

UNIVERSITÀ DEGLI STUDI DI NAPOLI “FEDERICO II”



FACOLTÀ DI INGEGNERIA

DIPARTIMENTO DI INGEGNERIA DEI MATERIALI E DELLA PRODUZIONE

**DOTTORATO IN INGEGNERIA DEI MATERIALI E DELLE STRUTTURE
XXII CICLO**

**Process tuning of physical properties of carbon
nanotubes polymer composites**

Ph.D. dissertation

by

Gabriella Faiella

Tutor: Dr. Michele Giordano

Coordinatore: Ch.mo Prof. Domenico Acierno

December 2009

*“By striving to the impossible,
man has always achieved what is possible.*

*Those who have cautiously done no more than they believed possible have never taken
a single step forward”*

Mikhail Bakunin

Contents

List of figures	iv
List of tables	x
Introduction.....	1
Chapter 1 - Carbon nanotubes physical properties and applications	5
1.1 Introduction	5
1.2 Structure of CNTs.....	6
1.3 Synthesis and growth of CNTs	8
1.4 Optical and electrical properties.....	11
1.5 Mechanical properties	15
1.6 Thermal properties	16
1.7 Characterization techniques of CNTs	17
1.7.1 Raman spectroscopy.....	19
1.8 Applications of CNTs.....	24
1.9 References.....	24
Chapter 2 - Carbon nanotubes polymer composites.....	28
2.1 Introduction	28
2.2 Carbon nanotubes suspensions	30
2.2.1 Thermodynamics of CNTs suspensions	30
2.2.2 Production of CNTs suspensions	37
2.3 Carbon nanotubes polymer composites fabrication	40
2.3.1 Nanotubes functionalization.....	40
2.3.2 Mechanical dispersion.....	42
2.3.3 Nanotubes alignment	45
2.4 CNTs composites properties.....	48
2.4.1 Mechanical properties	48
2.4.2 Rheological properties.....	51
2.4.3 Thermal conductivity	53

2.5	Electrical properties	57
2.5.1	Statistical and dynamic percolation	58
2.6	References.....	65
Chapter 3 - Monitoring the dispersion process of CNTs in aqueous solutions		71
3.1	Introduction	71
3.2	CNTs dispersion with surfactants as dispersing agent.....	72
3.3	Characterization of CNTs dispersion by means of spectroscopic techniques	74
3.3.1	UV-vis spectroscopy	74
3.3.2	Raman spectroscopy.....	76
3.4	Experimental.....	77
3.4.1	Materials and methods	77
3.4.2	UV-vis spectroscopy analysis.....	79
3.4.3	Raman spectroscopy analysis	84
3.4.4	Scanning Electron Microscopy.....	87
3.4.5	Atomic Force Microscopy.....	88
3.5	Conclusions	91
3.6	References.....	91
Chapter 4 - Carbon nanotubes based composites produced using Latex technology		93
4.1	Introduction	93
4.2	Latex technology.....	94
4.3	Fabrication and electrical characterization of SWNT/polystyrene composites.....	95
4.3.1	Materials and methods	96
4.3.2	Electrical measurements	97
4.4	Equivalent electrical circuit for SWNT/polystyrene composites.....	103
4.5	Morphological analysis of SWNT/polystyrene composites.....	105
4.5.1	Transmission Electron Microscopy	105
4.5.2	Environmental Scanning Electron Microscopy: charge contrast imaging mode	106
4.6	Thermal properties of SWNT/polystyrene composites	107
4.7	Conclusions	108
4.8	References.....	109

Chapter 5 - Tuning of the insulator to conductor transition in MWNTs/epoxy composites.....	110
5.1 Introduction	110
5.2 Dynamic percolation and hierarchical morphology of CNTs networks	111
5.3 Experimental.....	115
5.3.1. Epoxy system characterization	116
5.3.2. Materials and methods.....	118
5.3.3. Composite set 1 - CNTs/epoxy composites at fixed MWNTs concentration from different solvent	120
5.3.4. Composite set 2 - CNTs/epoxy composites at fixed MWNTs concentration and different sonication times.....	126
5.3.5. Composite set 3 - CNTs/epoxy composites at different MWNTs concentrations	131
5.3.6. Mechanically mixed epoxy composites.....	144
5.4 Conclusions	146
5.5 References.....	147
 APPENDIX A - CNTs alignment in polyurethane composites.....	149
A.1 Introduction	149
A.2 Fabrication and electrical characterization of MWNTs/TPU composites	151
A.3 MWNTs alignment in TPU composites	153
A.4 References.....	154
 Conclusions and perspectives	156

List of figures

Figure 1. 1 - Graphite structure: parallel stacking of 2D graphene sheet planes [8]	6
Figure 1. 2 - Structure of a) zig-zag, b) armchair and c) chiral nanotube.....	7
Figure 1. 3 - a) Single Walled Carbon Nanotube (SWNT) and b) Multi Walled Carbon nanotube (MWNT)	7
Figure 1. 4 - Arc-discharge production of CNTs	8
Figure 1. 5 - a) Schematic of Carbon Vapour Deposition (CCVD) technique; b) entangled CNTs grown by CVD; c) PECVD aligned nanotubes.....	9
Figure 1. 6 - SWNT tip closure	10
Figure 1. 7 - Bonds structure in a nanotube.....	11
Figure 1. 8 - Illustration of allowed wavevector lines leading to semiconducting and metallic CNTs and examples of bandstructures for semiconducting and metallic zigzag CNTs. [8]	12
Figure 1. 9 - Schematic of metallic and semiconducting tubes chirality	13
Figure 1. 10 - Bandgap versus radius for zigzag CNTs [8]	13
Figure 1. 11 - Measured optical absorbance between 0 and 3 eV of SWNT samples with 1.3 nm mean diameter. ES11, ES22, and EM11 are the lowest interband transitions in semiconducting (S) and metallic (M) SWNTs.....	14
Figure 1. 12 - Micrographs showing (a) the apparatus for tensile loading of MWCNTs and (b) the telescoping, “sword and sheath” fracture behavior of the MWCNT [39].	16
Figure 1. 13 - Measured temperature dependence of the thermal conductivity of bundles of SWNTs [42].	17
Figure 1. 14 - TEM images of a) and b) SWNT, c) DWNT [52], d) MWNT [from nanolab website]	19
Figure 1. 15 - Kataura-plot showing the electronic transition energies E_{ii} for all the (n,m) SWNTs with diameters ranging between 0.4÷3 nm.	20
Figure 1. 16 - Raman scattering spectrum of a SWNT.....	21
Figure 1. 17 - Atomic vibration of a nanotube in the radial breathing mode	22
Figure 1. 18 - a) Atomic vibration of a nanotube in the tangential modes; b) typical G-band spectrum of different nanotubes.....	23
Figure 2. 1 - The specific interaction potential between two parallel SWNT as a function of the distance between them, [28]	33
Figure 2. 2 - Repulsive interactions between grafted polymers on parallel CNTs as a function of the distance between the grafting surfaces, as calculated from a molecular theory [12]	35
Figure 2. 3 - The total interaction potential between parallel CNTs. The potentials are obtained by adding the vdW attractive contribution (fig. 2.1) and the steric repulsions (fig. 2.2) arising from the tethered polymers.....	36
Figure 2. 4 - a) The vdW interaction between two 4-tubes bundles; b) total interaction between two bundles composed by 4 CNTs each coated by different polymers.....	36

Figure 2. 5 - A schematic representation of the exfoliation concept (A-C) and of the subsequent polymer attaching and solution stabilization (D-G) [12].....	38
Figure 2. 6 - Schematic depiction of oxidative etching of SWNTs followed by treatment with thionyl chloride, and subsequent amidation.....	41
Figure 2. 7 - (a) SEM image of aligned electrospun fibers. (b) AFM image.....	46
of aligned individual SWNT after heating an electrospun fiber on a silicon substrate [83]	46
Figure 2. 8 - Schematic illustration of a) a polarised cylindrical particle in an electric..... Field; b) the interaction between aligned and polarised metallic cylindrical particles in an electric field	47
Figure 2. 9 - Transmission optical micrographs of epoxy composites containing 0.01 MWNT wt% a) cured in a DC field and in b) a AC field	48
Figure 2. 10 - Stress-strain profiles of SWNT-nylon-6 composite fibres at different SWNT loadings [93]	50
Figure 2. 11 - Composition dependence of the normalized tensile modulus ($E_{\text{composite}}/E_{\text{PDMS}}$) and the elongation at break ($L_{\text{break}}/L_{\text{initial}}$) for SWNT/PDMS nanocomposites [94].....	50
Figure 2. 12 - Mechanical properties of different CNTs/epoxy composites [95]	51
Figure 2. 13 - Mechanical properties of different CNTs/epoxy composites [96]	51
Figure 2. 14 - (a) Storage modulus (G') vs shear frequency for SWNT/PMMA nanocomposites with various nanotube loadings from 0 to 2.0 wt % (b) G' as a function of the nanotube loading for SWNT/PMMA nanocomposites at a fixed frequency, 0.5 rad/s [97].....	52
Figure 2. 15 - a) Storage modulus and b) loss factor of an epoxy/CNTs system [101]	53
Figure 2. 16 - (a) Electrical conductivity and (b) thermal conductivity as function of SWNT loading for PMMA composites [104].....	55
Figure 2. 17 - Time Dependence of room temperature electrical resistivity for 2.5 phr VGCF filled HDPE/PMMA (50/50) blend after hot-pressed at various temperatures [137]	62
Figure 2. 18 - Optical microscopy images and specific bulk AC conductivity of MWNT/epoxy composites produced by varying a) stirring temperature, b) stirring rate, c) curing temperature	64
Figure 2. 19 - DC conductivity during 2 h of annealing, transient shear, conductivity recovery and cooling to room temperature for different MWNT/PC composite [140].....	64
Figure 3. 1 - Surfactant adsorption on nanotube external wall	73
Figure 3. 2 - Evolution of the UV spectra of a) CoMoCAT, b) arc-discharge and c) HiPCO carbon nanotubes solution as function of the energy delivered during sonication.....	76
Figure 3. 3 - Evolution of the height of the peak located around 250 nm for an aqueous arc-discharge carbon nanotubes solution	76
Figure 3. 4 - Chemical structure of a) Sodium-Cholate, b) CTAB and c) Triton-X 100.....	78
Figure 3. 5 - UV-vis spectra of surfactant aqueous solutions.....	80

Figure 3. 6 - Evolution of the UV-vis spectra of aqueous surfactant-SWNTs solutions as a function of sonication time: a) Triton-X-SWNTs solution; b) CTAB-SWNTs solution; c) Sodium Cholate solution.....	80
Figure 3. 7 - Evolution of the UV-vis spectra (zoom image in the range 200-500nm) of aqueous surfactant-SWNTs solutions as a function of surfactant concentration: a) Triton-X; b) CTAB; c) Sodium Cholate	81
Figure 3. 8 - UV-vis absorbance spectra of (a) CTAB-SWNTs (b) Sodium-Cholate-SWNTs aqueous solutions at different sonication times.....	83
Figure 3. 9 - Area under the UV-vis spectra of a) CTAB-SWNTs and b) Sodium-Cholate-SWNTs aqueous solutions as a function of sonication time	83
Figure 3. 10 - Raman spectra of a) CTAB-SWNTs and b) Sodium-Cholate-SWNTs aqueous solutions at different sonication times; in the inset a zoom of RBM and G band is reported	84
Figure 3. 11 - Areas of G and G* bands as a function of sonication time for a) CTAB - SWNTs and b) Sodium-Cholate aqueous solutions.....	85
Figure 3. 12 - Raman intensities as a function of UV-vis absorbance for a) CTAB - SWNTs and b) Sodium-Cholate - SWNTs aqueous solutions evaluated at different sonication times	86
Figure 3. 13 - SEM micrographs of CTAB - SWNTs dried solutions at a) 10000 X and b) 60000 X magnifications.....	87
Figure 3. 14 - SEM micrographs of sodium-Cholate - SWNTs dried solutions at a) 10000 X and b) 60000 X magnifications	88
Figure 3. 15 - AFM height images of two different areas (a: (10x10) μm^2 and b: (7x7) μm^2) of the specimen prepared by CTAB and SWNTs-solution. The contrast covers height variations in the range 0 ÷ 195.2 nm and 0 ÷ 67.2 nm for a and b respectively	89
Figure 3. 16 - a) AFM height image of an area (2.5x2.5) μm^2 of the specimen prepared by CTAB and SWNTs-solution (the contrast covers height variations in the range 0 ÷ 37.8 nm and b) a cross section along the line indicated in figure 3.16 a).....	89
Figure 3. 17 - AFM height images of two different area (a: (10x10) μm^2 and b: (5x5) μm^2) of the SC-CNT dried sample. The contrast covers height variations in the range 0 ÷ 116.4 nm and 0 ÷ 25.9 nm for the two images a and b respectively	90
Figure 3. 18 - a) AFM height image of an area (2x2) μm^2 of the SC-CNT dried sample (the contrast covers height variations in the range 0 ÷ 24.4 nm and b) a cross section along the line indicated in figure 3.18 a).....	90
Figure 4. 1 - Schematic description of the multi-step process for the preparation of CNT/polymer composites by using latex technology	94
Figure 4. 2 - Electrical conductivity of a) polystyrene/SWNTs [3]and b) polystyrene/MWNT [6] composites as a function of wt%	95
Figure 4. 3 - SWNT/polystyrene composite powders resulting from the freeze drying process, from the most concentrated (5 SWNT wt%) to the pure polystyrene	97
Figure 4. 4 - a) DC conductivity of SWNT-PS composites; b) power law fit of data above percolation threshold.....	98
Figure 4. 5 - Current-Voltage characteristics of polystyrene composites at a) 1 SWNT wt%; b) 3 SWNT wt%; c) 5 SWNT wt%	99

Figure 4. 6 - Bode plot: absolute value of impedance as a function of angular frequency for the SWNT/polystyrene composites	100
Figure 4. 7 - a) AC conductivity σ' and b) imaginary part of complex permittivity for polystyrene composites at various SWNT wt%	101
Figure 4. 8 - Real part ϵ' of complex permittivity for PS - SWNT composites of various SWNT content	101
Figure 4. 9 - Static permittivity $\epsilon_s = \epsilon'(\omega \rightarrow 0)$ versus SWNT wt% in PS composites	102
Figure 4. 10 - Phase angle of SWNT-PS composites as a function of angular frequency..	103
Figure 4. 11 - Electrical equivalent circuit modeling 1.5 SWNT wt% composite	104
Figure 4. 12 - Best fitting of a) impedance and b) phase angle data: the solid line represent the fit curve and the dots represent experimental data.....	105
Figure 4. 13 - TEM micrograph of a 5 SWNT wt% sample	106
Figure 4. 14 - High resolution SEM images of a 2 SWNT wt% sample using an acceleration voltage of a) 20kV and b) 25kV	107
Figure 4. 15 - a) Overview and b) high resolution SEM images of a 3 SWNT wt% sample using an acceleration voltage of 25 kV showing straight and bended SWNTs.....	107
Figure 4. 16 - a) TGA curves of SWNT-PS composites with different SWNT content under atmosphere and b) a zoom of the curves in the range 30-500°C	108
Figure 5.1 - a) Comparative log-log plot of the MWNT/epoxy composites conductivity as a function of nanotube weight fraction for different sample preparation methods and b) the corresponding optical microscopy images.....	112
Figure 5. 2 - Small-angle scattering (SAS) data on SWNTs water solution [2]	113
Figure 5. 3 - a) Schematic representation of a suspension of SWCNTs showing a disordered network on two length scales [6] b) SEM and c) TEM images of CNTs water solution [7].....	114
Figure 5. 4 - Background-subtracted USAXS data for Epon 828 cured with SWCNT-loaded Jeffamine D-2000 [6]	114
Figure 5. 5 - Schematic representation of a branched wormlike cluster with persistence length L_p	115
Figure 5. 6 - Physical properties of the Epon 828 (by Hexion)	116
Figure 5. 7 - Total heat reaction during the curing of the epoxy system in dynamic conditions	117
Figure 5. 8 - Epoxy curing heat flow curves during curing in isothermal conditions at a) 30 °C, b) 70 °C, c) 120 °C	117
Figure 5. 9 - DC electrical measurements experimental set-up	119
Figure 5. 10 - Electrical conductivity of the four sets of manufactured nanocomposites and of pure epoxy as a function of curing temperatures	121
Figure 5. 11 - Transmission light micrographs at 20 X magnification (100 μm x 100 μm) of 0.05 MWNT wt% composites sonicated for a) 30' in TETA; b) 30' in Epon; c) 120' in TETA and d) 120' in Epon and then cured as curing conditions 1, 2 and 3	122
Figure 5. 12 - SAXS structural data referring to T and E samples sonicated for 30 and 120 minutes and cured as condition	123

Figure 5. 13 - a) Proposed multiscale nanotubes net for b) E and T composites [18]	125
Figure 5. 14 - Electrical conductivity of composites of set 2: a) the five sonication time groups as a function of curing temperature; b) the three curing temperatures groups as a function of sonication time.....	128
Figure 5. 15 - Transmission optical microscopy images (magnification 10X) of composites sonicated 45' and cured as indicated in curing conditions a) 1, b) 2 and c) 3 respectively.	129
Figure 5. 16 - Transmission optical microscopy images (magnification 10X) of composites sonicated 120' and cured as indicated in curing conditions a) 1, b) 2 and c) 3 respectively	129
Figure 5. 17 - Electrical conductivity as a function of curing condition of composites of set 3 at different MWNT wt% produced by a sonication for 10 minutes in Epon	133
Figure 5. 18 - Electrical conductivity of composites of set 3 at different MWNT wt% produced by a sonication of 30 minutes as a function of the curing conditions 1, 2 and 3	133
Figure 5. 19 - Electrical conductivity of composites of set 3 at different MWNT wt% produced by a sonication of 75 minutes as a function of the curing conditions 1, 2 and 3	134
Figure 5. 20 - Electrical conductivity of composites of set 3 at different MWNT wt% produced by a sonication of 120 minutes as a function of the curing conditions 1, 2 and 3	134
Figure 5. 21 - Percolative curves of composites of set 3 produced by a sonication of 10 minutes cured using the three different conditions	135
Figure 5. 22 - Percolative curves of composites of set 3 produced by a sonication of 30 minutes cured using the three different conditions	135
Figure 5. 23 - Percolative curves of composites of set 3 produced by a sonication of 75 minutes cured using the three different conditions	136
Figure 5. 24 - Percolative curves of composites of set 3 produced by a sonication of 120 minutes cured using the three different conditions	136
Figure 5. 25 - Transmission optical microscopy images of composites at 0.02 MWNT wt% produced by a sonication of 10 minutes and cured respectively following the curing conditions a) 1, b) 2 and c) 3	137
Figure 5. 26 - Transmission optical microscopy images of composites at 0.025 MWNT wt% produced by a sonication of 10 minutes and cured respectively following the curing conditions a) 1, b) 2 and c) 3	137
Figure 5. 27 - Transmission optical microscopy images of composites at 0.03 MWNT wt% produced by a sonication of 10 minutes and cured respectively following the curing conditions a) 1, b) 2 and c) 3	138
Figure 5. 28 - Transmission optical microscopy images of composites at 0.03 MWNT wt% produced by a sonication of 30 minutes and cured respectively following the curing conditions a) 1, b) 2 and c) 3	138
Figure 5. 29 - Transmission optical microscopy images of composites at 0.02 MWNT wt% produced by a sonication of 30 minutes and cured respectively following the curing conditions a) 1, b) 2 and c) 3	138

Figure 5. 30 - Transmission optical microscopy images of composites at 0.08 MWNT wt% produced by a sonication of 30 minutes and cured respectively following the curing conditions a) 1, b) 2 and c) 3	139
Figure 5. 31 - Transmission optical microscopy images of composites at 0.035 MWNT wt% produced by a sonication of 75 minutes and cured respectively following the curing conditions a) 1, b) 2 and c) 3	139
Figure 5. 32 - Transmission optical microscopy images of composites at 0.04 MWNT wt% produced by a sonication of 75 minutes and cured respectively following the curing conditions a) 1, b) 2 and c) 3	139
Figure 5. 33 - Transmission optical microscopy images of composites at 0.03 MWNT wt% produced by a sonication of 120 minutes and cured respectively following the curing conditions a) 1, b) 2 and c) 3	140
Figure 5. 34 - Transmission optical microscopy images of composites at 0.04 MWNT wt% produced by a sonication of 120 minutes and cured respectively following the curing conditions a) 1, b) 2 and c) 3	140
Figure 5. 35 - Percolation curves of composites of set 3 as a function of the curing condition a) 1, b) 2 and c) 3	142
Figure 5. 36 – Three roll mill calander Exakt 50	145
Figure 5. 37 - Electrical conductivity of mechanical mixed, 30 minutes sonicated in TETA and 30 and 120 minutes sonicated in Epon MWNT/epoxy composite cured at 70 °C	145
Figure A. 1 - Chemical formulation of a generic TPU	149
Figure A. 2 - TPU chemistry: hard and soft segments (from BASF)	151
Figure A. 3 - a) Current vs. Voltage curves for TPU/MWNTs composites; b) electrical conductivity of TPU and its composites at 1 and 3 MWNT wt% as a function of mixing conditions	153
Figure A. 4 - Electrical resistivity of the TPU composite before and after the electrical discharge	153
Figure A. 5 - Transmission optical microscopy images of TPU/MWNT composite a) before and b) after the electrical discharge	154

List of tables

Table 3. 1 - Solutions prepared using three different surfactants and concentrations.....	78
Table 4.1 - SWNT composite samples.....	97
Table 4.2 - Best fitting parameters.....	104
Table 5. 1 - Epoxy curing cycle and corresponding glass transition temperature	117
Table 5. 2 - Chemical gel times for epoxy systems evaluated at $\alpha = 0.54$	117
Table 5. 3 - CNTs/Epoxy composites set: manufacturing techniques.....	119
Table 5. 4 - Samples in composites set 1	121
Table 5. 5 - SAXS structural data referring to T and E samples sonicated for 30 and 120 minutes and cured as curing condition 1 and 3	124
Table 5. 6 - Samples of composites set 2.....	127
Table 5. 7 – Variation of MWNT wt% corresponding to an increase of conductivity from 10^{-12} to 10^{-6} S/m for the four sonication times set of composites	143
Table A. 1 - MWNT/TPU composites mixing conditions.....	152

Introduction

The work is settled in the framework of polymer based nanocomposites, that are composites constituted by a polymeric matrix and a nanometric filler, such as a particle having at least one dimension in the order of nanometer (10^{-9} m) and it concerns the fabrication and the characterization of carbon nanotubes (CNTs) polymers composites.

Carbon nanotubes are fullerenic structures that can be regarded as a graphene sheet rolled up into a cylinder with the diameter having dimensions in the order of few nanometers and the length in the order of microns. The high aspect ratio, such as the ratio between the length and the diameter (L/D), ranging from 100 to 1000 confers to these nanostructures the possibility to be used for a very wide range of applications with enormous beneficial results respect to the other nanoparticles.

CNTs possess unique electrical properties, because they are ballistic conductor along their length, but they can have also semiconductive nature depending on their chemical structure, such as on how the graphene sheet is rolled up. Moreover, CNTs have also extraordinary mechanical properties related to the strength of the C-C bounds, with Young modulus of about 2 TPa, very high stiffness and axial strength. Together with high electrical conductivity, CNTs also show a thermal conductivity of 3000 W/Km, twice as high as in the diamond and very high thermal resistance.

The intriguing properties of carbon nanotubes have led to an explosion of research efforts worldwide. Understanding these properties and exploring their potential applications have been a main driving force in this area. Thus far, nanotubes have been utilized individually for nanoelectronic applications or as filler in composite materials and in particular together with polymer matrices.

Such nanocomposites have attracted a big interest in scientific community because of their enhanced physical properties respect to the neat matrix. The addition of CNTs to insulating polymers leads to the production of the so called “conductive plastic” at concentrations of filler ten times lower than the ones used for carbon-black composites, for the same conductivity value. These results are possible because of the high aspect ratio of CNTs, that allows them to connect

in a conductive network at concentrations much lower respect to the other conductive particles having other geometrical forms.

The dissertation is divided into two part: in the first two chapters a state of art background of the CNTs physical properties as well as of their polymer based composites has been illustrated; in the second part, three experimental research experiences have been described. The first is based on the study of the dispersion process of CNTs; the second deals with the production and characterization of thermoplastic composites and the third describes the process induced properties of CNTs/thermoset composites.

The dissertation will start in chapter 1, with a description of CNTs structure and production techniques, passing then to a discussion of their physical properties, such as optical, electrical, mechanical and thermal. Physical properties characterization techniques and methods have been then described, paying particular attention to Raman spectroscopy, because it has been used as characterization technique in an experimental section of this work.

The main subject of this thesis has been introduced in chapter 2, with a description of the actual state of art on CNTs polymer based composites. The thermodynamics and the production techniques of CNTs suspensions have been discussed and then the attention has been then devoted to CNTs polymer composites. Composites fabrication techniques have been described distinguishing among the different polymer matrices and elucidating the advantages and drawbacks of both chemical and mechanical dispersion methods. On the basis of the thermodynamics theoretical concepts and the description of production techniques, the physical properties of CNTs composites have been described and related to their fabrications methods. Mechanical, rheological, thermal and electrical properties of polymer based composites having both thermoplastic and thermoset nature have been summarized, reporting elucidative literature results. In this part, particular attention has been paid to the discussion of the electrical properties of CNTs composites. The percolation phenomenon in different types of composites has been analyzed and, at the same time, examples of systems where the statistical theories were not sufficient to explain the electrical results have been provided. Hence, the concept of “dynamic percolation”, conferring a kinetic nature to the percolation phenomenon, has been introduced to explain most of the results reported in literature.

With chapter 3 the experimental part starts with the description of the production and characterization of CNTs aqueous solutions. In this part of the study, surfactants have been used as dispersing agent in SWNTs/water solutions and sonication as dispersion technique. The monitoring of the dispersion process has been studied by means of UV-vis and Raman spectroscopies and the exfoliation efficiency of different surfactants as well as of different sonication times has been evaluated by the combined analysis of the provided results. The

maximum UV absorbance and Raman intensity were found to be related to the maximum exfoliation of CNTs in solution. A strict correlation between the two spectroscopic techniques results was found, demonstrating that both techniques can be considered effective and reproducible methods to investigate the dispersion state of CNTs in solutions.

The results provided by the SWNTs dispersion study have been used for the production of polystyrene based composites produced by using Latex technology, described in chapter 4. The latter is a polymer type independent technique, based on the dispersion of CNTs in aqueous surfactant solution, then mixed with a polymer emulsion to obtain the final composite. SWNTs/polystyrene composites have been produced at different carbon nanotubes concentrations and an extensive electrical characterization has been carried out for the evaluation of the percolative behavior of such composites. Impedance spectroscopy has been also used for the study of the electrical behavior as a function of frequency in order to distinguish between the capacitive and resistive natures of the different composites. An equivalent electrical circuit model has been proposed to explain the frequency dependence of the composites, where both the capacitive nature of the matrix and the conductive behavior of the nanotubes have been considered and opportunely schematized. A good agreement between experimental and fitted data has been found to validate the model. Moreover, a morphological characterization by means of scanning electron microscopy using charge contrast imaging mode and thermo-gravimetric analysis have been performed on the composites to complete the materials characterization.

In chapter 5, the fabrication and the characterization of CNTs/thermoset composites have been carried out. The aim of this part of the work is the study of the dependence of the electrical properties of MWNTs/epoxy composites on the fabrication process, finalized to control the tuning of the electrical properties of the final composite by varying the process parameters. Starting from the same matrix and filler, various sets of materials have been produced by properly varying some fabrication parameters, such as the dispersion solvent, the sonication time, the curing temperature and finally the MWNTs concentration. The strict dependence of the final morphological properties on every of these parameters has been found to be crucial for the final electrical properties of the composites. The study of this dependence has been carried out starting from the assumption that CNTs arrange within a polymer matrix in networks with hierarchical morphology, having a multiscale dispersion state, where they are aggregated into disordered ropes that are further agglomerated into micron sized fractal clusters. Optical microscopy has been used to study the CNTs network morphology at the microscale level and a correlation between the evolution of the electrical conductivity with a temperature induced agglomeration has been found. The concepts of dynamic percolation and induced agglomeration have been mostly used as key factors to explain the electrical conductivity results. Moreover, a

notable result consists in the detection itself of structures at a nanoscale level by means of small angle X-ray analysis (SAXS), not yet observed in literature for MWNT/epoxy composites systems. The correlation between electrical, morphological and SAXS results has provided the formulation of a multiscale organization model of CNTs in the composites, where, starting from the single MWNT, two higher length scales have been assumed to exist, such as the nanosized bundles and the micron sized clusters, whose intrinsic electrical conductivity and connectedness determine the conductivity at the macroscopic scale.

Chapter 1

Carbon nanotubes physical properties and applications

1.1 Introduction

Due to their low dimensionality, nanostructures such as quantum dots, nanowires and carbon nanotubes (CNTs) possess unique properties that make them promising candidates for future technology applications. However, to truly harness the potential of nanostructures, it is essential to develop a fundamental understanding of the basic physics that governs their behavior in devices. This is especially true for CNTs, where research has shown that the concepts learned from bulk device physics do not simply carry over to nanotube devices, leading to unusual device operation.

Carbon nanotubes (CNTs) are amongst the most explored one-dimensional nanostructures and have attracted tremendous interest from fundamental science and technological perspectives. Albeit topologically simple, they exhibit a rich variety of intriguing electronic properties, such as metallic and semiconducting behavior. Furthermore, these structures are atomically precise, meaning that each carbon atom is still three-fold coordinated without any dangling bonds. CNTs have been used in many laboratories to build prototype nanodevices. These devices include metallic wires, field-effect transistors, electromechanical sensors and displays. They potentially form the basis of future all-carbon electronics. Together with their ballistic conduction, carbon nanotubes have extraordinary mechanical properties that render them ideal candidates for reinforcement in polymer composites. Moreover, because their high surface to volume ratio they are also used as sensors, and high-capacity hydrogen storage. Elemental carbon in the sp^2 hybridization can form a variety of amazing structures. Apart from the well-known graphite,

carbon can build closed and open cages with honeycomb atomic arrangement. First such structure to be discovered was the C₆₀ molecule by Kroto et al. [1]. Although various carbon cages were studied, it was only in 1991, when Iijima [2] observed for the first time tubular carbon structures. The nanotubes consisted of up to several tens of graphitic shells (so-called multi-walled carbon nanotubes (MWNTs)) with adjacent shell separation of about 0.34 nm, diameters of ~1 nm and large length/diameter ratio. Two years later, Iijima and Ichihashi [3] and Bethune et al. [4] synthesized single-walled carbon nanotubes (SWNTs). Nowadays, MWNTs and SWNTs are produced mainly by three techniques: arc-discharge, laser-ablation, and catalytic growth. The synthesized nanotube samples are characterized by means of Raman, electronic, and optical spectroscopies. Important information is derived by mechanical, electrical and thermal measurements. The experimental data is discussed in comparison with the results of theoretical models and computer simulations [5-7].

In this chapter the physical properties of carbon nanotubes will be illustrated, together with their possible applications.

1.2 Structure of CNTs

To understand the atomic structure of CNTs, one can imagine taking the structure of graphite, as shown in figure 1.1, and removing one of the two-dimensional planes, which is called a graphene sheet. A single graphene sheet is shown in figure 2(a). A CNT can be viewed as a rolled-up graphene strip which forms a closed cylinder as shown in figure 1.2.

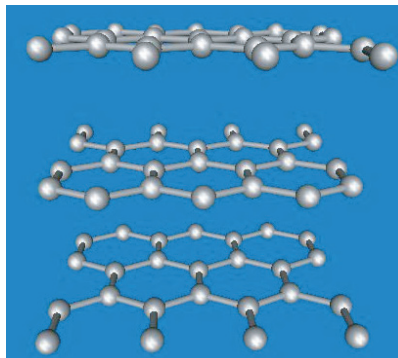


Figure 1. 1 - Graphite structure: parallel stacking of 2D graphene sheet planes [8]

The basis vectors $a_1 = a(\sqrt{3}, 0)$ and $a_2 = a(\frac{\sqrt{3}}{2}, \frac{3}{2})$ generate the graphene lattice, where $a = 0.142$ nm is the carbon-carbon bond length. A and B are the two atoms in the unit cell of

graphene. In cutting the rectangular strip, one defines a circumferential vector, $\mathbf{C} = na_1 + ma_2$, from which the CNT radius can be obtained:

$$R = \frac{C}{2\pi} = \frac{\sqrt{3}}{2\pi} a \sqrt{n^2 + m^2 + nm} \quad 1.1$$

There are two special cases shown in figure 1.2 a and b that deserve special mention. First, when the circumferential vector lies purely along one of the two basis vectors, the CNT is said to be of the ‘zigzag’ type. Second, when the circumferential vector is along the direction exactly between the two basis vectors ($n = m$), the CNT is said to be of ‘armchair’ type.

Figure 1.2 c shows a nanotube with arbitrary chirality (n, m), where the blue strip is generated by $m \neq n$.

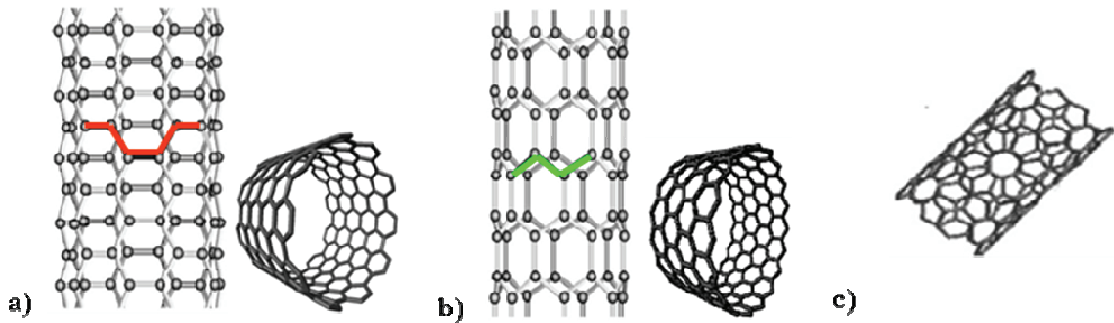


Figure 1. 2 - Structure of a) zig-zag, b) armchair and c) chiral nanotube

The individual tubes in the bundle are attracted to their nearest neighbors via the van der Waals interactions, with typical distances between the tubes being comparable to the interplanar distance of graphite which is 3.1 Å. The cross section of an individual nanotube in a bundle is circular if the diameter is smaller than 15 Å and deforms to a hexagon as the diameter of the individual tubes increases [8]. A close allotrope of the SWNT (fig. 1.3 a) is the multiwall nanotube (MWNT), which consists of nested SWNTs, in a Russian doll fashion as shown in figure 1.3 b. Again, the distance between the walls of neighbouring tubes is comparable to the interplanar distance of graphite.

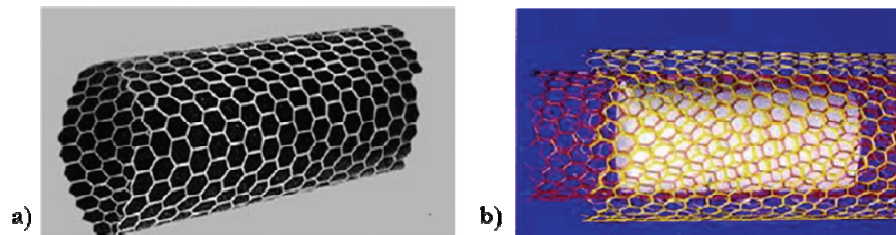


Figure 1. 3 - a) Single Walled Carbon Nanotube (SWNT) and b) Multi Walled Carbon nanotube (MWNT)

1.3 Synthesis and growth of CNTs

In 1991, Iijima reported the preparation of a new type of finite carbon structures consisting of needle-like tubes [2]. The tubes were produced using an arc-discharge evaporation method similar to that used for the fullerene synthesis (fig. 1.4). The carbon needles, ranging from 4 to 30 nm in diameter and up to 1 mm in length, were grown on the negative end of the carbon electrode used for the direct current (dc) arc-discharge evaporation of carbon in an argon-filled vessel (100 Torr). The TEM study of the growth morphology of the carbon microtubules synthesized by arc-discharge [9] revealed that there were many variations in shape, especially near the tube tips.

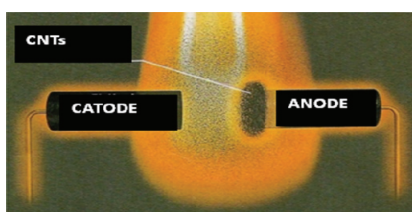


Figure 1. 4 - Arc-discharge production of CNTs

In 1996, Smalley and co-workers produced high yields ($>70\%$) of SWNTs by laser-ablation (vaporization) of graphite rods with small amounts of Ni and Co at $1200\text{ }^{\circ}\text{C}$ [10]. The X-ray diffraction and TEM showed that the synthesized nanotubes were remarkably uniform in diameters and that they formed ropes (or bundles) 5-20 nm in diameter and tens to hundreds of micrometers long.

The growth of the nanotubes was explained by a “scooter” mechanism. In this mechanism a single Ni or Co atom chemisorbs onto the open edge of a nanotube. The metal atom must have a sufficiently high electronegativity as to prevent formation of fullerenes and it must be highly effective in catalyzing the nanotube growth. The metal atom circulates (“scoots”) around the open-end of the tube and absorbs small carbon molecules and converts them into graphite-like sheet. The tube grows until too many catalyst atoms aggregate on the end of the nanotube. The large particles either detach or become over-coated with sufficient carbon to poison the catalysis. This allows the tube to terminate with a fullerene-like tip or with a catalyst particle. It was argued that the scooter mechanism favors the growth of armchair type nanotubes with of most probable type (10, 10) which corresponds to the experimental observations.

Both arc-discharge and laser-ablation techniques have the advantage of high ($>70\%$) yields of SWNTs and the drawback that (1) they rely on evaporation of carbon atoms from solid targets at

temperatures $>3000\text{ }^{\circ}\text{C}$, and (2) the nanotubes are tangled which makes difficult the purification and application of the samples.

Another very used technique to produce high quantity of nanotubes is based on the catalytic growth.

Generally, the CVD process includes catalyst-assisted decomposition of hydrocarbons, usually ethylene or acetylene, in a tube reactor at $550\text{--}750\text{ }^{\circ}\text{C}$ and growth of carbon nanotubes over the catalyst upon cooling the system. Best results are obtained with Fe, Ni or Co nanoparticles as catalyst. The same catalysts are found optimal in the arc-discharge and laserablation techniques, which is in favor of a common nanotube growth mechanism.

It was argued that the nanotubes grow out of the catalyst nanoparticle embedded in the pores by tip growth or base growth depending on the contact force between the catalyst particles and the substrate [11, 12]. Large-scale synthesis of aligned carbon nanotubes was achieved by the CVD technique and iron as catalyst by Li et al. [13]. A substrate containing iron nanoparticles embedded in mesoporous silica was placed in the reaction chamber. A mixture of 9% acetylene in nitrogen was introduced in the chamber at a flow rate of $110\text{ cm}^3/\text{min}$. Carbon nanotubes were formed on the substrate containing the iron nanoparticles by deposition of carbon atoms obtained by decomposition of acetylene at $700\text{ }^{\circ}\text{C}$ (fig. 1.5).

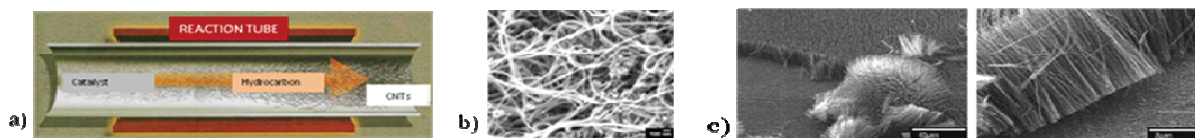


Figure 1. 5 - a) Schematic of Carbon Vapour Deposition (CVD) technique; b) entangled CNTs grown by CVD; c) PECVD aligned nanotubes

The samples were examined by SEM and energy-dispersive X-ray diffraction (EDX). The SEM image of the obtained thin films showed that MWNTs grew continuously from the bottom to the top of the film in lengths between 50 and $100\text{ }\mu\text{m}$.

High-quality SWNTs could be grown on silicon wafers patterned with micrometerscale islands of catalytic material by the CVD technique by Kong et al. [14]. Methane was used as carbon feedstock, high reaction temperatures in the range of $850\text{--}1000\text{ }^{\circ}\text{C}$ were necessary to form small diameter SWNTs. The optimal choice of a catalyst was a Fe/Mo species supported on a sol-gel derived alumina-silica multicomponent material. The TEM images revealed an abundance of individual and bundled SWNT. One unique aspect of CVD techniques is its ability to synthesize aligned arrays of carbon nanotubes with controlled diameter and length. The synthesis of well aligned, straight carbon nanotubes on a variety of substrates has been accomplished by the use of

plasma enhanced chemical vapor deposition (PECVD) where the plasma is excited by a DC source or a microwave source (fig 1.5 c) [15-20].

It has been experimentally established that transition metal catalysts are necessary for the growth of SWNTs but are not required for MWNTs. This fact suggests different growth mechanisms in both cases. Experimentally it is observed that the MWNTs grow both lengthening and thickening, and at some stage the nanotubes tend to close. Secondly, during the growth, the nanotubes remain open [17] although the large number of dangling bonds at the ends favor closing of the tubes. It was suggested that open-ended growth could be explained by a so-called lip-lip interaction [19] (fig. 1.6). Tight-binding calculations on MWNTs showed that the growing edge is stabilized by bridging carbon atoms thus prolonging the life of the open structure. It was found that strong covalent bonds connecting the exposed edges of adjacent walls stabilize the nanotubes against dome closure [20].

The growth of SWNTs with a narrow diameter distribution by the arc-discharge [21] and the laser-ablation techniques [10] requires and critically depends on the composition of the catalyst.

At experimental temperatures (2000-3000 K) the open-end of SWNTs closed spontaneously into a graphitic dome with no residual dangling bonds in accordance with the experimental fact that SWNTs do not grow in the absence of transition metal catalysts. The tip closure resulted in a substantial reduction in the localized density of electronic states on the tips close to the Fermi energy. This result suggested that the reactivity of closed nanotube tips should be considerably lower than that of open-end nanotubes. The most probable mechanism of catalyst-assisted tip-growth assumes that the metal atoms sit on the open edge of precursor fullerene clusters [10]. The metal atoms “scoot” around the open edge of the cluster preventing the formation of carbon pentagons and the dome closure. Additionally, the metal catalyst assists incoming carbon atoms in the formation of hexagons and thus in the lengthening of the tube. With time the metal atoms at the tube edge will tend to aggregate. These clusters will become gradually less reactive and less mobile. Eventually, when the size of the metal cluster reaches some critical value, the adsorption energy of the cluster will decrease to such a level that it will peel off the edge. In the absence of the catalyst at the tube edge, defects can no longer be annealed effectively, thus initiating tube closure.

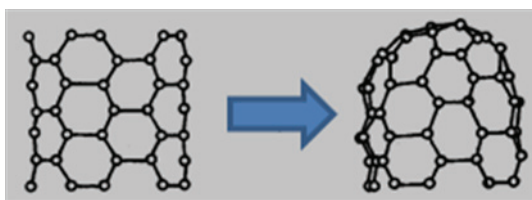


Figure 1. 6 - SWNT tip closure

1.4 Optical and electrical properties

The early theoretical studies of the electronic properties of SWNTs predicted that SWNTs could be either metallic or semiconducting depending on their structural parameters: one third of the nanotubes are metallic and two thirds are semiconducting depending on their indices (n, m), moreover some metallic nanotubes are very-small-gap semiconducting nanotubes[22-24].

- **Electronic band structure of SWNTs**

In the hexagonal graphite lattice, each carbon atom has six electrons: two are 1s, three are $2sp^2$ and 1 electron is 2p. The three electrons $2sp^2$ form three bonds in the graphite sheet, providing one unsaturated π -orbital (fig. 1.7).

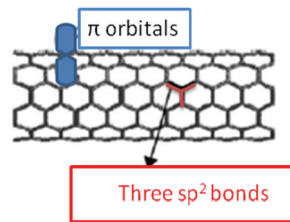


Figure 1. 7 - Bonds structure in a nanotube

Starting from the electronic structure of graphite it is possible to build up the electronic band structure of carbon nanotubes. Along the circumference of the nanotube the wavevector is quantized:

$$k \cdot c = k_x c_x + k_y c_y = 2\pi p \quad 1.2$$

where p is an integer.

This equation defines the lines in the plane (k_x, k_y) and each of this line gives a mono-dimensional energy band, intersecting the structure in bi-dimensional bands. The particular values of c_x , c_y and p determine where the lines intersect the band structures of the graphene and hence each nanotube has a different electronic structure. In particular, the nanotubes can be metallic or semiconducting whether or not these lines pass through the Fermi points (fig. 1.8). If the lines corresponding to wavevector pass through the Fermi points, the nanotubes are metallic, if they don't pass they are semiconducting, with a bandgap determined by the two lines that come closer to the Fermi points.

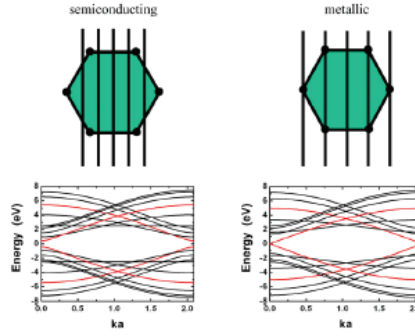


Figure 1. 8 - Illustration of allowed wavevector lines leading to semiconducting and metallic CNTs and examples of bandstructures for semiconducting and metallic zigzag CNTs. [8]

It is possible to mathematically represent the band structure of nanotubes defining the components of the wavevector perpendicular and parallel to the tube axis.

The energy is:

$$E = \frac{\hbar^2 k_c^2}{(2\pi)^2 2m^*} + \frac{\hbar^2 k_a^2}{(2\pi)^2 2m^*} \quad 1.3$$

Where k_c is the component of the momentum along the circumference, k_a along the cylinder axis and m^* the electron effective mass, accounting also for the interaction effect of the electron with the 2D periodic lattice. In the grapheme, the effective mass is 1/20 of the electron mass. Because k_c is quantized, the energy can be written as:

$$E = \frac{\hbar^2 n^2}{\pi^2 d^2 2m^*} + \frac{\hbar^2 k_a^2}{(2\pi)^2 2m^*} \quad 1.4$$

Hence, the energy is defined in sub-bands with minimum Energy depending on the number n determined by the nanotube diameter. In SWNTs, these bands have a separation gap of about 1 eV, that is higher than the thermal energy at room temperature, equal to 0.026 eV. The quantization of the momentum component along the circumference leads also to the removal of the zero gap condition of the graphene, providing the nanotube to be metallic or semiconducting whether the graphene sheet is rolled up. As discussed above, the condition for CNTs to be metallic is that some of the allowed lines $(2\pi p/c_y) - (c_x/c_y)k_x$ cross one of the Fermi points of graphene. This leads to the condition $|n - m| = 3 * I$, where I is an integer (fig. 1.9).

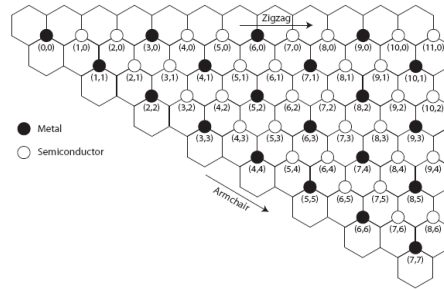


Figure 1. 9 - Schematic of metallic and semiconducting tubes chirality

Nanotubes for which this condition does not hold are semiconducting. Furthermore, it can be shown that the bandgap of semiconducting nanotubes decreases inversely with an increase in diameter as shown in figure 1.10. Nanotubes having smaller diameter have few allowed electronic states, that are far from each other. Upon an increase of the diameter, the allowed states increase and the bandgap between the valence and conduction bands decreases. In figure, it is possible to observe as the bandgap of a zig-zag nanotube decreases with increasing the tube radius. The tubes with bandgap equal to zero correspond to metallic tubes, satisfying the relation: $n-m=3*I$.

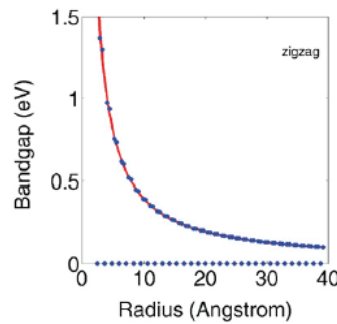


Figure 1. 10 - Bandgap versus radius for zigzag CNTs [8]

Summarizing, it is possible to say that the nanotube can behave like a metal or a semiconductor depending on the diameter and the chiral vector and this nature doesn't depend on the chemical bond between the Carbon atoms.

- **Optical absorption**

In figure 1.11 , the optical absorption spectrum of purified SWNT thin films measured by Kataura et al. [25] is presented.

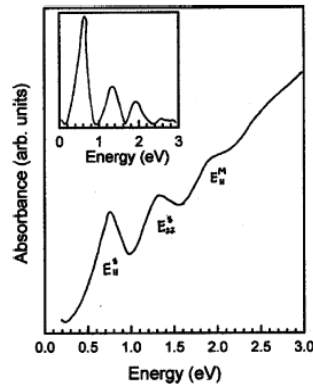


Figure 1. 11 - Measured optical absorbance between 0 and 3 eV of SWNT samples with 1.3 nm mean diameter. ES11, ES22, and EM11 are the lowest interband transitions in semiconducting (S) and metallic (M) SWNTs

The three peaks at 0.68, 1.2 and 1.7 eV were found to correspond to the density of states peaks of two semiconducting and one metallic tubes. It is possible to accurately determine the mean diameter and diameter distribution in bulk SWNT samples from a combined study of optical absorption, high-resolution electron energy-loss spectroscopy (EELS) in transmission and tight-binding calculations.

The optical response could be well described assuming a Gaussian distribution of nanotube diameters and the predicted inverse proportionality between the nanotube diameter and the energy of the absorption features. The obtained mean diameters and diameter distributions were in very good agreement with the values derived from other bulk sensitive methods such as electron diffraction, X-ray diffraction, and Raman scattering [26].

- **Electrical transport in perfect nanotubes**

Electrical transport through carbon nanotubes has attracted considerable interest due to the many possible applications of the nanotubes in nanoscale electronic devices, because they are nearly perfect 1D conductors. Ballistic transport has been observed and values for the conductance that approaches the theoretical limit have been measured at small biases. On the basis of the above illustrated concepts, it appears clear that nanotubes are unique material showing metallic behavior at single molecule level. Their conductance is ballistic, such as the electrons travel along the axis of the tube without any deviation from their path and the distances are quantized in unit of $2e^2/h$. On the contrary, in common metals the electrons travel on pathways where many collisions occur and the distance between two consequent collisions is of few nanometers. An electron in a 1D system can be deviated only if its pathway is completely inverted in direction, while in 2D and 3D systems, the electrons can be dispersed changing their

direction of small angles in the lattice. In metallic nanotubes, the lattice vibration have not sufficient energy to invert the direction of the moving electron. Ballistic resistor possess the unique properties that if they are connected in series, the total resistance is not the sum of the two resistance, but it is the higher between the two. The system behaves like the minor resistance is not present at all. This properties is based on the concept that each resistance independent on its length.

It was experimentally found that the current that could flow along a MWNT corresponds to a density of current of 10^8 A/cm². If the nanotube was a classic resistor, the power dissipated by a so much great current would have heated so much the wire to pulverize it.

1.5 Mechanical properties

Significant challenges exist in both the micromechanical characterization of nanotubes and the modeling of the elastic and fracture behavior at the nano-scale. Challenges in characterization of nanotubes and their composites include (a) complete lack of micromechanical characterization techniques for direct property measurement, (b) tremendous limitations on specimen size, (c) uncertainty in data obtained from indirect measurements, and (d) inadequacy in test specimen preparation techniques and lack of control in nanotube alignment and distribution.

The carbon nanotubes are expected to have high stiffness and axial strength as a result of the carbon-carbon sp² bonding [27]. The practical application of the nanotubes requires the study of the elastic response, the inelastic behavior and buckling, yield strength and fracture. Efforts have been applied to the experimental [28-31] and theoretical [32-37], investigation of these properties. Treacy et al. [28] first investigated the elastic modulus of isolated multi-walled nanotubes by measuring, in the transmission electron microscope, the amplitude of their intrinsic thermal vibration. The average value obtained over 11 samples was 1.8 TPa. Direct measurement of the stiffness and strength of individual, structurally isolated multi-wall carbon nanotubes has been made with an atomic-force microscope (AFM). The nanotube was pinned at one end to molybdenum disulfide surfaces and load was applied to the tube by means of the AFM tip. The bending force was measured as a function of displacement along the unpinned length, and a value of 1.26 TPa was obtained for the elastic modulus [30]. In the theoretical study of the mechanical properties of SWNTs and MWNTs it was obtained that the Young (E) and shear (G) moduli and chirality, having an average value of E=0.97 TPa and G=0.45 TPa. Together with these exceptional mechanical properties, CNTs have also flexibility, due to the ability of C-C bounds to hybridize with an hybridization dependent on the occurring deformation. Moreover,

they are characterized by a high deformation at break, about 40%, thanks to the plastic deformation and then to the rupture of C-C bonds.

However, nanotubes tend to aggregate in “ropes” of several tubes, having mechanical properties lower than the single tube. In particular as the rope diameter increases, the axial and shear moduli significantly decrease [38]. This phenomenon can be explained by a slipping between nanotubes occurring within the bundle. Yu and co-workers [39, 40] have investigated the tensile loading of multi-walled nanotubes and single-walled nanotube ropes. In their work, the nanotubes were attached between two opposing AFM tips and loaded under tension. Their experimental set-up is shown in fig. 1.12 a. For multi-walled carbon nanotubes the failure of the outermost tube occurred followed by pullout of the inner nanotubes. This ‘sword and sheath’ telescoping failure mechanism of multi-walled carbon nanotubes in tension is also shown in fig. 1.12 b.

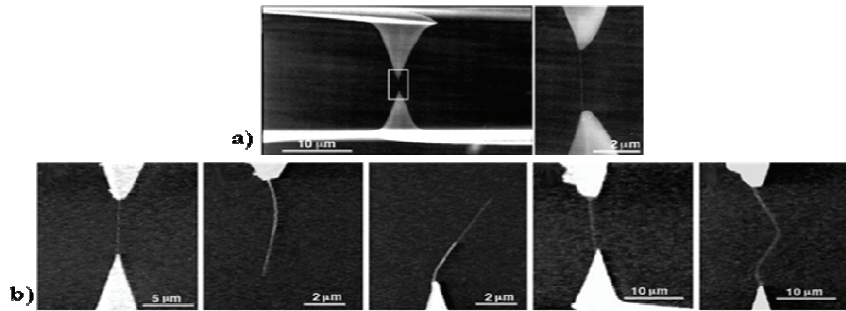


Figure 1. 12 - Micrographs showing (a) the apparatus for tensile loading of MWCNTs and (b) the telescoping, “sword and sheath” fracture behavior of the MWCNT [39].

The experimentally calculated tensile strengths of the outermost layer ranged from 11 to 63 GPa and the elastic modulus ranged from 270 to 950 GPa. In their subsequent investigation in the rope carried the load during the experiment, and they calculated tensile strengths of 13 to 52 GPa and average elastic moduli of 320 to 1470 GPa.

1.6 Thermal properties

Together with exceptional electrical properties CNTs possess also high thermal conductivity, being about twice as high as diamond, moreover they are thermally stable up to 2800 °C in vacuum. The thermal conductivity k of CVD-grown MWNTs measured from 4 to 300 K [41] was found to varied as T^2 , similar to that of graphite. The room temperature value of k is small, which is consistent with small system size and dominance of the grain-boundary scattering. Similar behavior was observed in the measurements of the temperature-dependent thermal conductivity of bundles of SWNTs from 8 to 350 K [42].

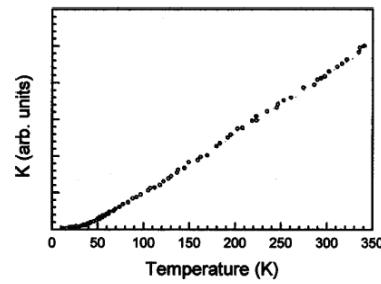


Figure 1.13 - Measured temperature dependence of the thermal conductivity of bundles of SWNTs [42]

The thermal conductivity decreased smoothly with the decrease of T and displayed linear temperature dependence below 30 K (fig. 1.13). The thermal conductivity of an individual MWNT was measured using a microfabricated suspended device [43]. The observed thermal conductivity was more than 3000 W/mK at room temperature, which is two orders of magnitude higher than the estimation of previous experiments that used macroscopic mat samples (about 20 W/mK [41] and 35 W/mK [42]).

As the diameter of the MWNT increases, the thermal conductivity versus T becomes similar to the bulk measurements.

1.7 Characterization techniques of CNTs

As previously observed, many are the difficulties in characterizing carbon nanotubes because of their dimensions and their high aspect ratio. In order to investigate the morphological and structural characterizations of nanotubes, a reduced number of techniques could be used. However, only few techniques are able to characterize CNTs at the individual level such as scanning tunneling microscopy (STM) and transmission electronic microscopy (TEM). X-ray photoelectron spectroscopy is helpful in order to determine the chemical structure of nanotubes while neutron and X-ray diffraction, infrared and Raman spectroscopy are mostly global characterization techniques.

Photoluminescence spectroscopy, based on the electronic properties of the tubes and in particular on the bandgap of semiconducting tubes, can be used for the identification of the nature (semiconducting or not), the geometries and the diameters of dispersed nanotubes. Moreover, the luminescence spectra seems to be very sensitive to the presence of chemical defects and to the purity of the samples [44].

Another useful technique for the knowledge of chemical structure of CNTs is the X-ray photoelectron spectroscopy (XPS). The most widely used data refers to the structure modification of the CNT walls due to the chemical interaction with organic compounds or gases adsorption, such as nitrogen [45].

Morphological investigations of CNTs structure can be carried out by means of Scanning tunneling microscopy (STM). STM images give directly the three-dimensional morphology of tubes and are consistent with the structure inferred from scanning electron microscopy [46]. Moreover, STM can resolve simultaneously both the atomic structure and the electronic density of state (DOS), giving information on the chiral angle, eventually present asymmetry of the tip, diameter and all the deriving properties. Furthermore, to investigate CNTs at larger scale X-ray diffraction or neutron diffraction is needed. Neutron diffraction is widely used for determination of structural features such as bond length and possible distortion of hexagonal network [47]. Moreover, contrary to X-ray diffraction, a wide range of scattering vector q can be explored due to the weak decrease of the atomic factor with q [48].

The latter characterization method is not sample destructive and is used to obtain some information on the interlayer spacing, the structural strain and the impurities. However, carbon nanotubes have multiple orientations compared to the X-ray incident beam. Diameters and chiralities distribution are also observed as well as various number of layers for MWNTs. This leads to a statistical characterization of carbon nanotubes. Due to their intrinsic nature, the main features of X-ray diffraction pattern of CNTs are close to those of graphite, hence the X-ray diffraction profile is not useful to differentiate microstructural details between the CNT and the graphite structure [49] but can help to determinate the sample purity, such as catalysts and functional groups. Some studies on the alignment of CNTs have been done using X-ray diffraction [50].

Another technique used for the morphological characterization is the infrared spectroscopy. This type of spectroscopy is often used to determine impurities remaining from synthesis or molecules capped on the nanotube surface. Numerous works are performed on organic molecules and CNTs: infrared spectroscopy exhibits all the modification of the CNTs structure and reveals the nature of compounds added to the CNTs [51].

Together with indirect morphological analysis, microscopic techniques are very useful tools for the characterization of the morphology of CNTs. Transmission electronic microscopy (TEM) is used for the identification of the nanotubes geometry, because with its high resolution is able to visualize and determine the geometry also of very small SWNT (fig 1.14).

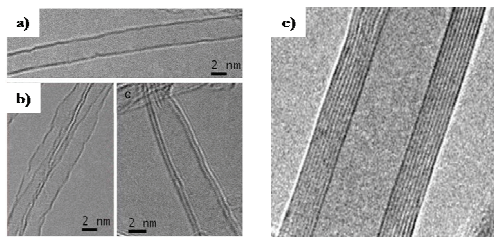


Figure 1. 14 - TEM images of a) and b) SWNT, c) DWNT [52], d) MWNT [from nanolab website]

TEM is used for all the studies concerning CNTs based nanodevices. Moreover, it can be used for the determination of the structures of CNTs within the bundles coupled with electron diffraction. The topology of a surface covered by CNTs can be analyzed using atomic force microscopy (AFM). The atomic force microscopy is a surface characterization technique that attributes the surface morphology by exploiting the interactions (usually Van der Waals forces) between the few atoms of the tip of the microscope and those that constitute the surface of the sample. It can work in different operating modes such as the contact and non-contact mode (or tapping mode) providing the details of the investigated sample. Moreover the AFM can be employed as manipulation tool for the molecules placed onto a substrate if we set the microscope in the contact mode. The AFM imaging generally doesn't require a sample preparation and the measurement can be performed either in air or in a controllable atmosphere without any vacuum stage. MWNTs can be also used as AFM probe tips, now commercially available, allowing to overcome the problems related to the tip dimensions.

Scanning electron microscopy (SEM), differently from TEM, having a lower resolution is used for the visualization of CNTs distribution on substrate or within composite. This latter visualization is very difficult to perform because of the same carbon based nature of polymers and CNTs, so most of the SEM images on composites are performed on fracture surfaces. A very powerful tool for the characterization of CNTs is Raman spectroscopy. for this technique, a more detailed discussion will be presented in the following paragraph.

1.7.1 Raman spectroscopy

Raman spectroscopy is one of the most powerful tools for characterization of carbon nanotubes. Without sample preparation, a fast and non-destructive analysis is possible. All allotropic forms of carbon are active in Raman spectroscopy [53]: fullerenes, carbon nanotubes, amorphous carbon, polycrystalline carbon, etc. The position, width, and relative intensity of bands are modified according to the carbon forms.

Raman technique is the only probe for gaining the structural information from the vibrations of the C-atoms arranged in a carbon nanotube structure, since infrared active modes are completely absent in CNTs. Moreover in order to enhance the information coming from the Raman investigation, the resonant technique is normally used. This technique consists in the choice of that laser line determining an electronic transition in the band gap of a nanotube and is clearly strongly influenced by the nanotube electronic structure. The optical spectra of carbon nanotubes are rich of indications about their structural parameters. The graph in figure 1.15 is well known as Kataura plot and it allows to know what nanotubes are in resonance with the laser line that we are using for their excitation [25].

Raman scattering consists of an inelastic scattering of a high frequency radiation as a consequence of an indirect coupling of the impinging photons with the internal motions (vibrations or rotations) that occur in a molecule or crystal. A Raman scattering can be interpreted as a consequence of a perturbation of the molecular polarizability (the easy of distortion of the electron cloud of the molecule) induced by the electric field of the radiation.

Because of the oscillations of the electron cloud, a subsequent rapid re-irradiation occurs in every direction, determining a scattering of the beam. If the scattered radiation has the same frequency of the incident radiation we have a Rayleigh scattering, i.e. an elastic scattering process.

Because of the internal motions (vibrations and rotations) of the molecule, the frequencies of the scattered radiation can vary of a quantity corresponding to the characteristic frequency of the vibration or rotation, with respect to the frequency of the incident beam. This is the case of an inelastic scattering or Raman scattering. A Raman scattering occurs very rarely compared to the Rayleigh scattering. As a matter of fact, the largest fraction of photons is scattered at the same optical frequencies of the incident photons while only a small fraction is scattered at a different optical frequency.

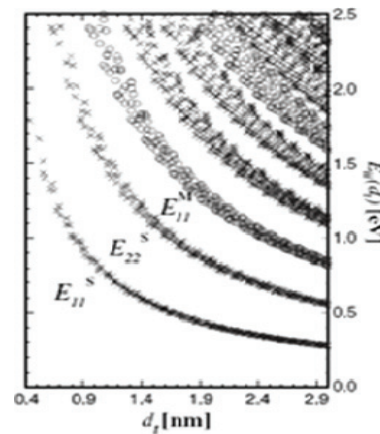


Figure 1. 15 - Kataura-plot showing the electronic transition energies E_{ii} for all the (n,m) SWNTs with diameters ranging between 0.4÷3 nm.

The structural properties of carbon nanotubes can be clearly evidenced by means of the Raman technique in the resonant configuration. Because of their all carbon and wrapped honeycomb structure, the CNTs don't have strong and permanent dipole moments, but essentially Raman active modes.

Moreover, because of their electronic structure, both the semiconducting and metallic nanotubes are characterized by direct band gaps. This occurrence allows a strong coupling of the electron clouds with an impinging radiation, once the van-Hove singularities are matched, and as a consequence of the polarizability of the CNT, this allows a coupling with vibrations in the honeycomb network. The non-resonant Raman investigation is used preferably for MWNTs or for dense assembly of SWNTs. In fact, in this case, the higher electronic density determined by the walls of the tube allows a significant coupling for the scattering process. Conversely, in the case of isolated SWNTs the completely hollow structure very hardly can provide a significant coupling with the wave.

A typical Raman spectrum of a SWNT is composed of many features visible in three distinct ranges of frequencies or bands. Between these structures, the most characteristic are the Radial Breathing Modes (RBM) in the low frequency range between $100 \div 500 \text{ cm}^{-1}$, the disorder-induced D-band in the intermediate range between $1200 \div 1400 \text{ cm}^{-1}$ and the High Energy Modes (HEM), also called G-band (from Graphite), in the high energy range between $1500 \div 1600 \text{ cm}^{-1}$ [54] A typical Raman spectrum of SWNTs bundles excited with 488 nm laser line is reported in figure 1.16 , where the three regions associated to RBM, D-band and G-band have been highlighted using three different colors.

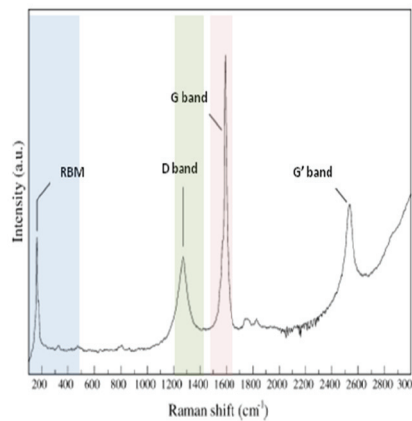


Figure 1. 16 - Raman scattering spectrum of a SWNT

- **Radial breathing mode - RBM**

Each RBM involves a single phonon mode which is a bond-stretching that occurs in such a way that the tube expands and relaxes with radial movements. This movement looks like a tube breathing (fig. 1.17).

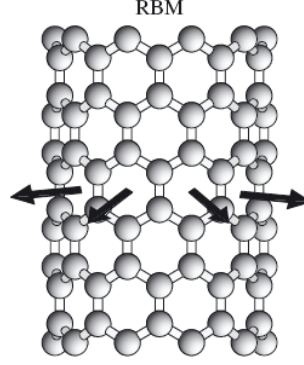


Figure 1. 17 - Atomic vibration of a nanotube in the radial breathing mode

This feature appears only in carbon nanotubes because it corresponds to the collective atomic vibrations of a set of carbon atoms bound together to form a tube. RBM of SWNTs are widely used to determine nanotube diameters because of the simple relation between their frequency and the diameter of the tube. In fact, we expect it is more difficult to deform a tube of small diameter than a tube of larger diameter. The dependence of the radial breathing mode frequency on the tube diameter is given by [55]:

$$\omega_{RBM} = \frac{C_1}{d^k} + C_2(d) \quad 1.5$$

where C_1 is a constant, C_2 depends on the diameter and k is an exponent.

A Raman measurement performed on an isolated SWNT can give complete structural information, i.e, the (n,m) indices obtained by calculating the tube diameter starting from RBM in the spectra [56]. On the other hand, the Raman spectra of SWNTs bundles cannot give the nanotubes diameters. In order to obtain information from the many tubes in a bundle, we should use several laser lines or a tunable laser source to enhance the resonance phenomena. Moreover, the RBM coming from the coaxial tubes of MWNTs are too weak to be observable, mainly because of the strong interaction of the walls.

- **Tangential modes - G band**

The high-energy modes (HEM) of carbon nanotubes are the vibrations associated with the optical mode of a graphene sheet at about 1580 cm^{-1} . In this energy range carbon atoms vibrate tangentially with respect to the nanotube walls.

Nonetheless, a new characteristic appears in the case of the SWNTs. In fact, in this case, the G peak can be resolved in a multi-peak structure with up to six peaks, that is completely different by the case of the graphite single G-peak. The most intense features of the G-band for the SWNTs are the G^- and G^+ peaks. The G^- peak is linked to the displacement of carbon atoms along the circumferential direction. The G^+ arises from the carbon atoms displacement along the tube axis. A schematic of the carbon atoms displacement in the RBM and G-bands is shown in figure 1.18 a. Moreover, the peaks of the G-band have different shapes depending on which CNTs we are considering: MWNT, semiconducting or metallic SWNTs (fig. 1.18 b).

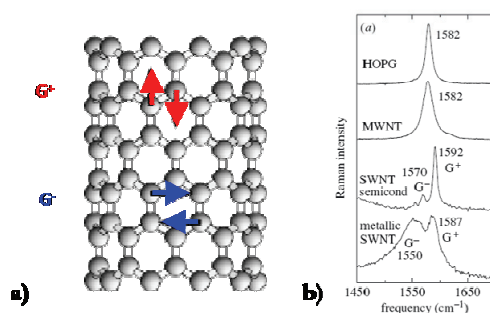


Figure 1. 18 - a) Atomic vibration of a nanotube in the tangential modes; b) typical G-band spectrum of different nanotubes

Because of the diameter distribution, the double peaks structure of the G-band of MWNTs becomes a broad single feature. Both semiconducting and metallic SWNTs show G^+ and G^- features, but the shape and intensity of the G^- peak is quite different in these two cases.

- **Disorder induced mode - D band**

Up to now we have described the vibrational modes that can occur in a perfect structure of carbon atoms arranged in the honeycomb tubular crystal of MWNTs or SWNTs. Nonetheless, the CVD growth process that forms the CNTs could introduce some defect in the structure, producing a structural disorder that gives rise to a new band named the D-band is not related to a Raman active vibration, but depends on the crystalline disorder of the material. In the disordered graphite and carbon fibers, this feature is associated to a symmetry lowering effect. The intensity of the peak around 1350 cm^{-1} , compared with the G-band intensity, provides information about the lowering of the crystal symmetry for a carbon nanotube as well as about the amount of

amorphous carbon. The D-band and in particular the ratio between the intensity of D and G bands is used for a qualitative evaluation of the defects introduced in the CNTs structure by functionalization process, that alters the crystalline structure [57].

1.8 Applications of CNTs

The intriguing properties of carbon nanotubes have led to an explosion of research efforts worldwide [7]. Understanding these properties and exploring their potential applications have been a main driving force in this area. Theoretical and experimental work has been focusing on the relationship between nanotube atomic structures and electronic structures, transport properties, electron-electron and electron-phonon interaction effects. Extensive effort has been made to investigate the mechanical properties of nanotubes, including their Young's modulus, tensile strength, failure processes and mechanisms. It has also been an important fundamental question regarding how mechanical deformation in a nanotube affects its electrical properties. Thus far, nanotubes have been utilized individually or as an ensemble to build functional device prototypes, as has been demonstrated by many research groups. Ensembles of nanotubes have been used for field emission based flat-panel displays, composite materials with improved mechanical properties and electromechanical actuators.

Bulk quantities of nanotubes have also been suggested as high-capacity hydrogen storage media. Individual nanotubes have been used for field emission sources, tips for scanning probe microscopy, nanotweezers and chemical sensors. Nanotubes are also promising as the central elements for future miniaturized electronic devices. The full potential of nanotubes for applications will not be realized until the growth of nanotubes can be further optimized and controlled. Real-world applications of nanotubes require either large quantities of bulk materials or device integration in a scale-up fashion. For applications such as composites and hydrogen storage, it is desired to obtain high quality nanotubes at the kilogram or ton level using growth methods that are simple, efficient and inexpensive [58]. Significant work has been carried out to tackle these issues. Nevertheless, many challenges remain in the nanotube growth area.

1.9 References

1. Kroto H.W., Heath J.R., O'Brien S.C., Curl R.F., Smalley R.E. - Nature 1985; 318:162-163
2. Iijima S. - Nature 1991; 354:56-58
3. Iijima S., Ichihashi T. - Nature 1993, 363:603-605

4. Bethune D.S., Kiang C.H., de Vries M.S., Gorman G., Savoy R., Vazquez J., Beyers R. - *Nature* 1993; 363:605-607
5. Dresselhaus M.S., Dresselhaus G., Eklund P.C. *Science of Fullerenes and Carbon Nanotubes*, Academic Press, New York, 1996.
6. Saito R., Dresselhaus G., Dresselhaus M.S., *Physical Properties of Carbon Nanotubes*, Imperial College Press, London, 1998.
7. Dresselhaus M.S., Dresselhaus G., Ph. Avouris (Eds.), *Carbon nanotubes: Synthesis, Structure, Properties, and Applications*, Springer-Verlag, Berlin, 2001.
8. Anantram M.P., Léonard F. - *Reports on Progress in Physics* 2006; 69:507-561
9. Iijima S., Ichihashi T., Ando Y. - *Nature London* 356 (1992) 776-778
10. Thess A., Lee R., Nikolaev P., Dai H., Petit P., Robert J., Xu C., Lee Y.H., Kim S.G., Rinzler A.G., Colbert D.T., Scuseria G.E., Tomanek D., Fischer J.E., Smalley R.E., - *Science* 1996; 273:483-487
11. Baker R.T.K. - *Carbon* 1989; 27:315-323
12. Amelinckx S., Zhang X.B., Bernaerts D., Zhang Z.F., Ivanov V., Nagy J.B. - *Science* 1994; 265:635-639
13. Li W.Z., Xie S.S., Qian L.X., Chang B.H., Zou B.S., Zhou W.Y., Zhao R.A., Wang G. - *Science* 1996; 274:1701-1703
14. Kong J., Soh H.T., Cassell A.M., Quate C.F., Dai H. - *Nature* 1998; 395:878
15. Ren Z.F., Huang Z.P., Xu J.W., Wang D.Z., Wen J.G., Wang J.H. - *Applied Physics Letters* 1999; 75:1086-1088.
16. Ren Z.F., Huang Z.P., Xu J.W., Wang J.H., Bush P., Siegal M.P. - *Science* 1998; 282:1105-1107.
17. Huang Z.P., Xu J.W., Ren Z.F., Wang J.H., Siegal M.P., Provencio P.N. - *Applied Physics Letters* 1998; 73:3845-3847.
18. Iijima S., Ajayan P.M., Ichihashi T. - *Physical Review Letters* 1992; 69:3100-3103
19. Guo T., Nikolaev B., Rinzler A.G., Tomanek D., Colbert D.T., Smalley R.E. - *Journal of Physical Chemistry* 1995; 99:10694-10697
20. Kwon Y.K., Lee Y.H., Kim S.G., Jund P., Tomanek D., Smalley R.E. - *Physical Review Letters* 1997; 79: 2065-2068
21. Journet C., Maser W.K., Bernier P., Loiseau A., Lamy de la Chapelle M., Lefrant S., Deniard P., Lee R., Fischer J.E. - *Nature* 1997; 388:756-758
22. Mintmire J.W., Dunlap B.I., White C.T. - *Physical Review Letters* 1992; 68:631-634
23. Hamada N., Sawada S., Oshiyama A. - *Physical Review Letters* 1992; 68:1579-1581
24. Saito R., Fujita M., Dresselhaus G., Dresselhaus M.S. - *Physical Review B* 1992; 45: 6234-6242
25. Kataura H., Kumazawa Y., Maniwa Y., Umez U., Suzuki S., Ohtsuka Y., Achiba Y. - *Synthetic Metals* 1999; 103:2555-2558
26. Liu X., Pichler T., Knupfer M., Golden M.S., Fink J., Kataura H., Achiba Y. - *Physical Review B* 2002; 66:45411
27. Robertson D.H., Brenner D.W., Mintmire J.W. - *Physical Review B* 1992; 45:12592-12595

28. Treacy M.M.J., Ebbesen T.W., Gilson J.M. - Nature 1996; 381:678-680
29. Krishnan A., Dujardin E., Ebbesen T.W., Yianilos P.N., Treacy M.M.J. - Physical Review B 1998; 58:14013-14019
30. Wong E.W., Sheehan P.E., Lieber C.M. - Science 1997; 277:1971-1975
31. Yu M.F., Lourie O., Dyer M.J., Moloni K., Kelly T.F., Ruoff R.S. - Science 2000; 287:637-640
32. Sanchez-Portal D., Artacho E., Soler J.M., Rubio A., Ordejon P. - Physical Review B 1999; 59:12678-12688
33. Popov V.N., Van Doren V.E., Balkanski M. - Physical Review B 2000; 61:3078-3084
34. Lu J.P. - Physical Review Letters 1997; 79:1297-1300
35. Yakobson B.I., Brabec C.J., Bernholc J., Physical Review Letters 1996; 76:2511-2514
36. Cornwall C.F., Wille L.T. - Solid State Communications 1997; 101:555
37. Hernandez E., Goze C., Bernier P., Rubio A. - Physical Review Letters 1998; 80:4502-4505
38. Salvétat J.P., Briggs G.A.D., Bonard J.M., Bacsá R.R., Kulik A.J., Stockli T. - Physical Review Letters 1999; 82:944-947
39. Yu M.F., Lourie O., Dyer M., Moloni K., Kelly T. - Science 2000; 287:637-640.
40. Yu M.F., Files B.S., Arepalli S., Ruoff R.S. - Physical Review Letters 2000; 84:5552-5555.
41. Yi W., Lu L., Zhang D.L., Pan Z.W., Xie S.S. - Physical Review B 1999; 59:R9015-R9018
42. Hone J., Whitney M., Piskoti C., Zettl A. - Physical Review B 1999; 59:R2514-R2516
43. Kim P., Shi L., Majumdar A., McEuen P.L. - Physical Review Letters 2001; 87:215502-215505
44. Lauret J.S., Voisin C., Cassaboís G., Roussignol P., Delalande C., Filoramo A., Capes L., Valentin E., Jost O. - Physica E 2004; 21:1057-1060
45. Droppa R., Hammer P., Carvalho A., Dos Santos M., Alvarez F. - Journal of Non-Crystalline Solids 2002; 299-302:874879
46. Sattler K. - Carbon 1995; 33:915-920
47. Burian A., Kolocz J., Dore J., Hannon A.C., Nagy J.B., Fonseca A. - Diamond and Related Materials 13 (2004) 1261-1265
48. Lambin P., Loiseau A., Culot C., Biro L. - Carbon 2002; 40:1635-1648
49. Zhu W., Miser D., Chan W., Hajaligol M. - Materials Chemistry and Physics 2003; 82:638-647
50. Cao A., Xu C., Liang J., Wu D., Wei B. - Chemical Physics Letters 2001; 344:13-17
51. Saito R., Matsushige K., Tanaka K. - Physica B: Condensed Matter 2002; 323:280-283
52. Sun Z., Barron A.R. <http://cnx.org/content/m22963/1.2/>
53. Arepalli S., Nikolaev P., Gorelik O., Hadjiev V., Holmes W., Files B., Yowell L. - Carbon 2004; 42:1783-1791
54. Maultzsch J., Reich S., Thomsen C. - Physical Review B 2002; 65:233402-233405
55. Jishi R. A., Venkataraman L., Dresselhaus G., Dresselhaus M.S. - Chemical Physics Letters 1993; 209:77-82
56. Jorio A., Saito R., Hafner J. H., Lieber C. M., Hunter M., McClure T., Dresselhaus G., Dresselhaus M.S., Physical Review Letters 2001; 86:1118-1121

57. Wang S., Liang Z., Liu T., Wang B., Zhang C. - Nanotechnology 2006; 17:1551-1557
58. Dai H. - Surface Science 2002; 500:218-241

Chapter 2

Carbon nanotubes polymer composites

2.1 Introduction

Carbon nanotubes based materials have inspired scientists for a range of potential applications [1]. Because of their unique atomic structure, very high aspect ratio and extraordinary mechanical properties (strength and flexibility) they are ideal candidates for reinforcing fibers in nanocomposites. CNT-based nanocomposites form a new class of lightweight super strong functional materials for air and space applications [2, 3], energy storage [4], molecular sensors [5] and biomedical applications [6, 7]. The structure and properties described in chapter 1 relate to the individual tube. Yet, these are hard to find: carbon nanotubes emerge from the synthesis as bundles or ropes that contain hundreds of well-aligned SWNT arranged in a close packed triangular lattice, the so called “ropes” or “bundles”.

The over-micron long ropes further entangle into networks, due to van der Waals (vdW) attraction rendering the carbon-powder insoluble in aqueous and organic liquids and thus unprocessable. Many efforts have been made to incorporate CNTs into polymers in order to take advantage of the exceptional properties of individual nanotubes. Unfortunately, colloidal materials based on nanotubes solutions are very difficult to produce because the tubes do not spontaneously suspend in polymers. Dispersion of nanotubes in polymer matrices has proven to be extremely difficult and the resulting composites do not show particularly enhanced properties [8]. Several methods have been reported to solve the dispersion problem through functionalization of carbon nanotubes as well as use of strong acids, certain solvents and surfactants.

When approaching to the fabrication of nanotubes composites and to the study of their physical properties, it is important to have in mind the concept that the properties of polymer nanocomposites containing carbon nanotubes depend on several factors in addition to the polymer: synthetic process used to produce nanotubes; nanotube purification process (if any); amount and type of impurities in the nanotubes; diameter, length, and aspect ratio of the nanotube objects in the composite (isolated, ropes, and/or bundles); nanotube orientation in the polymer matrix. These variations in nanotubes and nanotube/polymer composites account for many of the apparent inconsistencies in the literature. Reporting the nanotube concentration (specifying whether the concentration allots for the impurities or functionalization) and the matrix polymer alone is insufficient.

Fabrication methods have overwhelmingly focused on improving nanotube dispersion because better nanotube dispersion in the polymer matrices has been found to improve properties. Similar to the case of nanotube/solvent suspensions, pristine nanotubes have not yet been shown to be soluble in polymers illustrating the extreme difficulty of overcoming the inherent thermodynamic drive of nanotubes to bundle. The quality of nanotube dispersion in polymer matrices should be evaluated over a range of length scales and can be accomplished using a selection of these imaging methods: optical microscopy, polarized Raman imaging, scanning electron microscopy (SEM), and transmission electron microscopy (TEM). More recently, confocal microscopy has been successfully applied to evaluate the nanotube dispersion in MWNT/polystyrene nanocomposites [9].

Scattering methods remain difficult to interpret regarding dispersion in polymers because the contrast is low and the presence of rigid-rod behavior is not equivalent to good dispersion at all length scales. At a local length scale, UV-vis-near-IR spectroscopy qualitatively determines the nanotube dispersion state in CNTs solutions and nanocomposites because only individual or small bundles of SWNT exhibit sharp absorbance peaks (van Hove singularities), while large bundles exhibit only monotonically decreasing absorbance with increasing wavelength [10].

The methods of solution blending, melt blending, and in situ polymerization are widely applied to produce nanotube/polymer composites, together with latex technology, solid-state shear pulverization, and coagulation spinning methods.

In light of this assumption, the aim of this chapter is to propose a literature review on the fabrication processes of polymer carbon nanotubes composites, starting from thermodynamics of nanotubes suspensions and then illustrating the dispersion techniques of CNTs in different solvents and polymers as well as the corresponding physical properties and the methods that are used to characterize them.

2.2 Carbon nanotubes suspensions

2.2.1 Thermodynamics of CNTs suspensions

Several factors make the dispersion of nanophase carbon particularly troublesome. These factors are dominated by strong attraction between carbon species of both enthalpic and entropic origin. In addition, the low dimensionality of carbon nanotubes leads to an enhancement of these attractive forces. The origin of the attractive forces between graphitic structures is well known. Due to the extended π -electron system, these systems are highly polarizable, and thus subject to large attractive vdW forces. These forces are responsible for the secondary bonding that holds graphitic layers

together. In the case of carbon nanotubes, these forces lead to so called “ropes”, extended structures formed by side-by-side aggregation of the nanotubes.

When suspended in a polymer, an attractive force between filler particles also arises due to different factors of chemical and entropic natures. [11]

Being inherently large molecules composed of necklaces of functional groups, polymers may interact with CNTs via strong covalent or electrostatic interactions, π -stacking, or hydrogen bonding. These chemical CNT-polymers interactions result in strong coupling between the components, modify the tube surface chemistry and consequentially the intrinsic inter-tube interactions as well as tube-solvent interactions. The range and strength of the resulting interactions depend on the chemical details of the exposed surface, and cannot be easily tuned or generalized [12]

Alternatively, polymers and CNTs may interact via generic weak vdW interactions. Decoration of CNT by adsorbed or end-attached polymer triggers entropic interactions among the polymeric layers. Polymer chains in the corona region of the colloidal filler suffer an entropic penalty since roughly half of their configurations are precluded. Therefore there is a depletion of polymer in the corona, resulting in an osmotic pressure forcing the filler particles together. In these cases the range and strength of the interaction can be controlled by the molecular weight and density of the polymeric layers, rather than by the chemical composition of the monomers.

Indeed, evidence is emerging that cooperative effect of weak interactions between long-flexible chains and CNTs can be utilized for engineering the phase behavior of CNTs by modifying the shape, range, and depth of the intermolecular potential, while not affecting the intrinsic properties of the individual tube.

- **Strong coupling systems: wrapping polymers**

An instance of strong coupling interactions between polymer and nanotubes are the conducting polymers-CNT systems. Typical examples of conducting polymers are polyacetylene, polyaniline and polyphenylenevinylene (PPV). They are quasi-infinite conjugated π -system, extending over a large number of recurring monomer units, resulting in a band-like electronic structure. The conduction mechanism is based on the motion of charged defects within the conjugated framework, and strongly depends on the level of doping [13, 14]. It was found that the electronic structure of PmPV [15] as well as other types of conducting polymers is modified by the presence of CNTs [16, 17] indicating strong coupling between the MWNT and the polymer π -systems, that alters the final composite electrical properties. Hence, it is now well accepted that conjugated polymers and CNT are strongly tightly bound systems and the molecular geometry of this association is that of a helical wrapping of the tubes by the polymers [18]. This type of morphology has been found to occur also in other kinds of coiling polymer, for example biopolymers such as DNA and peptides. It was found that the specific interaction between CNTs and a particular type of DNA and a specific peptide configuration allows the visualization respectively of DNA [19] and the peptides [20].

- **Weak non specific interactions: entropic effects**

A very different scenario is expected, and observed, in the absence of specific chemical interactions: the free energy of interaction between CNT decorated by adsorbed (or grafted) polymeric layers is then dominated by the polymers confined in the region between the two highly curved (cylindrical) surfaces. In these systems, polymer structure, surface forces, geometry and topology as well as dimensionality of the different components shape the range and depth of the intermolecular effective potential, and consequentially the phase behavior of the combined systems. As expected, entropic effects arising from the conformational degrees of freedom of the polymer molecules play the major role.

A direct consequence (with non-trivial implications) of the nanometric diameter and microscopic length of CNTs is their relatively large surface area as compared to classical colloids. Thus, when CNTs are embedded within a polymeric medium, the systems become enriched by interfacial zones that are subjected to non-bulk potentials and forces. Complete description of polymer-surface interactions is a multidimensional task in which the polymer and surface structure, molecular weight, polymer concentration and type of solvent combine to determine the end result. Essentially, the presence of a surface reduces the conformational degrees of freedom of

polymers due to excluded volume interactions [21]. This reduction in the number of allowed conformations, and thus in chains entropy, has two interrelated major consequences. First, the shape of polymers residing in close vicinity to the surface is altered with respect to that of polymers in the bulk. Second, the loss of entropy translates into a repulsive interaction between the polymers and the surface. Thus, in the absence of additional attractive interactions, polymers are depleted from surfaces. In colloidal dispersions this results in an effective attractive force between the colloidal particles, known as ‘depletion force’ [22-25]. The range of this force is of the order of the radius of gyration of the polymers. It is then possible to tune the range and strength of the effective attractions by modifying the polymer characteristic size and tailor the phase diagram of the combined systems. A different scenario arises in the presence of an attractive

(enthalpic) interaction between the polymers and the surface. Attraction competes with the entropically driven repulsion, and leads to adsorption of polymeric chains. When the attractive component is localized (for example, at chain ends) the polymer molecules attach in a specific way to the surface and able to form a dense layer known as a ‘polymer brush’ [12]. This additional restriction on the polymeric molecules results in a more severe entropic penalty leading to an even more dramatic change in the range and strength of the interactions.

The high surface-to-volume ratio in CNT-filled polymers is manifested in a variety of surface-related effects: an increased degree of crystallinity was observed in semicrystalline matrices, as well as a modification of the glass transition temperature and an improvement of the mechanical properties with a clear dependence on the volume fraction of CNTs.

- **Effects of geometry: the high aspect ratio**

As mentioned above, a strong influence on the interactions between polymer and CNTs is their very high aspect ratio, that is about 1000 in SWNTs. This geometric characteristic results is very useful in CNTs polymer based systems, because it allows the formation of tubes network at very low CNTs concentrations. The transition between a non connected system to a networked CNTs path is known as percolation and the concentration at which this phenomenon occurs is the percolation threshold. Electrical properties are strongly affected by the presence of a percolative path, with increases of several orders of magnitude of the electrical conductivity in correspondence of the percolation threshold.

Some years ago, when few works on CNTs composites were present in literature, there were evidences of the fact that though the reported percolation values were about two orders of magnitude lower than the value for carbon black (a colloidal filler), these values were many times

higher than the theoretical predictions for randomly oriented objects of similar aspect ratio [26]. This was attributed to experimental flaws or to low quality of polymer coated CNTs contacts. Then, it was demonstrated that intermolecular interactions could lead to CNTs alignment with a consequent reduction of the electrical properties and increasing of the percolation threshold. Now, it is well accepted that a completely different phenomenon occurs in the CNTs polymer composites that consists in the formation of a percolative path at percolation thresholds well below the statistical percolation value. This phenomenon is related to the concept of “dynamic percolation”, that will be discussed later in this chapter.

Because of their dimensions, nanotubes differ from colloids by an inherent property: the inter-particle potential. Classical colloids are mesoscopic objects and dominated, in general, by long-ranged dispersive forces, while fullerenes [27] and SWNT are large molecules and interact via a short-ranged intermolecular potentials [28]. The difference originates from the fact that SWNTs and fullerenes are hollow structures with two (SWNT) or three (fullerenes) nanometric dimensions.

The intermolecular interaction potential between two individual SWNT in vacuum were derived using the Girifalco et al. model [29]. As presented in fig.2.1, a large attractive interaction at short inter-tube distance (less than 2 nm) is observed and it decreases within 2.5 nm. The potential for two tubes 1 μm long in contact predicts a contact energy of 40,000 times the thermal energy. Hence, there will be a very large tendency of the tubes to be found in the form of bundles, as experimentally observed. Indeed all the strategies developed for de-bundling CNT aim to modify the inter-tube potential.

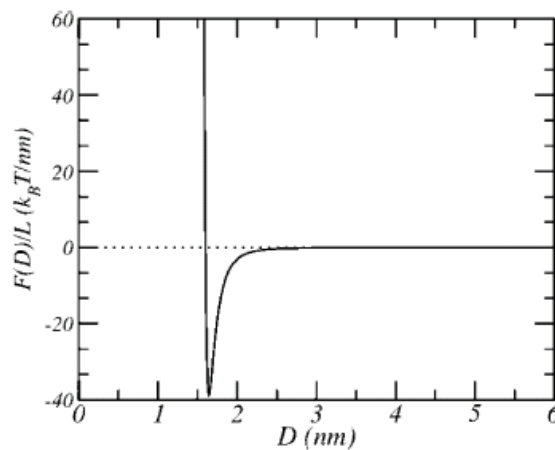


Figure 2. 1 - The specific interaction potential between two parallel SWNT as a function of the distance between them, [28]

The reduction of the attractive minimum via chemical modification of the extended π -systems (the origin of the strong vdW attraction), or the introduction of electrostatic repulsion, should enable exfoliation and dispersion of CNT. However, as described above, this approach leads to inherent diminishment of the unique properties of the individual tube. A different approach would be to take advantage of the short range of the potential: the behavior of objects interacting via a short ranged attraction is known to be highly sensitive to variations in the long-range tail of the inter-particle potential.

- **Long-ranged inter-particle potential**

In light of the concepts explained in the previous part, a way of modifying the short ranged attractions is varying the long-range inter-particle potential, hence a relatively weak, but long ranged repulsion, such as the osmotic (steric) repulsion among tails of tethered copolymers, in good solvent conditions, may lead to significant modification of the CNT's phase behavior. Weak, long-ranged interactions are not expected to interfere with the electronic structure of the tubes or modify the physical properties of the individual tube. As the approach does not rely on specific interactions, it is efficient for both aqueous and organic media [29]. Among the more efficient steric stabilizers are block-copolymers and end functionalized polymers. A model system which provides an upper bound for the repulsive interaction induced by attached polymers is a dense stretched 'polymer brush'. The strongest effect is expected when end-attached polymers assemble at a surface, in a good solvent environment and high surface coverage. The tethered chains stretch out in order to avoid intermolecular repulsions. In the so called "brush regime" the thickness of the tethered polymer layer, h , scales with the polymer chain length, N . The linear increase of the thickness with molecular weight serves as an important tool in the manipulation of the range of the interactions. Surface coverage highly affects both the range and the strength of the potential [30, 31]. The higher the surface coverage, the larger the distance at which the repulsive interaction diverges. This is due to overcrowding of polymer segments that occur as the distance between the surfaces decreases. Furthermore, we can see that longer chains increase the range of the interactions and the absolute strength of the repulsion for identical density of tethered chains (fig. 2.2).

Figure 2.2 shows the steric repulsion between two polymer- decorated CNTs for two different polymer molecular weights, as calculated using the molecular theory. In all cases, as the distance between the parallel tubes decreases, the repulsion increases. The variation of the potential is rather different from that of polymers grafted to planar surfaces. In fact, polymers end-attached to CNT exhibit repulsions at a range shorter than that of polymers attached to planar surfaces. At

an inter-tube distance of 3 nm of separation tubes attractions are already below the thermal energy. In light of the presented concepts, now the question is if the repulsion triggered by end-adsorbed polymers are strong enough to prevent the tubes to reach the attractive inter-tube region and the subsequent reaggregation. The repulsive barrier magnitude depends on the polymer surface coverage and chain length. Figure 2.3 shows the combined profiles of repulsive and attractive potentials, that is the total interaction potential. From this graph one can note that a local minimum positioned at the same location as that of the bare CNT shown in figure 2.1, is observed in all the cases.

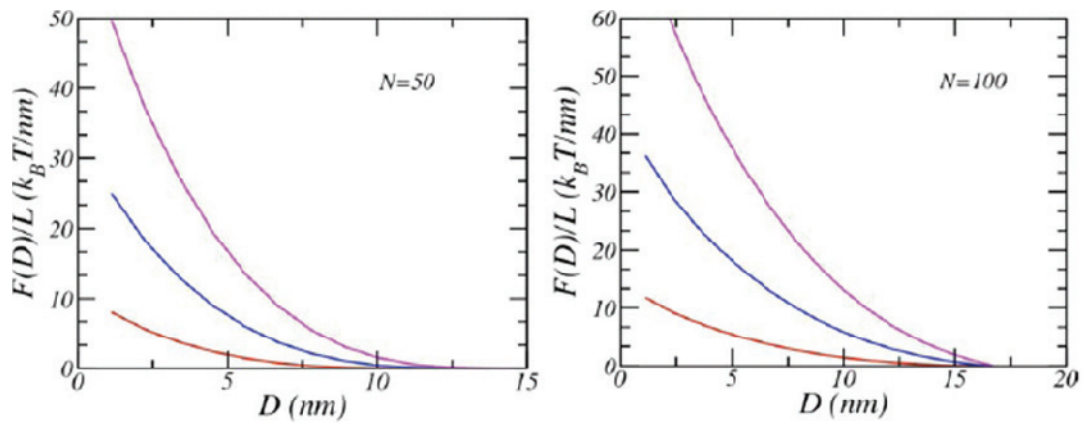


Figure 2. 2 - Repulsive interactions between grafted polymers on parallel CNTs as a function of the distance between the grafting surfaces, as calculated from a molecular theory [12]

The shape of the potentials shown in figure 2.3 and the fact that even relatively short polymer chains suffice to create a high enough barrier and prevent tube aggregation, is a result of the (short) range of the CNTs attraction. As described above, the latter is a direct consequence of the nanoscopic dimensions of CNT and the relative low density of interacting atoms due to the hollow nature of the tubes.

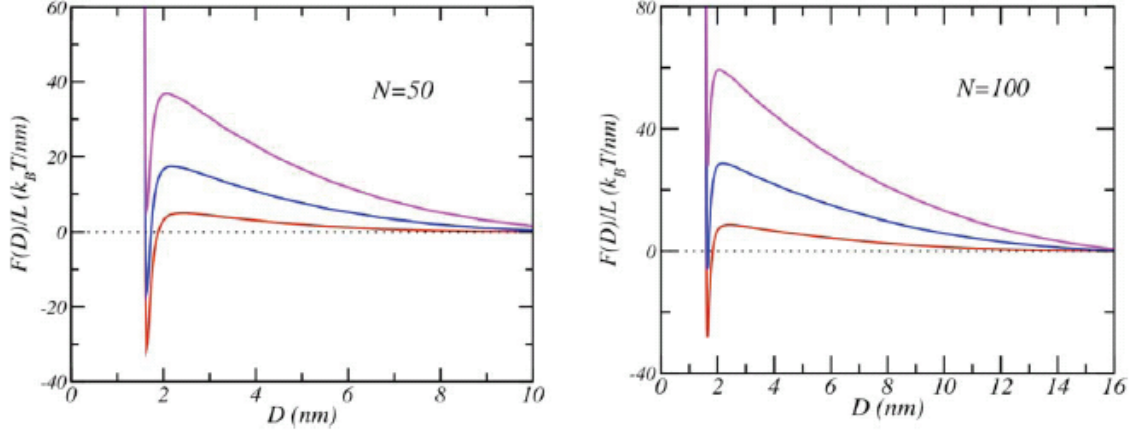


Figure 2. 3 - The total interaction potential between parallel CNTs. The potentials are obtained by adding the vdW attractive contribution (fig. 2.1) and the steric repulsions (fig. 2.2) arising from the tethered polymers.

The results presented above, apply to stabilization of exfoliated CNTs. However, a different behavior has to be expected for polymer chains tethered at the surface of CNTs bundles. It was found that the attractive between bundles is much deeper than for single tubes and it suggests that the polymer-induced repulsion in the case of small bundles is not as effective as in the case of single tubes. Moreover, only long chain of polymers resulted in a repulsive barrier, so it can be concluded that the formation of stable dispersions of CNTs bundles would require relatively long polymers at high grafting densities, while short polymer can be used for the preparation of individual suspended CNTs or small bundles dispersions (fig. 2.4 a and b).

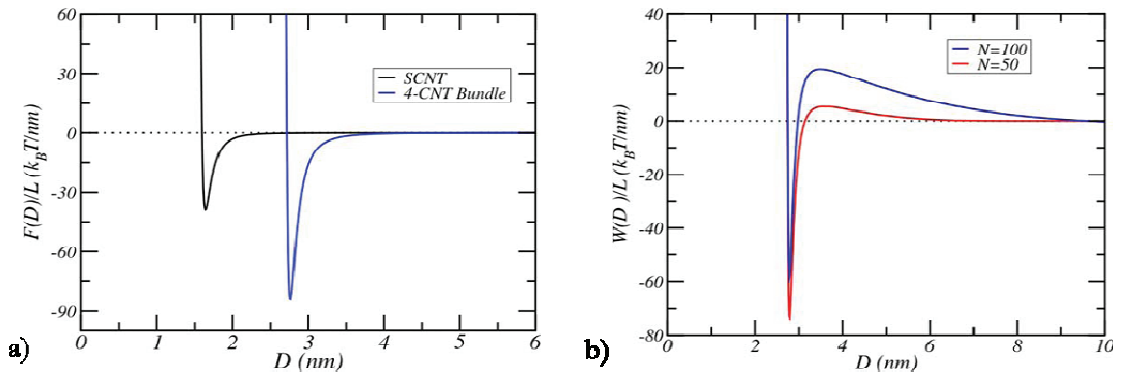


Figure 2. 4 - a) The vdW interaction between two 4-tubes bundles; b) total interaction between two bundles composed by 4 CNTs each coated by different polymers

To summarize the theoretical studies reported above, CNTs exhibit strong, short ranged, attractive vdW interaction. The range of the interaction is determined by the nanometric length scale characteristic of two of the three dimensions of the tubes. Polymers attached at the surface of CNTs introduce a repulsive (steric) barrier whose range and strength can be controlled by the

polymer chain length and surface density. Increasing the polymer molecular weight results in a longer range repulsive interaction. Moreover, increasing the density of grafted and adsorbed polymers increases the strength of the repulsive interactions. Moreover, it is important to emphasize that due to the geometry of the tubes the strength and range of the steric repulsion induced by the tethered polymer layers is qualitatively different than the steric repulsion between polymer chains grafted to planar surfaces.

Generally, the range of the attractive vdW interactions between particles is determined by the dimensions of the particle and the interaction range is a few times the particle size. Thus, in the case of CNTs the range of the attractive interactions is a couple of nanometers and adsorption of relatively short polymers, in good solvent conditions, suffices to present a steric barrier at a distance larger than the attractive inter-tube minimum, preventing tube aggregation. Furthermore, it was shown that the dispersion and prevention of bundles aggregation would require the tethering of much longer polymer chains at a higher density than the case of isolated tubes.

2.2.2 Production of CNTs suspensions

A true solvent for pristine nanotubes is yet to be found. As previously discussed the high aspect ratio of the nanotubes coupled with a strong intrinsic vdW attraction between each other provide the formation of ropes and bundles of several CNTs. Ropes refer to nanotubes collections having a degree of order and a quite uniform diameter, while bundles are disordered aggregates of tubes.

A typical scenario may utilize mild sonication (which does not damage the tubes [33]) for a primary exfoliation of the CNTs bundles, followed by adsorption or tethering of polymers. After the simple addition of carbon nanotubes in the solvent, they deposit on the bottom of the flask and only after a proper sonication process they can exfoliate in smaller bundles and single tubes.

A scheme summarizing this approach is presented in figure 2.5. The exfoliation can occur in different solvent and using either a dispersing agent or a compatible polymer or solvent.

Hence, with the aid of ultrasonication, nanotubes can be moderately dispersed in some solvents, to produce nanotube suspensions. Understanding nanotube suspensions is vital for controlling various solvent-based processes (phase separation, chemical derivatization, etc.) associated with preparing nanotube/polymer composites because the initial nanotube dispersion can impact the nanotube dispersion in the polymer matrix. Together with organic solvents, for biological applications water based CNTs solutions are studied.

Generally, for CNTs aqueous solutions amphiphilic molecules, such as ionic or nonionic surfactants, are used as dispersing agent and sonication as dispersion technique. A higher degree of debundling can be reached using a sonicator with dipping horn respect to the ultrasound bath. Good dispersing ability and long term stability in water were found for anionic surfactants and in particular for sodiumdodecyl sulphate (SDS) solutions [34-36]. Even if a quite consolidate knowledge of the dispersion properties of various surfactants is available in literature, it is yet well known as well that the procedure used to disperse nanotubes has a significant impact on the SWNT concentration, stability, and fraction of individual tubes in the final suspension. It is also accepted that it is not easy to replicate the same procedure used in dispersing nanotubes among different laboratories because of the many factors involved in this process that many times are not reported. In addition to the more commonly reported operating conditions, such as surfactant and nanotube concentration, sonication and centrifugation times, other parameters such as the total amount of liquid, the shape and size of the vial, the depth of the probe under the solution during sonication, the procedure used to avoid overheating the sample during sonication, and the different G-forces used during centrifugation can be critical in determining the degree of dispersion [37]. A detailed discussion on the surfactant assisted exfoliation is presented in chapter 3, together

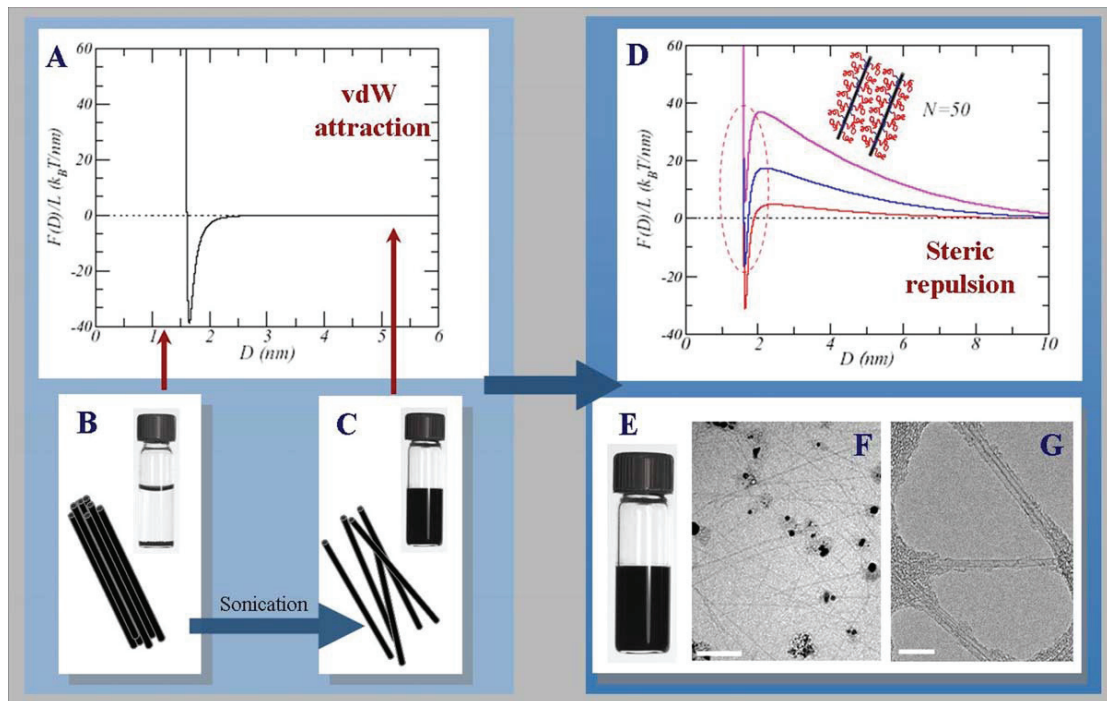


Figure 2. 5 - A schematic representation of the exfoliation concept (A-C) and of the subsequent polymer attaching and solution stabilization (D-G) [12]

with experimental results on surfactant assisted exfoliation of carbon nanotubes in water.

When handling with CNTs suspensions, an important issue to consider is the size distribution of the nanotube objects. This is critical because, for example, isolated tubes facilitate extensive chemical derivatization in suspension and provide the highest interfacial area for stress transfer to the polymer matrices. Given the variability in sizes (both diameter and length), size characterization is best accomplished with an imaging method, specifically atomic force microscopy (AFM). If one assumes that the objects on the substrate are representative of the suspension, then a thorough analysis of diameter (inferred from height), length, and aspect ratio is possible. Together with imaging method of characterization, other techniques are able to evaluate the degree of exfoliation in solution. One of the most useful tool for the evaluation of CNTs debundling in solvent is UV-vis absorbance analysis. Because nanotubes absorb in the UV wavelength range, the monitoring the absorbance of CNTs in suspensions at specific wavelengths can give an idea of the maximum degree of the occurrence of the bundles size and of the exfoliation process. However, this technique is qualitative, because it is not able to give an estimation of the real size of the CNTs structures present in solution. This question is readily addressed with scattering methods [38-42]

A limited number of researchers have used small-angle X-ray, neutron, or light scattering with wave vectors q in the range 10^{-3} - 100 nm^{-1} (corresponding to length scales 1-1000 nm) to investigate nanotubes structures in suspension. A suspension of isolated rigid rods with diameter D and length L exhibits scattering intensity that varies as q^{-1} for wave vectors $2\pi/L < q < 2\pi/D$. With typical nanotube aspect ratios higher than 100 and SWNTs diameters on the order of about 1 nm, the criteria of isolated rigid rods with good dispersion specifies very low nanotube concentration and correspondingly low scattering intensities from nanotube suspensions, wherein lies the challenge. Using small angle neutron scattering (SANS) and a dilute suspension of SWNTs (0.01-0.1 wt %) in water with the surfactant sodium dodecylbenzenesulfonate (NaDDBS), Zhou et al. [43] found an isolated rigid-rod behavior in these suspensions. In contrast, when the above suspensions were prepared with Triton X-100, a surfactant with less efficient nanotube dispersing ability, some sort of network of ropes was found.

An other important issue to be considered is the evaluation of the long term stability of the produced solutions. The stability of nanotube suspensions influences how they can be handled during processing and in applications. The experimental methods described above to probe size and rigidity can be used to follow nanotube suspensions as a function of time. Overall nanotube dispersions remain an active research area focusing on assessing the size distribution of suspended nanotube objects as well as their rigidity and stability and they are subjects also treated in this work.

2.3 Carbon nanotubes polymer composites fabrication

Much effort has been invested in developing approaches for reproducible dispersions of individual carbon nanotubes. As stated earlier, in order to develop high property CNT-based materials, fully utilizing unique properties of the tubes, the thermodynamic drive toward aggregation must be overcome. Therefore, a dispersion method, as an integral step of the production chain, has to be selected in accordance with the processing conditions of the CNT-based material.

There are two distinct approaches for dispersing carbon nanotubes: methods that are designed to alter the surface energy of the solids, either chemically (covalent treatment) or physically (non-covalent treatment) and mechanical methods.

2.3.1 Nanotubes functionalization

Local strain in carbon nanotubes, which arises from pyramidalization and misalignment of the π -orbitals of the sp^2 -hybridized carbon atoms, makes nanotubes more reactive than a flat graphene sheet, thereby paving the way to covalently attach chemical species to nanotubes [44]. Chemical methods use surface functionalization of CNTs to improve their chemical compatibility with the target medium (solvent or polymer solution and melt) and consequently to enhance wetting or adhesion characteristics and reduce their tendency to agglomerate. Hence, covalent functionalization can provide a means for engineering the nanotube/polymer interface for optimal composite properties. With respect to mechanical properties, for example, the interfacial adhesion could be modified through covalent or noncovalent interactions between the functional group on the nanotube and the polymer matrix to maximize load transfer. The open-end functionalization method is widely reported and uses an oxidative route (usually by refluxing in nitric acid) to form shortened nanotubes bearing carboxylic acid end groups that are subsequently converted into other functional groups via standard condensation reactions. In addition to cleaning of raw nanotube material by facilitating removal of amorphous and graphitic carbon (presumably made possible by differences in rate and extent of oxidation), these procedures cut (or ‘etch’) the SWNTs, as demonstrated by the length distributions determined by means of AFM. These cutting procedures leave the SWNTs open ended, the ends being decorated with a somewhat indeterminate number of oxygenated functionalities (fig. 2.6) [45]. It is understood that these oxidations also result in the introduction of moieties at defect sites along the sidewalls, and that functionalities other than carboxylic acids are formed (such as esters, quinones, and

anhydrides). Additionally, although only one per end is shown, there are expected to be multiple functionalities at each end.

The distribution of these functionalities has not been well characterized, they are presumed to exist primarily at the ends of nanotubes and at sites along the sidewalls in correspondence of structural defects, hence where increased curvature strain results in increased reactivity [46]. The concept of higher reactivity at defect sites, or sites of increased curvature and partial loss of conjugation (especially end caps and kinks) has been touched upon by a number of authors, as it has the increased reactivity of smaller diameter SWNTs.

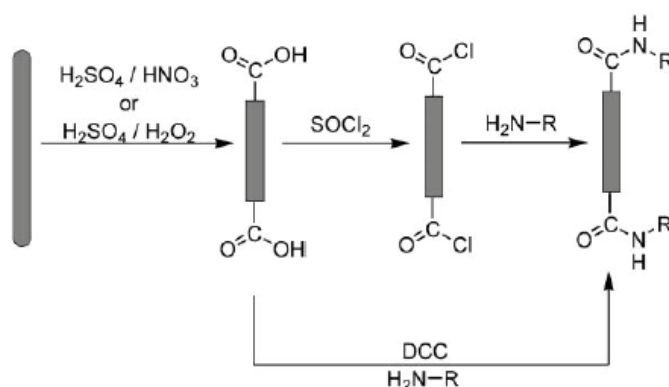


Figure 2. 6 - Schematic depiction of oxidative etching of SWNTs followed by treatment with thionyl chloride, and subsequent amidation.

Exploitation of the functionalities introduced by these oxidative procedures through further chemical elaboration has taken many forms. Most obviously, the presence of carboxylic acid functionalities gives access to the vast field of peptide chemistry, and many reports have demonstrated elaboration via amide linkages.

In these functionalized materials, the SWNTs ropes were reported to be largely exfoliated into individual tubes, in addition to having significantly increased solubility in organic solvents. This exfoliation of ropes is particularly important, as it facilitates manipulation and investigation of the spectroscopic properties of individual SWNTs.

In light of the above mentioned results, it is evident that these aggressive chemical functionalizations might introduce structural defects resulting in inferior properties for the tubes. A notable drawback of covalent functionalization is, in fact, the disruption of the extended π -conjugation in nanotubes. While the impact of disrupted π -conjugation is limited for mechanical and probably thermal properties, the impact on electrical properties is expected to be profound because each covalent functionalization site scatters electrons.

Although the electronic properties of nanotubes are compromised via functionalization, their utility for rheological modification of material blend remains profound. Functionalized nanotubes are also commercially available, with COOH and NH₂ attached functional groups, that are suitable for the production of high mechanical properties thermoplastic and thermoset composites.

Noncovalent functionalization is an alternate method for tuning the interfacial properties of nanotubes. This treatment is particularly attractive because of the possibility of adsorbing various groups on CNT's surface without disturbing the π -system of the grapheme sheets. Star et al.[16] achieved such functionalization by adsorbing different polymers onto SWNTs to improve their solubilisation. As previously reported, this process has been dubbed “polymer wrapping” of nanotubes, although periodic helical wrapping has only been demonstrated when the polymers are DNA. Good dispersions not implying the chemical functionalization can be also realized utilizing block-copolymers and end-grafted macromolecules of specific chemical composition as dispersing agents, coupling agents and adhesion promoters in polymeric matrices. Thus, once a specific polymeric matrix is defined as a target material for preparation of CNT-polymer composite, a proper dispersing and compatibilizing agent may be tailored and synthesized. The dispersing agent and the compatibilizer shall be properly chosen in such a way that the physical properties of the composites are not altered by their presence. For instance, a compatibilizer could act as a plasticizer and reduce the mechanical properties of a polymer composite; as surfactant at high concentration in the final composite could be regarded as a source of defects and hence the better dispersion of nanotubes induced by the surfactant is not advantageous because of its detrimental influence on the final mechanical properties of the composite.

2.3.2 Mechanical dispersion

Because of the damaging induced by chemical functionalization of carbon nanotubes, an alternative fabrication technique has to be considered for the fabrication of nanocomposites where it is necessary to preserve the physical properties and the original aspect ratio of the pristine nanotubes. Hence, various mechanical dispersion techniques have been considered depending on the polymer matrix nature and the final physical properties required in the composite.

Here, an overview of the different composites fabrication techniques is proposed [47].

- ***Solution blending***

This is the most common method for fabricating polymer nanocomposites because it is both amenable to small sample sizes and effective. Solution blending involves three major steps: disperse nanotubes in a suitable solvent, mix with the polymer (at room temperature or elevated temperature), and recover the composite by precipitating or casting a film. As mentioned earlier, it is difficult to disperse the pristine nanotubes, especially SWNT, in a solvent by simple stirring. High-power ultrasonication can be used to make metastable suspensions of nanotubes or nanotube/polymer mixtures in different solvents. The minimum sonication conditions (time, power) that produce CNT degradation are yet to be determined and will certainly depend on nanotube concentration and initial nanotube length distribution. One variation of the solution blending method uses surfactants to disperse higher loadings of nanotubes [48-50]. However, using surfactants to improve nanotube dispersion can be problematic because the surfactant remains in the resulting nanocomposite and might degrade transport properties.

For example, Bryning et al.[50] reported that the thermal conductivities of the surfactant-SWNT/epoxy composites are much lower (and the interfacial thermal resistances are higher) than that of the composites prepared without surfactant at the same loading. The surfactant molecules can also alter the polymer matrix as shown by Sundararajan et al.,[51] where Triton X-100 induced crystallization in polycarbonate (PC); crystallization might in turn affect the transparency and mechanical properties of the composites. When using solution blending, nanotubes tend to agglomerate during slow solvent evaporation, leading to inhomogeneous distribution of the nanotubes in the polymer matrix. The evaporation time can be reduced by putting the nanotube/polymer suspension on a rotating substrate (spin-casting [52]) or dropping the nanotube/polymer suspension on a hot substrate (drop-casting [53]).

To avoid agglomeration during solvent evaporation, Du et al.[54] developed the versatile coagulation method that involves pouring a nanotube/polymer suspension into an excess of nonsolvent. The precipitating polymer chains entrap the SWNT, thereby preventing the SWNT from bundling. When this coagulation method is applied to poly-(methyl methacrylate) (PMMA), optical microscopy, SEM, and Raman imaging indicate good dispersion of SWNT in the nanocomposite. This method has been adapted to polyethylene (PE), where the nanotube/polymer suspension is heated to promote polymer solubility and then cooled to accomplish the precipitation [55].

- **Melt blending**

Melt blending uses high temperature and high shear forces to disperse nanotubes in a polymer matrix and is most compatible with current industrial practices. However, relative to solution blending methods, melt blending is generally less effective at dispersing nanotubes in polymers and is limited to lower concentrations due to the high viscosities of the composites at higher nanotube loadings. Successful examples of melt blending include MWNT/polycarbonate [56] MWNT/nylon-6 [57] SWNT/polypropylene [58] and SWNT/polyimide [59] composites. Haggemueller et al. [60] combined solution and melt blending by subjecting a solvent cast SWNT/polymer film to several cycles of melt pressing. An approach developed by Jin et al.[61] introduces polymer-coated MWNT (rather than pristine MWNT) into the polymer melt to promote compatibilization.

- **In situ polymerization**

This fabrication strategy starts by dispersing nanotubes in monomer followed by polymerizing the monomers. As with solution blending, functionalized nanotubes can improve the initial dispersion of the nanotubes in the liquid (monomer, solvent) and consequently in the composites. Furthermore, in situ polymerization methods enable covalent bonding between functionalized nanotubes and the polymer matrix using various condensation reactions. Epoxy nanocomposites comprise the majority of reports using in situ polymerization methods [62-67], where the nanotubes are first dispersed in the resin followed by curing the resin with the hardener. Note that as polymerization progresses and the viscosity of the reaction medium increases, the extent of in situ polymerization reactions might be limited. Noteworthy extensions of in situ polymerization include infiltration methods in which the reactive agents are introduced into a nanotube structure and subsequently polymerized [68-71].

- **Pulverization and latex fabrication**

Rather than avoid the high viscosities of nanotube/polymer composites, some researchers have decreased the temperature to increase viscosity to the point of processing in the solid state. Solid-state mechanochemical pulverization processes (using pan milling or twin-screw pulverization) have mixed MWNT with polymer matrices. Pulverization methods can be used alone or followed by melt mixing. Nanocomposites prepared in this manner have the advantage of possibly grafting the polymer on the nanotubes, which account in part for the observed good dispersion, improved interfacial adhesion, and improved tensile modulus [72, 73].

An innovative latex fabrication method for making nanotube/polymer composites disperses nanotubes in water and then adds a suspension of latex nanoparticles [74-75]. Freeze-drying and subsequent processing of this colloidal mixture produces composites with uniform dispersion of nanotubes even in a highly viscous matrix like high molecular weight polystyrene. This promising method can be applied to polymers that can be synthesized by emulsion polymerization or formed into artificial latexes, e.g., by applying high-shear conditions. In chapter 4 experimental results on the production and characterization of latex polystyrene/CNTs composites will be reported.

- ***Fibers spinning***

Nanotube/polymer composites with very high nanotube loadings have been also produced. Vigolo et al.[76] developed a “coagulation spinning” method to produce composite fibers comprising predominately nanotubes. This method disperses SWNT using a surfactant solution, coagulates the nanotubes into a mesh by wet spinning it into an aqueous poly(vinyl alcohol) solution, and converts the mesh into a solid fiber by a slow draw process. In addition, Mamedov et al. [77] developed a fabrication method based on sequential layering of chemically modified nanotubes and polyelectrolytes to reduce phase separation and prepared composites with SWNT loading as high as 50 wt %.

2.3.3 Nanotubes alignment

Various are the experiments where carbon nanotubes orientation is achieved on dispersions of the tube in different liquid media, for instance for nanoelectronics applications. However, less examples of nanotubes alignment in fully processed composites, because of the difficulty deriving from viscosity and processing matters.

The high aspect ratios of nanotubes make them susceptible to orientation either intentionally via various fibre spinning methods or unintentionally via solvent casting, filtering, or melt pressing. Nanotube alignment can be achieved prior to composite fabrication where aligned nanotubes are incorporated into a polymer matrix by in situ polymerization. Raravikar et al.[68] and Feng et al.[69] prepared aligned nanotube composites of PMMA and polyaniline, respectively, by infiltrating monomers into CVD-grown arrays of aligned MWNT, followed by in situ polymerization.

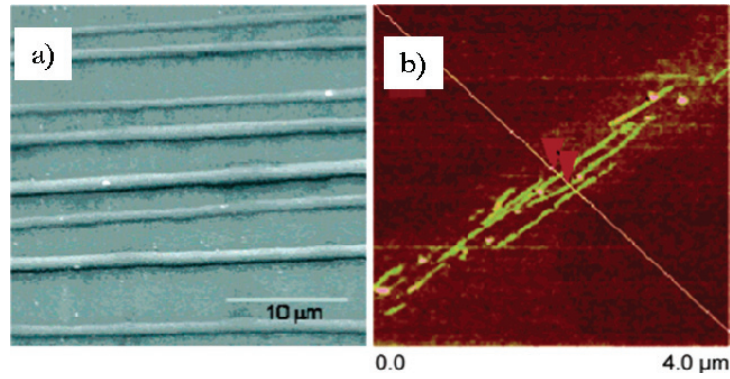


Figure 2. 7 - (a) SEM image of aligned electrospun fibers. (b) AFM image of aligned individual SWNT after heating an electrospun fiber on a silicon substrate [83]

Alternatively, in situ polymerization can be performed in the presence of an external field (e.g., a magnetic field [78]), where viscosity of the nanotube-monomer suspension affects the degree of alignment. The nanotubes can also be aligned during or after the composite fabrication by mechanical stretching [79] spin-casting [80] wet spinning, melt fibre spinning [81], and electrospinning [82-85], where the last two methods offer the greatest degree of alignment (fig. 2.7). In melt fibre spinning, the composite melt is extruded through a spinneret hole, and the extruded rod is air cooled and drawn under tension by a windup spool to produce aligned composite fibres.

Martin et al. produced aligned MWNTs/epoxy composites through the application of electric field [86]. They demonstrated that the application of both AC and DC fields during the nanocomposite curing induced the formation of aligned conductive nanotube networks between the electrodes. The carbon nanotube agglomeration mechanism was dominated by the electric field-induced forces acting on the nanotubes, which have a negative surface charge after processing in the epoxy. The network structure formed in AC fields was more uniform and more aligned compared to that in DC fields. The specific bulk composite conductivity of fully processed composite samples reflected the differences in the nanotube network structure.

In the presence of an electric field \vec{E} , each conductive nanotube experiences a polarisation \vec{P} . This polarisation can be divided into two contributing components, i.e. one parallel to the tube axis ($\vec{P}_{//}$) and one in the radial direction (\vec{P}_{\perp}). The magnitude of both components depends on the polarizability tensor of the nanotube, that leads to a torque N_E acting on the nanotube. Under the given conditions, this torque aligns the nanotube against the viscous drag of the surrounding medium in the direction of the electric field (fig. 2.8) [86].

Apart from this rotation and alignment, the behaviour of a carbon nanotube depends on the type of the applied electric field and its surface charge. In case of a DC field, charged carbon nanotubes move according to their electrophoretic mobility μ , towards the electrode with the opposite sign, where they discharge where:

$$\mu = \frac{v}{E} = \frac{\epsilon \zeta}{\eta} \quad 2.1$$

Here, ϵ is the dielectric constant and η the viscosity of the epoxy resin, respectively, and ζ is the zeta potential of the carbon nanotube, which is a measure of the surface charge [87].

In case of an AC field, the net electrophoretic mobility due to the zeta potential equals zero. However, aligned metallic carbon nanotubes cause inhomogeneities in the electric field, as shown schematically in figure 2.8b. One effect is a Coulombic attraction between oppositely charged ends of the nanotubes. In addition, the non-uniform electric field in the vicinity of the nanotube tips results in the movement of induced dipoles towards the area with the highest field strength, a behaviour which is called dielectrophoresis [88, 89]. This effect can also induce nanotube movement towards the electrode for those nanotubes in close proximity to the electrodes.

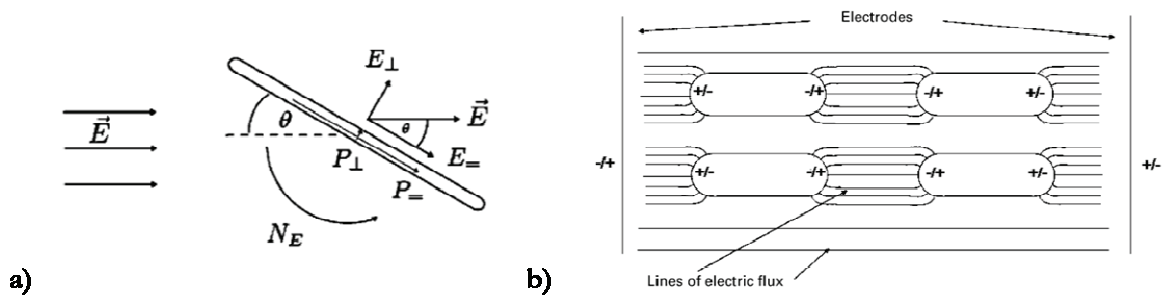
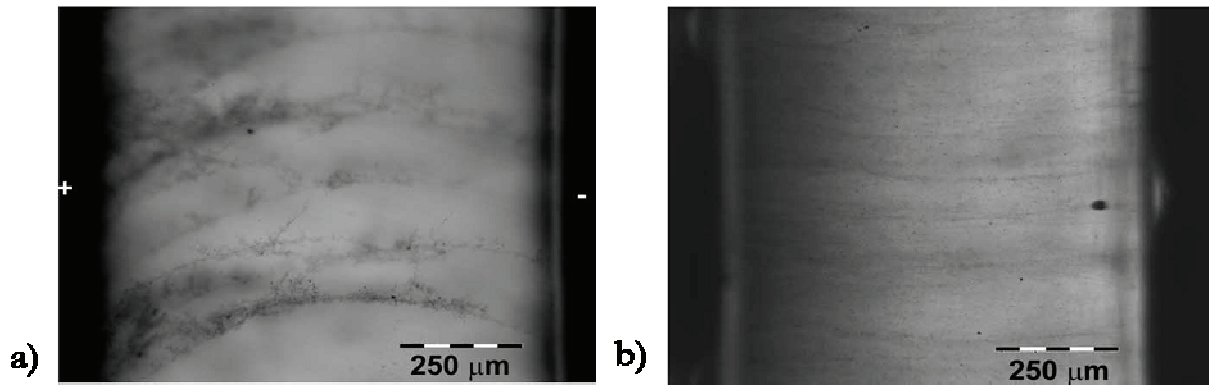


Figure 2. 8 - Schematic illustration of a) a polarised cylindrical particle in an electric Field; b) the interaction between aligned and polarised metallic cylindrical particles in an electric field

During the application of a DC electric field, a fraction of the carbon nanotubes was observed to move towards the anode, under electrophoresis. As soon as these nanotubes are close enough to the electrode to allow charge transfer, the nanotubes discharge and adsorb onto the anode. Tips of nanotubes connected to the electrode then become sources of very high field strengths and the location for adsorption of further filler particles. As a result, ramified nanotube network structures extend away from the anode, eventually reaching the cathode and providing conductive pathways throughout the sample (fig. 2.9 a).



**Figure 2. 9 - Transmission optical micrographs of epoxy composites containing 0.01 MWNT wt%
a) cured in a DC field and in b) a AC field**

In AC fields, more uniform, aligned nanotubes agglomeration was achieved. These agglomerates are also ramified and grow roughly along the electric field lines (fig. 2.9 b).

In appendix A, experimental results of an alignment process of MWNTs in a thermoplastic polyurethane composite are described. The alignment of the nanotubes has been achieved in solid matrix through the application of a high electric field and induced very high electrical conductivity materials.

2.4 CNTs composites properties

The physical properties of nanotube/polymer composites arise from the nanotube and polymer characteristics as well as from the microstructures produced while fabricating and processing these nanocomposites. Thus, ongoing efforts must improve our morphological control in nanotube/polymer composites using a combination of practicality and creativity. Note that the optimal microstructure for one physical property might not be the best microstructure of another physical property. Developing robust correlations (if not quantitative predictions) between nanotube/polymer composites and their properties will further advance the design and engineering of these composites.

Mechanical properties

In this section we will discuss results from the literature on mechanical properties of polymer nanotube composites. Many studies have been published each with a different focus.

The fiberlike structure of carbon nanotubes, their low density, high aspect ratio, and extraordinary mechanical properties make them particularly attractive for reinforcement in composite materials. In general, the tensile modulus and strength of polymer-rich nanotube composites are found to increase with nanotube loading, dispersion, and alignment in the matrix. However, the results at low nanotube concentrations typically remain far behind the idealized theoretical predictions from the rule of mixtures. While, at higher nanotube loadings, the extent of improvement in mechanical properties might be limited by the high viscosity of the composite and the resulting void defects [64].

The gap between the predictions and experimental results arises from imperfect dispersion and poor load transfer. Even modest nanotube agglomeration impacts the diameter and length distributions of the filler and overall is likely to decrease the aspect ratio (a parameter in the models). In addition, nanotube agglomeration reduces the modulus of the filler (another parameter in the models) relative to that of isolated nanotubes because there are only weak dispersive forces between nanotubes.

Schadler et al. [62] and Ajayan et al. [66] concluded from Raman spectra that slippage occurs between the shells of multiwall nanotubes and within single-wall nanotube ropes and may limit stress transfer in nanotube/polymer composites. While the load transfer at the nanotube/polymer interface is certainly less than ideal, there are several reports of strong interactions. For example, Wagner et al.⁸² found that the average interfacial stress required to remove a single MWNT from the polyethylenebutene matrix is 47 MPa, which is about 10 times larger than the adhesion level between the same type of polymer and carbon fibers; this example demonstrates the importance of filler size on the interfacial strength.

It is important to understand the mechanism of interfacial adhesion at the molecular level to further optimize the interface in nanocomposite systems. Using molecular mechanics simulations and elasticity calculations, Liao et al. [90] found that in the absence of atomic bonding between the nanotubes and the matrix the nanotube/matrix adhesion comes from (i) electrostatic and vdW interactions and (ii) stress/deformation arising from the mismatch in the coefficients of thermal expansion between nanotubes and the polymer matrix. Several other mechanisms [91] have been proposed to describe these interfaces, and further investigations are necessary to understand and then optimize nanotube/polymer interfaces.

Functional moieties on nanotubes typically provide better interfacial load transfer via bonding and/or entanglement with the polymer matrix. Experimentally, Geng et al. [92] obtained a 145% increase in tensile modulus and 300% increase in yield strength with 1 wt % fluorinated SWNT in a poly(ethylene oxide) matrix. In situ ring-opening polymerization of caprolactam by Gao et al. [93] in the presence of carboxylated SWNT produced SWNT/nylon-6 composites with nylon

chains grafted to the SWNT. The stress-strain profile of these composite fibers indicate a 153% increase in Young's modulus and 103% increase in tensile strength with 1 wt % carboxylated SWNT (fig 2.10). This suggests that the covalent bonding at the nanotube/polymer interface can be very effective in strengthening the material.

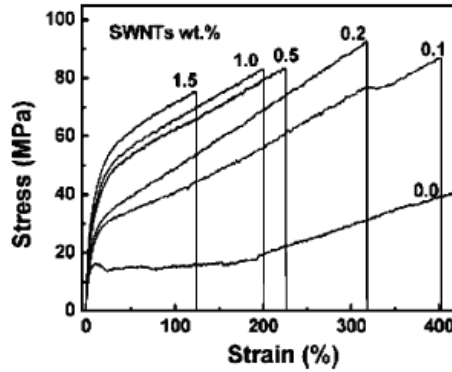


Figure 2. 10 - Stress-strain profiles of SWNT-nylon-6 composite fibres at different SWNT loadings [93]

However, the improvements in tensile strength and modulus in this case are coupled with a reduction in strain at break, indicating a decrease in polymer toughness and flexibility.

A promising result from Dyke et al. [94] reports the fabrication of poly(dimethylsiloxane) (PDMS) composites with functionalized SWNT, where they found that the tensile modulus and strength are considerably increased in these composites whereas the strain at break is largely unchanged (fig. 2.11).

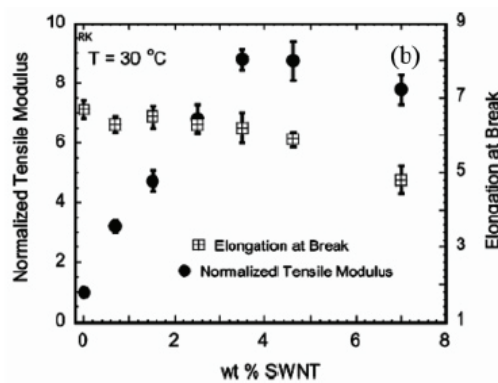


Figure 2. 11 - Composition dependence of the normalized tensile modulus ($E_{\text{composite}}/E_{\text{PDMS}}$) and the elongation at break ($L_{\text{break}}/L_{\text{initial}}$) for SWNT/PDMS nanocomposites [94]

Gojny et al. [95, 96] studied the influence of the geometrical and physical properties of various types of nanotubes on the mechanical properties of CNTs/epoxy composites. They found out

that the use of NH_2 functionalized nanotubes lead to an increase of the mechanical properties in terms of elastic modulus, elongation to break and fracture and tensile strengths (fig. 2.12). Moreover, they also found that in epoxy composite double-walled nanotubes (DWNT), up to a certain content, lead to the higher strength and elastic modulus, while for the same quantity of MWNTs a decrease of the strength respect to the neat resin (fig. 2.13) is found. From the table in fig. a common concept can be detected: the use of functionalized nanotubes leads to an increase of all the mechanical properties up to a certain content of nanotubes, above which the occurrence of agglomerates with micrometric dimensions creates defect points in the composites and a consequent decrease of all the mechanical performances.

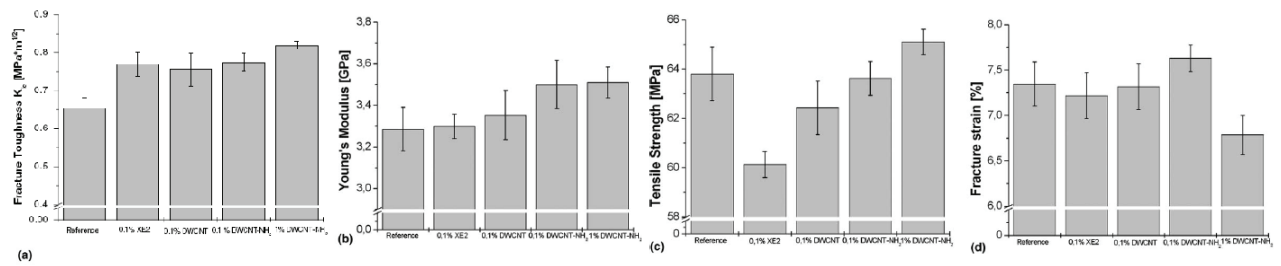


Figure 2. 12 - Mechanical properties of different CNTs/epoxy composites [95]

Mechanical properties of nanoparticle reinforced composites				
	Filler type/content (wt%)	Young's modulus (MPa)	Ultimate tensile strength (MPa)	Fracture toughness K_{Ic} (MPa m ^{1/2})
Epoxy	0.0	2599 (±81)	63.80 (±1.09)	0.65 (±0.062)
Epoxy/CB	0.1	2752 (±144)	63.28 (±0.85)	0.76 (±0.030)
	0.3	2796 (±34)	63.13 (±0.59)	0.86 (±0.063)
	0.5	2830 (±60)	65.34 (±0.82)	0.85 (±0.034)
Epoxy/SWCNT	0.05	2681 (±80)	65.84 (±0.64)	0.72 (±0.014)
	0.1	2691 (±31)	66.34 (±1.11)	0.80 (±0.041)
	0.3	2812 (±90)	67.28 (±0.63)	0.73 (±0.028)
Epoxy/DWCNT	0.1	2785 (±23)	62.43 (±1.08)	0.76 (±0.043)
	0.3	2885 (±88)	67.77 (±0.40)	0.85 (±0.031)
	0.5	2790 (±29)	67.66 (±0.50)	0.85 (±0.064)
Epoxy/DWCNT- NH_2	0.1	2610 (±104)	63.62 (±0.68)	0.77 (±0.024)
	0.3	2944 (±50)	67.02 (±0.19)	0.92 (±0.017)
	0.5	2978 (±24)	69.13 (±0.61)	0.93 (±0.030)
Epoxy/MWCNT	0.1	2780 (±40)	62.97 (±0.25)	0.79 (±0.048)
	0.3	2765 (±53)	63.17 (±0.13)	0.80 (±0.028)
	0.5	2609 (±13) ^a	61.52 (0.19) ^a	^a
Epoxy/MWCNT- NH_2	0.1	2884 (±32)	64.67 (±0.13)	0.81 (±0.029)
	0.3	2819 (±45)	63.64 (0.21)	0.85 (±0.013)
	0.5	2820 (±15)	64.27 (±0.32)	0.84 (±0.028)

^a High viscosity disabled degassing – composite contained numerous voids.

Figure 2. 13 - Mechanical properties of different CNTs/epoxy composites [96]

Rheological properties

The viscoelastic properties of nanotube/polymer composites have both practical importance related to composite processing and scientific importance as a probe of the composite dynamics

and microstructure. Figure 2.14 shows the storage modulus (G') as a function of frequency for a typical response of nanotube/polymer composites with good nanotube dispersion [97].

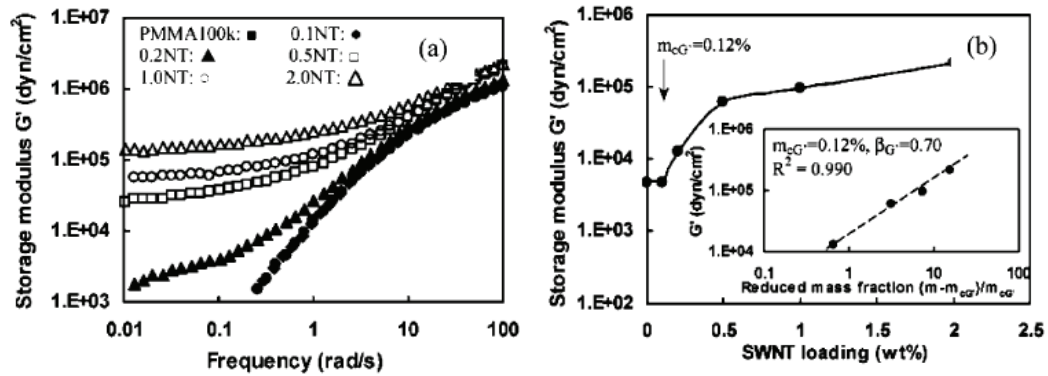


Figure 2. 14 - (a) Storage modulus (G') vs shear frequency for SWNT/PMMA nanocomposites with various nanotube loadings from 0 to 2.0 wt % (b) G' as a function of the nanotube loading for SWNT/PMMA nanocomposites at a fixed frequency, 0.5 rad/s [97]

At high frequencies, the response is not sensitive to the filler concentration, indicating that the short-range polymer dynamics are not influenced by the nanotubes. In a consistent manner the glass transition temperatures of the composites are constant in the absence of strong interfacial bonds and at low nanotube loadings. At low frequencies, the rheological behavior progresses from a liquidlike response to a solid like response, where G' is independent of the frequency as the nanotube concentration increases. Applying a power law function to the G' vs nanotube loading data provides a rheological percolation threshold ($m_{cG'}$) corresponding to the onset of solidlike behavior.

The rheological percolation has been found to depend on CNTs dispersion, aspect ratio, and alignment. Mitchell et al. [98] improved dispersion by functionalizing SWNT such that the rheological percolation threshold dropped from 3 wt % when using pristine SWNT to 1.5 wt % in functionalized SWNT/polystyrene composites. The values of G' at low frequencies were also higher for the functionalized composites, indicating better load transfer between the nanotube network and the polymer.

Within a given system (nanotubes and polymers), the linear viscoelastic response can serve as an indirect qualitative measure of the dispersion state of the nanotubes in the composites, where better dispersion corresponds to higher value of G' or a lower slope. Potschke et al. [99] also found that the rheological percolation threshold is strongly dependent on temperature. In their SWNT/PC composite, the percolation threshold decreases from 5 to 0.5 MWNT wt % upon increasing the temperature from 170 to 280 °C. They suggest that the superposition of the entangled polymer network and the combined nanotube-polymer network rather than the

nanotube network alone dominates the rheological properties. The concentration of nanotubes required to form a reinforcing nanotube-polymer network should be lower than the electrical percolation threshold, which requires nanotube-nanotube contacts to form a conductive network.

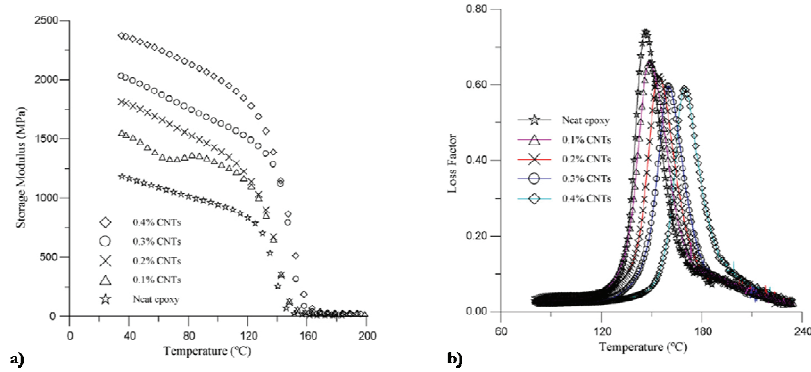


Figure 2. 15 - a) Storage modulus and b) loss factor of an epoxy/CNTs system [101]

In fact, in a set of SWNT/PMMA composites, Du et al.[97] found that the rheological percolation threshold, 0.12 wt %, was significantly smaller than the percolation threshold for electrical conductivity, 0.39%. The absence of a matrix in the solutions leads to higher rheological percolation thresholds. Moreover, because of the rod like geometry and the high aspect ratio of the CNTs the rheological percolation threshold is higher respect to other nanofillers, for instance carbon black and silicates. It was also seen that the thermo-mechanical properties of thermoset matrices can be improved by the addition of nanotubes, as can be noted from the storage modulus of an epoxy/CNTs composite in figure 2.15 a, while the $\tan\delta$ peak decreases upon an increase of the CNTs concentration (fig. 2.15 b) [100, 101].

However, from literature it seems that there is a lack of certain results about a determined percolation threshold, also for the same composite system. This occurrence can be explained with two considerations. When nanotubes form a network where all the tube are well dispersed at single state, the entanglement limit can be overcome. In this case, the rheological response should be similar to an elastic solid. On the contrary, the mechanical percolation could occur also when aggregates or clusters of tubes come in contact with each other, forming a sort of chain. This second type of dispersion provides the as named nanotubes “jamming effect”, that is responsible for the higher percolation thresholds and elastic moduli in the CNTs composites.

Thermal conductivity

Recent studies have demonstrated that carbon nanotubes have high thermal conductivity: 6000 W/Km for Single Walled Carbon Nanotubes (SWNT) and about 3000 W/Km for Multi Walled Carbon Nanotubes (MWNT) [102, 103]. The ballistic conduction mechanism of current and heat typical of carbon nanotubes makes CNTs ideal candidate for being used as electrical and thermal conductive fillers in polymer composites. However, an important factor to be pointed out is that the contemporary enhancement of good electrical, mechanical and thermal properties in the same CNTs composite is not simple to obtain, because the phenomena related respectively to the electrical conduction, stress transfer and heat transport are physically very different. For instance, the chemical functionalization providing a good interfacial adhesion between matrix and tubes and consequent good mechanical properties, induces the formation of an insulating matrix layer between tubes that is detrimental for the electrical properties as well as for thermal conduction. Moreover, the use of high aspect ratio tubes is very useful for obtaining high electrical and mechanical properties, but it produces negative effects in terms of thermal conductivity of the final composite.

The conduction mechanisms of electrical and thermal conductivity are physically different because the first is related to the electrons and the second to the phonons travelling along the tubes. The substantial difference between these two mechanism is encountered when a network of nanotubes is formed. The percolation pathway responsible for the electrical conduction is not always sufficient for the heat transport too, because the electrical conduction occurs by hopping mechanism, that requires close proximity between nanotubes in the composite, so it occurs even if there isn't a direct contact between tubes. On the contrary, the heat transport between tubes occurs via phonons coupling and a thermal energy scattering is unavoidable. Hence, the heat transport in nanocomposites is limited by the interaction between tubes and by the interaction between tubes/matrix/tubes, where the loss of energy is even higher than in a tube/tube contact [104]. It was found that the thermal conductivity of a buckypaper constituted by a free standing network of carbon nanotubes is two orders of magnitude lower than the one related to the single tube (from 10^3 to 10 W/Km) [105]. Therefore, the thermal conduction mechanisms within a nanocomposite is not yet ballistic, but governed by diffusion in both polymer matrix and nanotubes in a junction. As a consequence of this high thermal resistance at the interface, the thermal conductivity of a nanocomposite is several orders of magnitude lower than the single tube, being about 0.2 - 1 W/Km.

In 2002 Biercuk et al. measured a thermal conductivity of about 0.5 W/Km, in a an epoxy composite with 1 SWNT wt%, with an increase of 125% in comparison to the neat resin [106]. Du et al. using a particular infiltration technique, produced epoxy composites showing a thermal

conductivity of 0.61 W/Km at 2.5 SWNT wt%, with an enhancement of 220% respect to the neat resin (fig 2.16) [104].

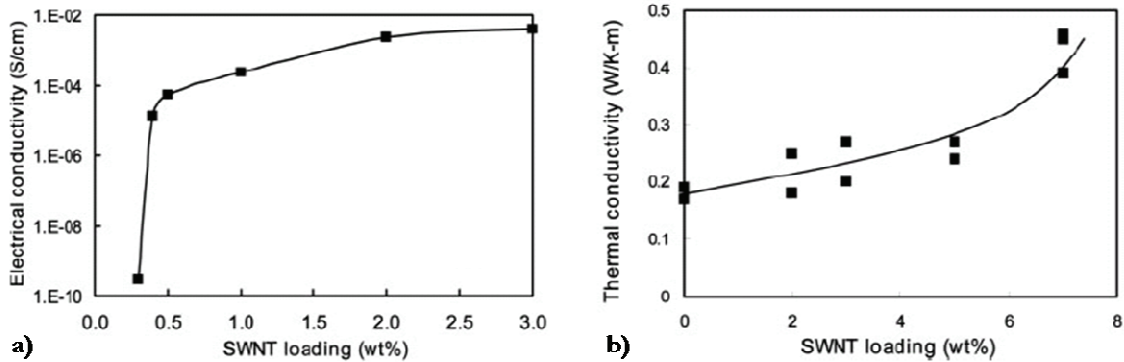


Figure 2. 16 - (a) Electrical conductivity and (b) thermal conductivity as function of SWNT loading for PMMA composites [104]

The effects of functionalization on the thermal conductivity of a nanocomposite is a controversial matter. Yang et al. experimentally demonstrated that a way to improve the heat transport between tubes within an epoxy matrix is the chemical functionalization of the tubes with an aliphatic amine [107]. They showed that the existence of a covalent bonding between tubes and matrix reduces the thermal resistance and facilitates the heat transport at the interface. Their epoxy composites showed a thermal conductivity of 1.3 W/Km at a high filler content of 10 MWNT wt%. On the contrary, Gojny et al. found out that a strong interfacial adhesion of the nanotube with the surrounding epoxy matrix has to be avoided, because it induces an intensive coupling between the two different media, CNTs with a high thermal conductivity and the poor conductive epoxy [108]. In light of the abovementioned basic concepts, it appears clear that the main problem for the heat transport is related to the interface between polymer and nanotubes in such a way that the interface thermal resistance is reduced. Together with the geometrical characteristics another important properties for a good heat transport is the absence of defects inducing phonon scattering. Hence, the higher the defect density and the larger the provided interface, the lower the efficiency as thermal conductor.

It was experimentally observed that while the electrical conductivity increases upon an increase of CNTs content, thermal conductivity doesn't show the same behavior and seems to be not influenced very much by the filler weight content. While, a substantial correlation between thermal conductivity and SSA was found. From a comparison between SWNTs and MWNTs with different length and diameters, it resulted that the largest improvement occurs for MWNTs, that exhibit the smallest SSA [108]. Despite the higher potential thermal conductivity of single SWNTs, they exhibit the largest SSA and hence the lowest enhancement of thermal conductivity

in a nanocomposite. In this context, Double Walled Carbon Nanotubes (DWNT) show intermediate properties between MWNTs and SWNTs. Moreover, internal layers of MWNTs, not interacting with the matrix, allow the phonon conduction minimizing the coupling losses. Moisala et al. reported that for the same content of MWNTs and SWNTs dispersed in an epoxy resin, the first lead to an increase of thermal conductivity, while the second show a decrease of it, remaining lower than the pure polymer matrix over a wide range of weight fractions [109]. On the contrary, for the same composite systems, electrical conductivity shows a percolation behavior with a threshold of only 10^{-3} MWNT wt% and 10^{-2} SWNT wt%. Theoretically, a high aspect ratio would improve the heat transport through CNTs over a longer distance, avoiding the coupling with the matrix in the transitions between particles, but at the same time it increases the interface with the matrix, so its influence has a limited importance if it is not correlated with the SSA. Hence, not only the nature of CNTs, but also their length is an important factor to be taken into account. Wang et al. used microtome shortened SWNTs to produce epoxy based composite and showed that shortening considerably improved the SWNTs dispersion because of the short aspect ratio, with a consequent improvement of the thermal conductivity of the 40% in comparison to the neat resin, passing from 0.18 to 0.252 W/Km for a content of 0.5 SWNT wt% [110].

Together with the intrinsic properties of nanotubes as thermal conductive fillers, as for the other functional properties of the CNTs based composites, a fundamental aspect influencing the final performances of the composite is the dispersion quality and the contact nature between fillers.

It was experimentally found that carbon nanotubes thermal conduction mechanisms in a composite can be described using percolation concepts as electrical conductivity or “effective medium” theories. The substantial difference between these two approaches is the fact that in the first case the topology of the CNTs network controls the thermal transport, while in the second case the formed pathway doesn’t influence the final thermal properties of the composite, because it is regarded as a mixture of a conductive filler and an thermal insulating medium. The occurrence of one of the two configuration strongly depends on the polymer matrix thermal properties: if the polymer is not a thermal insulator, the final thermal properties of composite are affected by diffusion conduction through the polymer, hence, irrespective of the CNTs structure, the thermal conductivity can be theoretically calculated using mixtures rules. On the contrary, when the contrast between the conductive properties of filler and matrix is substantial, a percolation theory can be used to describe the conduction mechanism within the composite and, consequently, the topology of the conducting network assumes a big importance. However, also in this case, the contrast problem related to percolation phenomenon is a matter of controversy, because up to now it is not yet well understood what it should be the proper contrast entity so

that one can consider percolative the conduction behavior [111, 112]. The assumption of a contrast factor of 10 rather than 10^4 between matrix and filler can lead to misunderstandings about the dependence of the nanocomposite thermal conductivity on the CNTs content.

2.5 Electrical properties

Polymers contain a very low concentration of free charge carriers, and are therefore generally good electrical insulators. However, conducting plastics or thermosets are useful for many applications. Electrical conductivity can be achieved by incorporation of highly conductive fillers, such as carbon-black (CB) particles, carbon fibers, metallic fillers, or intrinsically conducting polymers.

Since the discovery of carbon nanotubes and of their physical properties, they have been considered ideal candidates as fillers in insulating matrix for the enhancement of the electrical conductivity of the final composite and the potential of nanotubes as conducting fillers in multifunctional polymer composites has been successfully realized. Several orders of magnitude enhancement in electrical conductivity has been achieved with a very small loading of CNTs (less than 0.1 wt%) in different matrices, contemporary maintaining the other performance aspects of the polymers such as optical clarity, mechanical properties, low melt flow viscosities, so that the processing properties of the composites are not affected by the introduction of such a filler. Much lower amount of carbon nanotubes is needed respect to other conductive particles, for example carbon black, to reach the same conductivity values.

A variety of applications are being pursued using these conductive composites: electrostatic dissipation, electrostatic painting, electromagnetic interference (EMI) shielding, printable circuit wiring, and transparent conductive coating [113].

Electrical properties of such composite materials have been widely studied. The dc conductivity is related to the formation of a network of filler particles within the matrix; it increases sharply at a characteristic conducting particle concentration (p_c) known as the percolation threshold.

To describe the insulator-to-conductor transition a large variety of models have been proposed in the literature [114, 115]

This so-called percolation threshold coincides with the formation of a system spanning, conduction network of filler particles in the continuous polymer phase. Far above the percolation threshold, the conductivity of the nanocomposite levels off and does not increase significantly with the further addition of CNTs. Interestingly, there is a considerable body of evidence for the presence of an insulating layer between the CNTs even above the percolation threshold, as in fact

also seems to be the case for other types of conductive fillers including carbon black [116-118]. This then implies that the percolating filler particles are not in actual contact with each other, and that conductivity must occur via some tunnelling or hopping process through the insulating layer that separates them. This can only happen if the shortest distance between two neighboring particles is below a certain value, estimated to be in the order of a couple of nanometers. The type of electron transport involved should be strongly dependent on the CNT/polymer system in hand, and depends in particular on the statistics of inter-particle separations. It follows that the percolation threshold is not only purely geometrically defined, as usually tacitly implied, but also physically defined, exactly because the particles need not quite touch for conduction to take place.

The influencing factors of the electrical properties of CNTs composites are:

1. aspect ratio;
2. degree of debundling;
3. size and shape polydispersity;
4. interaction between filler particles;
5. degree of orientation;
6. processing conditions.

The influence of processing conditions is an interesting aspect to analyze, because it means that the measured percolation thresholds might not be the lowest possible for a given material system and that one should be weary comparing theoretical predictions that are often based on equilibrium percolation arguments [119]. Many experimental evidences reporting the influence of these factors on electrical properties are reported in literature [120-125].

In this part, a particular emphasis will be given to the influence of processing conditions on the electrical properties of CNTs composites because in chapter 5 the problem will be experimentally treated, with the production and testing of MWNT/epoxy composites by varying the fabrication conditions.

2.5.1 Statistical and dynamic percolation

The most prominent model is the statistical percolation model, proposed by Kirkpatrick and Zallen [126, 127]. It allows forecasting both geometric and electrical quantities. It is based on the assumption that the fillers are not interacting with each other or, in other words, that they are randomly dispersed within the matrix. Under such a condition a binary mixture can be modelled with a lattice possessing a given fraction of active sites \sim or bounds! randomly chosen, i.e.,

independently of the occupation status of their neighbors. Sufficiently close to the transition, the statistical percolation predicts a power-law variation for the measurable quantities with the volume fraction of fillers. The aim of the statistical percolation theory is to forecast the behavior of a not completely connected set of objects. By varying the number of connections, this model allows us to describe the transition from a local to an infinite “communication” state. The percolation threshold p_c is defined as the critical volume fraction separating these two states. The classical theory has proven to be relevant for describing both geometrical and transport properties of composite materials with power-law equations. The correlation length is the average distance between two sites belonging to the same cluster. It is directly related to the cluster formation and reaches very high values on both sides of the transition. Close to the threshold this parameter follows a power-law divergence $\xi = |p - p_c|^{-\nu}$, with a value of 0.88 for ν in 3D dimensional systems. In the statistical percolation theory the divergence of the correlation length or, in other words, the formation of an infinite cluster, is not due to any agglomeration, which should involve a driving force and a diffusion process, but to the random position of occupied sites.

The dc electrical conductivity σ , or the dielectric constant ϵ also exhibit a power-law dependence close to the percolation threshold

$$\epsilon \propto |p - p_c|^{-s} \quad 2.2$$

and for $p > p_c$

$$\sigma \propto (p - p_c)^t \quad 2.3$$

The exponents s and t , characterizing the transition, are assumed to be universal, i.e., to depend only upon the dimensionality of the system. In three-dimensional systems the universal values are $t \approx$ and $s \approx 0.7$ for the conductivity and for dielectric constant, respectively [128, 129].

The statistical percolation threshold evaluated following the excluded volume concept, for conductive particles individually dispersed in an insulating matrix, Φ_{st} , coincides with the onset of the insulator to conductor transition. In the case of rigid rods in the limit of $L/D \gg 1$ such as the case of CNTs, the percolation threshold is:

$$\Phi_{st} = \frac{D}{2L} \quad 2.4$$

The high aspect ratio of CNTs has been identified as a key parameter in reducing the critical concentration to obtain a percolative insulator to conductor transition [131]. Considering an aspect ratio of about 1000, following the equation 4 the statistical percolation threshold of CNTs composite systems should be 0.1 wt%. However, many evidences of the fact that the percolation

threshold cannot be univocally defined are present in literature. The variation of many parameters like CNT type, synthesis method, treatment and dimensionality as well as polymer type and dispersion method impeded a thorough understanding of the processes involved. Since the early observation of percolation-dominated electrical conductivity in a CNT/PmPV composite by Coleman et al. [131] more than 30 polymer matrices have been investigated with respect to percolation of CNT's filler loading.

From an analysis of the percolation thresholds measured of several composite systems, Bauhofer and Kovacs [132] found out that only few composites showed a percolation threshold higher than 0.2 CNT wt% and that in most of them the percolation threshold was lower than 0.1 CNT wt%, that reproduce the above mentioned value as statistical percolation threshold.

Hence, in a number of experimental studies, the theoretical percolation approach has been found to be inadequate and a new concept has been introduced, the “dynamic percolation”.

For the explanation of the concept of dynamic percolation, some aspects of colloid theory, widely explained in chapter 2, can be applied to describe the behavior of dispersions containing fine filler particles.

In figure 2.3 the total potential energy is plotted as a function of particle distance. Depending on the amount of charging, the coulombic force can cause a potential barrier. This barrier may be able to hinder the particles from coming into close enough contact with each other to be conductive, hence conducting agglomerates cannot form. In order to achieve a permanent contact in the primary minimum and hence to induce the agglomeration process, the potential energy barrier must be surmounted. It is very unlikely that thermal energy alone is sufficient to surmount an existing potential energy barrier within a reasonable time, but there are two possibilities to accelerate this process. The barrier can be surmounted either by external shear forces, which can be produced by stirring the dispersion or by reduction of the repulsive coulombic force by increasing the ionic concentration. Above a critical salt concentration, for instance, the barrier is lowered to such an extent that the thermal jostling or convection can drive particles into the primary minimum.

Particles dispersed in liquid media, like in polymers above their melting temperature, are influenced by the above mentioned forces but also by thermal and shear forces. Hence, they can migrate through the hosting medium. As a consequence of the influence of these external forces, the collision of particles could induce them to stick together. So, even if initially homogeneously dispersed, particles can agglomerate within the matrix, forming bigger clusters.

The model of Kirkpatrick and Zallen generally used for the description of the percolative behavior is based on the assumption that after the dispersion, filler particles are statistically distributed and blocked in a fixed position. However, this condition can be met only if a medium

of high viscosity is considered as a matrix and when the time required for the composite production is very short. Experimental results reported on agglomeration phenomena both in thermoplastic and thermoset matrices, such as in high and low viscosity systems. For particles dispersed in a lower viscous medium, such as a resin, the agglomeration process should be much faster and take place even if a relatively short production time is needed.

When the described prerequisite conditions are met, agglomerates start to form in many parts within the polymer and finally combine to a continuous network. Within an agglomerate, the number of particles N is proportional to its radius R to the power of its fractal dimension D . since D is below 3, the particle density n of an agglomerate decreases with its size, as follows [133]:

$$n = \frac{N}{\frac{4}{3}\pi R^3} \propto \frac{1}{R^{3-D}} \quad 2.5$$

A low percolation threshold can hence be obtained when the fractal dimension is low and the network is made up of large agglomerates. The fractal dimension is influenced by the conditions during and after the agglomeration process. Generally, it is between 1.8 and 2.5 [134, 135]. After a longer dispersion time, D increases. Hence, to achieve a percolation threshold as low as possible, this should be avoided.

Schueler et al. [133] studied these phenomena in carbon black epoxy composites and found out that the dispersion of CB in epoxy resin is an electrostatically stabilized suspension, so that the particles cannot reach the potential minimum because of a potential barrier. The formation of a conductive network is influenced by the shearing or by increasing the ionic concentration. Both treatments are proved to have an effect on the morphology, with the occurrence of a particle agglomeration also visible by optical microscopy of the filler network and strongly influencing the percolation threshold.

On the basis of the reported results, it appears evident that the percolation threshold doesn't depend only on the filler concentration, but also on the production conditions and hence to explain the formation of the percolative network the statistical models are not enough.

In such a context, the conductive particles filled polymer composites have to be regarded as thermodynamic non-equilibrium systems, in which the formation of conductive networks is temperature and time dependent, that is the percolation has a kinetic nature [136].

Based on this assumption, Zhang et al. [137] carried out a real-time measurement method to trace the dynamic process of conductive network formation during the production of thermoplastic vapor grown carbon fibers (VGCF) composite. They found out that at a given temperature, the electrical resistivity decreases slightly with increasing pressing time at the early stage, and then

decreases rapidly at a critical time, indicating the formation of a conductive network in the composite. This phenomenon undoubtedly originates from the aggregation and rearrangement of short carbon fibers in the matrix phase during the melt pressing process, indicating that percolation should be considered in terms of kinetics (fig. 2.17). They defined a critical time at which the first conductive network is constructed throughout the composite named percolation time t_p , that decreases with increasing the pressing temperature in the HDPE/PMMA composite production and upon an increase of the VGCF content. They attributed this phenomenon respectively to the lower viscosity of the matrix at a higher temperature and to the smaller gaps between the conductive fibers, that corresponds to a shorter time for the fibers coagulation during heating.

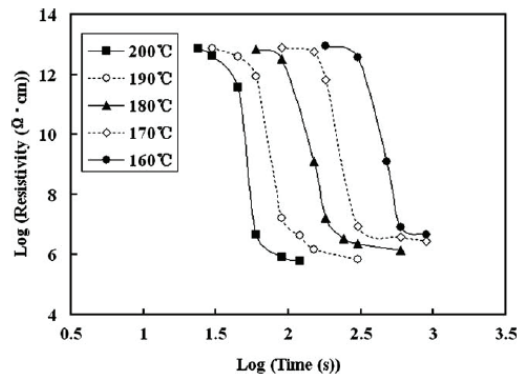


Figure 2. 17 - Time Dependence of room temperature electrical resistivity for 2.5 phr VGCF filled HDPE/PMMA (50/50) blend after hot-pressed at various temperatures [137]

According to the studies of Sumita [138, 139], the dispersion process of filler particles in the polymer matrix never lead to a thermodynamic equilibrium. Both of them emphasized the importance of the interfacial interaction at the boundary between the individual filler particles and the polymer host for the conductive network formation, and interpreted the percolation phenomenon as a phase separation process. As mentioned above, the flocculation rate of conductive particles would be controlled by the viscosity of polymer matrix and the size of the filler particles (or aggregates). The higher the value of melt viscosity or the bigger the size of filler particle, the longer time it will take to achieve the coagulation. So, it is not surprising that the percolation time decreases with increasing annealing temperature due to the low values of melt viscosity at high temperatures. Because all the dynamic percolation curves have similar features in their shapes, Zhang et al. tried to build a master curve by shifting these curves along the horizontal axis, with a shift factor α_t defined as:

$$\alpha_t = \frac{t_p(T)}{t_p(T^*)} \quad 2.6$$

where T^* is a reference temperature.

They found out a good linear relationship between the logarithmic shift factor and the reciprocal of temperature. The concepts reported for general filler particles polymer dispersions can be applied also to carbon nanotubes composites.

Martin et al. [134] studied the electrical properties of MWNT/epoxy composites produced using mechanical mixing by varying the process condition such as stirring temperature and rate, and curing temperature.

In figure 2.18 the AC electrical conductivity of the composites produced at different stirring rates and temperatures as well as using different curing temperatures is plotted as a function of frequency. In the same figure the optical microscopy images of the corresponding samples are shown. The authors found out a strict correlation between the electrical properties and the morphology existent within the composites. In particular, an agglomeration process occurs corresponding to an enhancement of the electrical conductivity. Initially, high stirring rates and shear-forces have to be applied in order to separate the nanotubes and to produce a charge-stabilised dispersion in the resin. After the addition of the hardener, small nanotube aggregates are formed, using high temperatures or small shear-forces to help the nanotubes overcome their mutual electrostatic repulsion. The nanotube aggregates subsequently agglomerate to form a macroscopic network which covers large volume fractions of the epoxy. High curing temperatures further enhance this network formation of nanotube clusters by enhancing nanotubes mobility.

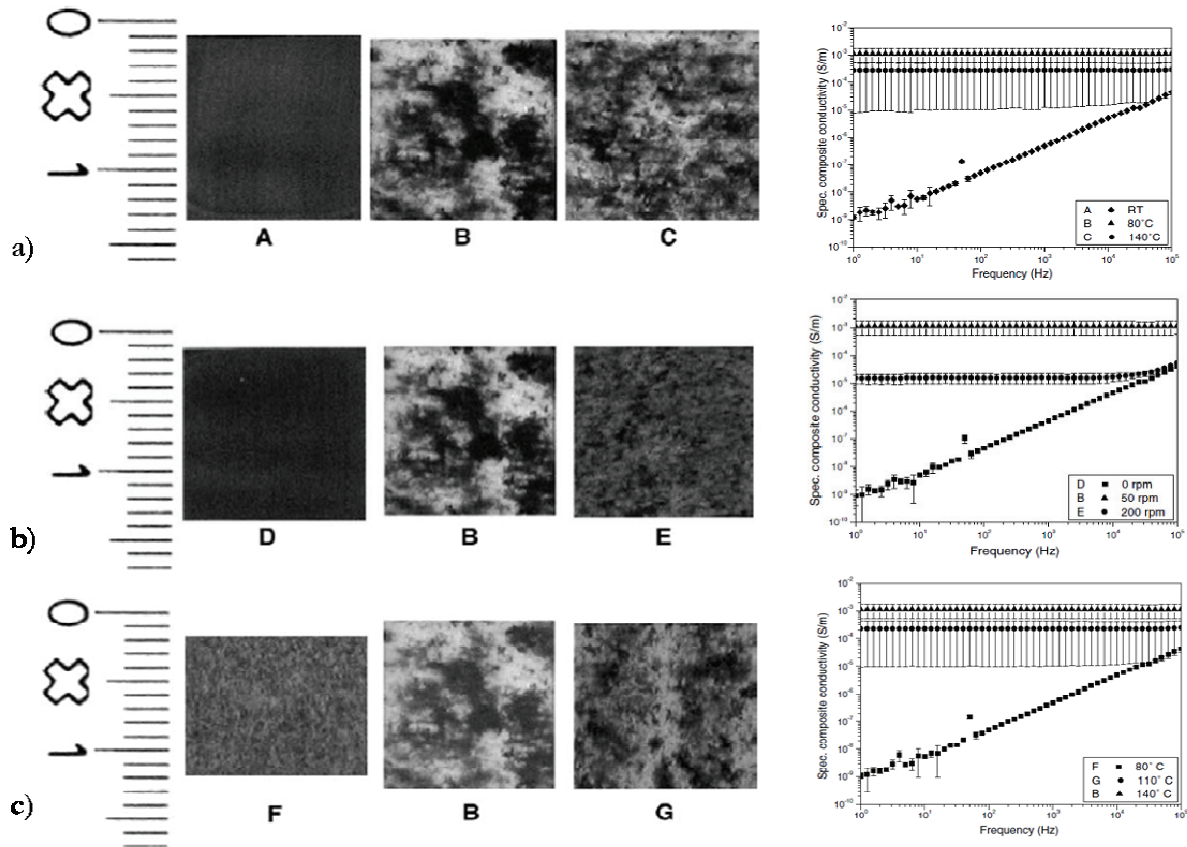


Figure 2. 18 - Optical microscopy images and specific bulk AC conductivity of MWNT/epoxy composites produced by varying a) stirring temperature, b) stirring rate, c) curing temperature

Examples of thermoplastic CNTs composites showing electrical properties depending on the production parameters have been reported in literature.

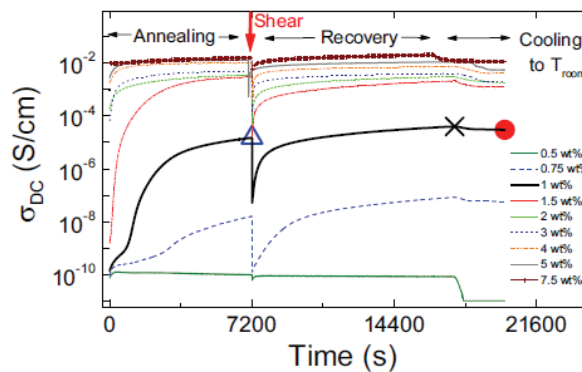


Figure 2. 19 - DC conductivity during 2 h of annealing, transient shear, conductivity recovery and cooling to room temperature for different MWNT/PC composite [140]

Alig et al. [140] studied in real-time the influence of thermal and mechanical prehistory on the insulator-conductor transition for PC/MWNT composites. They found out that during annealing of MWNT/PC composites the DC conductivity showed a percolation like transition due to the dynamic formation of a conductive network in polymer melts. During a short shear deformation

applied to the melt, the conductivity showed a tremendous decrease, with a recovery after some time, that can be explained with the rupture and the consequent reconstruction of the agglomerates network. This network keeps stable in polymer matrix after cooling to the glassy state (fig. 2.19).

2.6 References

1. Dresselhaus, M. S., Dresselhaus G., Avouris P. 2001, Carbon Nanotubes: Synthesis, Structure, Properties and Applications: Berlin, Springer.
2. Ajayan PM, Charlier JC, Rinzler AG. - Proceedings of the National Academy of Science 1996; 96:14199.
3. Baughman RH, Zakhidov AA, de Heer WA. - Science 2002; 297:792.
4. Niu C, Sichel EK, Hoch R, Moy D, Tennent H. - Applied Physics Letters 1997; 70:1480.
5. Kong J, Franklin NR, Zhou C, Capline MG, Peng S, Cho K, - Science 2000; 287:622.
6. Mattson MP, Haddon RC, Rao AM. J Mol - Neuroscience 2000; 14:175.
7. Chen X, Lee GS, Zettle A, Betoizzi CR. Angewandte Chemie International Edition 2004; 43:6111.
8. Bower, C., Kleinhammes A., Wu Y., Zhou O. - Chemical Physics Letters 1998; 288:481-486.
9. Bellayer, S.; Gilman, J. W.; Eidelman, N.; Bourbigot, S.; Flambard, X.; Fox, D. M.; De Long, H. C.; Trulove, P. C. - Advanced Functional Materials 2005; 15:910-916.
10. Chatterjee, T.; Yurekli, K.; Hadjiev, V. G.; Krishnamoorti, R. - Advanced Functional Materials. 2005; 15:1832-1838.
11. Bechinger, C., Rudhardt D., Leiderer P., Roth R., Dietrich S. - Physical Review Letters 1999; 83:3960-3963.
12. Szleifer I., Yerushalmi-Rozen R. - Polymer 2005; 46:7803-7818
13. Bredas JL, Silbey R. Conjugated polymers. Dordrecht: Kluwer Academic Publishers; 1991.
14. Dai H, Mau AWH. - Journal of Physical Chemistry B 2000; 104:1891.
15. Dalton A.B., Blau W.J., Chambers G., Coleman J.N., Henderson K, Lefrant S - Synthetic Metals 2001; 121:1217-1218
16. Star A, Stoddart F, Steuerman D, Diehl M, Boukai A, Wong EW - Angewandte Chemie International Edition 2001; 40:1721-1725
17. (Steuerman DW, Star A, Narizzano R, Choi H, Ries RS, Nicolini C. - Journal of Physical Chemistry B 2002; 106:3124-3130
18. Steuerman DW, Star A, Narizzano R, Choi H, Ries RS, Nicolini C, - Journal of Physical Chemistry B 2002; 106:3124-3130
19. Guo Z, Sadler PJ, Tsang SC. - Advanced Materials 1998; 10:701-703
20. Dieckmann GR, Dalton AB, Johnson PA, Razal J, Chen J, Giordano GM - Journal of American Chemical Society 2003;124:1770-1777

21. de Gennes PG. Scaling concepts in polymer physics. Ithaca, NY: Cornell University; 1979.
22. Joanny JF, Leibler L, de Gennes PG. - Journal of Polymer Science B: Polymer Physics 1979; 17:1073-1084
23. de Gennes PG. - Macromolecules 1980; 13:1069-1075.
24. Binder K, Milchev A, Baschnagel J. - Annual Review of Materials Science 1996; 26:107-134
25. Wu DT, Fredrickson GH, Carton JP, Ajdari A, Leibler L. J - Journal of Polymer Science B: Polymer Physics 1995; 33:2373-2389
26. Balberg I, Binenbaum N, Wagner N. - Physical Review Letters 1984; 52:1465-1468
27. Girifalco LA. - Journal of Physical Chemistry 1992; 96:858-861
28. Girifalco LA, Hodak M, Lee RS. - Physical Review B 2000; 62:13104.
29. Shvartzman-Cohen R, Levi-Kalisman Y, Nativ-Roth E, Yerushalmi-Rozen R. - Langmuir 2004; 20:6085-6088
30. Milner ST. - Science 1996; 905:251.
31. Szleifer I, Carignano MA. - Adv Chem Phys 1996;96:165.
32. Lu KL, Lago RM, Chen YK, Green MLH, Harris PJF, Tsang SC. - Carbon 1996; 34:814-816
33. Strano MS, Moore VC, Miller MK, Allen MJ, Haroz EH, Kittrell C. - Journal of Nanoscience and Nanotechnology 2003; 3:81-86
34. Grossiord N., Regev O., Loos J., Meuldijk J., and Koning C.E., - Analytical Chemistry 2005; 77:5135-5139
35. Vaisman L., Wagner H.D., Marom G. - Advances in Colloid and Interface Science 2006; 128-130 37-46
36. Junrong Y., Grossiord N., Koning C.E., Loos J. - Carbon 2007; 45:618-623
37. Tan Y., Resasco D.E. - Journal of Physical Chemistry B 2005; 109:14454-14460
38. Yurekli, K.; Mitchell, C. A.; Krishnamoorti, R. Journal of the American Chemical Society 2004; 126: 9902-9903.
39. Zhou W., Islam F. Wang H., Ho D. L., Yodh A. G., Winey K. I., Fischer J. E. - Chemical Physics Letters 2004; 384:185-189.
40. Wang H.; Zhou W., Ho D. L., Winey K. I., Fischer J. E., Glinka C. J., Hobbie E. K.- Nano Letters 2004; 4:1789-1793.
41. Schaefer D. W., Zhao, J., Brown J. M., Anderson D. P., Tomlin D. W. - Chemical Physics Letters 2003; 375:369-375.
42. Bauer B. J., Hobbie E. K., Becker, M. L. - Macromolecules 2006; 39:2637-2642.
43. Zhou W., Islam M. F., Wang H., Ho D. L., Yodh A. G., Winey K. I., Fischer J. E. - Chemical Physics Letters 2004; 384:185-189.
44. Niyogi S., Hamon M. A., Hu H., Zhao B., Bhowmik P., Sen R., Itkis M. E., Haddon R. C. - Accounts of Chemical Research 2002; 35:1105-1113.
45. Bahr J.L., Tour J.M. - Journal of Materials Chemistry 2002;12:1952-1958

46. Chen Y., Haddon R. C., Fang S., Rao A. M., Eklund P. C., Lee W. H., Dickey E. C., Grulke E. A., Pendergrass J.C., Chavan A., Haley B.E., Smalley R.E. - *Journal of Materials Research* 1998; 13:2423-2431.
47. Moniruzzaman M., Winey K.I. - *Macromolecules* 2006; 39:5194-5205
48. Islam M. F., Rojas E., Bergey D.M., Johnson A.T., Yodh A.G. - *Nano Letters* 2003; 3:269-273.
49. Barrau S., Demont P., Perez E., Peigney A., Laurent C., Lacabanne C. - *Macromolecules* 2003; 36:9678-9680.
50. Bryning M.B., Milkie D.E.; Islam M. F., Kikkawa J.M., Yodh A.G. - *Applied Physics Letters* 2005; 87:1611-1619/3.
51. Sundararajan P.R., Singh S., Moniruzzaman M. - *Macromolecules* 2004; 37:10208-10211.
52. De la Chapelle M. L., Stephan C., Nguyen T. P., Lefrant, S., Journet C., Bernier P., Munoz E., Benito A., Maser W. K., Martinez M. T., De la Fuente G. F., Guillard T., Flamant G., Alvarez L., Laplaze D. - *Synthetic Metals* 1999; 103:2510-2512.
53. Benoit J.M., Corraze B., Lefrant S., Blau W.J., Bernier P., Chauvet O. - *Synthetic Metals* 2001; 121:1215-1216.
54. Du F., Fischer J.E., Winey, K.I. - *Journal of Polymer Science Part B: Polymer Physics* 2003; 41:3333-3338.
55. Haggenmueller R., Fischer J.E., Winey K.I. - *Macromolecules* 2006; 39:2964-2971.
56. Poetschke P., Bhattacharyya A.R., Janke A., Goering H. - *Composite Interfaces* 2003; 10:389-404.
57. Liu T., Phang I.Y., Shen L., Chow S.Y., Zhang W.D. - *Macromolecules* 2004; 37:7214-7222.
58. Bhattacharyya A.R., Sreekumar T.V., Liu T., Kumar S., Ericson L.M., Hauge R.H., Smalley R.E. - *Polymer* 2003; 44:2373-2377.
59. Siochi E.J., Working D.C., Park C., Lillehei P.T., Rouse J. H., Topping C.C., Bhattacharyya A.R., Kumar S. - *Composites Part B* 2004; 35B:439-446.
60. Haggenmueller R., Gommans H.H., Rinzler A.G., Fischer J.E., Winey K.I. - *Chemical Physics Letters* 2000; 330:219-225.
61. Jin Z., Pramoda K.P., Goh S. H., Xu G. - *Materials Research Bulletin* 2002; 37:271-278.
62. Schadler L. S., Giannaris S.C., Ajayan P.M. - *Applied Physics Letters* 1998; 73:3842-3844.
63. Zhu J., Kim J., Peng H., Margrave J.L., Khabashesku V.N., Barrera E.V. - *Nano Letters* 2003; 3:1107-1113.
64. Zhu J., Peng H., Rodriguez-Macias F., Margrave J.L., Khabashesku V.N., Imam A.M., Lozano K., Barrera E.V. - *Advanced Functional Materials* 2004; 14:643-648.
65. Gong X., Liu J., Baskaran S., Voise R.D., Young J.S. - *Chemical Materials* 2000; 12:1049-1052.
66. Ajayan P.M., Schadler L.S., Giannaris C., Rubio A. - *Advanced Materials* 2000; 12:750-753.
67. Moniruzzaman M., Du F., Romero N., Winey K.I. - *Polymer* 2006; 47:293-298.
68. Ravavikar N.R., Schadler L.S., Vijayaraghavan A., Zhao Y., Wei B., Ajayan P.M. - *Chemical Materials* 2005; 17:974-983.
69. Feng W., Bai X.D., Lian Y.Q., Liang J., Wang X.G., Yoshino K. - *Carbon* 2003; 41:1551-1557.

70. Du F., Guthy C., Kashiwagi T., Fischer, J.E., Winey K.I. - Journal of Polymer Science Part B: Polymer Physics 2006; 44:1513-1519.
71. Huang H., Liu C., Wu Y., Fan S. - Advanced Materials 2005; 17:1652-1656.
72. Xia H., Wang Q., Li K., Hu G.H. - Journal of Applied Polymer Science 2004; 93:378-386.
73. Kasimatis K.G., Nowell J.A., Dykes L.M., Burghardt W.R., Thillalyan R., Brinson L.C., Andrews R., Torkelson J.M. PMSE Prepr. 2005; 92:255-256.
74. Regev O., ElKati P.N.B., Loos J., Koning C.E. - Advanced Materials 2004; 16:248-251.
75. Dufresne A., Paillet M., Putaux J.L., Canet R., Carmona F., Delhaes P., Cui S. - Journal of Materials Science 2002; 37:3915-3923.
76. Vigolo B., Penicaud A., Coulon C., Sauder C., Pailler R., Journet C., Bernier, P., Poulin P. - Science 2000; 290:1331-1334.
77. Mamedov A.A., Kotov N.A., Prato M., Guldi D.M., Wicksted J.P., Hirsch A. - Nature Materials 2002; 1:190-194.
78. Kimura T., Ago H., Tobita M., Ohshima S., Kyotani M., Yumura M. - Advanced Materials 2002; 14 :1380-1383.
79. Jin L., Bower C., Zhou O. - Applied Physics Letters 1998; 73:1197-1199.
80. Safadi B., Andrews R., Grulke E.A. - Journal of Applied Polymer Science 2002; 84:2660-2669.
81. Haggenmueller R., Zhou W., Fischer J.E., Winey K.I. - Journal of Nanoscience and Nanotechnology 2003; 3:105-110.
82. Ge Jason J., Hou H., Li Q., Graham Matthew J., Greiner A., Reneker Darrell H., Harris Frank W., Cheng Stephen Z.D. - Journal of American Chemical Society 2004; 126:15754-15761.
83. Gao J., Yu A., Itkis M. E., Bekyarova E., Zhao B., Niyogi, S., Haddon R.C. - Journal of American Chemical Society 2004; 126:16698-16699.
84. Hou H., Ge J.J., Zeng J., Li Q., Reneker D.H., Greiner A., Cheng S.Z.D.- Chemistry of Materials 2005, 17, 967-973.
85. Ko F., Gogotsi Y., Ali A., Naguib N., Ye H., Yang G., Li C., Willis P. - Advanced Materials 2003;15:1161-1165.
86. Martin C.A., Sandler J.K.W., Windle A.H., Schwarz M.K., Bauhofer W., Schulte K., Shaffer M.S.P. - Polymer 2005; 46:877-886
87. Brezesinski G, Mo"gel H-J. Grenzfl"chen und Kolloide. Mu"nchen: Spektrum Akademischer Verlag; 1993.
88. Pohl HA. Dielectrophoresis. Cambridge: Cambridge University Press; 1978.
89. Jones TB. Electromechanics of particles. London: Cambridge University Press; 1995.
90. Liao K., Li S. - Applied Physics Letters. 2001, 79, 4225-4227
91. Lordi V., Yao N. - Journal of Materials Research 2000; 15:2770-2779.
92. Geng H., Rosen R. Zheng B., Shimoda H., Fleming L., Liu J., Zhou O. - Advanced Materials. 2002; 14:1387-1390.

93. Gao J., Itkis M.E., Yu A., Bekyarova E., Zhao B., Haddon R.C. - Journal of American Chemical Society 2005; 127:3847-3854.
94. Dyke, C. A.; Tour, J. M. Journal of Physical Chemistry A 2004; 108:11151-11159.
95. Gojny F.H., Wichmann M. H. G., Kopke U., Fiedler B., Schulte K. - Composites Science and Technology 2004; 64:2363-2371
96. Gojny F.H., Wichmann M. H. G., Fiedler B., Schulte K. - Composites Science and Technology 2005; 65:2300-2313
97. Du F., Scogna R.C., Zhou W., Brand S., Fischer J.E., Winey K.I. - Macromolecules 2004; 37:9048-9055.
98. Mitchell C.A., Bahr J.L., Arepalli, S., Tour J.M., Krishnamoorti R. - Macromolecules 2002; 35:8825-8830.
99. Poetschke P., Abdel-Goad M., Alig I., Dudkin S., Lellinger D. - Polymer 2004; 45:8863-8870.
100. Hernandez-Perez A., Aviles F., May-Pat A., Valadez-Gonzalez A., Herrera-Franco P.J., Bartolo-Perez P. - Composites Science and Technology 2008; 68:1422-1431
101. Zhou Y., Pervin F., Lewis L., Jeelani S. - Materials Science and Engineering A 2007; 452-453:657-664
102. Kim P., Shi L., Majumdar A., McEuen P.L. - Physical Review Letters 2001; 87:2155021-4
103. Hone J., Whitney M., Piskoti C., Zettl A., phys rev b 1999; 59:2514-2516
104. Du F., Guthy C., Kashiwagi T., Fischer J.E., Winey K. - Journal of Polymer Science Part B 2006; 44:1513-1519
105. Hone J., Batlogg B., Benes Z., Llaguno M.C., Nemes N. M. Johnson A.T. Fischer J.E. - Materials Research Society Symposium Proceedings 2001 633 A17.1.1-A17.1.12
106. Biercuk M.J., Llaguno M.C., Radosavljevic M., Hyun J.K., Johnson A.T. Fischer J.E. - Applied Physics Letters 2002; 80:2767-2769
107. Yang K., Gu M., Guo Y., Pan X., Mu G. - Carbon 2009; 47 1723-1737
108. Gojny F.H., Wichmann M.H.G., Fiedler B., Kinloch I.A., W. Bauhofer, Windle A.H., Schulte K. - Polymer 2006; 47:2036-2045
109. Moisala A., Li Q., Kinloch I.A., Windle A.H. - Composites Science and Technology 2006; 66:1285-1288
110. Wang S., Liang R., Wang B., Zhang C. - Carbon 2009; 47:53-57
111. Bonnet P., Sireude D., Garnier B., Chauvet O. - Applied Physics Letters 2007 ; 91 :201910-2
112. Song Y.S. Youn J.R. - Carbon 2005; 43:1378-1385
113. Baughman R.H., Zakhidov A.A., de Heer W.A. - Science 2002; 297:787-792
114. Clerc J. P., Giraud G., Laugier J. M., Luck J. M. - Adv. Phys. 1990 ; 39 :191-
115. Lux F. - Journal of Material Science 1993; 28:285-
116. Kilbride B.E., Coleman J.N., Fraysse J., Fournet P., Cadek M., Drury A. - Journal of Applied Physics 2002; 92:4024-4030
117. Kim Y.J., Shin T.S., Choi H.D., Kwon J.H., Chung Y-C., Yon H.G. - Carbon 2005; 43: 23-30
118. Sandler J.K.W., Kirk J.E., Shaffer M.S.P., Windle A.H. - Polymer 2003; 44:5893-5899

119. Zakri C, Poulin P. - Journal of Materials Chemistry 2006;16:4095-4098
120. Kyrylyuk A.V., P. van der Schoot - Applied Physics Science 2008; 105:8221-8226
121. Vigolo B., Coulon C., Maugey M., Zakri C., Poulin P. - Science 2005 ; 309 :920-923
122. Zakri C., Poulin P. - Journal of Materials Chemistry 2006; 16: 4095-4098
123. Kovacs J. Z., Velagala B. S., Schulte K., Bauhofer W. - Composites Science and Technology 2007; 67:922-928
124. Grossiord N., Kivit P.J.J., Loos J., Meuldijk J., Kyrylyuk A.V., van der Schoot P., Koning C.E. - Polymer 2008; 469:2866-2872
125. Pegel S., Pötschke P., Petzold G., Alig I., Dudkin S. M., Lellinger D. - Polymer 2008; 49:974-984
126. Kirkpatrick S. - Reviews of Modern Physics 1973; 45:574-588
127. Zallen R., in The physics of Amorphous Solids, Wiley, New York, 1983
128. Song Y., Noh T. W., Lee S. I., Gaines J. R. - Physical Review B 1986; 33:904-908
129. Ezquerro T. A., Kulesza M., Balta`-Calleja F. J. - Synthetic Metals 1991; 41:915-920
130. Stauffer D., Aharony A., in Introduction to percolation theory 2nd edition (CRC Press 1994).
131. Coleman J.N., Curran S., Dalton A.B., Davey A.P., McCarthy B., Blau W., Barklie R.C. Physical Review B 1998;58:R7492-7495.
132. Bauhofer W., Kovacs J.Z. - Composites Science and Technology 2009; 69:1486-1498
133. Schueler R., Petermann J., Schulte K., Wentzel H-P. - Journal of Applied Polymer Science 1997; 63:1741-1746
134. Martin C. A., Sandler J.K.W., Shaffer M.S.P., Schwarz M.-K., Bauhofer W., Schulte K., Windle A.H., Composites Science and Technology 2004; 64:2309-2316
135. Bryning M.B., Islam M.F., Kikkawa J.M., Yodh A. G. - Advanced Materials 2005; 17:1186-1191
136. Zhang C. Doctor Thesis. Zhejiang University; 1998
137. Zhang C., Wang P., Ma C., Wu G., Sumita M. - Polymer 2006; 47:466-473
138. Sumita M., Asai S., Miyadera N., Jojima E., Miyasaka K. - Colloid & Polymer Science 1986;264:212-217
139. Sumita M., Sakata K., Asai S., Miyasaka K., Nakagawa H. - Polymer Bulletin 1991; 25:265-271
140. Alig I., Skipa T., Lellinger D., Bierdel M., Meyer H. - Physica Status Solidi (b) 2008; 245, No. 10, 2264-2267

Chapter 3

Monitoring the dispersion process of CNTs in aqueous solutions

3.1 Introduction

Carbon nanotubes (CNTs) have been attracted great interest due to their wide scope of possible applications, ranging from composite reinforcement materials to nanoelectronics and sensing too. Offering attractive mechanical, electrical and thermal properties, together with an high geometrical aspect ratio (ratio between length and diameter) CNTs could constitute a good candidate as nanoscale added fillers to achieve a significant improvement in bulk properties of different types of materials.

The current bottleneck to carbon nanotubes application in composite materials field consists in the difficulty of dispersing them in solvents. As a result of strong van der Waals interactions, as produced CNTs are tightly bundled in ropes of several tubes, rendering the carbon-powder insoluble in aqueous and organic liquids, and thus unprocessable [1]. Moreover, nano-scale dimensions turn dispersion into a challenge, since as the surface area of a particle increases, so does the attractive forces between aggregates.

The insolubility of SWNT in either water or organic solvents has prompted research efforts focused on nanotube functionalization combined with dissolution in organic solvents, or mixture of organic solvents and water. Many of functionalization attempts made use the possibility of dispersing CNTs in various organic solvents by acid attack in concentrated sulfuric-nitric mixtures, but introducing a significant number of defects in raw material that damage CNTs'

mechanical and electrical properties [2]. Despite this significant progress in SWNT suspension in organic solvents, the interest in applications that require water-soluble SWNT is growing. Water dispersions of SWNTs could have important implications in biochemistry and biomedical engineering, in which compatibility with living organisms is necessary [3]. Moreover, in the case of composite materials, it is very important to separate individual nanotubes from bundles to maximize the effect of intrinsic mechanical properties of CNTs and to facilitate the incorporation of individual nanotubes into the matrix for reinforcement of the composite materials. The use of surfactant can help both the integration of nanotubes in the matrix and the bonding between them. In order to achieve a good dispersion without impairing CNTs' physical properties, many attention is being directed to the study of surfactants aqueous solutions, in which surfactants can successfully suspend carbon nanotubes without formation of chemical bonds.

3.2 CNTs dispersion with surfactants as dispersing agent

The dispersion state in solutions with particulate in the submicron or nanometersized ranges is particularly influenced by the surface chemistry, hence it is extremely important to learn about the manipulation of the surface properties in order to achieve a stable and uniform dispersion. The property of the surfactant to adsorb onto surfaces has been widely used to promote stable colloidal dispersions in different media. Those amphiphilic molecules have both the polar and apolar groups, respectively a hydrophilic head and a hydrophobic tail. This duality infers a distinct structural feature to the molecule and its characteristics are classified according to the charge on their head groups in cationic, anionic and nonionic surfactants.

The adsorption of surfactant molecules onto inorganic or organic surfaces depends on the chemical characteristic of particles, surfactant molecules and solvent. Hence, the driving force for the adsorption of ionic surfactants on charged surfaces is the Coulombic attractions, while the mechanism by which nonionic surfactants adsorb onto a hydrophobic surface is based on a strong hydrophobic attraction between the solid surface and the surfactant's hydrophobic tail.

In a typical dispersion procedure, ultrasonication for minutes or hours helps surfactants debundling and exfoliating nanotubes: according to the so-called “unzippering” mechanism, surfactant has to get in the small spaces between bundles and individual nanotubes in the bundle in order to exfoliate the tubes. The role of ultrasonic treatment is to provide high local shear at the bundle end, so that a gap between tubes forming the bundle is formed. The surfactant adsorb onto the tube wall at the free end and get inside the gap, propagating the space and finally separating individual tubes or little bundles from the big one. Hence, by Coulombic or hydrophilic

interactions surfactant and sonication combined use can overcome van der Waals forces among individual nanotubes leading to the adsorption of surfactant molecules on CNTs external wall. Colloidal stability originates from electrostatic and steric repulsion between surfactant polar (or non polar) heads remaining in solution; this repulsion has the added effect of inhibiting the reattachment of nanotubes, making the suspension more stable in the time. Islam et al observed that the colloidal stability of some of these dispersions is maintained for several months [4]. Although it has been shown that the use of surfactant assisted exfoliation process results in an improved dispersion, the mechanism is not totally understood. Matarredona et al. [3] demonstrated that SWNT are not solubilized inside an existing cylindrical micelle, but the surfactant adsorbs with its tail on the external surface of the nanotubes and the resulting configuration takes the appearance of a cylindrical micelle with a nanotube in its interior (fig. 3.1).

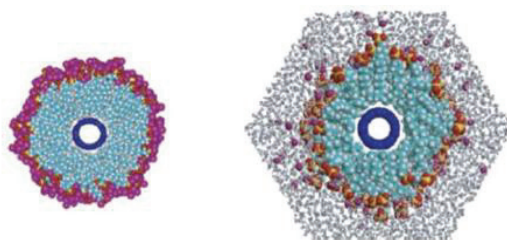


Figure 3. 1 - Surfactant adsorption on nanotube external wall

The formation of such a stable monolayer results in the stabilization of individual tubes suspended in solution. However, this phenomenon doesn't occur for all surfactant concentrations, but a minimum concentration is necessary for the solubilization of a fixed nanotubes content. This concentration strictly depends upon the critical micelles concentration (cmc), the nature and the chemical structure of surfactant that influence hydrophobic interactions between surfactant tails and between tails and substrate. Surfactant concentration must be adjusted on an optimum that occurs when interactions between adsorbed molecules and molecules in solution become dominant [5]. For some surfactants the solubilization of CNTs doesn't have to necessarily coincide with the formation of micelles and the surfactant can be used at a concentration below or above the cmc. The choice of surfactant chemical formula together with concentration is an important parameter in the optimization of nanotubes solubilization process.

Tan et al. [6] studying the dispersion ability of different surfactants using UV-vis spectroscopy concluded that not only the charge of the head group but also the dimension of surfactant hydrophobic tail is determinant for a good CNTs dispersion. Surfactants with too long or too

large hydrophobic groups have difficulties in penetrating in the intertube region between CNTs forming a bundle during the sonication, with a resulting lower electrostatic charge after adsorption, which eventually reduces the debundling efficiency of that surfactant. For instance, benzene group in the hydrophobic tail of many surfactants is thought to be one of the main reasons for their high nanotube dispersing ability [4] as well as the presence of a naphthalene group, provides a good surfactant-nanotube interaction [6].

Moreover, even with aromatic groups in the hydrophobic tail, non-ionic surfactants are not as effective as ionic ones.

Generally, ionic surfactant are preferable for CNT/water solutions, while nonionic surfactants are used as dispersing agent in organic solvents. However, at actual knowledge, the effect of head-group charge was investigated for various CNT-based systems, revealing no clear conclusions on the superiority of either cationic or anionic surfactants in dispersing tubes [7]

For many applications, the use of surfactants mixture is effective too, because of repulsive/attractive forces between head groups.

3.3 Characterization of CNTs dispersion by means of spectroscopic techniques

Besides the mentioned difficulty in obtaining stable and homogeneous dispersions of nanotubes, another complication is finding a valid method to evaluate their state of dispersion.

Electrical measurements could indirectly indicate the state of filler dispersion in CNT-based composite materials. Moreover, optical microscopy enables to access mainly the micrometer-sized agglomerates, while Atomic Force Microscopy (AFM) is used to monitor suspended CNT at nano-scale level. Another useful imaging technique is Scanning Electron Microscopy (SEM) used in contrast imaging mode, that, exploiting the conductive nature of carbon nanotubes, enables the visualization of CNTs as bright lines in the dark polymer matrix.

3.3.1 UV-vis spectroscopy

An effective method for the study of the dispersion state of CNTs in solution is the UV-vis spectroscopy. All kinds of CNTs are active in UV-vis region and spectra obtained are characterized by a fine structure of bands caused by additional absorption due to 1D van Hove singularities. In particular, SWNTs give rise to three transitions corresponding to three van Hove singularities, such as those related to semiconductive tubes S11 (800-1400), S22 (550-800

nm) and those related to metallic tubes M11 at (440-600 nm). Obtained spectra are characterized by a structure of bands corresponding to different diameters and chiral vectors [8]. Even if the peak are not individually resolved, their locations is related to some extent to the nanotube diameter distribution in the sample [9]. Hence, bundled CNTs are hardly active in the wavelength region between 200 and 1200 nm. Therefore, it is possible to detect individual CNTs via spectroscopic technique, implying that there is a relationship between individually suspended CNTs in solution and the intensity of absorption spectrum. CoMoCAT CNTs have much more pronounced spectral features than HiPCO, showing two peaks at two determined wavelengths at about 600 nm and 900 nm [6]. This characteristic allows a dispersion analysis based on the study of the modification of these spectral features with different parameters, such as solution sonication time, surfactant nature and concentration: better resolved spectral features indicate a higher fraction of individual nanotubes in the suspension. Another difference exists between HiPCO and arc-discharge CNTs. For these types of nanotubes, the spectral analysis has to be focused in the wavelength range 200-500 nm, because both show spectral feature in this region. Arc-discharge CNTs are characterized by the presence of a peak at 250 nm and as a consequence, the dispersion analysis is conducted by studying the modification of the absolute value of absorbance at this wavelength upon the variation of different process parameters: an increase of exfoliated CNTs in the solution results in an increase of the absorbance value. HiPCO nanotubes show different spectral features, where two peaks are present, one before 250 nm and the other after 300 nm [9, 10]. In this case, the dispersion study is conducted by analyzing the increasing of the area below the absorbance spectra upon an increase of the sonication time. Generally, this trend ends at a certain sonication time, because further sonication cannot induce a further increase of absorbance values. From this observation, one can conclude that spectral features characterize the type of nanotube, because they depend on chirality, diameter and purity. Hence, UV-vis spectra are specific for each type of dispersed nanotubes.

Moreover, the nature of CNTs influences also the effect that sonication has on the dispersion process in terms of maximum absorbance. For instance, CNTs produced by arc-discharge reach their maximum absorbance values after 5 minutes of sonication; while, for HiPCO nanotubes, the highest absorbance value is reached after 90-100 minutes of sonication [9, 10]. This behavior can be due to the presence of impurities in arc-discharge CNTs, hence they are interconnected via catalyst particles. On the contrary, HiPCO CNTs are characterized by an higher purity, that implies a strong interaction between nanotubes, stronger van der Waals interactions and hence a slower exfoliation process (fig. 3.2).

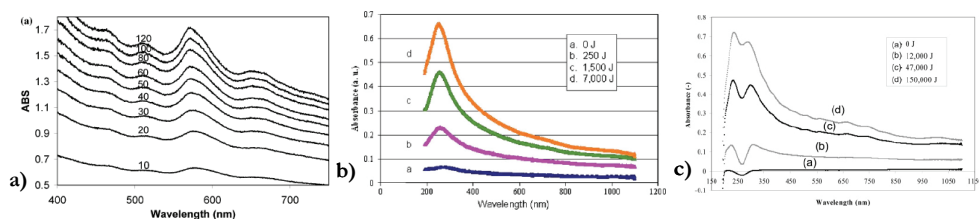


Figure 3. 2 - Evolution of the UV spectra of a) CoMoCAT, b) arc-discharge and c) HiPCO carbon nanotubes solution as function of the energy delivered during sonication

The common point consists in the fact that in all these cases the absorbance gradually decreases from UV to near-IR and increases as the sonication time increases. During sonication, the increasing amount of exfoliated SWNT results in an increasing area below the lines representing the absorbance.

It is possible to report the value of absorbance of the carbon nanotubes solution at a specific wavelength as a function of the total energy supplied to the solution during sonication (fig. 3.3).

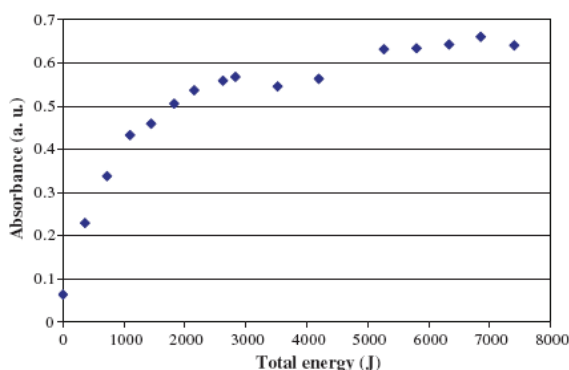


Figure 3. 3 - Evolution of the height of the peak located around 250 nm for an aqueous arc-discharge carbon nanotubes solution

The levelling off and the ultimate highest limit of the absorbance, which follows the initial increase, correspond to the maximum achievable degree of exfoliation of the SWNTs. An higher sonication could induce damages in nanotubes.

This technique for monitoring the exfoliation of carbon nanotubes can be used not only to evaluate the maximum sonication time, but also to determine the minimum concentration of surfactant required to exfoliate the nanotubes in an aqueous medium and to check the stability in time.

3.3.2 Raman spectroscopy

As previously described in chapter 1, resonance Raman scattering is a powerful tool to study electronic and vibrational properties of nanotubes. This technique is used not only for the determination of nanotubes dimensions, chirality and purity, but also for the evaluation of the degree of chemical functionalization [11-13] and processing induced defects.

The position and intensity of bands in Raman spectra are strongly dependent on the laser excitation energy because nanotubes with different diameters and chiralities are in resonance conditions at each excitation energy. In this way, Raman excitation profiles can be used to probe the unique geometric dependence of these transitions.

Kukovecz et al. [14] analyzed HiPco nanotubes using a series of excitation wavelengths and modeled peak shapes of tangential and disorder modes, also describing the radial breathing mode diameter dependence. However, all the raw material characterization studies involved aggregated nanotubes and ropes, that have shown to experience strong perturbations to their electronic structure, that complicate the interpretation of the profiles. Dresselhaus et al. experienced experimental techniques enabling single nanotube spectroscopy to circumvent this limitation [15], while Doorn et al. [16] used a solution phase dispersion of CNTs to yield individually isolated species, previously characterized by fluorescence microscopy, to map the radial breathing modes (RBM) as a function of the excitation energy.

Glamazda et al. [17] studied the effect of noncovalent interaction of SWNTs with a surfactant and DNA in solution and in dried film on Raman spectra. They found out that the line shape of G⁻ band is very sensitive to an interaction among nanotubes in bundles or between nanotubes and surrounding molecules, so that it can be used as a parameter for the evaluation of sticking behavior of CNTs in solution with different solvents and in dried solutions.

However, up to now no clear evidences on the effective utility of Raman spectroscopy for the evaluation of CNTs dispersion state have been reported in literature, even if a strict correlation between the number of exfoliated nanotubes in solution and the intensity of G bands can be supposed, because of the higher scattering properties of isolated tubes.

In this experimental part of the work, Raman scattering have been used for the evaluation of SWNT degree of exfoliation and related to UV-vis spectroscopy results.

3.4 Experimental

3.4.1 Materials and methods

Open ended single-walled carbon nanotubes produced by HiPCO process have been purchased

by Carbon Nanotechnologies inc. According to the manufacturer, the purity of the batch is 91% and the remaining 9% consists of Fe particles. The length of nanotubes has been reported to be 4-5 μm and their diameter about 1.5 nm. The chirality varies from 0° to 30° , having the material metallic and semiconductive properties.

Three types of surfactant have been used: anionic (Sodium-Cholate - 3,7,12 α -Trihydroxy-5 β -cholan-24-oic acid sodium salt), cationic (CTAB - Cetyl Trimetil-Ammonium Bromide) and non-ionic (Triton X-100 - 4-(1,1,3,3-Tetramethylbutyl)phenyl-polyethylene glycol) (fig. 3.4).

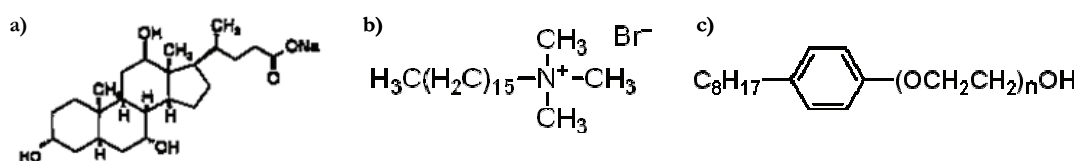


Figure 3. 4 - Chemical structure of a) Sodium-Cholate, b) CTAB and c) Triton-X 100

In order to study the dispersion state, aqueous solutions of SWNTs using surfactants at different concentrations have been prepared exploiting ultrasonication as dispersion technique.

Table 3. 1 - Solutions prepared using three different surfactants and concentrations

Sample	Concentration [wt%]
Triton-X 1	0.500
Triton-X 2	0.575
Triton-X 3	0.650
CTAB 1	0.100
CTAB 2	0.115
CTAB 3	0.130
Sodium-Cholate 1	2.000
Sodium-Cholate 2	2.300
Sodium-Cholate 3	2.600

The aim of this study is the comprehension of the influencing parameters on CNTs dispersion quality such as surfactant type, sonication time and surfactant concentration.

In particular, samples at three different concentrations for each surfactant have been prepared collecting nine samples in total (table 3.1), maintaining a constant SWNTs content of 0.006g (0.02 wt% respect to the total solution of 30 g).

Each of this sample has been sonicated for a total time of two hours in pulsed mode (4 seconds on and 2 seconds off) using a ultrasonicator with an immersion probe directly placed in the solution (Ultrasonic Processor S4000, Misonix, Inc.). The flask containing the solution has been placed in a bath of ice water during sonication in order to prevent rising of the temperature, that has been monitored during the sonication and kept below 40 °C.

3.4.2 UV-vis spectroscopy analysis

- *Part 1*

In order to study the influence of sonication time on the nanotubes dispersion, samples have been taken regularly during the sonication process every 10 minutes of sonication, diluted by a factor of 100 and analyzed using a spectrophotometer (Scinco UV-vis-NIR S 3100). Quartz cuvettes with an optical path of 10 mm have been employed and the blanks used as reference for the measurements were surfactants aqueous solutions under the same conditions of the samples themselves.

The first spectroscopic test has been performed on aqueous solutions of the three surfactants without CNTs at the same dilution used for the nanotubes dispersion analysis. From spectra analysis in the range 200-500 nm (figure 3.5) one can observe that CTAB and Sodium-Cholate don't show any spectral features after 200 nm; on the contrary, Triton-X shows two peaks, at wavelengths above 200 nm (223 nm and 274 nm), due to the presence of the aromatic ring and its substituent groups.

After the simple addition of carbon nanotubes to the aqueous surfactant solutions, SWNTs are deposited on the bottom of the flask and only after the sonication process black solutions can be obtained. By a first observation with bare eye, a longer sonication time resulted in a darker CNTs solution, which is an indication of a better and better CNTs exfoliation.

Figure 3.6 shows the absorbance vs. wavelength spectra of samples labeled "1" in table 1 for each surfactant as a function of sonication time. As expected, absorbance increases upon an increase of the sonication time, corresponding to an increase of the amount of exfoliated CNTs and the area under the UV-vis spectra increases upon an increase of the sonication time.

In the case of Triton-X solution (fig. 3.6 a), one can observe higher absorbance values, moreover the absorbance is less influenced by the sonication time than the other solutions. Furthermore, the spectral features of Triton-X in UV region influence the spectra of the nanotubes solutions, showing peaks not present in the other surfactant solutions. In CTAB solutions spectra (fig. 3.6

b) a relevant improvement of exfoliation process can be appreciated from 60 minutes and 90 minutes of sonication time, while a deep increase in absorbance can be appreciated between 10 and 30 minutes for Sodium-Cholate solutions (fig. 3.6 c). Samples labeled with “2” and “3” listed in table 1 show the same time sonication dependence, with an increase of exfoliation upon an increase of sonication time up to 120 minutes.

From this preliminary results, it seems that the best sonication time is 2 hours, because a longer sonication time could damage CNTs’ physical properties [8].

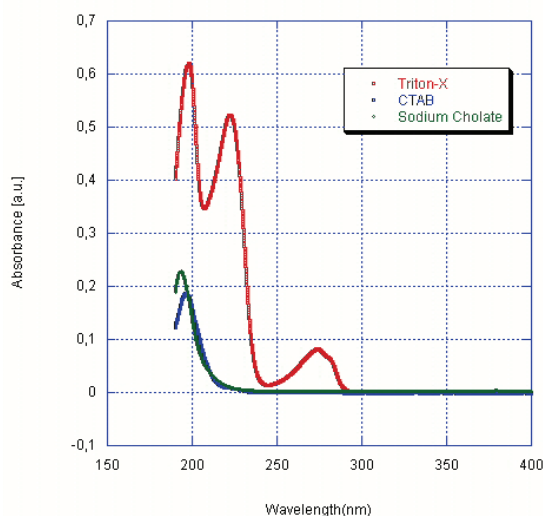


Figure 3. 5 - UV-vis spectra of surfactant aqueous solutions

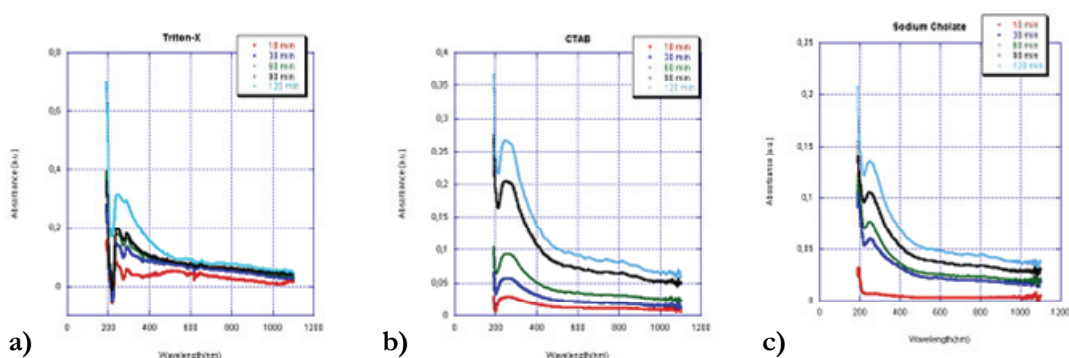


Figure 3. 6 - Evolution of the UV-vis spectra of aqueous surfactant-SWNTs solutions as a function of sonication time: a) Triton-X-SWNTs solution; b) CTAB-SWNTs solution; c) Sodium Cholate solution

In order to evaluate what is the concentration providing the best SWNTs dispersion for each surfactant, a comparison among the 120 minutes sonicated solutions at the mentioned three different concentrations was made (fig. 3.7).

As in the previous case, Triton-X solution is almost not affected by the concentration after 230 nm and absorbance values are higher than the other surfactants' spectra.

CTAB and Sodium-Cholate solutions show interesting concentration dependence behaviors. In the first case, absorbance increases from 0.100 wt% to 0.115 wt% of surfactant, but shows lower values at 0.130 wt%. Sodium-Cholate solutions show absorbance values decreasing for surfactant concentrations of 2.3 wt% and then increasing for 2.6 wt%.

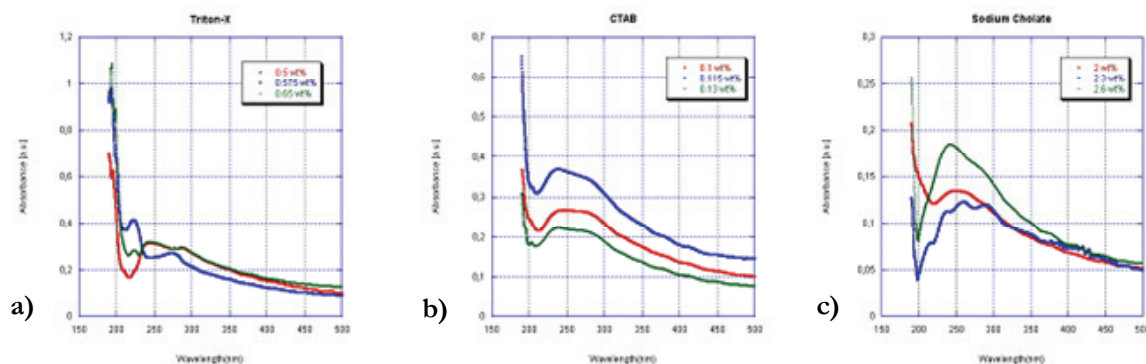


Figure 3. 7 - Evolution of the UV-vis spectra (zoom image in the range 200-500nm) of aqueous surfactant-SWNTs solutions as a function of surfactant concentration: a) Triton-X; b) CTAB; c) Sodium Cholate

From this analysis, one can draw a conclusion about the surfactant content related to each type of them, providing the best dispersion in terms of quantity of nanotubes in suspension. In this case, it is possible to assume that Triton-X is a good dispersing agent for HiPCO SWNTs, mostly independent on its content and we assume that the best dispersion is obtained in Triton-X 2 sample, with 0.65 wt% of surfactant, because of its higher absorbance spectra. CTAB solution shows its highest absorbance spectra in correspondence of 0.115 wt%, while the best Sodium-Cholate dispersed solution is obtained at 2 wt% of surfactant.

- *Part 2*¹

However, although Triton-X showed higher absorbance values in the wavelength range investigated, this surfactant doesn't show a good time stability. After some weeks, a sedimentation of nanotubes could be observed in the solutions. Because of its nonionic nature, it is better suitable for organic solvents than water, even if for short times it seems to have good dispersion properties even in water.

¹ The results reported in this part have been published by Faiella et al in [18].

Hence, only the cationic and anionic surfactants were considered for the progress of this study, aimed at a better understanding of the dispersion properties of surfactants as well as of the performances of UV-vis spectroscopic technique for the evaluation of the nanotubes dispersion. A more deepened dispersion study on the surfactant-SWNT solutions was carried out on the CTAB and Sodium-Cholate solutions at the concentrations showing the best results from the preliminary analysis. The same content of SWNT (0.006 g) was added to 0.115 CTAB wt% and 2.6 SC wt% aqueous solutions, that were processed in the same way reported above, but the sonication time was increased up to 4 hours. The UV-vis spectroscopic analysis was conducted on samples taken every 10 minutes during sonication and the absorbance at 237 nm was evaluated for each sample. Absorbance spectra of CTAB and Sodium-Cholate SWNTs-solutions at different sonication times are shown in figure 3.8 a and b respectively (for simplicity, only spectra recorded every 30 minutes of sonication are shown). UV -vis spectra present a broad absorption band in the UV region between 200 and 400 nm specific of a π -plasmon [11]. Moreover spectra have a linear baseline distinguishable in the visible region, that increases with frequency of incident light. This phenomenon is main due to the light scattering from little aggregates present in solution and whose dimensions are comparable to wavelengths of light beam. As previously observed the absorbance increases with sonication time for the two investigated systems corresponding to a gradual increase in concentration of exfoliated nanotubes in solution.

In figure 3.9 a and b the areas of UV spectra are reported as a function of sonication time. A linear baseline in the visible region of spectrum (500-700 nm) was chosen in order to cut off the background due to the light scattering in the absorbance spectra, then the area under the curve in the range 200-400 nm was evaluated. For Sodium Cholate solutions a linear increase of the absorbance area is observed up to a certain sonication time, above which a plateau is reached. An increase of absorbance is observable for CTAB too, but a real plateau seems to be approached only up to 240-250 minutes of sonication.

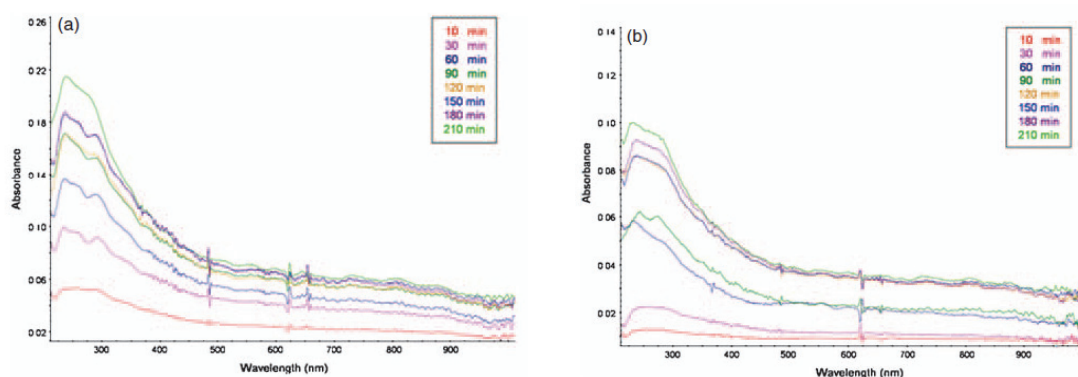


Figure 3. 8 - UV-vis absorbance spectra of (a) CTAB-SWNTs (b) Sodium-Cholate-SWNTs aqueous solutions at different sonication times

It seems that a longer sonication time is necessary to get a constant absorbance value for the cationic surfactant. The observed behaviors are due to the different dispersing ability of the two surfactants, which, in turn, depends on their chemical structure and ionic behavior.

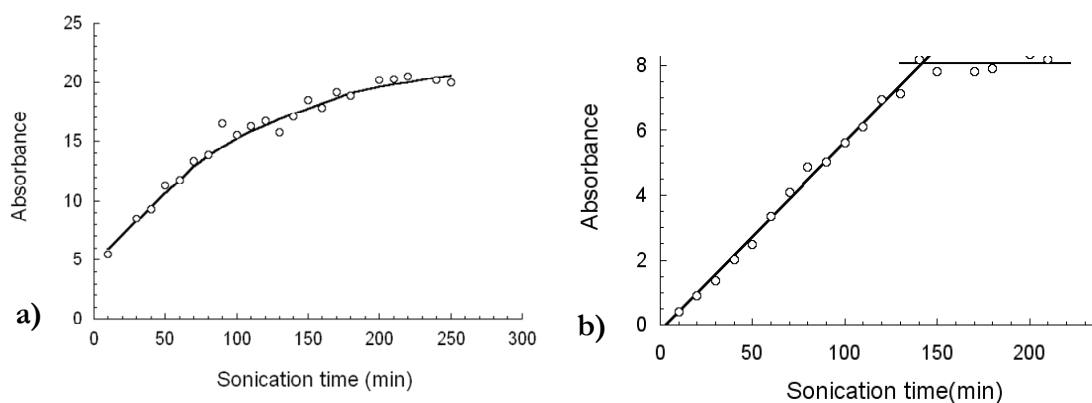


Figure 3. 9 - Area under the UV-vis spectra of a) CTAB-SWNTs and b) Sodium-Cholate-SWNTs aqueous solutions as a function of sonication time

From the absorbance vs. sonication time plot, it can be deduced that the exfoliation occurs during the first minutes of sonication process corresponding to the linear path of the absorbance vs. sonication time. At the plateau, maximum exfoliation occurs and further sonication could induce nanotubes damaging [8]. As mentioned above, even if the resolution of the spectral features improves when a higher fraction of individual nanotubes is in suspension [6], from an analysis of the shape of these spectra it was found that an assignment of one peak to a specific kind of nanotube is not possible, because of the superposition of different electronic transitions deriving from the different CNT species.

3.4.3 Raman spectroscopy analysis

The exfoliation process of the nanotubes in the surfactant solutions was studied using Raman spectroscopy too. Raman spectra were taken with a confocal Raman spectrometer Mod. Aramis, from Jobin-Yvon, operating with a 632.8 nm He-Ne laser source. The incident laser beam was driven through the path of a 50x optical microscope and focused on a 2.0 μm spot into the sample. The 180° back-scattered radiation collected by the microscope objective was focused onto a Peltier-cooled CCD detector (Synapse Mod. 354308) operating in the Raman-shift range 3000 - 50 cm^{-1} .

Sample holders for the the SWNT's-solutions were 200 μm thick glass capillaries. The focus of the microscope was placed in the middle of the capillary to maximize the signal and acquisitions were run in same condition for all samples.

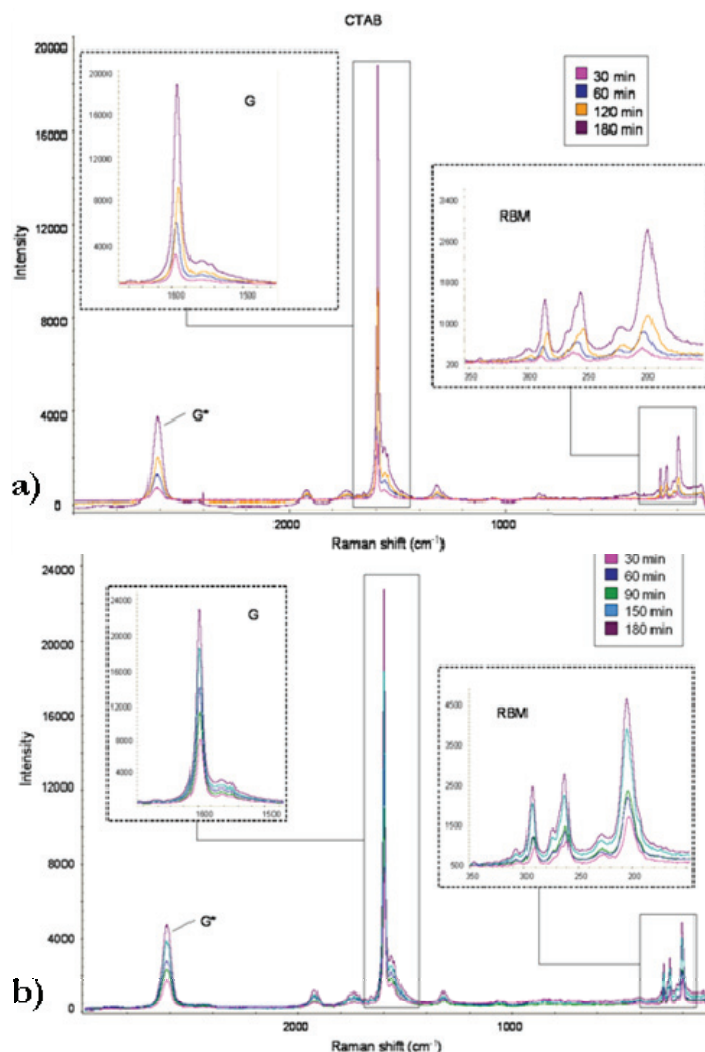


Figure 3. 10 - Raman spectra of a) CTAB-SWNTs and b) Sodium-Cholate-SWNTs aqueous solutions at different sonication times; in the inset a zoom of RBM and G band is reported

In figure 3.10 the Raman spectra of CNTs solutions at different times of sonication for both CTAB and SC surfactants are reported.

The Raman spectra of SWNTs display three characteristic features located, respectively, in the 100 - 500 cm^{-1} wavenumber range (radial breathing modes, RBM), in the 1200 - 1400 cm^{-1} range (disorder-induced D-band) and between 1500 and 1600 cm^{-1} (G bands) [6]. In particular, the radial breathing (a vibration of all Carbon atoms in the radial direction) has a distinct $1/d_t$ diameter dependence, which can be useful to characterize the geometry of the dispersed nanotubes. The very high intensity of the Raman spectra of SWNTs (which allows one to detect concentrations lower than 0.01 wt %) and their strong dependence on laser excitation energy were interpreted in terms of a resonance Raman scattering (RRS) process [12].

According to the RRS mechanism, the amount of unelastically scattered radiation is strongly enhanced by a concurrent electronic transition induced by the laser source. Thus, the gradual increase of intensity of the whole Raman spectrum as a function of sonication time (figs. 3.10 a, b) can be interpreted by arguments analogous to those used for UV spectroscopy. Evidently, also the electronic transitions in resonance with the laser radiation are active for isolated nanotubes, while remaining quiescent for bundles or aggregates and the intensity of the single Raman peaks is proportional to the concentration of exfoliated SWNTs in solution. In view of these effects, it is envisaged that Raman spectroscopy can be even more useful than UV for the characterization of SWNT solutions, since the Raman peaks are fully resolved and more information is available from their quantitative analysis (fig. 3.11 a and b)

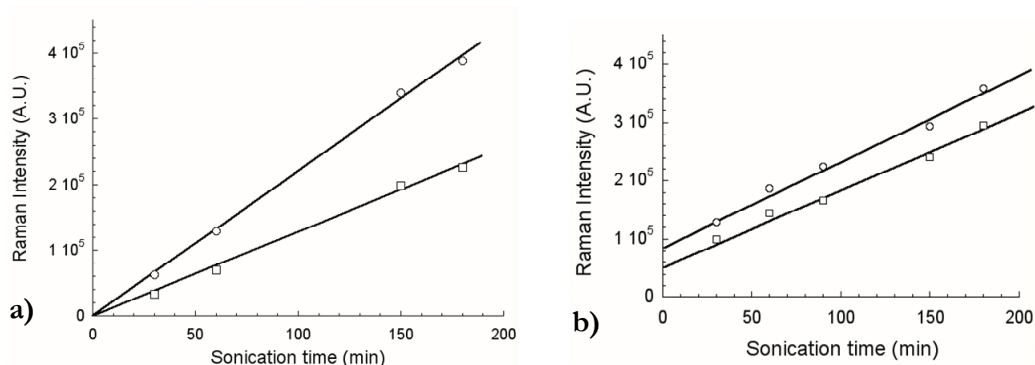


Figure 3. 11 - Areas of G and G* bands as a function of sonication time for a) CTAB - SWNTs and b) Sodium-Cholate aqueous solutions

Intensity of all Raman bands increases upon an increase of sonication time, indicating the enrichment in the solution of species able to involve the Raman scattering process, properly single nanotubes and little bundles, denoting the efficiency of the dispersion method. Moreover,

in figure 3.12 Raman intensity data are reported as a function of UV absorbance, which highlights the strict correlation between the two employed spectroscopic techniques.

From the analysis of all the spectroscopic results, it is possible to notice that Sodium-Cholate is particularly efficient in dispersing SWNTs in water.

Sodium Cholate has been found to be better than CTAB, because it is able to disperse a bigger amount of single nanotubes and little bundles in solution. Its good dispersing ability is due to its molecular structure and anionic nature. From figure 3.4, one can notice the presence in the Sodium-Cholate tail of three six-member rings and one five-member ring. Generally, the benzene ring in a surfactant hydrophobic tail is responsible for its high CNTs dispersing ability, as well as naphthalene phenyl groups [11]. In this case, Sodium-Cholate provides good surfactant-nanotube interaction because of the presence of saturated rings in its hydrophobic tail. The strong anionic nature of the surfactant is, moreover, responsible for the good colloidal stability of the prepared aqueous solutions.

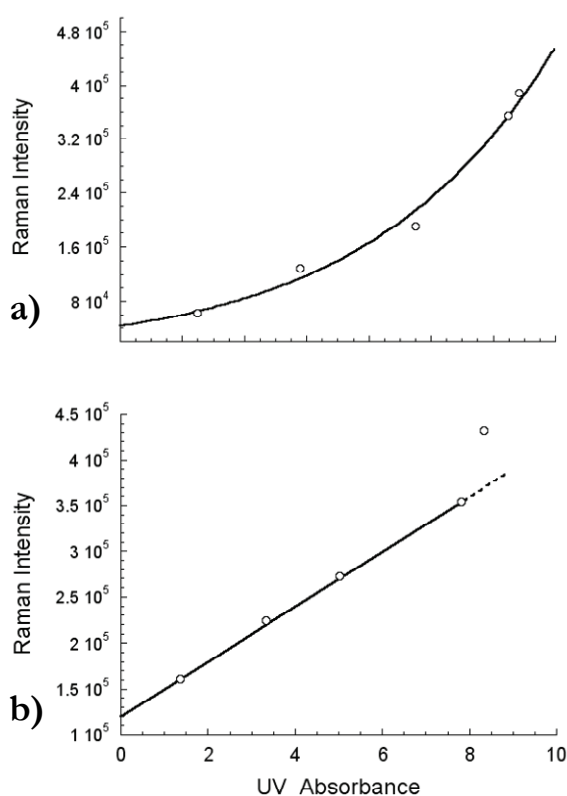


Figure 3. 12 - Raman intensities as a function of UV-vis absorbance for a) CTAB - SWNTs and b) Sodium-Cholate - SWNTs aqueous solutions evaluated at different sonication times

3.4.4 Scanning Electron Microscopy

Microscopic analysis was performed by means of Scanning Electron Microscopy using an ESEM equipped with a field emission electron source (Quanta 600 FEG, Fei).

SEM observations were carried out on 180 minutes sonicated dried solutions deposited on carbon substrates in low vacuum condition and without any coating treatment of the surface. Voltage and current values were optimized for each observation in order to better appreciate the morphological characteristics of the films.

Figures 3.13 a and b and figures 3.14 a and b show SEM micrographs of CTAB and Sodium-Cholate respectively casted film. A substantial difference between the two morphologies can be observed. A network like structure based on a homogeneous coverage of the surface was found for CTAB solution, where isolated tubes and little bundles can be observed. Sodium-Cholate solution presents a non homogeneous surface coverage, with bundles of aligned nanotubes and interstitial regions with networked nanotubes.

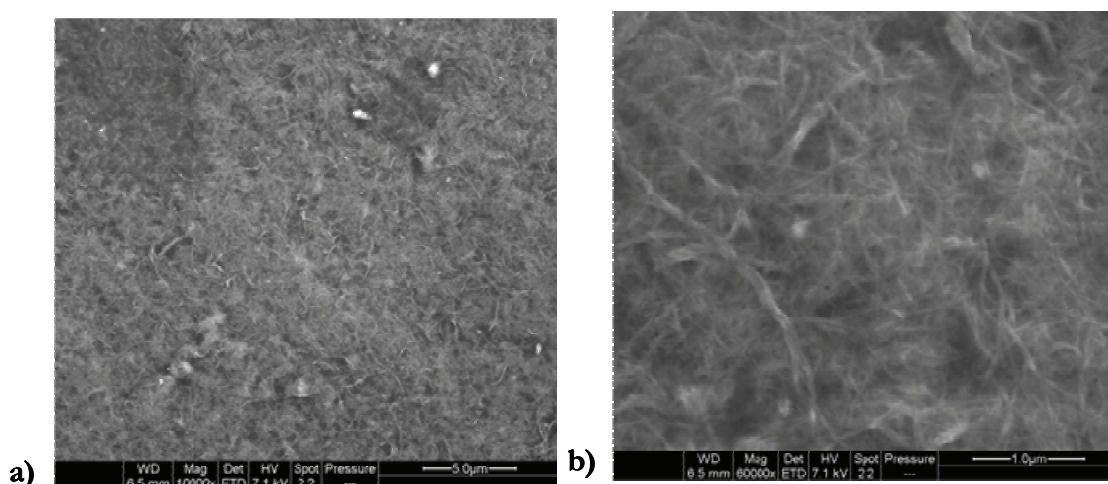


Figure 3. 13 - SEM micrographs of CTAB - SWNTs dried solutions at a) 10000 X and b) 60000 X magnifications

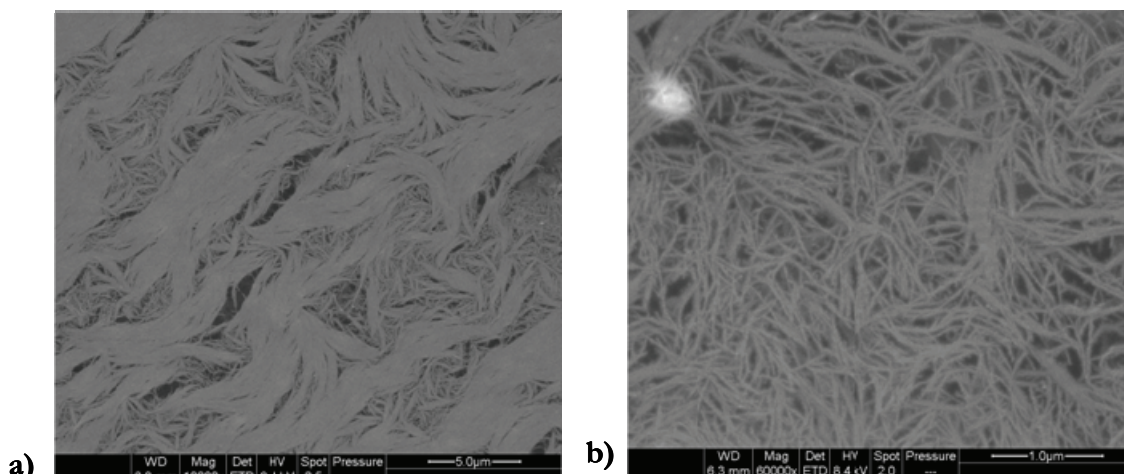


Figure 3. 14 - SEM micrographs of sodium-Cholate - SWNTs dried solutions at a) 10000 X and b) 60000 X magnifications

3.4.5 Atomic Force Microscopy

Atomic Force Microscopic analysis was performed using Nanonics Multiview 1000 AFM/SNOM integrated system.

AFM observations were carried out on 180 minutes sonicated solutions, depositing a droplet of each solution on a mica substrate and allowing water to evaporate before the scanning. All investigations were performed under ambient conditions using a commercial scanning probe microscope equipped with Nanonics AFM glass probes (Cantilevered pulled optical fiber probes) with a terminal diameter of 10 nm, resonance frequencies between 20 and 390 kHz and a nominal cantilever spring constant between 1 and 20 N/m. Tapping mode AFM (TM-AFM) was used as operation mode for all the analysis. In the TM-AFM the cantilever is forced to oscillate with the probing tip at its resonance frequency ω_0 , with an amplitude of A_0 . The cantilever is then brought close to the specimen and got to tap the surface with a given reduced set-point amplitude A_{sp} . As in the usual TM-AFM imaging the specimen surface is scanned at a set-point amplitude A_{sp} kept constant by a feedback loop. During the scan the vertical displacements Δz are displayed as height image reflecting the sample topography. The TM-AFM observations described in the present paper were carried out at a set-point amplitude of 75% in order to achieve the necessary conditions for obtaining optimum topographical information. All figures were elaborated using “WSxM free software downloadable at <http://www.nanotec.es>”.

Figures 3.15 a and b and 3.16 a show a series of AFM height images of different regions of the CTAB-SWNTs film. As shown in figure 3.16 b) the finest observed bundle has a lateral dimension of about 70 nm.

Figures 3.17 (a, b) and 3.18 (a) show a series of AFM height images of different regions of the specimen prepared by SC and SWNTs-solution. As shown in figure 3.18 b) the finest observed bundle has again a lateral dimension of about 70 nm.

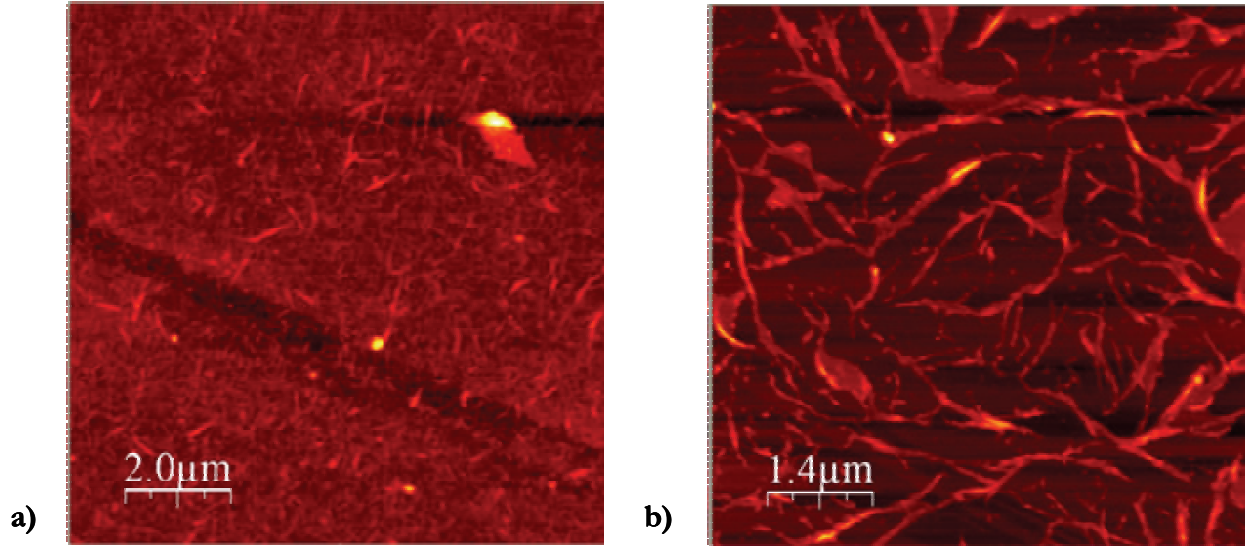


Figure 3. 15 - AFM height images of two different areas (a: $(10 \times 10) \mu\text{m}^2$ and b: $(7 \times 7) \mu\text{m}^2$) of the specimen prepared by CTAB and SWNTs-solution. The contrast covers height variations in the range $0 \div 195.2 \text{ nm}$ and $0 \div 67.2 \text{ nm}$ for a and b respectively

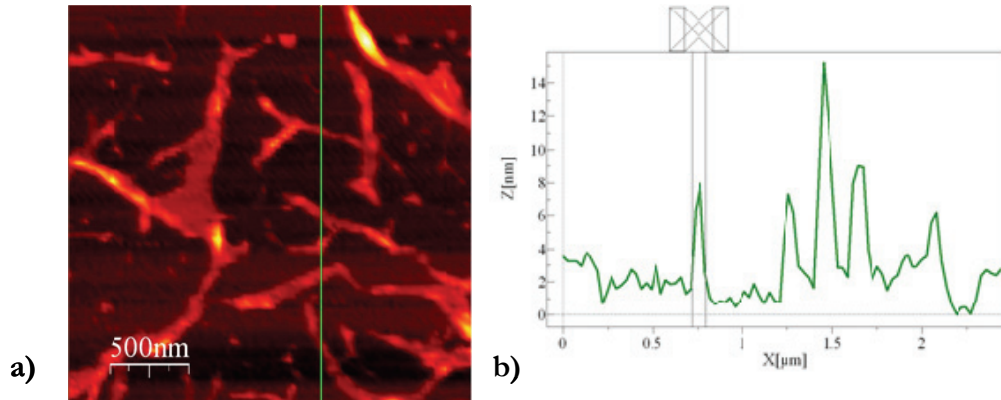


Figure 3. 16 - a) AFM height image of an area $(2.5 \times 2.5) \mu\text{m}^2$ of the specimen prepared by CTAB and SWNTs-solution (the contrast covers height variations in the range $0 \div 37.8 \text{ nm}$ and b) a cross section along the line indicated in figure 3.16 a)

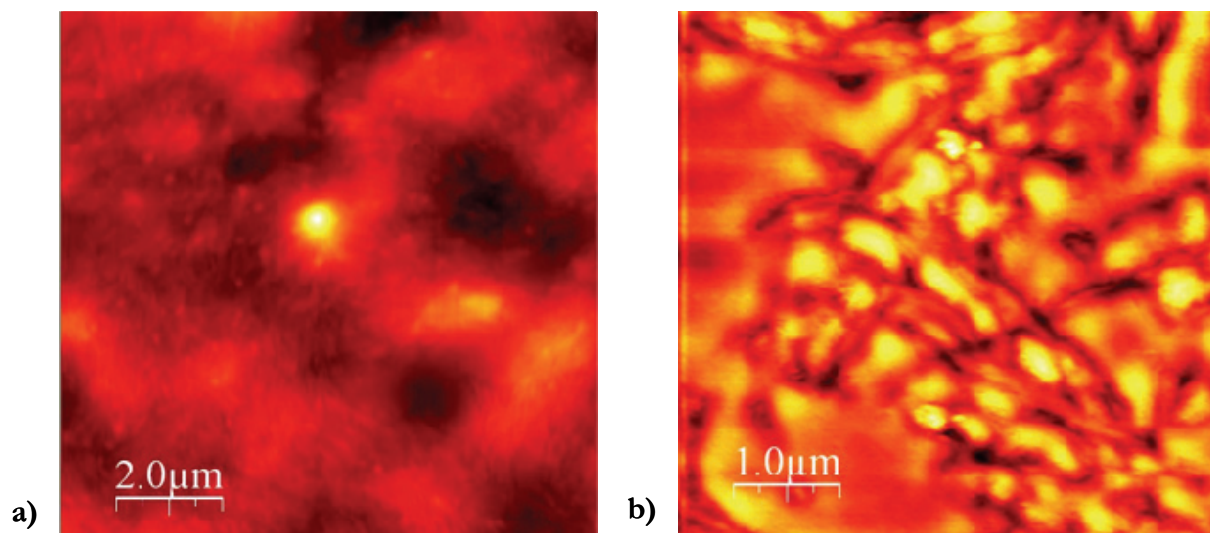


Figure 3. 17 - AFM height images of two different area (a: $(10 \times 10) \mu\text{m}^2$ and b: $(5 \times 5) \mu\text{m}^2$) of the SC-CNT dried sample. The contrast covers height variations in the range $0 \div 116.4 \text{ nm}$ and $0 \div 25.9 \text{ nm}$ for the two images a and b respectively

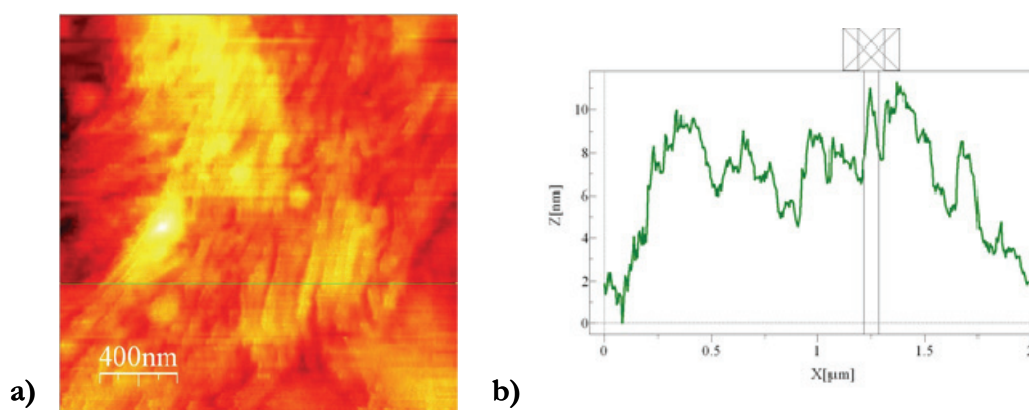


Figure 3. 18 - a) AFM height image of an area $(2 \times 2) \mu\text{m}^2$ of the SC-CNT dried sample (the contrast covers height variations in the range $0 \div 24.4 \text{ nm}$ and b) a cross section along the line indicated in figure 3.18 a)

The reported AFM analysis reveals the different morphological configurations for the two surfactant solutions already observed by SEM analysis, but it provides quantitative information about the minimum size of SWNT's bundle. Even if the drying of surfactant based solutions leads to a sticking of the nanotubes when the water is completely evaporated, little bundles are still observable.

For CTAB and Sodium-Cholate dried solutions from the shown cross section one can notice that the Z dimension, that is the height of the structures, is not higher than 15 nm.

Hence, from the measured structure lateral dimension and height, one can conclude that single tubes and little bundles are either directly attached on the substrate or to other nanotubes layers and stacked one near each other wall to wall. Moreover, from these dimensions one can also

predict that the observed bundles are constituted by an exiguous number of nanotubes, about ten, considering the dimension of the surfactant attached on the adjacent walls.

3.5 Conclusions

In this experimental part, the study of the dispersion process of SWNTs aqueous solutions prepared by using different surfactants as dispersing agents and ultrasonication as exfoliation method has been reported. The dispersion was monitored by means of UV-vis and Raman spectroscopic techniques as a function of sonication time.

The maximum UV absorbance and Raman intensity were found to be related to the maximum exfoliation of CNTs in solution. A strict correlation between the two spectroscopic techniques results was found, demonstrating that both techniques can be considered effective and reproducible methods to investigate the dispersion state of CNTs in solutions.

Raman resulted to be more specific than UV-vis spectroscopy, because its features are very sensitive to isolated CNTs than UV-vis absorbance.

Moreover, two different dispersing behaviors were found for the cationic and anionic surfactants, highlighted by both the spectroscopic results. Sodium-Cholate provided to be more effective, because the maximum exfoliation corresponding to the UV absorbance plateau was reached in a shorter time than in the CTAB dispersion. From Raman spectra analysis, in particular from the deconvolution of spectra in the RBM region, preliminary results show that a correlation between the chemical nature of the surfactants and the SWNTs diameter and chirality can be found. The study of the dependence of the nanotubes chirality on the surfactant nature in terms of selective dispersing ability is still in progress.

3.6 References

1. Thostenson E.T., Ren Z., Chou T.W. - Composites Science and Technology 2001; 61:1899-1912
2. Szleifer I. Yerushalmi-rozen R. - Polymer 2005; 46:7803-7818
3. Matarredona O., Rhoads H., Li Z., Harwell J.H., Balzano L., Resasco D.E. - Journal of Physical Chemistry B, 2003; 107:13357-13367
4. Islam M.F., Rojers E., Bergey D.M., Johnson A.T., Yodh A.G. - Nano Letters 2003; 3:269-273
5. Christian S.D., Scamehorn J.F., Eds., Marcel Dekker, New York 1995
6. Tan Y., Resasco D.E. - Journal of Physical Chemistry B 2005; 109:14454-14460

7. Vaisman L., Marom G., Wagner H.D. - *Advanced Functional Materials* 2006; 16:357-363
8. Ryabenko A.G., Dorofeeva T.V., Zvereva G.I. - *Carbon* 2004; 42:1523-1535
9. Grossiord N., Regev O., Loos J., Meuldijk J., Koning C.E. - *Analytical Chemistry* 2005; 77:5135-5139
10. Grossiord N., Loos J., Meuldijk J., Regev O., Miltner H.E., Van Mele B., Koning C.E. - *Composites Science and Technology* 2007; 67:778-782
11. Kataura H., Umazawa Y.K., Maniw Y., Umezu I., Suzuki S., Ohtsuka Y., Y.Achib - *Synthetic Metals* 1999; 103: 2555-2558
12. Jorio A., Saito R., Dresselhaus G., Dresselhaus M. S. - *Philosophical Transaction of the. Royal Society A* 2004; 362:2311-2336
13. Hu C., Chen Z., Shen A., Shen X., Li J., Hu S. - *Carbon* 2006; 44:428-434
14. Kukovecz A., Kramberger C., Georgakilas V., Prato M., Kuzmany H. - *European Physical Journal B* 2002; 28:223-230
15. Dresselhaus M.S., Dresselhaus G., Jorio A., Souza A.G., Pimenta M.A., Saito R. - *Carbon* 2002; 40:2043-2061
16. Doorn S.K., Heller D.A., Barone P.W., Usrey M.L., Strano M.S. *Applied Physics A* 2004; 78:1147-1155
17. Glamazda A.Y., Dettlaff-Weglikowska U., Leontiev V.S., Mateichenko P.V., Karachevtsev V.A. - *Fullerenes, Nanotubes and Carbon Nanostructures* 2006; 14:221-225
18. Faiella G., Musto P., Di Florio G., Buosciolo A., D'Orazio L., Antonucci V., Giordano M. - *Journal of Nanoscience and Nanotechnology* 2009; 9:6026-6033

Chapter 4

Carbon nanotubes based composites produced using Latex technology

4.1 Introduction

Carbon nanotubes (CNTs) have been attracted great interest due to their wide scope of possible applications, ranging from composite reinforcement materials to nanoelectronics and sensing too. Offering attractive mechanical, electrical and thermal properties, together with a high geometrical aspect ratio L/D , CNTs could constitute a good candidate as nanoscale added fillers to achieve a significant improvement in bulk properties of different types of materials. For example, as conductive filler in polymers, CNTs are quite effective compared to traditional carbon black microparticles.

The current bottleneck to CNTs' application in composite materials field consists in the difficulty of dispersing them in a polymeric matrix. As a result of strong van der Waals interactions, as produced CNTs are tightly bundled in ropes of several tubes and insoluble in aqueous and organic liquids, and thus unprocessable [1]. To unlock the potential of carbon nanotubes for application in polymer nanocomposites much effort has been invested over the last years in achieving good dispersion methods for CNTs in polymer matrices [2]. Some of the nanotubes based composites used the polymer matrix as dispersing medium and the direct two components mixing as dispersion technique, without the use of a second dispersing agent. In these systems, the polymer itself is optimized in order to be a good dispersing agent for the nanotubes or CNTs are functionalized for an enhancement of the compatibility with the matrix. The first method

introduces a limitation on the type of matrix that can be used, because it has to be suitable as dispersing agent for nanotubes; while, for the exploitation of the second method the functionalization of nanotubes is necessary, determining a damaging of the electrical and mechanical properties of the tubes and consequently of the final composite.

It appears evident that a good compromise between the polymer type and the use of a dispersing agent is necessary for the exploitation of the final performances of the composite.

4.2 Latex technology

A useful technique recently developed for the incorporation of CNTs in highly viscous polymeric matrices is Latex technology. This technique can be used with any type of polymer matrix that can be obtained by emulsion polymerization. Stable aqueous solutions of CNTs are obtained by sonicating nanotubes in water using a surfactant as dispersing agent. The aqueous solutions are sometimes centrifuged in order to separate the catalyst particles and big agglomerates. As prepared CNT's solutions are then mixed with the aqueous solution of latex nanoparticles. This composite solution is then freeze-dried in order to obtain a powder that is subsequently processed to prepare a composite consisting of homogeneously dispersed CNTs in a polymer matrix of choice (fig 4.1) [3].

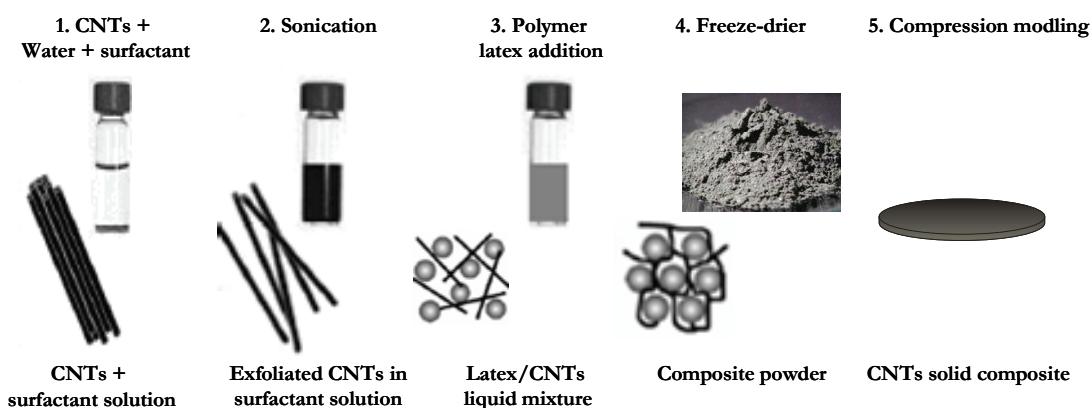


Figure 4. 1 - Schematic description of the multi-step process for the preparation of CNT/polymer composites by using latex technology

Studies reported in literature using emulsion-based approach for the integration of CNTs in polymer composites indicate conductivity percolation threshold values in the range of a few weight percent CNTs [4, 5].

Regev et al. [3] used highly viscous polystyrene as matrix for the preparation of SWNTs based composites, in which these nanotubes were reported to be not dispersible, by means of latex technology, founding out a very low percolation threshold of 0.28 SWNT wt% (fig. 4.2).

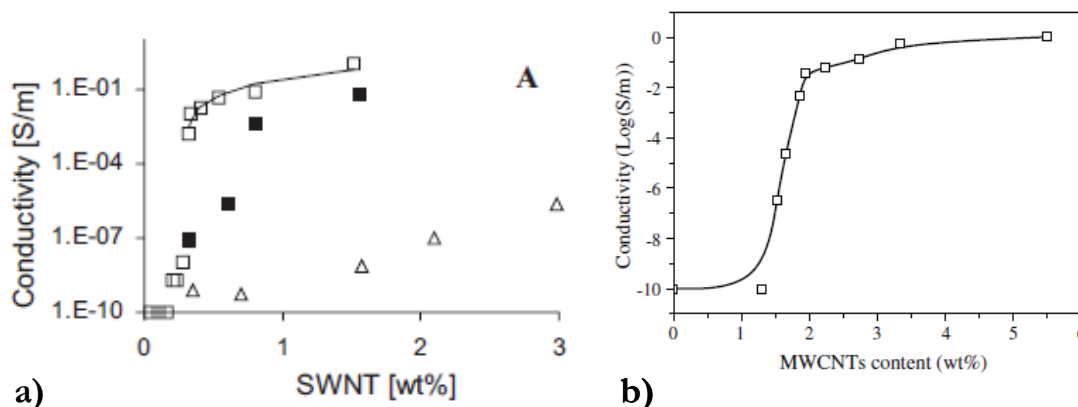


Figure 4. 2 - Electrical conductivity of a) polystyrene/SWNTs [3] and b) polystyrene/MWNT [6] composites as a function of wt%

Together with SWNTs, also MWNTs have been used as fillers in polymer composites obtained using latex technology. Yu et al. [6] investigated the electrical properties of MWNTs dispersed in PS matrix by means of latex technology and found out a percolation threshold of 1.5 wt%.

4.3 Fabrication and electrical characterization of SWNT/polystyrene composites²

In this study, latex technology was used to fabricate SWNT polystyrene composites at different nanotubes content.

DC Electrical measurements have been performed on the composites in order to study the percolative behavior. Moreover, a more accurate study of the electrical properties of the composite system has been carried out by means of impedance spectroscopy technique. On the basis of these results, an equivalent electrical circuit has been proposed to model the electrical behavior of the nanocomposites.

A morphological analysis of the composite has been carried out by means of TEM and SEM. The latter technique has been exploited using the charge contrast imaging mode, that is a particular technique able to visualize nanotubes embedded in polymeric matrices.

² The results reported in this paragraph have been published by Antonucci et al. in [7].

Thermal analysis of the composite at different SWNT content has been carried out, in order to understand the contribution of the nanotubes to the thermal stability of a composite.

4.3.1 Materials and methods

Closed-ended arc-discharge SWNTs were purchased from Carbolex. The tubes average diameter was 1.4 nm with a length of 2-5 μm ; the purity was about 70% and the residual catalysts consisting of Ni, Y particles. Samples include both semiconducting and metallic tubes.

Polystyrene latex at 20 PSwt% ($M_w = 690 \text{ kg/mol}$) was prepared by emulsion polymerization using Sodium Dodecyl Sulfate (SDS) as a dispersing agent in a reactor at 75 °C for 24 hours.

SWNTs (0.2 wt%) were dispersed in an aqueous solution of Sodium Dodecyl Sulfate (1 wt%) by ultrasonication technique (Ultrasonic Processor Fisher mod GEX 500) and then put in the thermal bath for one hour. As prepared solution was centrifuged for one hour, providing a phase-separation into a solid precipitate and an ink-like supernatant, which was decanted and used further.

Calculation of the amount of SWNT in weight percent was based on the assumption that all CNTs were in solution. Actually, the real content of CNTs in solution after the centrifugation was not the same as the initial one. The solid precipitate consisted not only in catalyst particles, but also in heavy carbonaceous nanoparticles and big bundles of nanotubes, so that an undefined amount of nanotubes was lost during the centrifugation. An attempt in evaluating the real amount of nanotubes present in the final solution was done by collecting the solid precipitate, depriving of the water and SDS and then weighting it, so that the remaining material should be only nanotubes. This sediment study led to the conclusion that more than 70% of the raw material was lost during the centrifuge. However, it was not possible to identify the real concentration for each sample, so that the SWNT concentrations indicated in this study are nominal.

Different amounts of the as treated aqueous solution were added to a defined quantity of polystyrene latex in order to prepare composite samples at various SWNT wt% having the same weight (table 1). As prepared composite solutions were freeze-dried over-night. The resulting powders, showed in figure 4.3, were hot-pressed providing thin films having a thickness of about 0.1 mm. A proper pressing cycle has been used for avoiding any air trapping inside the final composite.



Figure 4. 3 - SWNT/polystyrene composite powders resulting from the freeze drying process, from the most concentrated (5 SWNT wt%) to the pure polystyrene

Table 4.1 - SWNT composite samples

Sample	SWNT wt%
Film 1	0
Film 2	1
Film 3	1.5
Film 4	2
Film 5	2.9
Film 6	3
Film 7	5

The powders prepared by solution at a SWNT concentration less than 0.5 wt%, are not homogenous at a preliminary bare eye analysis, presenting visible black agglomerates within a white polystyrene powder. On the contrary, for higher concentration it seems that a homogeneous dispersion was induced in the samples by the described dispersion process. The poor dispersion properties associated to the lower SWNT content can be ascribed to a very small amount of surfactant present in the composite latex solutions. In fact, for each composite solution the latex quantity is always the same, because the final weight of the composite has to be the same for each sample, while the SWNT solution content varies depending on the desired SWNT wt%. When a so small amount of aqueous solution is mixed with the latex, the SDS quantity present in it is not enough to be able to separate the nanotubes and assure the emulsion stability, so the nanotubes tend to agglomerate in big bundles. This effect is also visible in the liquid solution during the mixing of the two components.

4.3.2 Electrical measurements

An extensive experimental analysis was conducted in order to evaluate composites electrical behavior. All composite samples were electrically characterized both in DC and AC mode in order to evaluate percolative and dielectric behaviors

- **Direct Current electrical measurements**

Room-temperature DC conductivity was measured by using a Keithley Picoammeter and Voltage source 6487. Samples (all the films listed in table 1) were shaped in a square form and placed on a plate between two copper electrodes. A tension in the range -50 - 50 V was applied between the electrodes and the current circulating in the samples was measured by the picoammeter and its values were acquired using Labview with a standard IEE-488. Conductivity values for each sample was calculated from current and voltage data and plotted against SWNT wt% in order to evaluate the percolative threshold (figure 4.4).

The introduction of nanotubes increases the conductivity of the composite by up to six orders of magnitude. Between 1.5 and 2 SWNT wt% the composite conductivity displays a dramatic increase by two orders of magnitude. 1.5 SWNT wt% was detected as the percolation threshold for the composite system. This indicates that for weight fractions of SWNTs below 1.5 wt%, nanotubes are almost isolated and the electrical conductivity governed by the electrical characteristics of the polymer.

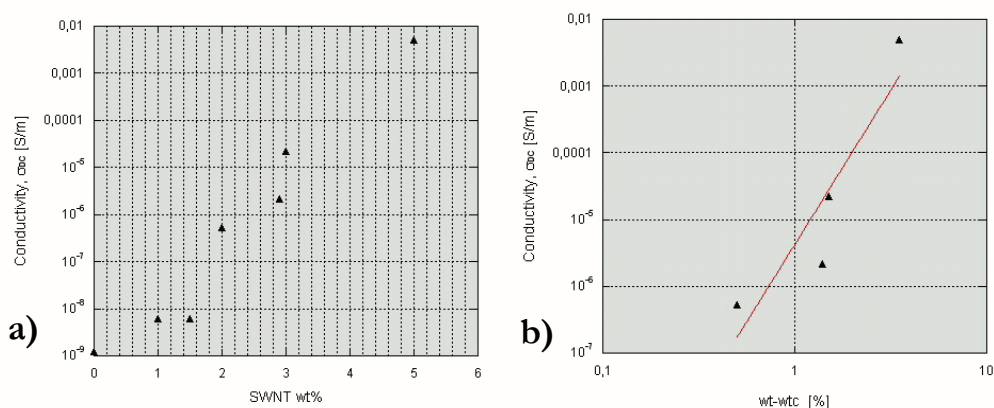


Figure 4. 4 - a) DC conductivity of SWNT-PS composites; b) power law fit of data above percolation threshold

As the fraction of SWNTs increases further, the average distance between the nanotubes becomes sufficiently small for electrons to tunnel through the polymer or to induce contact between nanotubes.

Thus, the electrical response of the composite was described by the power law:

$$\sigma = 2.59^{-6} \cdot (\text{wt} - 1.5)^{4.9} \quad 4.1$$

found out by fitting the data above the percolation threshold (fig. 4.4 b).

From DC electrical data it was also possible to analyze the current-voltage characteristic of the composites at different SWNT concentrations. I-V curves for samples at low and high SWNT

concentrations is nearly linear, while for samples with an intermediate concentration, for example 3 SWNT wt% composite, the trend is not linear (fig. 4.5).

This phenomenon can be addressed to the simultaneous occurring in the composites of different electrical transport mechanisms. Because of the presence of polymer matrix, a series of different mechanisms could occur, such as tunneling and hopping. The concomitance of these different electrical conduction mechanisms, the possible lack in homogeneity of the composite, together with the mixed nature of the raw nanotubes, that can be metallic or semiconducting, could cause deviations from linearity in the IVC.

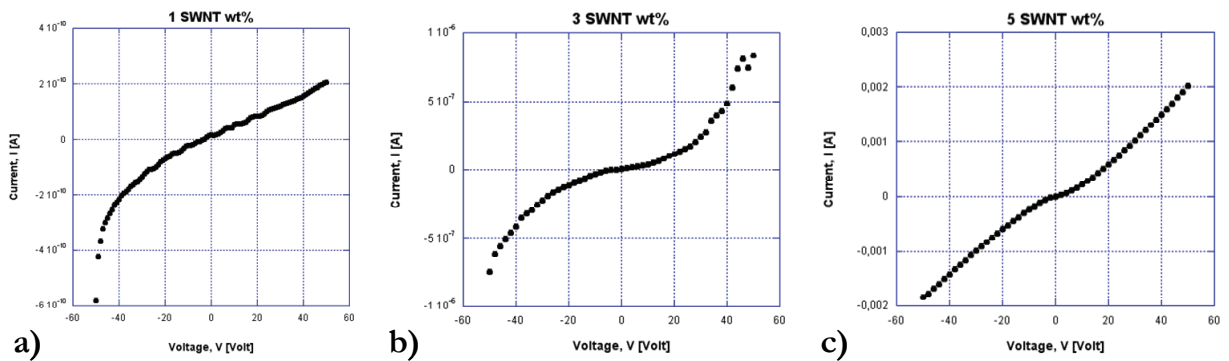


Figure 4. 5 - Current-Voltage characteristics of polystyrene composites at a) 1 SWNT wt%; b) 3 SWNT wt%; c) 5 SWNT wt%

- Alternate Current measurements and dielectric spectroscopy

The use of dielectric spectroscopy in CNT filled systems represents a novel and quite interesting research area. The knowledge of the frequency dependence of complex impedance, expressed as its modulus and phase, is a very useful technique to investigate AC behavior of composite materials [9].

Impedance measurements in a frequency range 42Hz - 5MHz were performed by using a Hioki 3532-50 LCR Tester. A thin Al coating was deposited on both sample surfaces in order to improve electrical contact with the tester leads. Experimental set-up consisted in a capacitor-like system where the sample was placed between two copper parallel surface biased by an alternating voltage.

Hioki Tester data output were recorded by a standard IEE-488, and consist of modulus (Z), real part (R) and imaginary part (X) of the impedance.

Figure 4.6 shows the impedance modulus Z as a function of the logarithm of angular frequency ω (the so-called Bode plot) for some of the samples listed in table 1. Impedance decreases with increasing SWNT content because of the higher conductive filler content.

Moreover, at 1.5 SWNT wt% impedance assumes a constant value in the range 700-4000 Hz. By the analysis of 1.5 SWNT wt% Bode plot the value of resistance can be obtained from the intersection of the frequency-independent line and $\log |Z|$ axis, and it is possible to observe that at higher frequencies the dielectric response is purely capacitive the impedance being directly proportional to frequency with a slope of about $-1 \text{ Hz}/\Omega$. Upon increasing SWNT content this plateau disappears, up to 5 SWNT wt%, where the sample shows a quite nonlinear behavior, approaching a nearly frequency independent value at $f \geq 1 \text{ MHz}$.

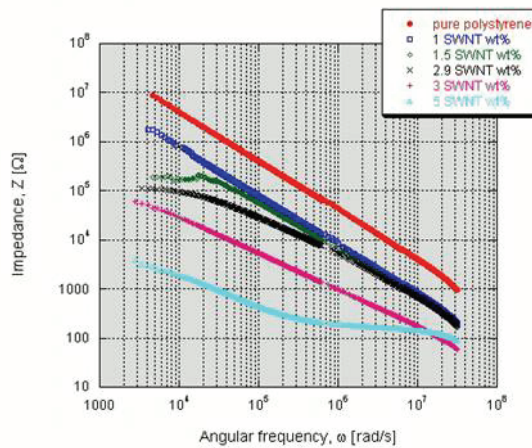


Figure 4. 6 - Bode plot: absolute value of impedance as a function of angular frequency for the SWNT/polystyrene composites

In order to evaluate both the complex conductivity and complex permittivity, and describe their frequency dependence, it is necessary to find a relation between these macroscopic quantities and molecular properties, by postulating a reasonable model able to describe the way the material responds to the applied field.

In this study an “equivalent circuit model” for the composite material in which a resistance and a capacitance are placed in series is proposed, treating the percolative system as a random mixture of resistors and capacitors: carbon nanotubes percolation clusters of high conductivity embedded in a polymer matrix of considerable lower conductivity.

The complex conductivity and the complex permittivity can be written as $\sigma^*(\omega) = \sigma'(\omega) - i\sigma''(\omega)$ and $\epsilon^*(\omega) = \epsilon'(\omega) - i\epsilon''(\omega)$, respectively. The real part of AC conductivity, *i.e.* $\sigma'(\omega)$, for selected nanotube concentrations is presented in figure 4.7 a as a function of angular frequency, while the imaginary part of permittivity, *i.e.* $\epsilon''(\omega)$, is shown in figure 4.7 b. Composites with a SWNT content lower than 1.5 SWNT wt% show a weak frequency dependence of ϵ'' , whereas at SWNT contents higher than 1.5 wt% ϵ'' decreases appreciably with increasing frequency.

Extrapolated static values of the DC conductivity as $\sigma_{AC} (\omega \rightarrow 0)$ are in agreement with conductivity values measured in DC mode. The percolation composition is confirmed to be 1.5 SWNT wt%, since at this value of concentration a significant change in conductivity is observed. In figure 4.8 the real part of permittivity is plotted against angular frequency. Composites with SWNT content lower than 1.5 SWNT wt% have a nearly constant ϵ' value, whereas composites with SWNT loading higher than 1.5 SWNT wt% show significant deviations from the previous law.

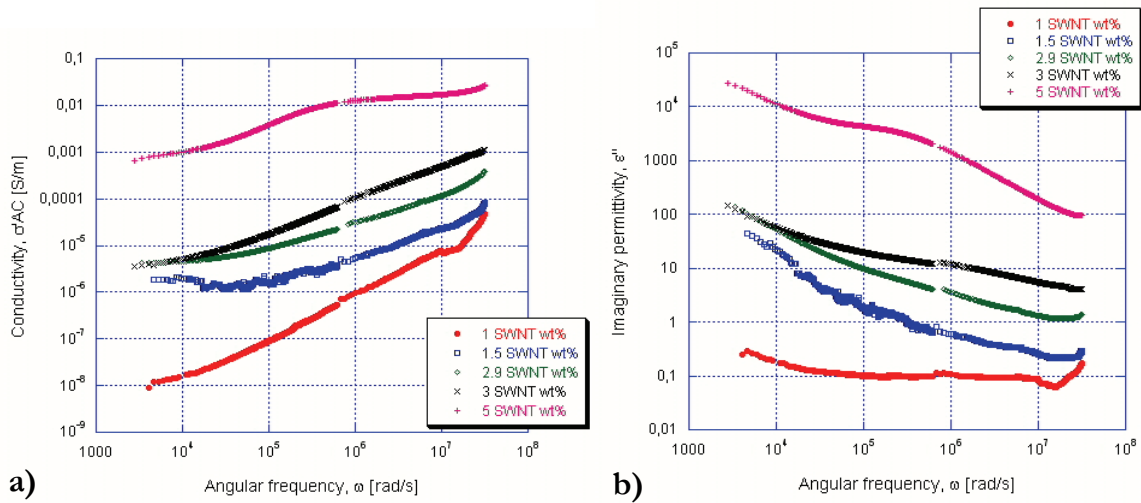


Figure 4. 7 - a) AC conductivity σ' and b) imaginary part of complex permittivity for polystyrene composites at various SWNT wt%

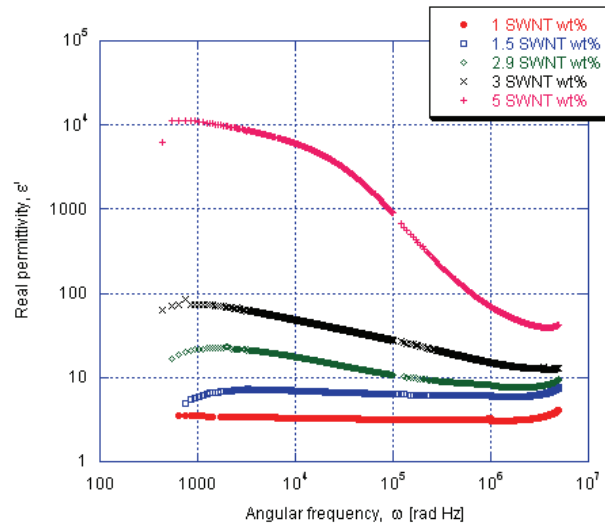


Figure 4. 8 - Real part ϵ' of complex permittivity for PS - SWNT composites of various SWNT content

Experimental data allow to estimate the static permittivity $\epsilon_s = \epsilon'$ in the limit $\omega \rightarrow 0$. Static permittivity's composition dependence was found to be:

$$\varepsilon_s \propto |wt - wt_c|^{-s} \quad 4.2$$

for both $wt > wt_c$ and $wt < wt_c$ [9, 10] where wt_c is the percolative threshold. Static permittivity is expected to diverge in correspondence of percolation threshold, increase with increasing SWNT content approaching the percolation threshold at small concentrations and decrease above.

In figure 4.9 extrapolated values of static permittivity ε_s are plotted against SWNT content. It is possible to observe that ε_s increases above wt_c but does not decrease as expected from the theoretical law (3). Such a behavior can be related to a phenomenon occurring in nanocomposites, reported earlier for polymer composites containing carbon black [11]. It can be addressed to the presence of “micro-capacitors” that remain in the composite also above wt_c . Such capacitors are probably constituted by a gap between CNT filled by some insulating polymer matrix. Nevertheless, the occurrence of these micro capacitors is unavoidable, because of the presence of CNTs not contributing to the percolation network and the free ends of the percolation structure cannot be ruled out.

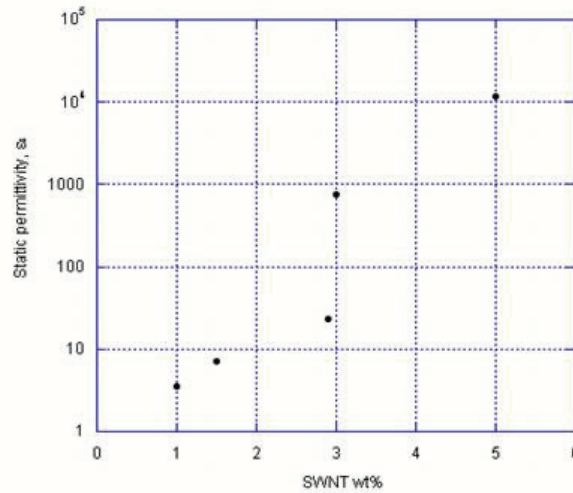


Figure 4. 9 - Static permittivity $\varepsilon_s = \varepsilon'(\omega \rightarrow 0)$ versus SWNT wt% in PS composites

In figure 4.10 phase angle Φ , representing the out of phase between current and voltage, is plotted against the angular frequency, ω . Φ was evaluated from imaginary and real parts of impedance:

$$\Phi = \arctg \frac{X}{R} \quad 4.3$$

A frequency-constant capacitance is shown by the pure polystyrene, that behaves like a dielectric material with a phase angle of about -90° . Upon increasing SWNTs content, phase angle shows a not linear trend as function of angular frequency. Because of the conductive nature of nanotubes, the material loses its dielectric nature, behaving more and more as a conductor. Moreover, this

curve confirms that the conductive nature is predominant at low frequencies, while at higher frequencies the capacitive behavior provides a constant value for the phase curve. As mentioned above, the different behavior for 5 SWNT wt% sample can be observed also in the phase curve. For this sample, the phase is not linear for the entire frequency range, as the other samples, but moreover, it doesn't show a constant value of the phase at high frequencies. This phenomenon can be due to the conductive nature of the composite where SWNT's content is predominant on the dielectric polymer.

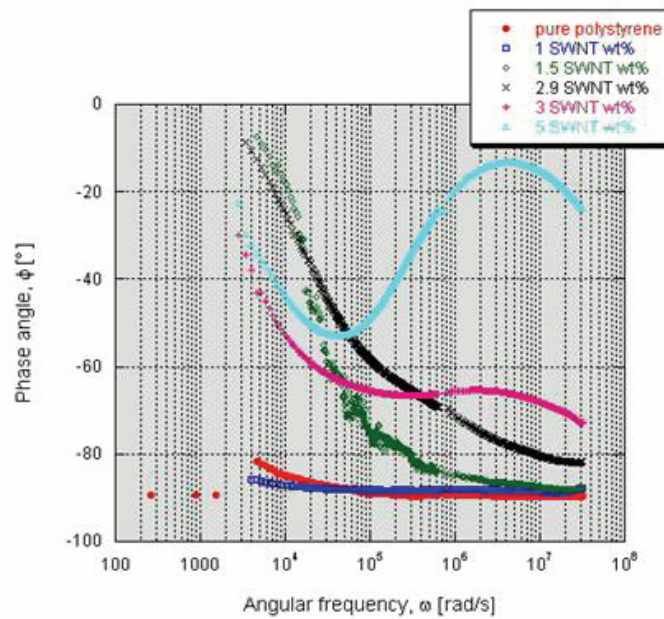


Figure 4. 10 - Phase angle of SWNT-PS composites as a function of angular frequency

4.4 Equivalent electrical circuit for SWNT/polystyrene composites

In order to better understand the mechanism governing the composite AC behavior an attempt to electrically model the material was done.

The simplest modeling approach for a dielectric material is a R-C parallel circuit. However, in the case of a composite constituted by polymer matrix and nanotubes, the model should be more complex, in order to account the not ideal conductive behavior of nanotubes and the not ideal capacitive behavior of polymer. In this study, the nanocomposite was modeled as a circuit where a series of a resistance and a capacitance was in parallel with a parallel of a resistance and a capacitance. The first series represents the conductive nature of the composite, that consists in the nanotubes, and the parallel represents the polymer matrix (figure 4.11).

conductive nature of the composite can be detected at low frequencies and the capacitive one at higher frequencies (figure 4.12).

A good agreement between experimental and fitted data was found, that confirms the good formulation of the equivalent circuit, that is hence able to describe the interaction between the percolative nanotubes network and the surrounding polymer matrix.

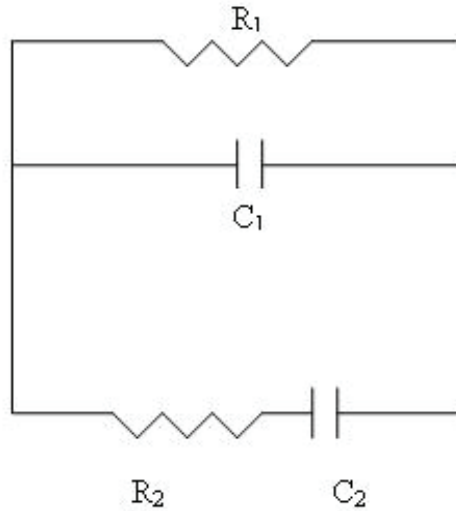


Figure 4. 11 - Electrical equivalent circuit modeling 1.5 SWNT wt% composite

Table 4.2 - Best fitting parameters

Parameter	Value
R_1	$7.380\text{e}+08$ [Ω]
C_1	$1.085\text{e}-09$ [F]
R_2	$1.858\text{e}+05$ [Ω]
C_2	$1.350\text{e}-06$ [F]

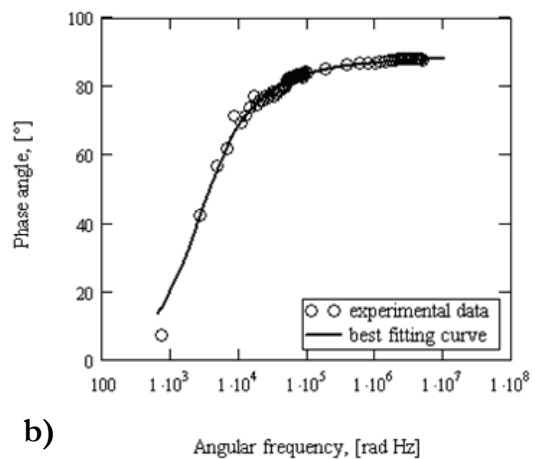
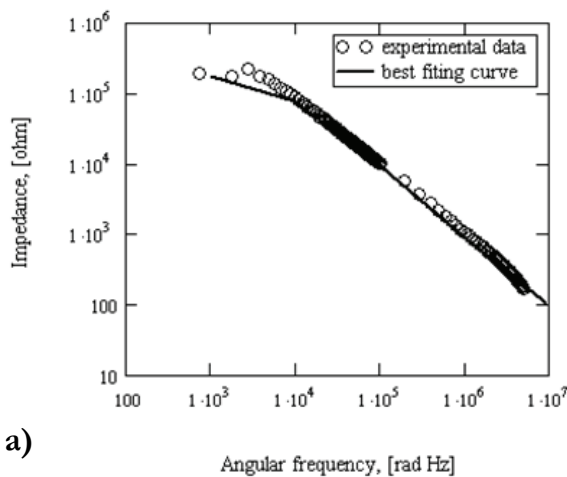


Figure 4. 12 - Best fitting of a) impedance and b) phase angle data: the solid line represent the fit curve and the dots represent experimental data

In this model four parameters were identified: R_1 , C_1 , R_2 , C_2 . These parameters have been used to best fit experimental data. The best fitting was performed on Z modulus and phase angle of 1.5 SWNT wt%, that corresponds to the percolative threshold concentration. Parameters values are indicated in table 4.2. R_1 and C_1 represent polymer properties and R_2 , C_2 the conductive nature of composite. The first two parameters affect Z modulus fitting curve in its high frequency region, while the other two parameters influence its low frequency region, coherently to the fact that the

4.5 Morphological analysis of SWNT/polystyrene composites

In order to understand the physical mechanisms involved for charge transport and able to assure the conductive nature of the composite, it would be very useful the knowledge of the local organization of nanotubes in the percolative network. However, direct microscopic observation of SWNT dispersion in the polymer matrix is very difficult to apply, due to the extreme smallness of the nanotubes and their high aspect ratio. The observation and the identification of nanotubes in a polymer matrix with conventional techniques is more difficult because of the similar nature of nanotubes and polymer matrix that provides a low contrast between the two phases.

In this study two microscopic techniques were used to analyze the composite's morphology: Transmission Electron Microscopy and Environmental Scanning Electron Microscopy used in charge contrast imaging mode. The first technique allows the observation of single nanotubes and the identification of their geometry, the second one provides the possibility of understanding nanotubes distribution in the polymer matrix and a sort of their bulk organization.

4.5.1 Transmission Electron Microscopy

Room-temperature TEM characterization of the composite films was conducted after embedding a 5 SWNT wt% sample in an epoxy resin and sectioning the cured composite by microtome. Direct microscopic observation of the SWNT dispersion in nanocomposites is difficult to apply due to their extreme high aspect ratio, i.e. the extreme difference in radial and axial dimensions. Figure 4.13 shows a SWNT having a diameter of about 2 nm and a few darker catalyst particles in its vicinity.

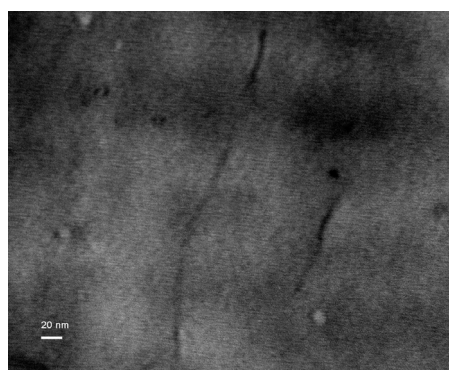


Figure 4. 13 - TEM micrograph of a 5 SWNT wt% sample

4.5.2 Environmental Scanning Electron Microscopy: charge contrast imaging mode

Based on results obtained by TEM it is difficult to draw conclusions about homogeneity of the SWNT distribution in the matrix, hence of organization of the conductive network. In order to go over this problem a room temperature SEM characterization was performed by means of an Environmental Scanning Electron Microscope equipped with a field emission electron source (Quanta 600 FEG, Fei) applying high vacuum conditions and using a secondary electron detector for image acquisition. No additional treatment such as sample coating with conductive layer was applied. Because of the different capabilities for charge transport of the conductive nanotubes and the insulating polymer matrix, SWNTs appear like bright lines in a dark surrounding. This technique for the observation of nanotubes embedded in polymeric matrices is known as “charge contrast imaging mode”.

Charge contrast imaging is not possible at low acceleration voltage, because SWNTs charging is prevented. In this study acceleration voltage of 20 kV and 25 kV were used.

Figure 4.14 shows two high resolution SEM images of two different regions of a SWNT-PS composite at a 2 SWNT wt% and figure 4.15 shows two SEM images of the same part of the 3 SWNT wt% sample at two different magnifications. By the comparison of TEM and SEM images it is possible to note that nanotubes dimensions appear different. This phenomenon can be explained by the local charging of the polymer matrix around the SWNTs, that renders the average diameters of nanotubes larger than the value measured by TEM. From images analysis, it is possible to observe that a substantial amount of CNTs is homogeneously distributed over the entire area of the image, allowing the assumption that the overall distribution of the nanotubes is homogeneous in the sample and providing the presence of the percolative network responsible for the composite conductive nature.

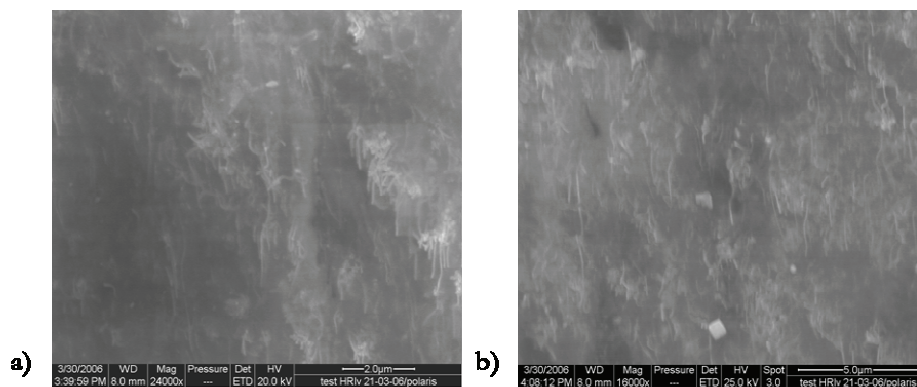


Figure 4. 14 - High resolution SEM images of a 2 SWNT wt% sample using an acceleration voltage of a) 20kV and b) 25kV

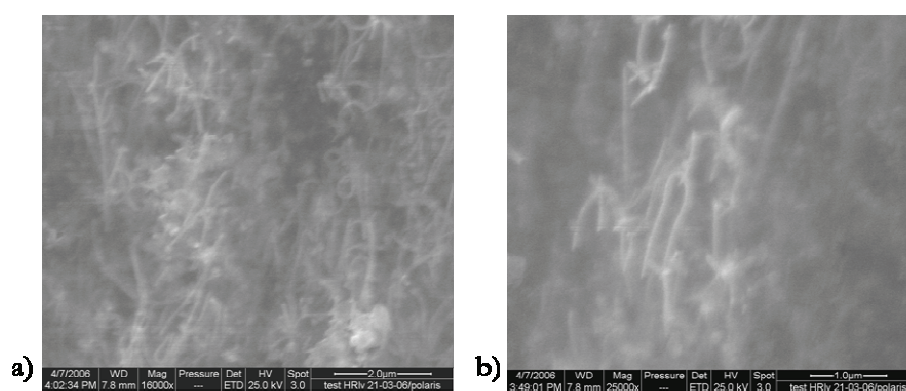


Figure 4. 15 - a) Overview and b) high resolution SEM images of a 3 SWNT wt% sample using an acceleration voltage of 25 kV showing straight and bended SWNTs.

4.6 Thermal properties of SWNT/polystyrene composites

Thermal properties of CNT/polymer composites also attracted many attentions from scientists because CNTs have very high thermal stability. The addition of CNTs in polymer matrix can cause some composites to degrade at lower temperature [12] or to promote an increase in thermal stability [13]. The structure of the polymer matrix and the interaction between CNTs and the matrix may be the key factors for the thermal degradation behaviour of CNTs filled polymer composites.

In this study, thermogravimetric analysis on five samples at different SWNT wt% (films 1, 2, 3, 7) was performed using a HiRes TGA 2950 Thermogravimetric Analyzer (TA Instruments). The thermal decomposition studies of the composites were performed over a temperature range of 30-1000 °C under air environment at the heating rate of 10 °C/min. TGA curves of pure polystyrene and SWNT-PS composites are shown in figure 4.16.

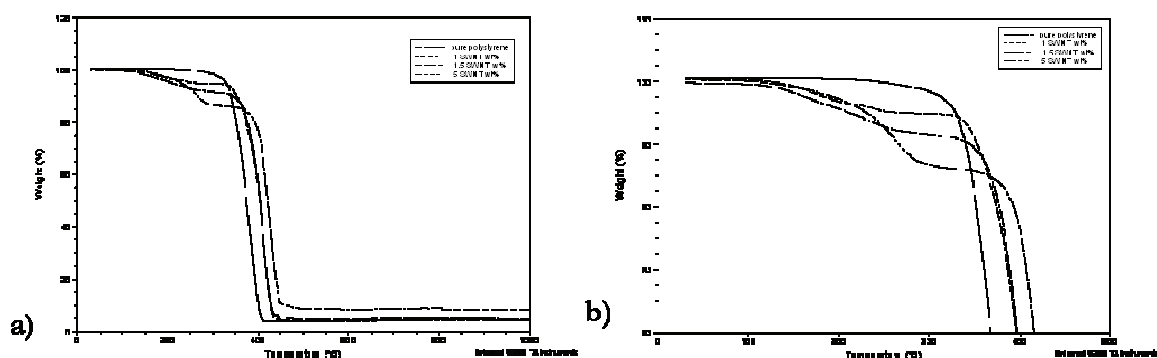


Figure 4. 16 - a) TGA curves of SWNT-PS composites with different SWNT content under atmosphere and b) a zoom of the curves in the range 30-500°C

One step decomposition is found for the pure polymer and a two-step decomposition for the composite samples in the range 30-450 °C. The presence of CNTs induces the comparison of a plateau that is lower for higher SWNT wt%.

Pure polystyrene starts to lose weight at 98 °C and is burned out at 417 °C. The oxidation of the composites starts with PS oxidation, because CNTs generally starts to degrade at about 500 °C. Many researchers have reported that CNTs can stabilize polymer [14]. Our observation is similar, as can be seen in figure 4.16 b degradation temperature of the composite increases upon an increase of SWNT content. The increased thermal stability of SWNT-PS composites over that of the pure PS is likely to be a result of absorption, by activated carbon nanotubes surface, of free radicals generated during the polymer decomposition.

4.7 Conclusions

In this experimental part, SWNTs/polystyrene composites at different filler concentrations have been fabricated using Latex Technology, with the aid of a surfactant as dispersing agent. Microscopic analysis using Scanning Electron Microscopy in charge contrast imaging mode has been performed on the samples, in order to visualize the CNTs dispersion inside the matrix.

Electrical characterization both in DC and AC modes was performed on the composite samples for the investigation respectively of their percolative and dielectric behavior. By the study of the impedance and phase angle dependence on frequency, an equivalent electrical circuit model has been formulated to describe the electrical behavior of the composite sample corresponding to the percolative threshold. Both the non ideal capacitive and conductive natures respectively of the matrix and the nanotubes has been taken into account for the identification of the model parameters. The good agreement found between experimental and fitted data has lead to the

conclusion that the formulated equivalent circuit was able to describe the composite nature of this analyzed material. Together with electrical also thermal properties have been investigated, demonstrating an enhancement of the thermal stability of the CNT's composites respect to the neat polymer.

4.8 References

1. Thostenson E.T., Ren Z., Chou T.W. - *Composites Science and Technology* 2001; 61:1899-1912
2. Szleifer I., Yerushalmi-rozen R. - *Polymer* 2005; 46:7803-7818
3. Regev O., ElKati P.N.B., Loos J., Koning C.E. - *Advanced Materials* 2004; 16:248-251
4. Barraza H.J., Pompeo F., O'Rear E.A., Resasco D.E. - *Nano Letters* 2002; 2:797-802
5. Dufresne A., Paillet M., Putaux J.L., Canet R., Carmona F., Delhaes P., Cui S. - *Journal of Materials Science* 2002; 37:3915-3923
6. Yu J., Lu K., Sourty E., Grossiord N., Koning C.E., Loos J. - *Carbon* 2007; 45:2897-2903
7. Antonucci V., Faiella G., Giordano M., Nicolais L., Pepe G.P. - *Macromolecular Symposia* 2007; 247:172-181
8. McLachlan D.S., Chimete C., Park C., Wise K.E., Lowther S.E., Lillehei P.T., Siochi E.J., Harrison J.S. - *Wiley InterScience* 2005
9. Bergman DJ, Imry Y. - *Physical Review Letters* 1977; 39:1222-1225
10. Stroud D., Bergman DJ. - *Physical Review B* 1982; 25:2061-2064
11. Flandin L., Prasse T., Schueler R., Schulte K., Bauhofer W., Cavaille J.Y. - *Physical Review B* 1999; 59:14349-14355
12. Yang S.Y., Castilleja J.R., Barrera E.V., Lozano K. - *Polymer degradation and Stability* 2004; 83:383-388
13. Kashiwagi T., Grulke E., Hilding J., Harris R., Awad W., Douglas J. - *Macromolecular rapid Communications*
14. Zou Y., Feng Y., Wang L., Liu X. - *Carbon* 2003; 42:271-277

Chapter 5

Tuning of the insulator to conductor transition in MWNTs/epoxy composites

5.1 Introduction

As reported in the previous chapters, the final properties of a CNTs polymer composite strongly depends on dispersion technique and processing parameters. The process used for the dispersion of the nanotubes within the matrix is related to the chemical and physical nature of the hosting polymer, hence a different technique is used if the matrix is a thermoplastic or a thermoset polymer. Moreover, an efficient exploitation of the electrical and mechanical properties of the final composite is related to the morphology of the CNTs networks forming within the matrix. This morphology is strongly affected by the chemical interactions between the nanotubes and the surrounding matrix and by external forces acting as modifier of the filler-polymer system.

In this chapter, after a brief description of the scientific background, with some reminds to previously treated subjects such as dynamic percolation and SAXS analysis, the main experimental work on thermoset CNTs composites is presented. The manufacturing techniques used for the production of thermoset polymer based CNTs composites are described. Moreover, experimental results on the characterization of the physical properties of CNTs/epoxy resin composites are reported. Finally, the discussion will focus on the effects of the processing on the composites physical properties and a model for the explanation of the morphology organization of CNTs network is proposed.

5.2 Dynamic percolation and hierarchical morphology of CNTs networks

In chapter 2, a panoramic view of the CNTs polymer properties as well as of the problems related to the manufacturing of high performances composites has been reported. It was illustrated how polymer nanocomposites have attracted enormous interest from the scientific community because of their theoretically promising substantial improvement of mechanical and electrical properties at very low filler loadings. As it was possible to understand in the discussion about percolation in CNTs polymer composites reported in chapter 2, a strong dependence on the manufacturing process and dispersion procedures exists for the final composites physical properties.

Kovacs et al [1] investigated the effect of shear rates on the promotion of a particle network at concentrations below and above the statistical percolation threshold. Their system consisted of MWNTs dispersed in an epoxy resin which possesses a fluid state of low viscosity during processing. Variable shear rates were exerted by controlling the stirring rate of the agitator and the temperature of the dispersion during the final mixing step. They demonstrated that two types of percolation thresholds exist for composite systems possessing a fluid state of low viscosity during processing. The higher threshold is determined by statistical percolation theory and therefore is unchangeable by processing methods. The lower one can be shifted down to lower concentrations by stimulating particle flocculation and network formation.

Through the comparison of the conductivity measurements with light microscopy images, it was possible to note that the emergence of flocs and the steep conductivity increase occurred at lower filler concentrations than predicted by percolation theory for statistically distributed particles (fig. 5.1).

As it was previously discussed, this phenomenon can be addressed to the existence of a percolation characterized by kinetic nature that overlaps the statistical one. In light of the reported results, it seems that engineered materials having specific characteristics can be produced by tuning the final physical properties of the composites through a proper manufacturing process. In this context it appears evident how big is the importance of the knowledge of the network morphology existent within CNTs polymer composites.

In fact, although claims of exceptional enhancement of mechanical and electrical properties exist, these claims are often offset by measurements that show little or no improvement, especially for the mechanical performances. The lackluster performance of nanocomposites has been attributed to a number of factors including poor dispersion, poor interfacial load transfer or poor contact in conductive networks. In this context, the filler morphology is a key factor for understanding why some polymer nanocomposites had a great commercial success (i.e. carbon black filled rubber)

while others demonstrated marginal performances. When nanoparticles are considered as fillers for polymer composites, whatever can be their dimensionality, it is worth noting that their morphology has a great impact on the physical properties of the final composite. Because of high attraction forces existent at this low dimensional scale, even well dispersed nanofillers naturally aggregate to form clusters whose size extend to length scales exceeding $1\ \mu\text{m}$ [2].

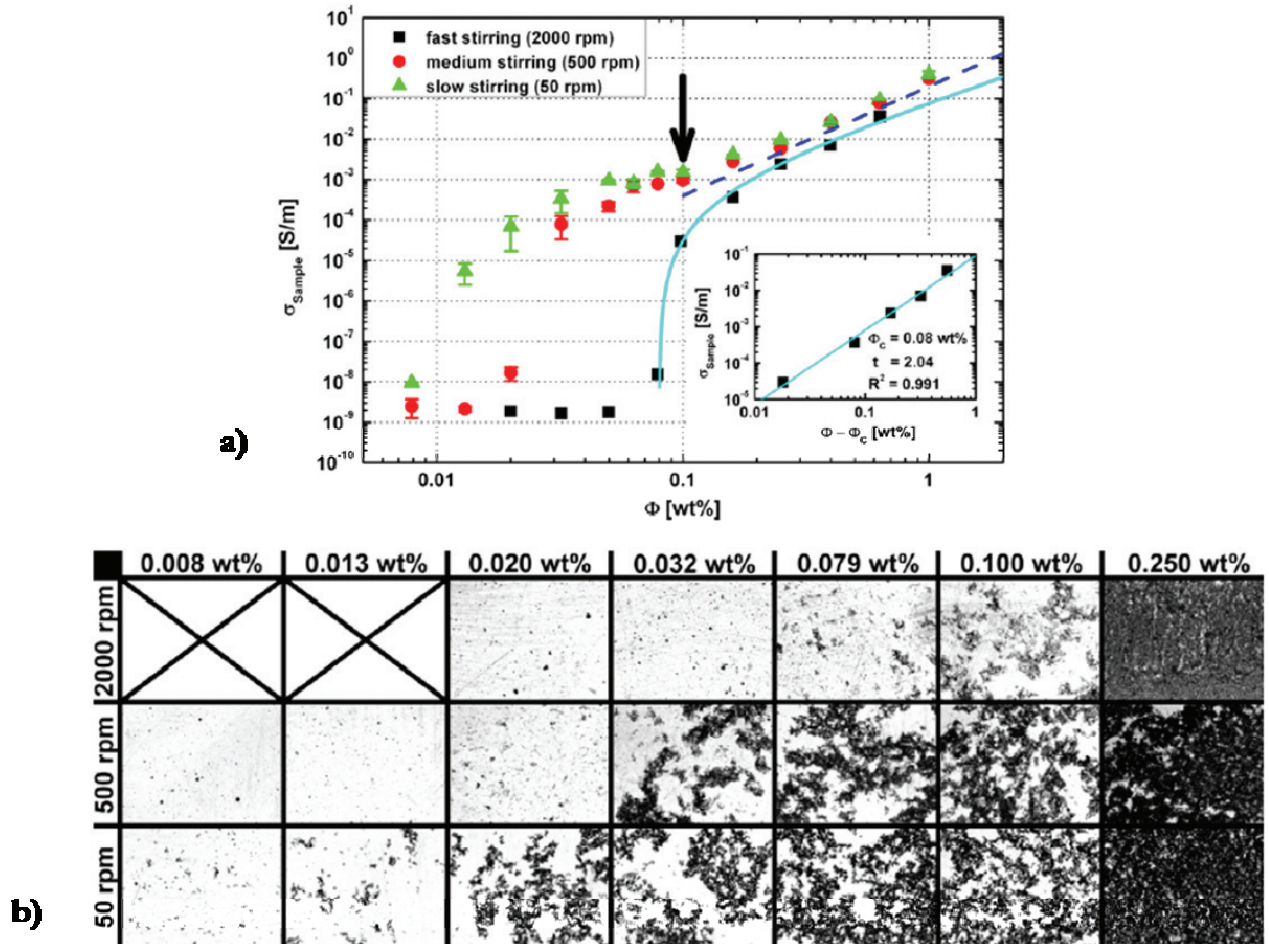


Figure 5.1 - a) Comparative log-log plot of the MWNT/epoxy composites conductivity as a function of nanotube weight fraction for different sample preparation methods and b) the corresponding optical microscopy images

Due to its two dimensional nature, imaging is of limited value when analyzing network morphology of nanocomposites. Optical microscopy, SEM, TEM all produce two-dimensional images. However, filler network within composites are three-dimensional, hence the characterization of such networks is compromised on the onset if treated only by means of these techniques. One of the investigations techniques used for the determination of the degree of dispersion of such nanoparticles within polymer matrices is X-ray scattering, that is a promising tool for the evaluation of the large-scale morphology of nanocomposites, because it provides quantitative, three-dimensional, morphological information. Microscopy and scattering are

actually complementary and experimental data from each of these techniques are useful for the understanding of the particles network morphology [3].

In figure 5.2 a combined light scattering and ultra-small angle X-ray scattering (USAXS) plot of data from SWNT/water solution are reported [4].

The most notable feature of the profile is the absence of a power-law scattering with an exponent of -1, that is the signature of the presence of a one-dimensional scatterer. Over the entire region where a rodlike power-law (slope -1) profile is expected, the measured intensity of orders of magnitude greater than the value calculated assuming isolated SWNTs [5].

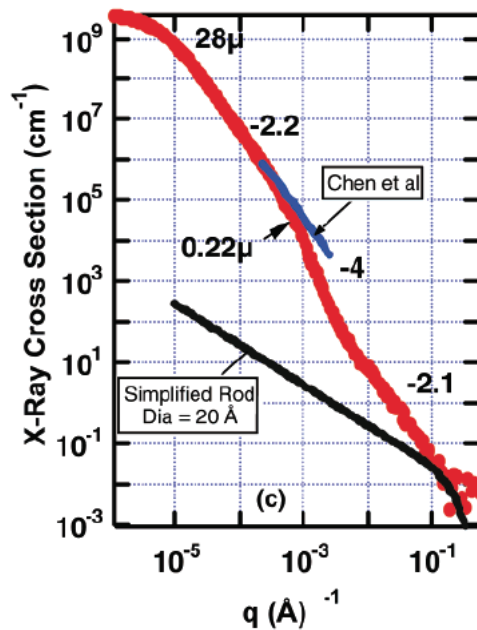


Figure 5. 2 - Small-angle scattering (SAS) data on SWNTs water solution [2]

The excess scattering at small q presumably arises because SNWTs clusters are present. Clustering leads to larger mass per unit volume and therefore enhanced intensity at small q . These clusters can be visualized by optical microscopy, even if their internal structure cannot be resolved using this technique. From SAXS analysis, one can calculate the dimension of the rope and by a comparison between them and the dimensions resulted by SEM, it is possible to figure out a morphology organization of the nanotubes in solution. Brown et al. [6] proposed a hierarchical morphology for the explanation of the CNTs disordered ropes organization on two length scales but retains some semblance of ropelike character (fig. 5.3). On large scales there is a network of ropes, that are constituted themselves by isolated SWNTs at a smaller length scale. Instances have been reported in literature where power-law scattering with exponents of -1 has been observed in SWNTs suspensions [7], while, generally, the visualization of carbon nanotubes embedded in polymer matrices is very difficult, especially SWNTs.

Because of the difficulty in gathering light scattering data on solid samples, direct evidence regarding the large-scale morphology of nanotubes in solid matrices is sparse.

Brown et al. [6] analyzed the scattering data from SWNT/Epoxy composites, founding out that no Guinier crossovers were present, even at high sonication times, hence it was not possible to associate any length scales with the dispersed nanotubes. They concluded that SWNTs were aggregated on all observable length scales, because the micro-sized aggregates were so large to exceed the resolution of the USAXS (fig 5.4)

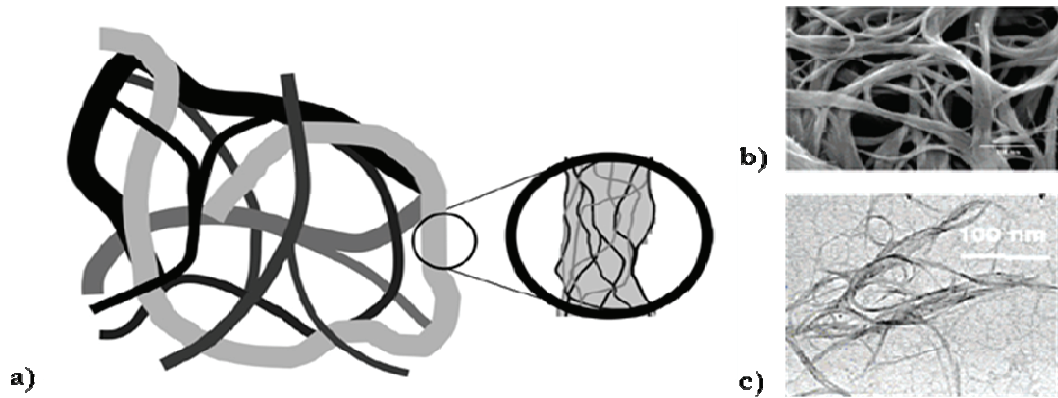


Figure 5. 3 - a) Schematic representation of a suspension of SWCNTs showing a disordered network on two length scales [6] b) SEM and c) TEM images of CNTs water solution [7]

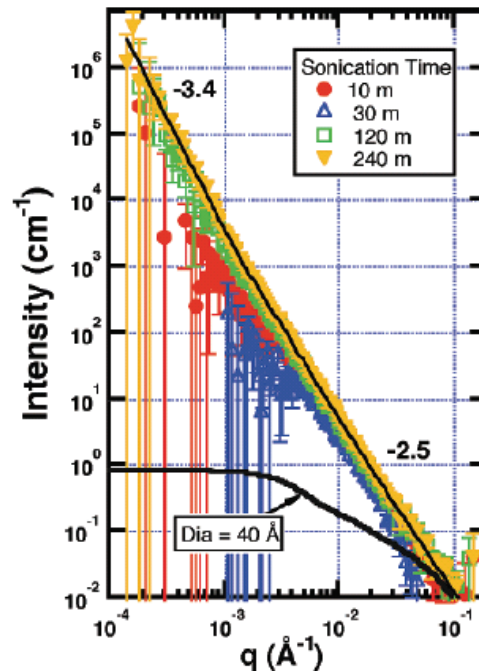


Figure 5. 4 - Background-subtracted USAXS data for Epon 828 cured with SWCNT-loaded Jeffamine D-2000 [6]

Justice et al. proposed a model for the schematization of the hierarchical structure of the CNTs network organization [8]. They assumed isolated tubes for distances less than a persistence length, L_p , while for distances larger than L_p , a mass fractal network morphology with fractal dimension, d_m , is assumed, with isolated wormlike tube clusters (figure 5.5). If such clusters are part of a percolated network, fractal correlations would exist up to a correlation range beyond which the carbon distribution would be uniform, similar to the situation in a semidilute polymer solution. If this cutoff length scale is larger than $1\ \mu\text{m}$, it exceeds also the USAXS resolution.

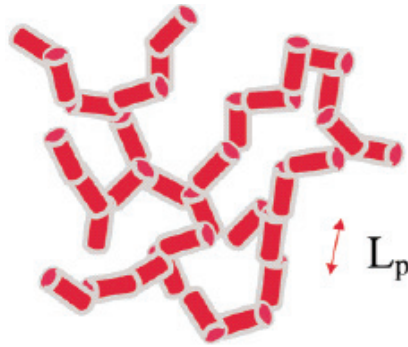


Figure 5. 5 - Schematic representation of a branched wormlike cluster with persistence length L_p .

In light of the reported information regarding both CNTs suspensions and composites, it is possible to conclude that SAXS, and particularly USAXS, is a valuable technique for studying the nanocomposites morphology, even if the dispersion of the nanofillers within the matrix is fundamental for a good exploitation of the technique potentialities.

5.3 Experimental

In line with this argument, in this chapter the work will focus on the manufacturing of Multiwalled Carbon Nanotubes (MWNT) bi-component epoxy based composites whose percolative insulator to conductor transition has been tuned by using different process parameters. Main objective of this part of the work is to produce CNTs based composite materials whose electrical connectedness varies according to the development of different nanotubes networks within the composite, induced by different processing techniques. Two main manufacturing processes have been used, both based on the use of sonication as dispersion technique, in the first case the sonication of MWNTs occurred in the liquid hardener, in the second case the nanotubes were dispersed in the more viscous resin.

An electrical characterization was carried out on the prepared nanocomposites for the evaluation of the dependence of the electrical conductivity on the production technique.

In order to visualize the MWNTs microstructure, transmission optical micrographs were taken on samples. Moreover, Small Angle X-ray Scattering technique was used to obtain information about the submicron-scale structures forming the CNTs agglomerates.

For simplification purposes, in the following, after a first unified explanation of the materials and methods used for the preparation of the different composite systems, the characterization results corresponding to the final composites will be discussed separately depending on the varying process parameters.

5.3.1. Epoxy system characterization

The thermoset resin used for the production of the carbon nanotubes composites is a bi-component epoxy system constituted by a bisphenol-A/epichlorohydrin derived liquid epoxy resin (Epon 828) with an aliphatic amine-based curing agent, triethylenetetramine, TETA (Epikure 3234) both supplied by Hexion. The stoichiometric ratio between the two components is 13 phr (13 parts of amine per 100 parts of resin in weight). The physical properties of the resin Epon 828 are illustrated in figure 5.6. In order to estimate the thermo-chemical behaviour of the neat epoxy system the reaction heat and the glass transition temperature have been measured by calorimetric investigations using a differential scanning calorimeter (TA DSC Q1000). The two components have been mixed in the stoichiometric ratio and a scanning from 20 to 180 °C has been performed on the sample in the DSC and the curing heat of the complete cure has been evaluated. The reaction heat has been estimated to be equal to 420 J/g and $T_{g\infty}$ equal to 104 °C (fig. 5.7).

Property	Test Method	Unit	Value
Epoxide Equivalent Weight ¹	ASTM D1652	g/eq	185-192
Viscosity @ 25°C ²	ASTM D445	P	110-150
Color	ASTM D1544	Gardner	1 max.
Pounds per Gallon @ 25°C (77°F)		lbs/gal	9.7
Density @ 25°C (77°F)		g/ml	1.16
Physical form			Clear liquid
Vapor pressure @ 77°C (170°F)		mm Hg	0.03
Refractive index @ 25°C (77°F)			1.573
Specific heat		BTU/lb/°F	0.5

¹ ASTM D1652 (Epoxy Content of Epoxy Resins – Perchloric Acid Method)

² ASTM D445 (Kinematic Viscosity - Determination of the Viscosity of Liquids by Ubbelohde Viscometer).

Figure 5. 6 - Physical properties of the Epon 828 (by Hexion)

The epoxy system has been cured in three different conditions and the corresponding glass transition temperatures have been measured and summarized in table 5.1. Moreover, in order to evaluate the conversion, α , calorimetric investigations in isothermal conditions have been performed on epoxy samples produced using a stoichiometric ratio of hardener by means of DSC. In figure 5.8 the heat flow curves corresponding to the three curing cycles recorder during a curing process in DSC as a function of time for each temperature are shown.

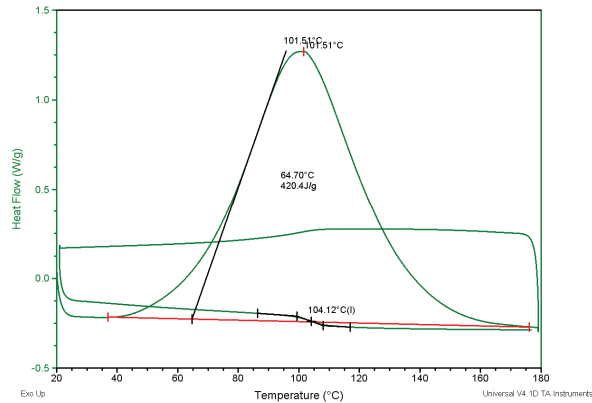


Figure 5. 7 - Total heat reaction during the curing of the epoxy system in dynamic conditions

Table 5. 1 - Epoxy curing cycle and corresponding glass transition temperature

Curing cycle	T _g [°C]
24 h @ 25 °C + 2h @ 120 °C	108
1 h @ 70 °C + 2 h @120 °C	105
2 h @120 °C	118

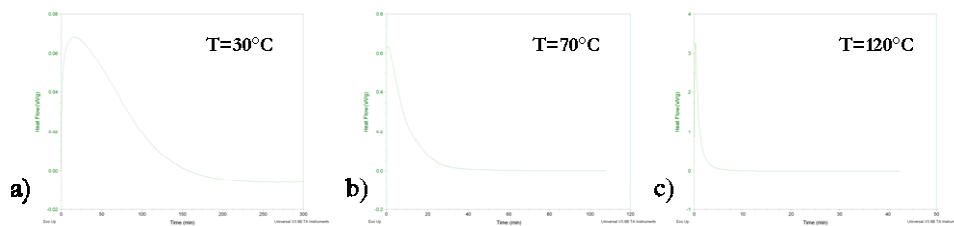


Figure 5. 8 - Epoxy curing heat flow curves during curing in isothermal conditions at a) 30 °C, b) 70 °C, c) 120 °C

The chemical gel times (table 5.2) have been estimated referring to a conversion of 0.54, as indicated by Antonucci et al. in [9].

Table 5. 2 - Chemical gel times for epoxy systems evaluated at $\alpha = 0.54$

Temperature [°C]	Gel time [min]
30	57

70	21
120	15

5.3.2. Materials and methods

MWNT 3150 produced by catalytic carbon vapour deposition (CCVD) process were supplied by Nanocyl S.A.. The tubes have an average diameter of 9.5 nm, an average length less than 1 μm and a purity exceeding 95% (with less than 5% of metal oxide impurity). The aspect ratio (L/D) for these nanotubes is 100, so the statistical percolation threshold in weight, calculated as D/L, is 1 wt%.

The epoxy system Epon 828 and TETA whose properties are described in 5.3.1 has been used as matrix for the production of MWNT/epoxy composites.

The common nanocomposites production technique went through the following steps:

1. dispersion of nanotubes in TETA or Epon using sonication;
2. addition of the second element, such as TETA or Epon;
3. mixing of the components;
4. curing in isothermal conditions.

The processing parameters that have been modified to induce different CNT's network morphologies are:

- A sonication solvent;
- B curing temperature;
- C sonication time;
- D MWNT's concentration.

Sonication has been carried out by means of a dipping tip ultrasonicator (Misonix S4000). The second component has been added to the as prepared composite solution in a stoichiometric ratio, that corresponds to 13 phr of TETA. in Epon for a total quantity of composite of 30 g. A first attempt of manually mixing the two components have been done, then a planetary vacuum mixer (Thinky Mixer ARV-310) has been used for a standardization of the mixing step.

For each sonication time, concentration and solvent set of samples, three different nanocomposites have been produced using three different curing conditions:

1. 25 °C for 24 hours + 2 hours at 120 °C;
2. 70 °C for 1 hour + 2 hours at 120°C;
3. 120 °C for 2 hours.

A summary of all the prepared composites is shown in table 5.3.

Table 5. 3 - CNTs/Epoxy composites set: manufacturing techniques

Composites set	Solvent	MWNT wt%	Sonication time [min]	Mixing technique	Curing conditions
1	TETA - Epon	0.05	30,120	Manual	1 - 2 - 3
2	TETA	0.05	30,45,90,105,120	Thinky	
3	Epon	0.01 ÷ 0.09	10,30,75,120	Thinky	

In addition, control samples of neat epoxy cured at the three different temperatures have been manufactured and considered as a reference.

An electrical characterization was carried out on the prepared nanocomposites for the evaluation of the dependence of the electrical conductivity on the production technique. Samples with a thickness of about 1 mm were polished and painted on the largest surfaces with silver conductive paint. The DC electrical conductivity was calculated from electrical resistance measurements using a pico-ammeter connected to a two-probes station (Signatone 1160 probe station). The probes were pointed to the silver electrodes on the sample largest surfaces, so that the current circulating in the thickness was measured applying a constant voltage of 40 V (fig. 5.9).

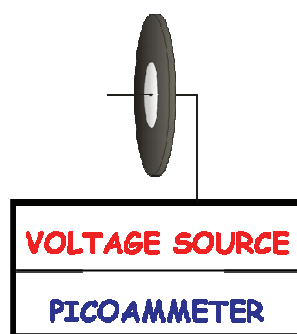


Figure 5. 9 - DC electrical measurements experimental set-up

SAXS experiments were performed with a SAXSess Instrument manufactured by Anton Paar, using copper K_α radiation $\lambda = 0.1542$ nm. The apparatus is equipped with a 2D imaging plate detection system. The X-Ray generator was operated at 40 kV and 50 mA and a line collimation was used to ensure a high radiation intensity. The measurements were performed on samples in the form of thin films. The q -range analyzed was $0.07 \div 1$ nm⁻¹, where q is the magnitude of scattering vector:

$$q = \frac{4\pi}{\lambda} \sin \theta \quad 5.1$$

and 2θ is the scattering angle. Each spectrum was collected for 90 minutes in order to assure a good signal/noise ratio.

The procedure used to process the spectra involved different steps:

- 1) subtraction of the dark current;
- 2) normalization of the primary beam;
- 3) normalization for the transmittance value, calculated dividing the scattering intensity by the sample thickness;
- 4) subtraction of the corresponding neat epoxy system, cured as previously described. This is performed by assuming that the structure of epoxy matrix does not change with addition of carbon nanotubes, as verified by WAXS analyses;
- 5) subtraction of the incoherent scattering;
- 6) correction for de-smearing.

5.3.3. Composite set 1 - CNTs/epoxy composites at fixed MWNTs concentration from different solvent

The aim of this part of the work is the study of the influence of initial solvent for two sonication times on the physical properties of the composites.³

- **Production**

For this set of composites, a fixed MWNTs concentration has been used for the preparation of all the composites, while the initial solvent, the curing temperature and the sonication time have been varied. The fixed MWNTs concentration used to prepare these epoxy nanocomposites is 0.05 wt%, hence a value much lower than the calculated statistical percolation threshold. The proper amount of nanotubes necessary to have this final concentration in the composite has been added alternatively to TETA or Epon and the components have been manually mixed. After the mixing, each composite has been cured following the three curing conditions 1, 2 and 3 previously reported in 5.3.2.

In the following, for clarity purposes the samples are named as “*starting letter of the solvent_sonication time_curing condition*” (table 5.4). For instance, T_30_1 is a composite produced sonicating in TETA for 30 minutes and cured for 24 hours at 25 °C with a postcuring of 2 hours at 120 °C.

³ The results reported in this paragraph have been published by Faiella et al. in [19].

It's worth nothing that E and T initial mixtures do intentionally differ each other not only by the mere chemo-physical solvents properties but primarily by the MWNTs concentrations due to the stoichiometric amounts of the epoxy and its hardener within the final thermoset polymer. In particular, composites prepared in TETA solvent started from a more concentrated solution of MWNTs respect to the composites prepared starting from Epon as solvent.

Table 5. 4 - Samples in composites set 1

SAMPLE	SOLVENT	SONICATION TIME	CURING CONDITION
T_30_1	TETA	30	24 h@25 °C + 2 h@120 °C
T_30_2			1 h@70 °C + 2 h@120 °C
T_30_3			2 h@120 °C
T_120_1		120	24 h@25 °C + 2 h@120 °C
T_120_2			1 h@70 °C + 2 h@120 °C
T_120_3			2 h@120 °C
E_30_1	EPON	30	24 h@25 °C + 2 h@120 °C
E_30_2			1 h@70 °C + 2 h@120 °C
E_30_3			2 h@120 °C 3
E_120_1		120	24 h@25 °C + 2 h@120 °C
E_120_2			1 h@70 °C + 2 h@120 °C
E_120_3			2 h@120 °C

- Electrical measurements

Figure 5.10 shows the electrical conductivity of the composites set 1 as a function of the curing temperature for the two solvent systems.

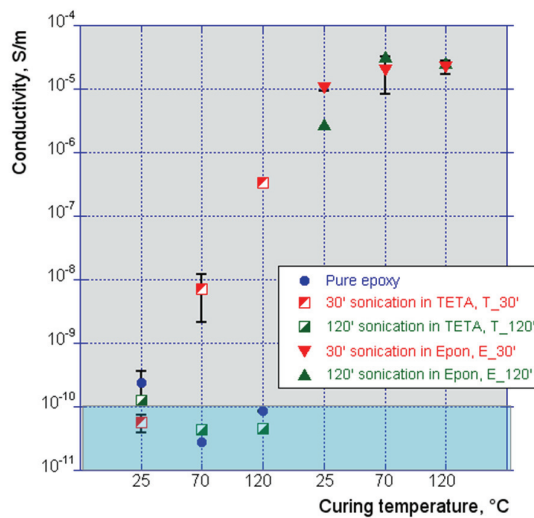


Figure 5. 10 - Electrical conductivity of the four sets of manufactured nanocomposites and of pure epoxy as a function of curing temperatures

- **Optical microscopy analysis**

It appears evident that only a notable difference in CNTs network morphologies within the composites could induce a so strong variation of the material properties. Hence, a microscopic analysis has been carried out on the samples of set 1.

Transmission optical microscopy images of thin nanocomposite films is shown in figure 5.11a-d.

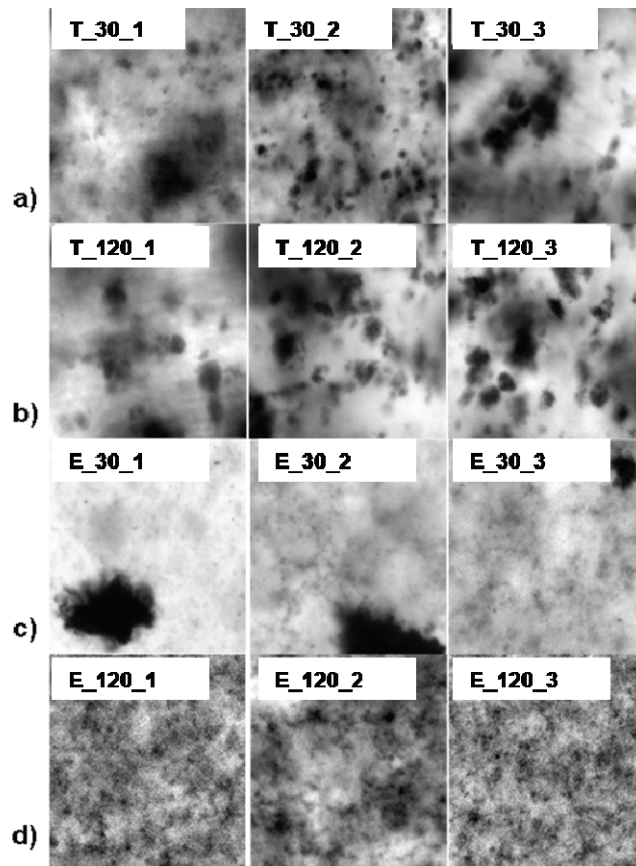


Figure 5. 11 - Transmission light micrographs at 20 X magnification (100 μm x 100 μm) of 0.05 MWNT wt% composites sonicated for a) 30' in TETA; b) 30' in Epon; c) 120' in TETA and d) 120' in Epon and then cured as curing conditions 1, 2 and 3

The micron scale morphology of the 'T' composites is characterized by a coarse distribution of particles having dimensions ranging from few microns to some tens of microns. Upon an increase of curing temperature, the number of the observable particles increases ('T_2) as does the particle agglomeration ('T_3). On the contrary, the composites prepared by sonication in Epon have all shown a finer and more homogeneous space filling topology than 'T' samples. This morphological difference is mainly due to the structure induced during the initial sonication. For 'T' samples, both the high numerical concentration of nanotubes within the initial sonicated

mixture and their high affinity with ammine hardener promote the formation of a micron sized cluster structure, not disassembled during the quiescent curing step. While, for E composites the preparation from a dilute solution of MWNTs in epoxy, leads to a more homogenous dispersion state [6].

This different dispersion state strongly affects the electrical conduction mechanisms: in E samples the electrons transport occurs through a fully percolated network of conductive rods or bundles; in T samples, the electrical percolative network is very “weak” (removal of few bonds can reduce it to a non percolative net) and it is dominated by the particle clusters that act as “blobs” for the electron transport [10].

- **Small Angle X-Ray Scattering (SAXS)**

SAXS investigations have been further used to assess the morphology of MWNTs within the composites at length scales ranging between 10 and about 90 nm, evaluated as $d=2\pi/q$, where q is the scattering vector. The Porod plot (log-log) of the scattering intensity, I vs. q may show both linear regions, where the power law with $-D$ exponent is related to the fractal dimension of the nanotubes structure, and Guinier regimes, where crossover features are reasonably associated with the size of scattering objects [11]. It is worth noting that the D exponent is a measure of either the compactness or the surface topology of the scattering objects. In particular, it represents a sharp and smooth interface when D is equal to 4, a fractal surface for $3 < D < 4$, and a mass fractal for $1 < D < 3$, respectively.

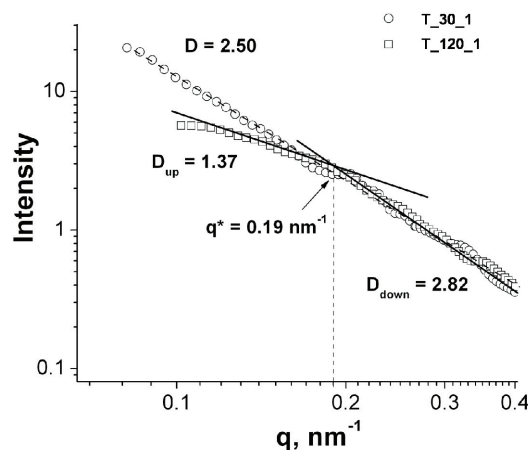


Figure 5. 12 - SAXS structural data referring to T and E samples sonicated for 30 and 120 minutes and cured as condition

Figure 5.12 shows the Porod plots of the background subtracted SAXS spectra related to T_25°C samples. The spectra have been obtained by subtracting the scattering intensity due to the neat epoxy structure. For $q > 0.5 \text{ nm}^{-1}$, data are affected by large error due to the comparable magnitude of the pure epoxy matrix and nanocomposites scattering intensity signals and they have been omitted for sake of the graph quality. The T_30_1 sample spectrum is linear within the investigated range and it is characterized by a single D exponent, while the T_120_1 sample exhibits a knee-scattering feature with a crossover at a q^* , that separates two linear regions associated with two different fractal like morphologies, i.e. D_{up} and D_{down} for $q < q^*$ and $q > q^*$ respectively.

Although the background subtraction may introduce additional uncertainty in estimating the contribution of the MWNTs, the cross-over is a reliable scattering feature that is related to a peculiar morphology of manufactured composite systems.

Table 5.5 summaries the data from the analysis of the SAXS spectra features of the 25 and 120 °C cured T and E samples, both sonicated for 30' and 120'.

Regardless the dispersing medium, 120' sonicated samples exhibit a knee-scattering feature with a crossover which reasonably leads to the estimation of the size of the smallest scattering object within the composites, evaluated as $d^* = 2\pi/q^*$ [12].

In this case, for $q > q^*$ the scattering objects exhibit a fractal dimension, D_{down} , related either to a mass or a surface fractal morphology. In particular, the fractal morphology is more compact than that of the 30' sonicated samples cured at the correspondent temperature, and the scattering objects surface corresponds to a fractally rough surface. Scaling exponent, D_{up} , for $q < q^*$ has been always found to be lower than D_{down} , approaching the value 1, indicating the existence of somehow linear or flexible linear objects.[5]

Table 5. 5 - SAXS structural data referring to T and E samples sonicated for 30 and 120 minutes and cured as curing condition 1 and 3

	25°C		120°C		25°C		120°C			
30'	2.5		2.72		2.5		3.32		D	
120'	31		30		32		48		d* [nm]	
	2.82	1.37	3.45	2.23	3.12	1.43	2.95	1.72	D_{down}	D_{up}
	TETA				EPON					

Regardless the dispersing medium, 30' sonicated samples do not show any scattering structure. The scaling exponents do reveal the existence of mass fractal objects whose compactness increased with the curing temperature [13, 14].

A notable result is the detection itself of such nanostructures by means of SAXS, not yet observed in literature for MWNT/epoxy composites systems. SAXS analysis indeed reveals that for both T or E samples, irrespective of the topological morphology of the microsized dimensional scale, nanosized structures are formed as the sonication time is increased.

- **Results discussion and morphological model**

Such findings not only confirm the debundling action of the sonication technique,[15-17] but also suggests that the energy provided by the sonication enables and promotes nanotubes rearrangements within the bundles network. In E samples because of the persistence of a percolative network of nanotubes, the variations of the nano scale structural parameters do not induce significant electrical conductivity modulation on the macroscale. On the other hand, for T samples, where the composite conductivity is associated to the “weakness” [10] of the percolative path, the variation of nano scale structural parameters influences the conductivity modulation on the macroscale. In fact, the ‘T_120’ resulted not conductive at all due to the presence of small matrix isolated nanotubes bundles, that do not contribute to the formation of the percolation path and contemporary increase the number of electrical junctions between tubes. Moreover, sonication could induce damaging and shortening of the nanotubes with the reduction of their aspect ratio and the consequent decreasing of the electrical conductivity [18].

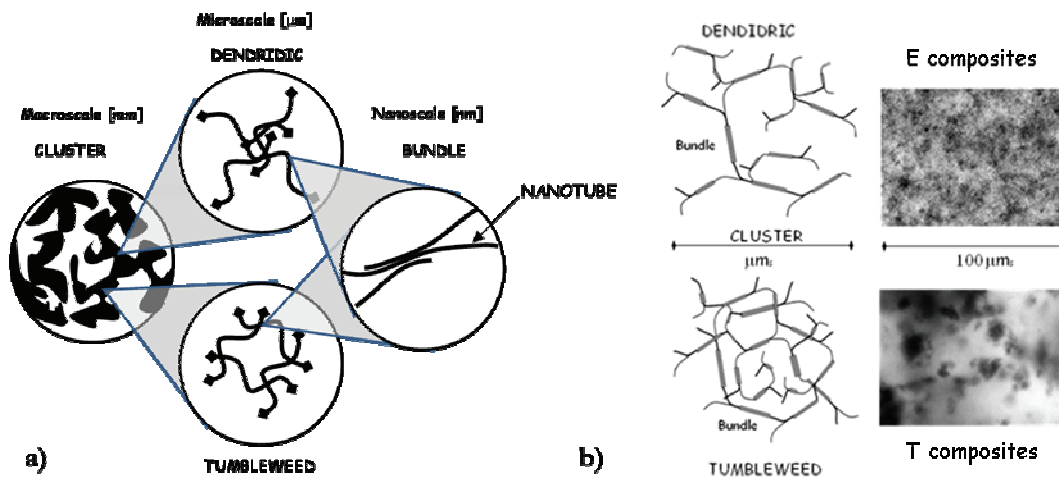


Figure 5.13 - a) Proposed multiscale nanotubes net for b) E and T composites [18]

Based on the present experimental findings and partially according to Brown et al,[6] a picture of the multi scale organization of CNTs has been proposed [19]. Starting from the single MWNT, two higher length scales have been observed, such as the nano sized bundles and the micron sized clusters, whose intrinsic electrical conductivity and connectedness determine the

conductivity at the macroscopic scale. Moreover, on the micron scale two different topologies are here proposed for the structure of the clusters. Both the topologies have to be regarded as constituted by CNTs bundles (whose dimensions and connectedness depend on the sonication time) that is the building block of the resulting micro-networks. For T systems, a “tumbleweed” topology is proposed, in which bundles connect each other mainly forming closed micrometric loops. In the case of the E systems, microscopic observations suggest the presence of a “dendritic” morphology, in which bundles are connected mainly forming branched open structures (figure 5.13 a and b).

In summary, MWNTs/epoxy composites at a fixed tubes concentration below the statistical percolation threshold having an electrical conductivity fully modulated between the insulator to the conductor behavior have been produced. It was shown that by varying the initial dispersion medium, the sonication time and the curing temperature the electrical behavior of such composites can be tuned because the morphology of the CNTs network induced by external forces substantially modifies.

Two distinct cluster topologies within the final composite induced by means of sonication aided dispersion procedure have been found by SAXS analysis. Moreover the extent of conductivity tuning is regulated by such nano scale bundle structures. So far, increasing the concentration of isolated bundles it is possible to modify the weak percolative net and in turn the whole nanocomposite electrical conductivity. A multiscale organization of nanotubes in bundles then in micron sized clusters has been proposed accounting for the development of the conductive percolative path.

5.3.4. Composite set 2 - CNTs/epoxy composites at fixed MWNTs concentration and different sonication times

The aim of this part of the work is the study of the influence of sonication time on the physical properties of the composites.

- **Production**

For this set of composites, a fixed MWNTs concentration (0.05 wt%) and the same initial solvent (TETA) have been used, while the curing temperature and the sonication time have been varied. The proper amount of nanotubes necessary to have a final concentration in the composite of 0.05 wt% has been added to TETA and different solutions have been prepared, sonicating for 30,

45, 90, 105 and 120 minutes. As prepared solution has been mixed with Epon using a planetary vacuum mixer (Thinky Mixer ARV-310), at 2000 rpm for two minutes with the vacuum applied.

Table 5. 6 - Samples of composites set 2

SAMPLE	SONICATION TIME [min]	CURING CONDITION
30_1	30	24 h@25 °C + 2 h@120 °C
30_2		1 h@70 °C + 2 h@120 °C
30_3		2 h@120 °C
45_1	45	24 h@25 °C + 2 h@120 °C
45_2		1 h@70 °C + 2 h@120 °C
45_3		2 h@120 °C
90_1	90	24 h@25 °C + 2 h@120 °C
90_2		1 h@70 °C + 2 h@120 °C
90_3		2 h@120 °C
105_1	105	24 h@25 °C + 2 h@120 °C
105_2		1 h@70 °C + 2 h@120 °C
105_3		2 h@120 °C 3
120_1	120	24 h@25 °C + 2 h@120 °C
120_2		1 h@70 °C + 2 h@120 °C
120_3		2 h@120 °C

This mixer, by rotation and revolution movements is able to contemporary mix and squeeze out air bubbles.

Each composite has been processed using the curing conditions 1, 2 and 3 reported in 5.3.2.

Sample codification of composites in set 2 is illustrated in table 5.6. The samples are named as “*sonication time_curing condition*”. For instance, 45_1 is a composite at 0.05 MWNT wt% produced sonicating in TETA for 45 minutes and cured for 24 hours at 25 °C with a postcuring of 2 hours at 120 °C.

- **Electrical measurements**

Figure 5.14a shows the electrical conductivity values measured by DC electrical measurements of the composites of set 2, grouped for sonication time as a function of curing temperature.

An interesting phenomenon to be noted in this set of samples is that the tuning of the electrical properties through the curing temperature is more evident as the sonication time increases. In fact, a tuning of the conductivity of five orders of magnitude occurs in the samples sonicated for 120 minutes passing from 25 to 120 °C, while the composites sonicated for 45 minutes show an almost constant conductivity with the curing temperature.

Moreover, from figure 5.14b what appears evident is that a decrease of conductivity occurs upon an increase of sonication time: passing from 30_25 to 120_25, a decrease of six orders of magnitude can be detected. This phenomenon is more evident at low curing temperature, such as 25 and 70 °C, respect to 120 °C, where a decrease of only two orders of magnitude has been measured.

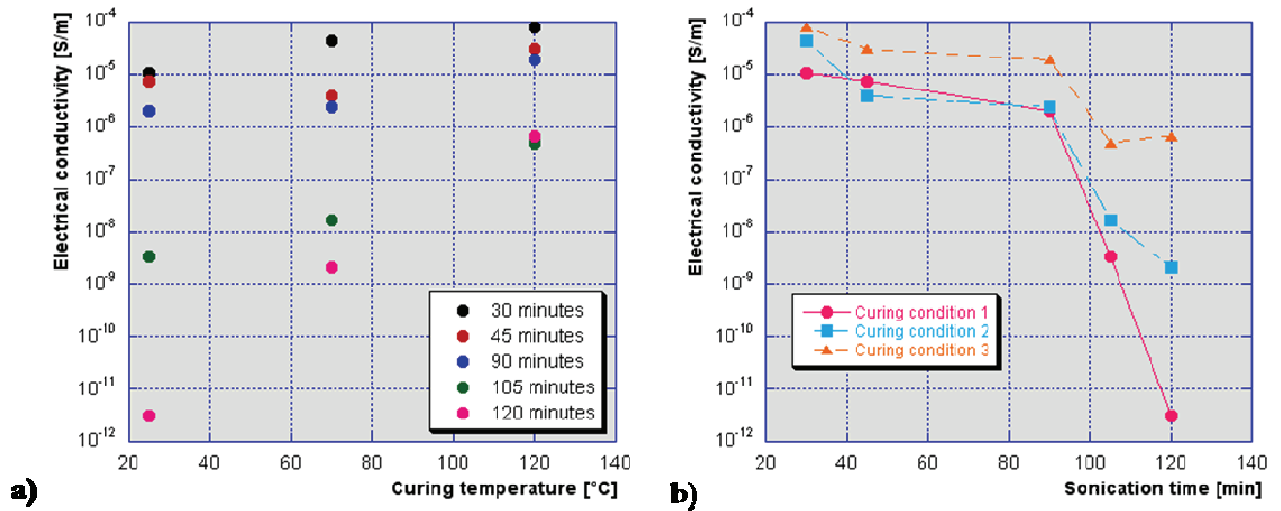


Figure 5. 14 - Electrical conductivity of composites of set 2: a) the five sonication time groups as a function of curing temperature; b) the three curing temperatures groups as a function of sonication time

The decrease of conductivity associated to the increase of sonication time could be addressed to a nanotubes shortening due to a longer sonication or to the better exfoliation that causes a better adhesion of the matrix to the tubes wall, and hence an insulating layer between nanotubes, that is detrimental for the electrical conduction.

- Optical microscopy

On the basis of the previous results, the reasons for these changes in conductivity can be searched in the morphological differences of the CNT's network topology within the composites. In figure 5.15 transmission optical transmission images from thin composite films of composite sonicated for 45 minutes and cured as indicated in curing conditions 1, 2 and 3 are shown.

As can be noted by a comparison between the three composites cured at the three different temperatures, the morphology is almost the same, without the presence of evident differences between them. The dispersion is quite homogenous and the material seems to be constituted by dense CNTs networks with a high degree of connectedness.

In figure 5.16, optical microscopy images of the composites obtained by 120 minutes of sonication at the three curing temperatures are shown. Differently from the 45 minutes sonicated samples, here one can note an evolution in the morphology of the CNTs networks. It seems that upon an increase of curing temperature, the visible aggregates are bigger. In particular an evident difference can be noted between 25 and 120 °C of curing temperature, where the morphology passes from a homogenous CNTs to coarse micro-aggregates dispersion.

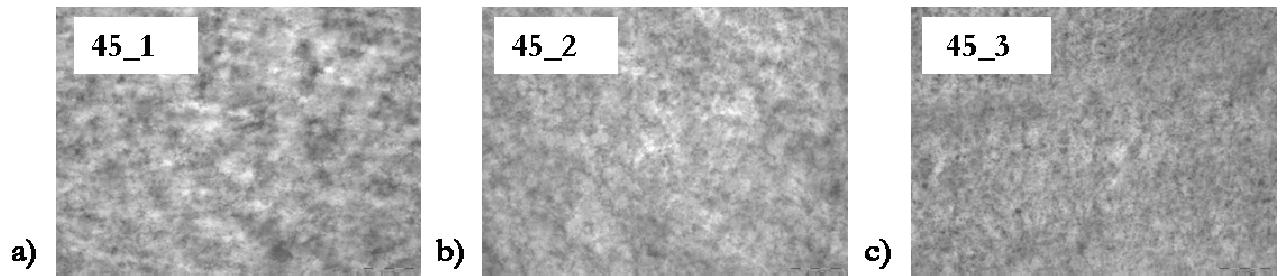


Figure 5. 15 - Transmission optical microscopy images (magnification 10X) of composites sonicated 45' and cured as indicated in curing conditions a) 1, b) 2 and c) 3 respectively

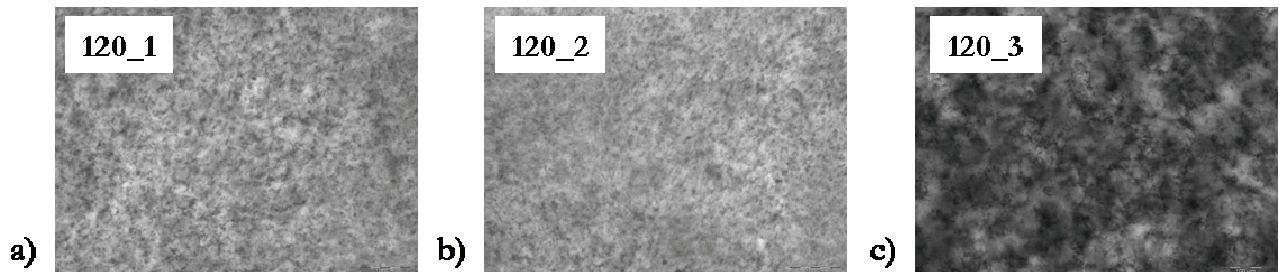


Figure 5. 16 - Transmission optical microscopy images (magnification 10X) of composites sonicated 120' and cured as indicated in curing conditions a) 1, b) 2 and c) 3 respectively

- **Results discussion**

The important difference between the composites set 1 and the composites set 2 consists in the mixing technique. In fact, in the second case, all the TETA/MWNTs solutions have been mixed with Epon by means of a planetary mixer. The rotation and revolution technology of this mixer allows to simultaneously stir and degases the material, stabilizing the quality of the final solution. The rotation movement of the container generates a strong whirlpool flow in the material, able to

stir and disperse particles within it. In this work, the mixer has been used for a standardization of the TETA-Epon mixing step, so all composites can start to cure from the same conditions and the effect of the curing temperature on the different solutions can be studied independently on the quality of the prior mixing, that was not completely assured by hand mixing. Moreover, the possibility to eliminate air bubbles from the solution leads to a higher homogeneity and stability of it. A first attempt of directly mixing resin and nanotubes using Thinky has been carried out, but with bad results. The dispersion was not uniform at all and even at high MWNTs concentration the electrical conductivity assumed low values, because aggregates were present in the solution. So, the planetary mixer has been used only for the mixing of the two components Epon and TETA. Even if the production conditions of composites set 1 and 2 are not the same, a common result for the two composites sets is the strict correlation between CNTs aggregation behavior and electrical properties, resulting from the comparison between the electrical behavior and the morphology characteristics. For instance, the electrical conductivity of the composites produced sonicating for 45 minutes doesn't change with the curing temperature, as does the morphology visible by optical microscopy. In the same way, for samples sonicated for 120 minutes, the electrical conductivity varies as the morphology does.

However, a big difference between the two types of composite can be found in the electrical properties. While for T₃₀_{1,2,3} samples of composites set 1 the tuning of the electrical properties was possible passing from 25 to 120 °C of curing temperature, here for 30_{1,2,3} samples the electrical conductivity is almost constant with the temperature and the same constant behavior is also found for 45_{1,2,3} and 90_{1,2,3}. On the contrary, here for 120_{1,2,3} a tuning of the electrical properties can be induced in the material. This could be explained considering that the use of a mechanical mixing method instead of a manual one leads to a better dispersion of the nanotubes, confirmed by the fact that the morphology of the 45₁ sample appears more homogenous than the T₃₀₁ of the previous set. Hence, it is possible to say that further dispersion can be induced by shear in the composite after the addition of Epon if a previous sonication of the nanotubes has been performed on the TETA/MWNTs solutions.

This further dispersion can also explain the decrease of the electrical conductivity upon an increase of sonication time, because a higher degree of dispersion is induced in the composites by the mechanical mixing, hence the tubes connectedness is lowered by a higher content of insulating matrix present between them. It seems that there exist a sort of threshold for the sonication time, that in this case is 90 minutes, above which the conductivity dramatically decreases. The correlation between electrical properties of the composites and exfoliation of the TETA/MWNTs solutions could be related to the same dispersion concepts reported for CNTs water solutions in chapter 3 and in [17]. There, the exfoliation process could be monitored by

means of spectroscopic techniques, that were effective tools for the identification of the maximum sonication time above which further sonication would have induced only tubes damaging. Here, the loss of electrical properties can be related to the lowering of tubes connectedness due to the increasing of the probability to have insulating matrix between conductive networks.

Small angle X-ray experiments even in this case could be an effective tool for understanding the real reason on the basis of these results, because it could help to evaluate the nanoscale morphology of this set of composites [19]. This study is still in progress.

5.3.5. Composite set 3 - CNTs/epoxy composites at different MWNTs concentrations

The aim of this part of the work is to investigate the percolation behavior of epoxy composites produced starting from Epon as solvent at two different sonication times.

- **Production**

For this set of composites, different MWNTs concentration (from 0.01 to 0.1 wt%) and the same initial solvent (Epon) have been used, while the curing temperature and the sonication time have been varied. The proper amounts of nanotubes necessary to have the desired final concentrations in the composite have been added to Epon and each solution has been sonicated for four different times: 10, 30, 75 and 120 minutes. Then the solutions have been mixed with TETA using the planetary vacuum mixer. Each composite has been cured as indicated in the curing conditions 1, 2 and 3.

For results clarity purposes a sample codification of the materials is used. The samples are named as “*concentration_sonication time_curing condition*”. For instance, 0.03_30_1 is a composite at 0.03 MWNT wt% produced sonicating in Epon for 30 minutes and cured for 24 hours at 25 °C with a postcuring of 2 hours at 120 °C.

- **Electrical measurements**

The DC electrical conductivity of all the composites in set 3 has been measured. In the following the electrical behaviors of the four groups of composites will be shown firstly as a function of curing temperature, then the percolative behavior, such as the dependence of the electrical conductivity on the MWNTs concentration, will be illustrated.

In the figures from 5.17 to 5. 20, the electrical conductivity of the composites produced by sonication for 10, 30, 75 and 120 minutes at different MWNTs weight percentages are reported as a function of curing cycle. The points corresponding to electrical conductivity and curing condition are connected to each other only to make faster the analysis of the data.

From these plots it is possible to appreciate the variation of the electrical conductivity with the curing temperature for each MWNTs concentration. In particular, it is possible to take evidence of the fact that only at some concentrations the conductivity appreciably varies with the curing temperature, with increments even of 6 orders of magnitude passing from curing condition 1 to 3. Furthermore, the concentration corresponding to the tuning of the electrical conductivity with the curing temperature increases upon an increase of sonication time passing from 0.02 wt% at 10 to 0.04 wt% at 120 minutes of sonication. Another interesting result is that, for each batch of composites there exist at least one other concentration close to the one corresponding to the tuning showing a sharp increase in conductivity for curing condition 3, being very low for curing conditions 1 and 2.

In the figures from 5.21 to 5. 24 the percolative behaviors of the four sets of composites are shown in graphs where the electrical conductivity is plotted against MWNT wt%. A notable result consists in the dependence of the percolation threshold on the curing temperature. It is possible to see that the percolation threshold decreases upon an increase of curing temperature for each sonication time. For the same group of composites, the biggest difference between the percolation curves can be noted in the composites sonicated for 120 minutes, where for curing conditions 1, 2 and 3 the percolation thresholds are respectively 0.04 wt%, 0.035 wt% and 0.03 wt%. Furthermore, another important effect is the increase of the percolation threshold upon an increase of sonication time. In fact it passes from 0.01 wt% to 0.04 wt% from 10 to 120 minutes of sonication.

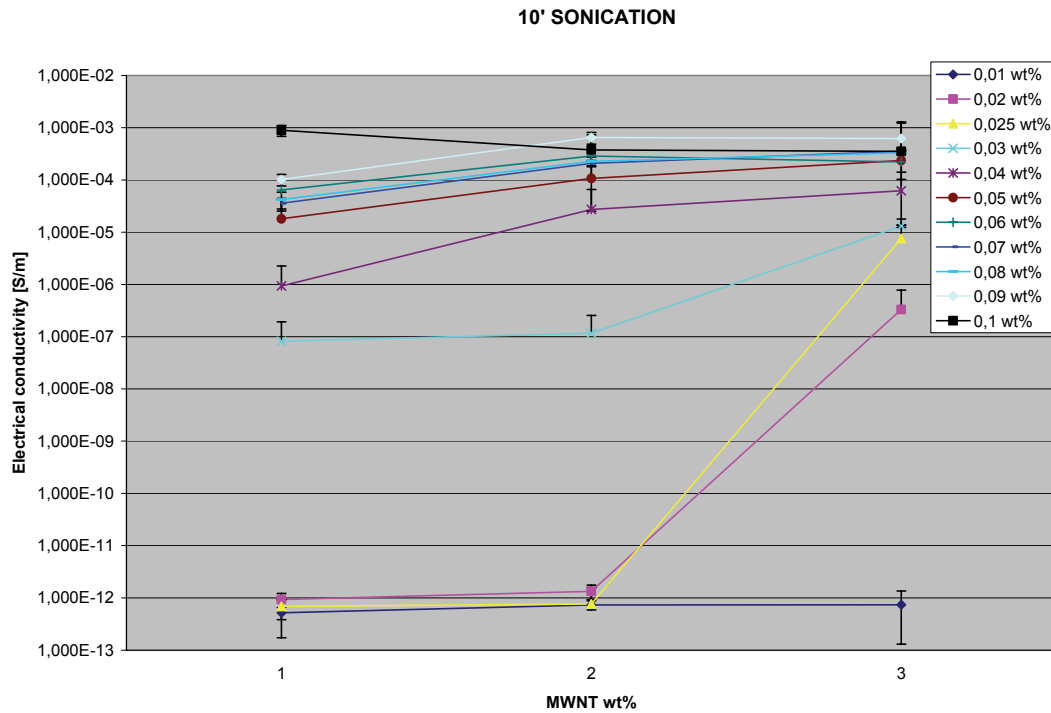


Figure 5. 17 - Electrical conductivity as a function of curing condition of composites of set 3 at different MWNT wt% produced by a sonication for 10 minutes in Epon

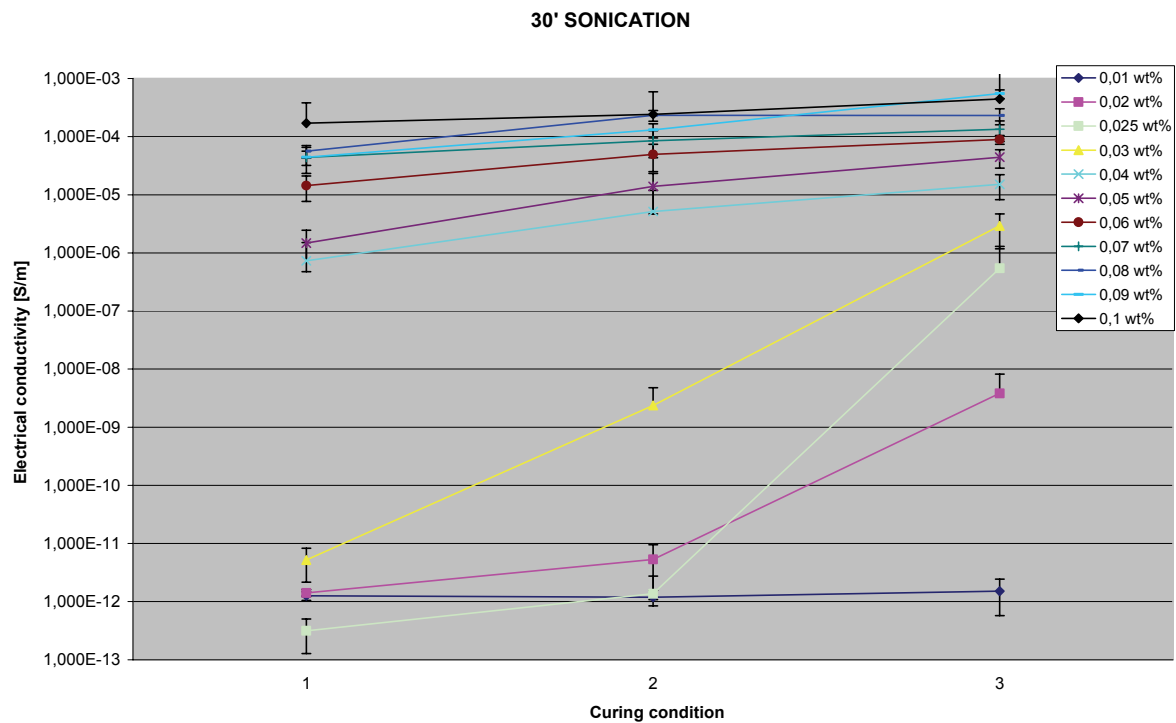


Figure 5. 18 - Electrical conductivity of composites of set 3 at different MWNT wt% produced by a sonication of 30 minutes as a function of the curing conditions 1, 2 and 3

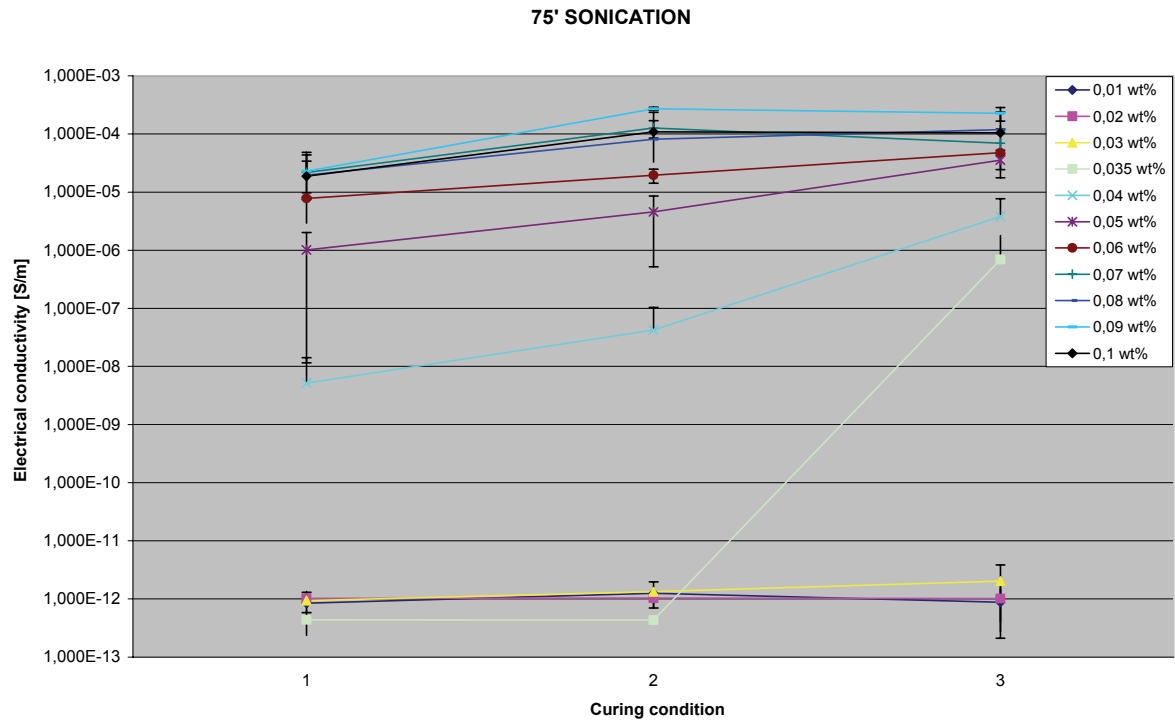


Figure 5. 19 - Electrical conductivity of composites of set 3 at different MWNT wt% produced by a sonication of 75 minutes as a function of the curing conditions 1, 2 and 3

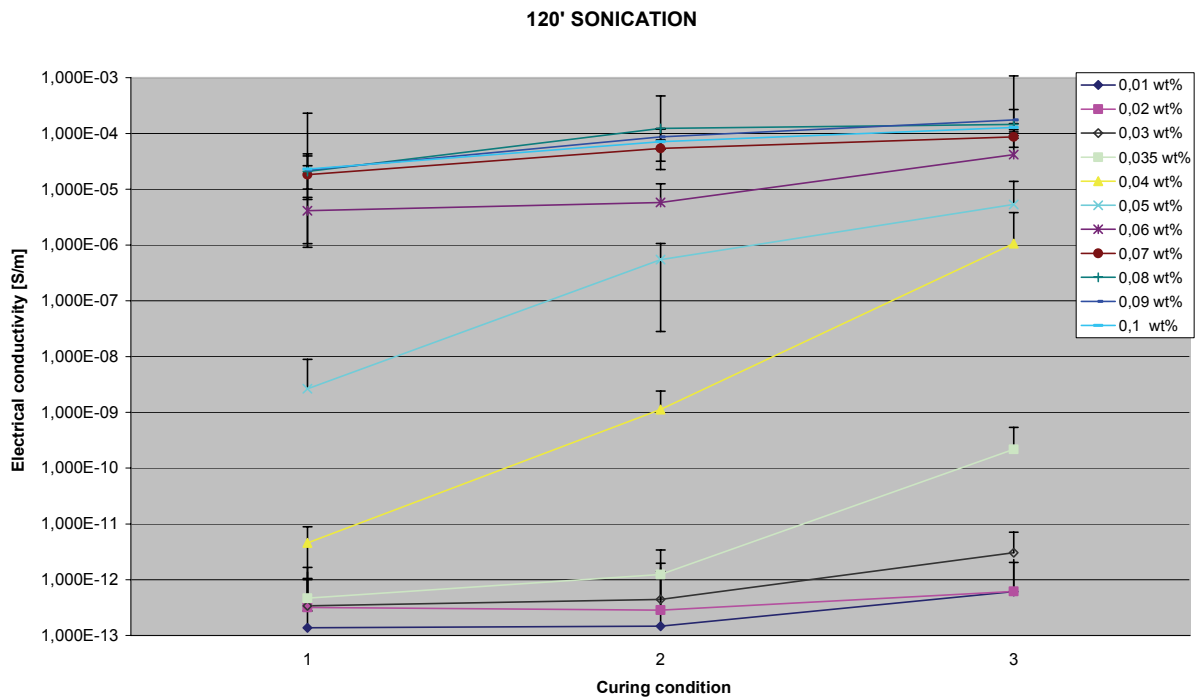


Figure 5. 20 - Electrical conductivity of composites of set 3 at different MWNT wt% produced by a sonication of 120 minutes as a function of the curing conditions 1, 2 and 3

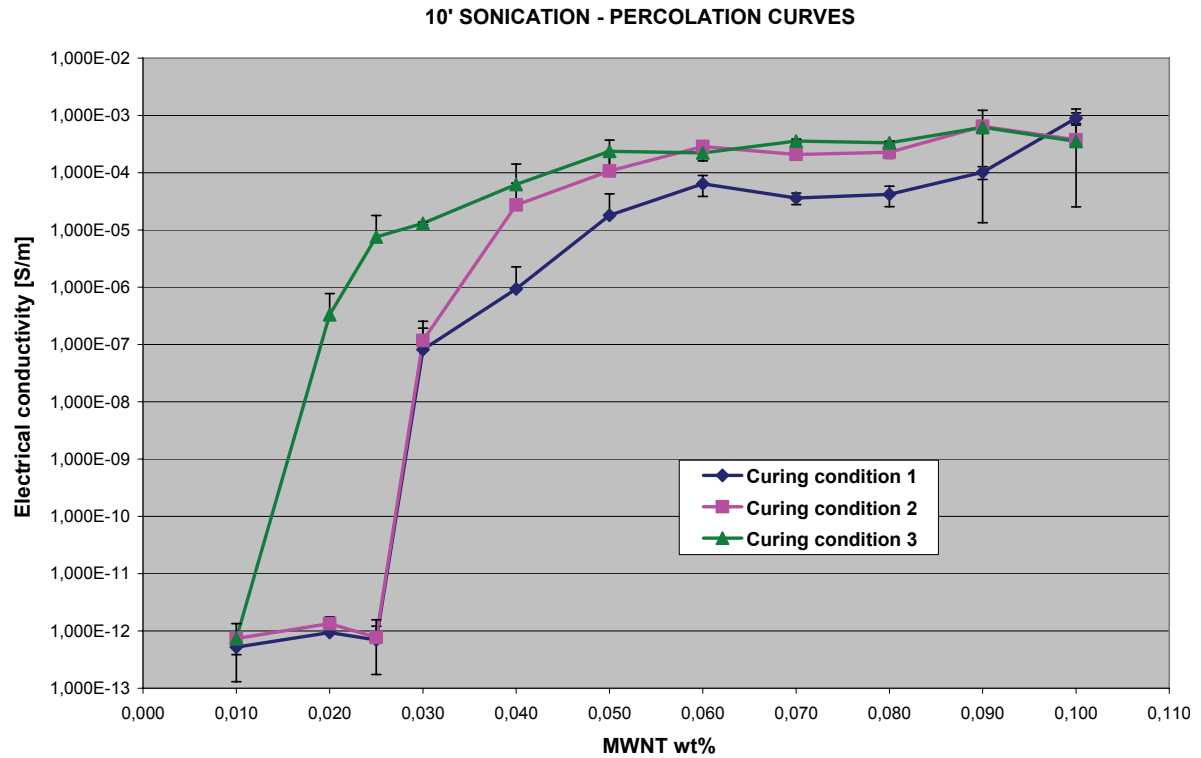


Figure 5. 21 - Percolative curves of composites of set 3 produced by a sonication of 10 minutes cured using the three different conditions

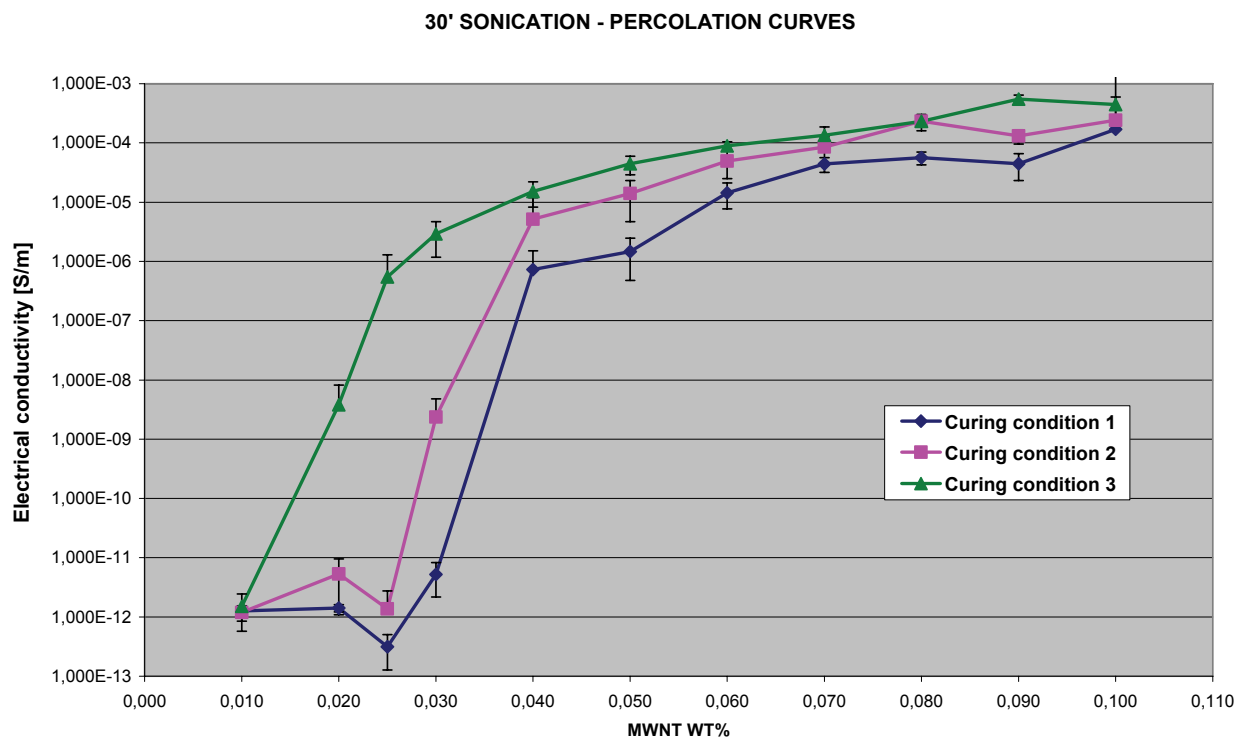


Figure 5. 22 - Percolative curves of composites of set 3 produced by a sonication of 30 minutes cured using the three different conditions

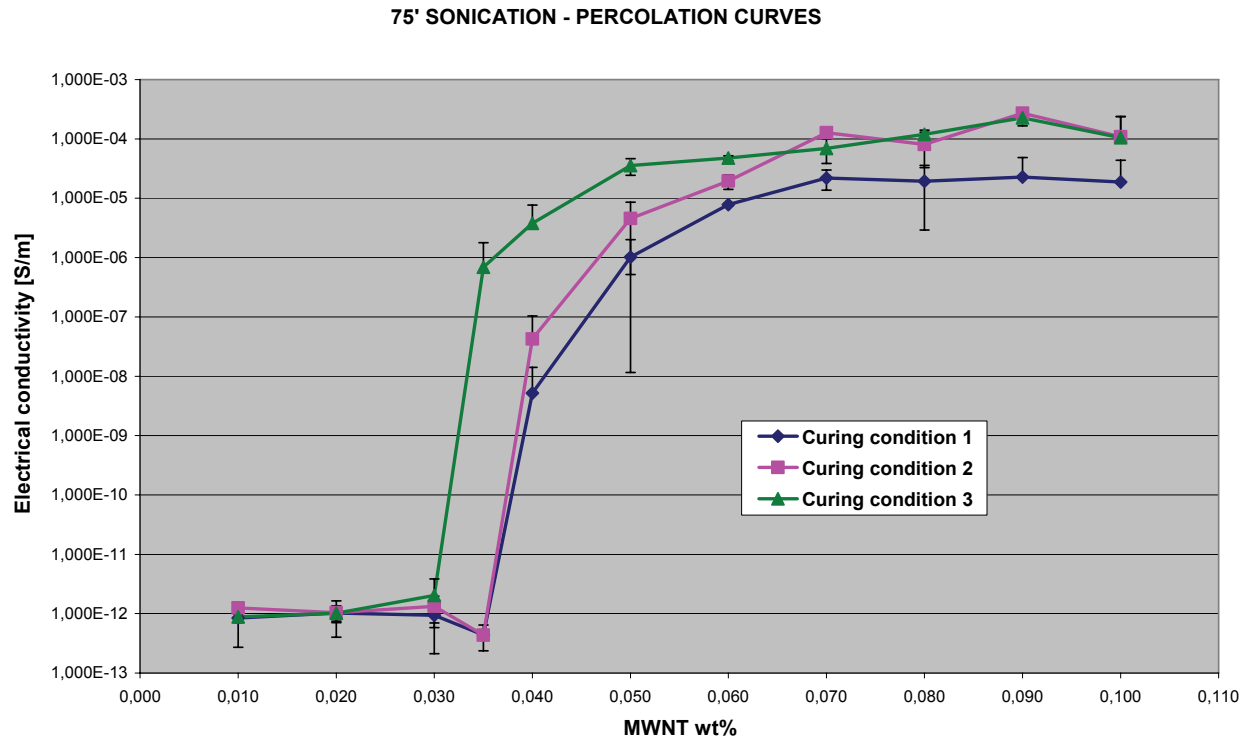


Figure 5. 23 - Percolative curves of composites of set 3 produced by a sonication of 75 minutes cured using the three different conditions

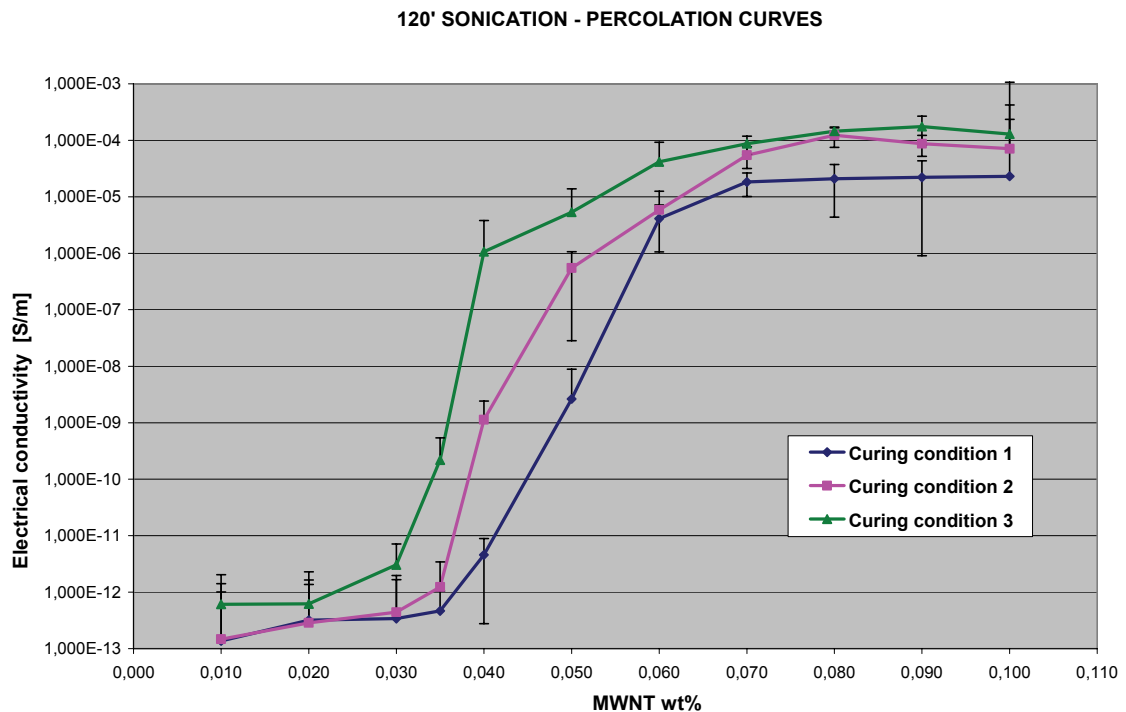


Figure 5. 24 - Percolative curves of composites of set 3 produced by a sonication of 120 minutes cured using the three different conditions

- Optical microscopy

Optical microscopy images of the composites corresponding to the temperature induced tuning of the electrical properties are compared to the ones of the samples at concentration below and above this critical one.

From figure 5.25 to 5.34, optical microscopy images of the composites at 10, 30, 75 and 120 minutes of sonication are shown.

In figures 5.25, 5.26 and 5.27 optical microscopy images respectively of samples at 0.02, 0.025 and 0.03 MWNT wt% sonicated for 10 minutes are shown. From these pictures, it is possible to follow the evolution of the microstructure modification occurring within the composites passing from curing condition 1 to 3. A sort of agglomeration process occurs in the composite at higher curing temperature, with the appearance of darker micro-areas where the CNTs networks morphology becomes denser of agglomerates upon an increase of curing temperature.

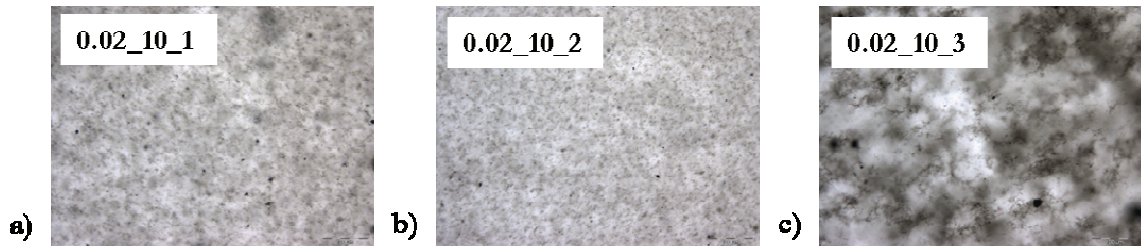


Figure 5. 25 - Transmission optical microscopy images of composites at 0.02 MWNT wt% produced by a sonication of 10 minutes and cured respectively following the curing conditions a) 1, b) 2 and c) 3

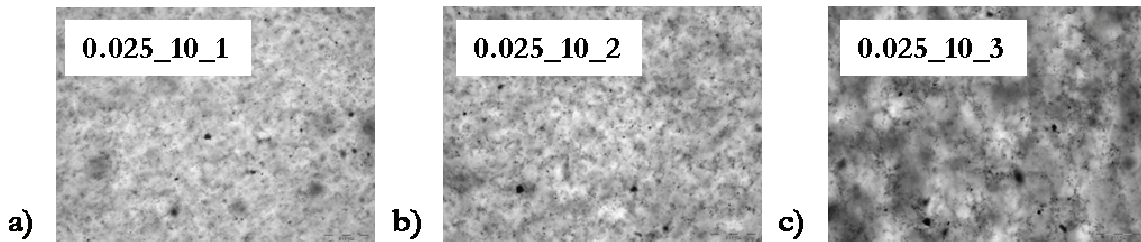


Figure 5. 26 - Transmission optical microscopy images of composites at 0.025 MWNT wt% produced by a sonication of 10 minutes and cured respectively following the curing conditions a) 1, b) 2 and c) 3

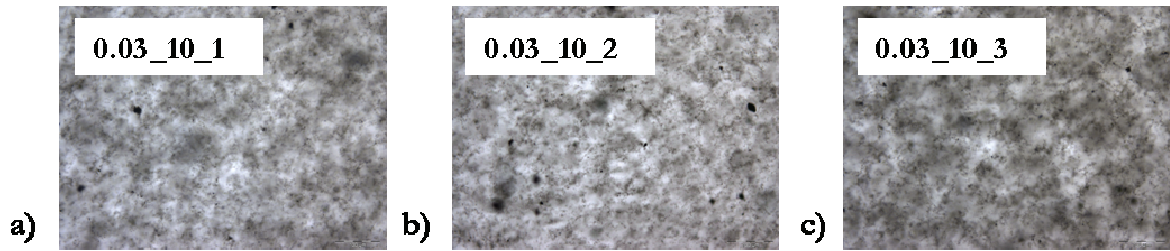


Figure 5. 27 - Transmission optical microscopy images of composites at 0.03 MWNT wt% produced by a sonication of 10 minutes and cured respectively following the curing conditions a) 1, b) 2 and c) 3

In figures 5.28, 5.29 and 5.30 optical microscopy images of samples sonicated for 30 minutes respectively at 0.02, 0.03 and 0.08 MWNT wt% are shown. The agglomeration process is particularly visible passing from 0.02_30_2 to 0.02_30_3, while an evolution of the process is visible passing from 0.03_30_1, 2, 3. For higher concentrations any evolution in the morphology is visible, as it appears from the images of the composites 0.08_30.

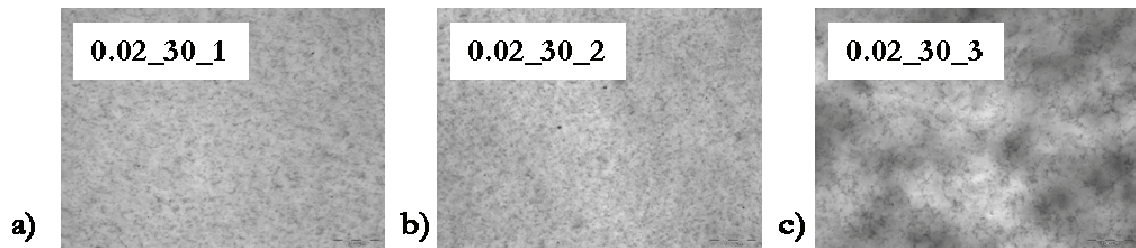


Figure 5. 28 - Transmission optical microscopy images of composites at 0.03 MWNT wt% produced by a sonication of 30 minutes and cured respectively following the curing conditions a) 1, b) 2 and c) 3

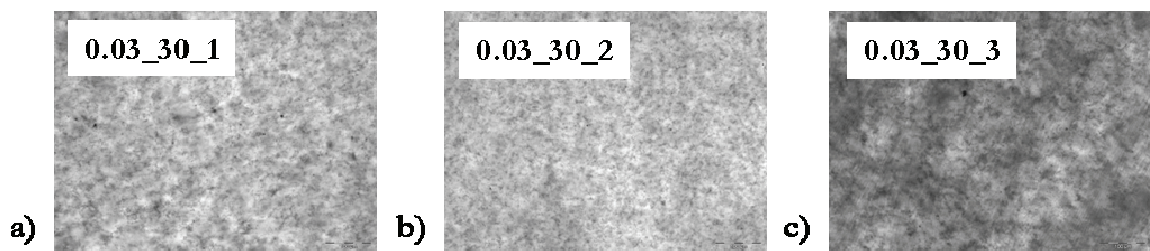


Figure 5. 29 - Transmission optical microscopy images of composites at 0.02 MWNT wt% produced by a sonication of 30 minutes and cured respectively following the curing conditions a) 1, b) 2 and c) 3

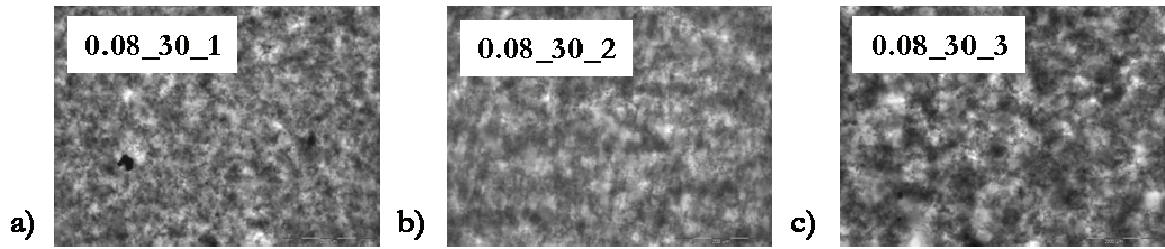


Figure 5. 30 - Transmission optical microscopy images of composites at 0.08 MWNT wt% produced by a sonication of 30 minutes and cured respectively following the curing conditions a) 1, b) 2 and c) 3

In figures 5.31 and 5.32 the morphologies of the composites sonicated for 75 minutes at 0.035 and 0.04 MWNT wt% are shown. Again here, the morphology becomes characterized by denser agglomerates passing from curing condition 2 to 3 at 0.035 MWNT wt% and an evolution of this process is visible throughout the three curing conditions at 0.04 MWNT wt%.

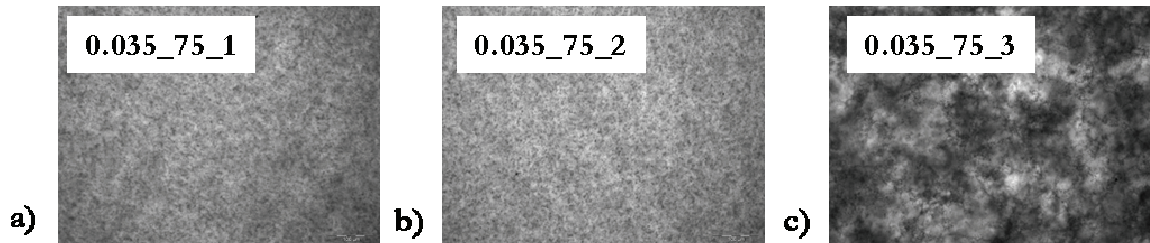


Figure 5. 31 - Transmission optical microscopy images of composites at 0.035 MWNT wt% produced by a sonication of 75 minutes and cured respectively following the curing conditions a) 1, b) 2 and c) 3

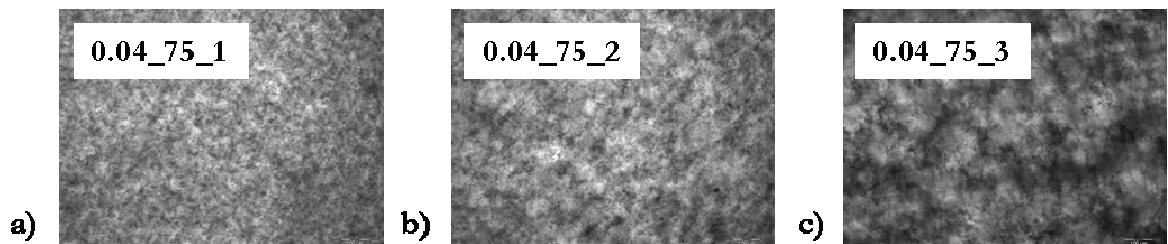


Figure 5. 32 - Transmission optical microscopy images of composites at 0.04 MWNT wt% produced by a sonication of 75 minutes and cured respectively following the curing conditions a) 1, b) 2 and c) 3

In figures 5.33 to 5.34 optical microscopy images of the samples sonicated for 120 minutes at 0.04 and 0.03 MWNT wt% are shown. As in the previous cases, again here a densification of the CNTs agglomerates can be seen upon an increase of curing temperature, passing from 0.04_120_1, 2, 3, samples while any agglomeration phenomena can be detected in the composites at 0.03 MWNT wt%. Moreover, it is also possible to note that a finer texture characterizes the

morphology of the samples sonicated for longer times respect to the ones sonicated for 10 minutes.

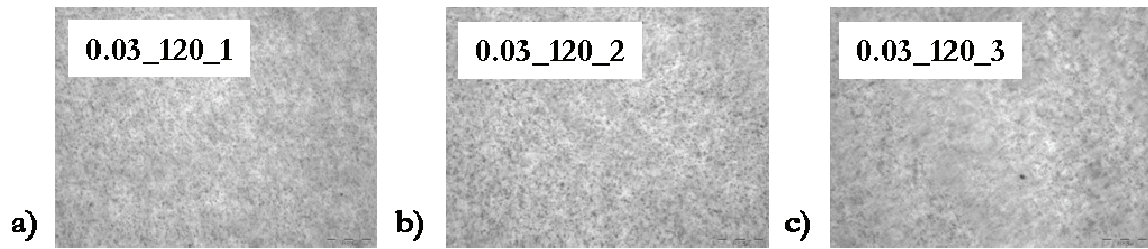


Figure 5.33 - Transmission optical microscopy images of composites at 0.03 MWNT wt% produced by a sonication of 120 minutes and cured respectively following the curing conditions a) 1, b) 2 and c) 3

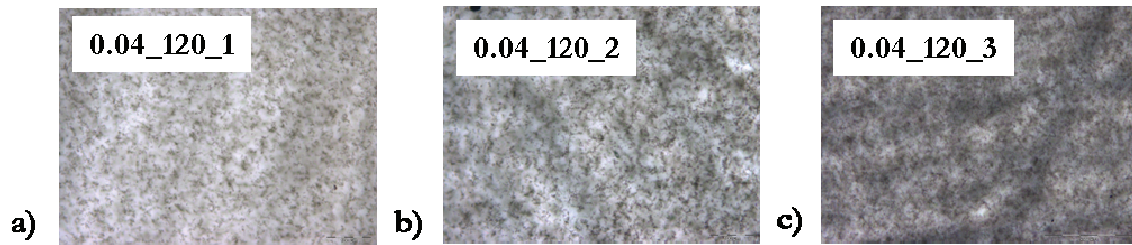


Figure 5.34 - Transmission optical microscopy images of composites at 0.04 MWNT wt% produced by a sonication of 120 minutes and cured respectively following the curing conditions a) 1, b) 2 and c) 3

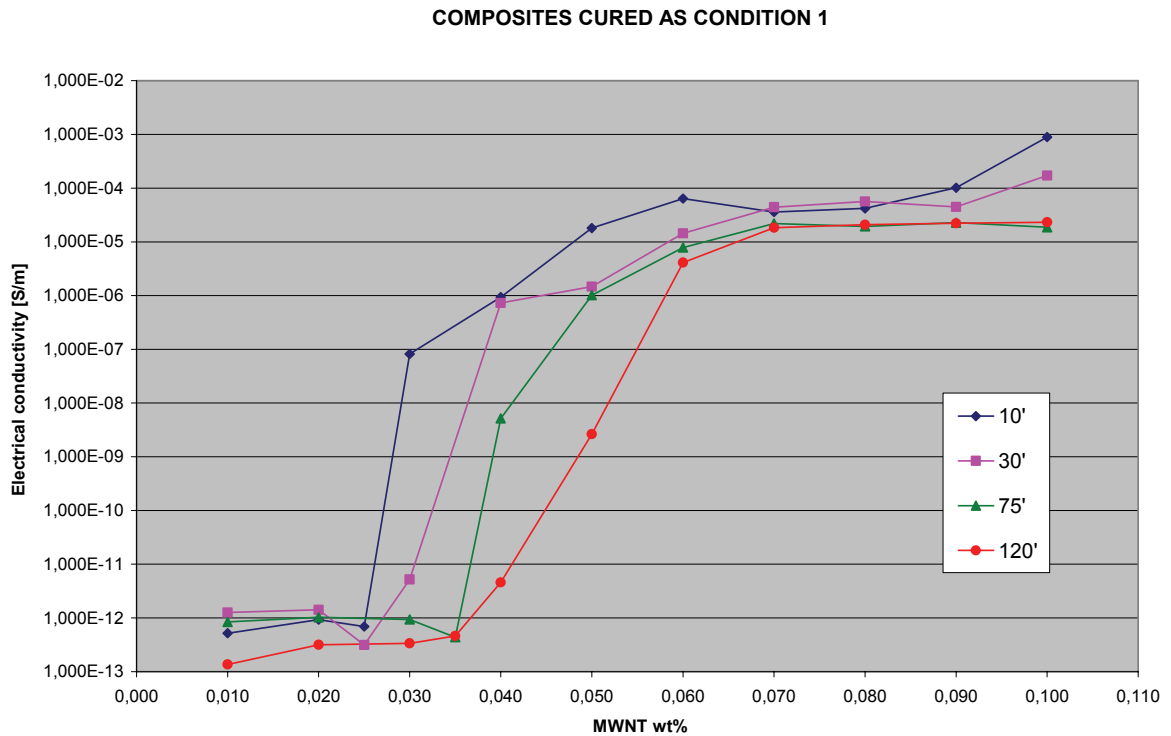
- **Results discussion**

It appears quite evident from the analysis of these results that the curing temperature and sonication time strongly affects the electrical behavior of the composites as a consequence of their influence of intern material morphology.

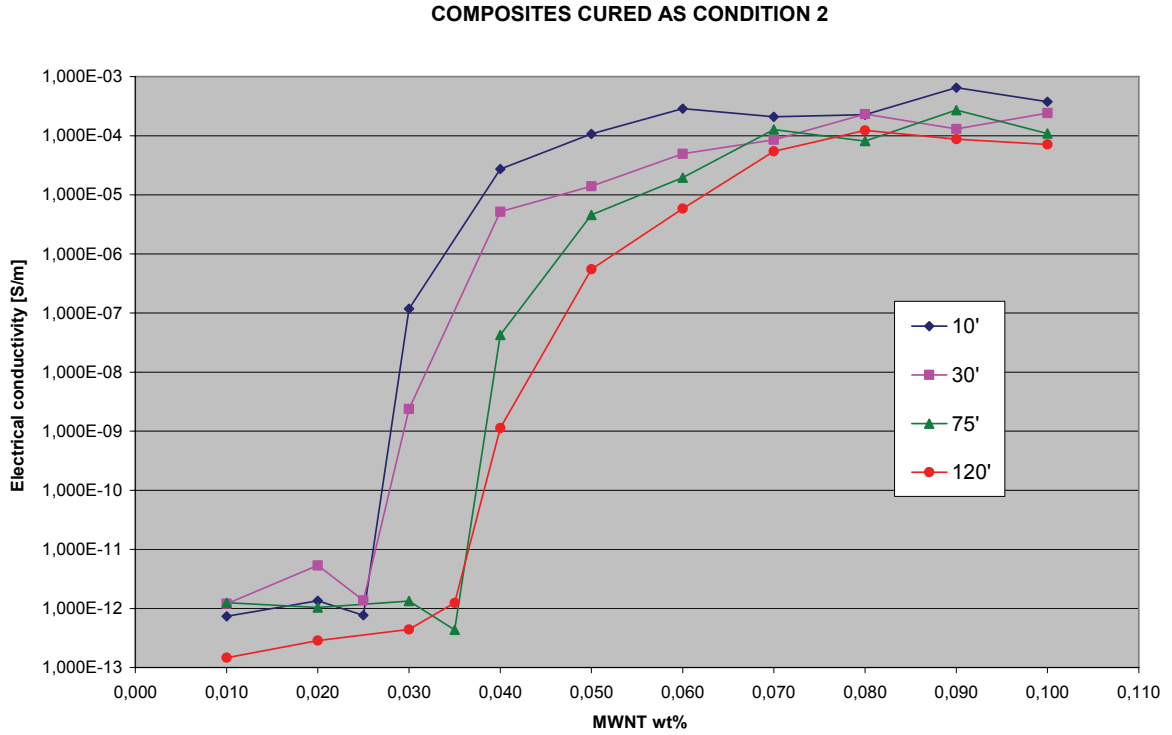
In general terms, it is possible to say that the percolation threshold decreases upon an increase of curing temperature. This phenomenon is an important example of “dynamic percolation”. The temperature effects occurring in the composites induce morphological modifications of the CNTs networks visible at the micro-scale. From the microscopic investigations, it appears that the formation of CNTs agglomerates corresponds to an increase in conductivity. This agglomeration is correlated to an increase of the connectedness of the CNTs networks that leads to an increase in conductivity. This temperature effect is a common phenomenon in all the examined systems occurring at different MWNTs concentrations for each sonication time. The dependence of conductivity on curing temperature occurring at different concentrations is hence induced by different morphologies present in the Epon/MWNTs solutions right after the sonication, before any other subsequent treatment. The formation of a conductive network

within the composite induced by increasing curing temperature is very sensitive to the energy provided for the agglomeration. In fact, one can observe that for certain concentrations the conductive network is formed only at the highest curing temperature, such as 120 °C of condition 3, while 70 °C of curing condition 2 are not sufficient for the agglomeration process resulting in the conductive network. This is the case of 0.02_10_2, 0.02_30_2, 0.035_75_2 and 0.035_120_2.

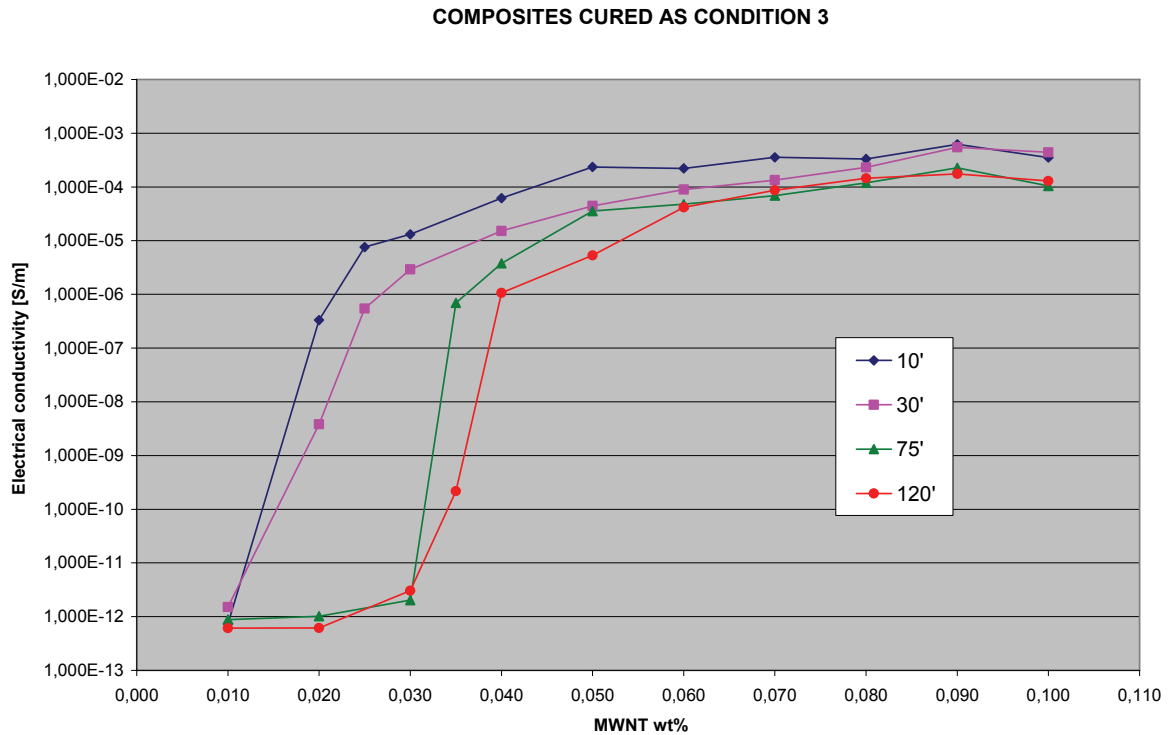
A more complete overview of the data can be derived from the analysis of the percolation behavior of the different systems. From this comparison one can note that an increase of sonication time corresponds to an increase in percolation threshold for all the curing temperatures, while the maximum electrical conductivity value is the same for all the sonication times at the maximum concentration (figures 5. 35 a, b, c). This means that after a certain concentration a plateau can be reached for all the systems, even if each of them in different ways.



a)



b)



c)

Figure 5. 35 - Percolation curves of composites of set 3 as a function of the curing condition a) 1, b) 2 and c) 3

This is the confirmation that a prolonged sonication is not beneficial for the electrical properties of the final composite. Such reduction could be explained considering two possible reasons: the

reduction of the length of CNTs due to sonication process or the very fine dispersion of the fillers in the matrix. However, the occurrence of the sonication induced damaging is not the actual case, because the length of the MWNTs used is not enough high to induce shortening [18]. Hence the other effect has been considered for the explanation of the increasing of percolation threshold with the sonication time. A very fine dispersion of CNTs in little bundles of few tubes leads to the formation of less efficient conductive networks, where the insulating matrix is present between the tubes, providing a lowering of the conductivity of the whole network, if any. This causes the necessity to increase the MWNTs content to enhance the conductivity. Moreover, the formation of isolated little bundles increasing the number of electrical junctions between tubes, increases the overall resistance of the system.

Furthermore, a synergic effect of the two varying parameters, such as curing temperature and sonication time, can be highlighted from the comparison between the percolation behaviors at fixed curing condition and variable sonication time. It appears that the effect of temperature on percolation mentioned above is much more evident as sonication time increases (figs 5.35 a, b, c). If one measures the variations in concentration corresponding to the same variation in conductivity (from 10^{-12} to 10^{-6} S/m) for all the sonication times at the three different curing conditions, he can observe that for 10 and 30 minutes of sonication, the variations in concentration (Δ MWNTwt%) are constant all over the varying curing conditions, while they decrease in the same batch for 75 and 120 minutes of sonication, passing from curing condition 1 to 3 (table 5.7).

Table 5. 7 – Variation of MWNT wt% corresponding to an increase of conductivity from 10^{-12} to 10^{-6} S/m for the four sonication times set of composites

Curing condition Sonication time	Δ MWNTwt%			
	10 min	30 min	75 min	120 min
1	1.5	1.5	1.5	2
2	1.5	1.5	1	1.5
3	1.5	1.5	0.5	1

This experimental evidence explains the higher mobility due to the little dimension of CNTs bundles provided by higher sonication times, that, however, it is not efficient for the formation of conductive networks. This can be also evident from the comparison between 75 and 120 minutes sonicated composites, where the variations in MWNT wt% measured at 75 minutes corresponding to the three curing conditions, are lower than the ones found for 120 minutes sonicated composites for the same curing condition. This is consistent with the assumption that

bigger bundles form more efficient networks, although the higher mobility during diffusion processes of agglomeration of the smaller bundles. This analysis has been conducted for an evaluation of the efficiency in the formation of the conductive network of the different CNTs structures, whose final dimensions depend upon the sonication time and whose connectedness depends upon the curing temperature. Hence, the final conductivity of the composites is a very difficult balance between the two opposite effects caused by the variation of the two process parameters.

On the basis of these results, one can say that the lowest percolation threshold can be reached for the lowest sonication time at the highest curing temperature, and the highest threshold for the highest sonication time and the lowest curing temperature.

In summary, it is possible to get evidence of the fact that for the produced composites the percolation thresholds are all well below the statistical one (two orders of magnitude), that is a notable result in terms of processability of the material. Moreover, the reported electrical behaviors are very reproducible even for very sensitive concentrations if all the process is well controlled.

These results provide, furthermore, the possibility to produce materials having very fine tunable electrical behavior in a very wide range of conductivity, with a high reliability.

The study on the morphology of the as produced MWNTs/epoxy composites at nano-scale levels by means of SAXS analysis is still in progress. This technique has been proved to be a very useful tool for the comprehension of the network structures forming within the CNTs composites and consequently of the type and degree of connectedness of the nanotubes [19].

5.3.6. Mechanically mixed epoxy composites

MWNTs/epoxy composites produced also by means of mechanical mixing have been produced for comparison purposes with composites produced by sonication. A three roll mill calander (Exakt 50) has been used for the nanotubes dispersion. Using this mixer, particle sizes are reduced and agglomerates are dispersed by the combined crushing force of the rollers and the extremely high shearing force resulting from different roller speeds.

The proper amount of MWNTs has been added to Epon component in order to have final cured composites at 0.01, 0.05 and 0.1 MWNT wt%. A first manual mixing has been carried out up to the disappearance of big CNTs aggregates. Then, the composite solution has been fed into a hopper, where it has been drawn between the feed and center rollers. When pre-dispersed, the solution sticks to the bottom of the center roller, which transports it into the second gap. In this

gap, the paste has been dispersed to the desired degree of fineness. With the scraper system the finished product has been removed from the apron roller. A preliminary mixing at 20 rpm has been done for all the solution, then a second mixing step has been performed at 120 rpm (fig. 5.36).



Figure 5. 36 – Three roll mill calander Exakt 50

The as prepared Epon/MWNT solution has been manually mixed with the TETA hardener and the final composites have been cured at 70 °C for 1 hour with a postcuring at 120 °C for two hours.

The electrical conductivity has been measured and compared with the conductivity of the other composite systems cured in the same conditions, such as the ones produced using sonication for 30 minutes in the TETA and for 30 and 120 minutes in Epon.

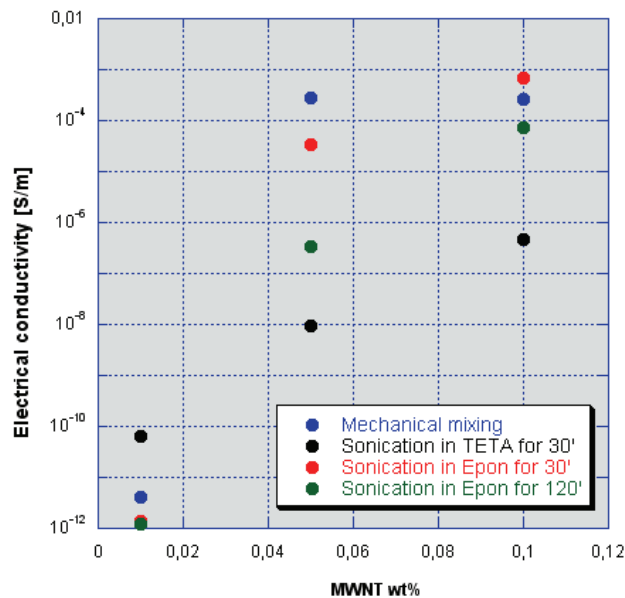


Figure 5. 37 - Electrical conductivity of mechanical mixed, 30 minutes sonicated in TETA and 30 and 120 minutes sonicated in Epon MWNT/epoxy composite cured at 70 °C

From figure 5.37 it is possible to note that for concentrations higher than 0.01 wt% the electrical conductivity of the composites produced by sonication in the hardener are lower than the ones produced by mechanical mixing and by sonication in Epon, both the 30 and 120 minutes sonicated ones. By the analysis of these data it can be found out that composites system produced by mechanical mixing has a percolation thresholds lower than 0.05 MWNT wt%, because high values of conductivity can be detected already at this concentration and they remain constant also at 0.1 MWNT wt%. This graph is a significant example of the influence of the production technique on the electrical properties of CNTs composites. In fact, for the same MWNTs content (0.05 wt%) and the same curing temperature, four different electrical conductivity values can be found, with a spanning of more than four orders of magnitude. In correspondence of higher concentrations, this phenomenon is not so evident, if one excludes the samples prepared by sonication in TETA. There exist concentrations where the percolative path is not stable and hence different manufacturing technique or the modification of a production parameter can cause substantial variations of the physical properties of the composite.

5.4 Conclusions

In this part of the experimental work, the fabrication and characterization of MWNTs epoxy composites have been carried out using the same matrix and filler, but different production methods. A strict correlation between the production technique and the final morphological and electrical properties of the composites has been found for all the investigated materials. Such as, for the same final CNTs concentration in the cured final composites, very different values of electrical conductivity have been found upon a variation of process parameters, in particular initial solvent, sonication time and curing temperature. The notable result consists in the possibility of exploiting a fine tuning of the insulator to conductor behavior of the epoxy composites, by controlling the CNTs network morphology forming within the composite, through the variation of the mentioned fabrication parameters.

Thanks to SAXS analysis, an explanation of such a morphology variation has been proposed starting from the dynamic percolation concepts and arriving to the definition of a multi-scale model, able to elucidate the hierarchical morphology existent in the CNTs structures. Two distinct cluster topologies within the final composite have been induced by means of sonication aided dispersion procedures in the two different solvents (TETA and Epon) that mainly differ each other by the nanotubes concentration. The modulation of nanocomposite electrical conductivity has been obtained by changing the state of aggregation of such clusters by means of

the variation of curing temperature. A high curing temperature provides an agglomeration process of the clusters and consequently a higher connectedness between conductive parts, that leads to higher conductive materials. The sonication time has been identified as a key factor in determining the mean dimension of the such initial clusters and it works in decreasing it for longer sonication times. The synergistic effect of sonication time and curing temperature provides the possibility to produce very tunable electrical properties upon a proper variation of process parameters.

5.5 References

1. Kovacs J.Z., Velagala B.S., Schulte K., Bauhofer W. - Composites Science and Technology 2007; 67:922 - 928
2. Schaefer D.W., Justice R.S. - Macromolecules 2007; 40 (24) November 27
3. Justice R.S. Small-angle scattering from nanocomposites: elucidation of hierarchical morphology/property relationships - 2007 Phd thesis
4. Chen Q., Saltiel C., Manickavasagam S., Schadler L. S., Siegel R.W., Yang H. C. J. - Journal of Colloid and Interface Science 2004; 280:91-97
5. Zhao C., Hu G., Justice R., Schaefer D. W., Zhang S., Yang M., Han C.C. - Polymer 2005; 46:5125-5132
6. Brown J.M., Anderson D.P., Justice R.S., Lafdi K., Belfor M., Stroing K.L., Schaefer D.W. - Polymer 2005; 46:10854-10865
7. Schaefer, D. W.; Zhao, J.; Brown, J. M.; Anderson, D. P.; Tomlin, D. W. - Chemical Physical Letters 2003; 375:369-375
8. Justice R. S., Wang D. H., Tan L.-S., Schaefer D. W. - Journal of Applied Crystallography 2007; 40:88-92
9. Antonucci V., Giordano M., Nicolais L. - Journal of Polymer Science Part A: Polymer Chemistry 2002; 40:3757-3770
10. Stauffer D., Aharony A., in Introduction to percolation theory 2nd edition (CRC Press 1994).
11. Beaucage G., Ulibarri T.A., Black E.P., Schaefer D.W., in Hybrid Organic-Inorganic Composites, Eds : J. E. Mark, C. Y-C Lee, P. A. Bianconi, ACS Symposium Series 585 (1995).
12. Rozes L., Fornasieri G., Trabelsi S., Creton C., Zafeiropoulos N. E., Stamm M., Sanchez C. - Progress in Solid State Chemistry 2005; 33:127-135
13. Hernández J. J., García-Gutiérrez M. C., Nogales A., Rueda D. R., Ezquerro T. A. - Composites Science and Technology 2006; 66:2629-2632
14. García-Gutiérrez M.C., Nogales A., Hernández J.J., Rueda D.R., Ezquerro T. A. - Optica Pura y Aplicada 2007; 40:195-205

15. Bryning M.B., Islam M.F., Kikkawa J.M., Yodh A.G. - *Advanced Materials* 2005; 17:1186-1191
16. Hecht D., Hu L., Grüner G., *Applied Physics Letters* 2006; 89:133112
17. Faiella G., Musto P., Di Florio G., Buosciolo A., D’Orazio L., Antonucci V., Giordano M. - *Journal of Nanoscience and Nanotechnology* 2009; 9:6026-6033
18. Badaire S., Poulin P., Maugey M., Zakri C. - *Langmuir* 2004 ; 20 :10367-10370
19. Faiella G., Piscitelli F., Lavorgna M., Antonucci V., Giordano M. - *Applied Physics Letters* 2009; 95:153106

APPENDIX A

CNTs alignment in polyurethane composites

A.1 Introduction

In this part of the dissertation, an experimental finding happened working on carbon nanotubes composites will be described. The experiment deals with the alignment of CNTs in a thermoplastic polyurethane composite for the production of highly conductive material.

The work lead to the wording of a patent [1]

Polyurethane (PU) is one of the most versatile materials today. It is widely used in coatings, adhesives, thermoplastic elastomers and composite, because of its useful properties such as excellent flexibility, elasticity and damping ability. PU generally consists of a soft segment which is a high molecular weight polyester or polyether macrodiol and a hard segment which is composed of diisocyanate and low molecular weight diol or diamine [2].

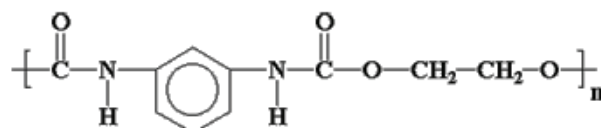


Figure A. 1 - Chemical formulation of a generic TPU

The most important feature of PU's structure is the microphase separation arising from the thermodynamic incompatibility of hard and soft segments. The modification of polyurethane

mainly focuses on the mechanical properties and thermal stability. In general, there are two approaches: the first is to change the molecular structure of polyurethane by modification of its three basic building blocks: polyol, diisocyanate, and the chain extender. The second is to introduce an inorganic filler into the polyurethane matrix, with, however, a worsening of the fatigue behavior and a reduction of the elongation at break.

In this context, a great effort has been devoted in scientific community for the production of polyurethane composites using carbon nanotubes as filler. However, few reports can be found in literature on this type of nanocomposites. This is probably due to the difficulty of dispersing nanotubes in polyurethane without the deterioration of the matrix properties[3-7]. Different dispersion techniques have been used for exploiting high mechanical, thermal and electrical properties of the final composites. The choice of proper fabrication process parameters, such as sonication time, stirring speed, dispersing solvents and mixing temperature is fundamental for achieving a good dispersion of the nanotubes in PU [8].

Most of the literature papers describes mechanical properties of CNTs PU composites, while very few works describe their electrical properties.

Xia et al. [2] in 2005 dispersed MWNTs and SWNTs in polyurethane matrix by means of in situ polymerization, prior a dispersion of the fillers into polyol by mechanochemical milling with the aid of a dispersing agent. From dynamic mechanical analysis (DMA), they found out that the addition of MWNT lead to a slight decrease of glass transition temperature and to an enhancement of the elastic modulus upon an increase of nanotubes content. While the addition of SWNTs lead to an increase of the final elongation and to a decrease of the damping properties. Both the types of nanotubes provided an increase of the thermal stability and conductivity due to the separation of the two PU phases, that is more evident for SWNTs than MWNTs composites. This could explain why SWNT-TPU composites showed a higher final elongation and strength respect to MWNT-TPU ones.

Very different results were found out by Xiong et al. [4], which prepared MWNT-polyurethane composites by means of a functionalization of nanotubes, able to create a strong chemical linkage with the matrix. Their results indicate that the glass transition temperature of the composite increased of about 10 °C at 2 MWNT wt% respect to the pure polyurethane. Moreover, an improvement of thermal stability, modulus and tensile strength were also found.

Abdullah et al. [9] prepared polyurethane composites filled with CNTs by mixing and injection molding. From DMA analysis they found out that the storage modulus of the composites increased with filler concentration, with a corresponding increase of the stiffness and a broadening and lowering of the peak of $\tan \delta$. This means that the polyurethane

composite became more elastic because a good adhesion between the filler and the matrix occurs. Moreover, the addition of carbon fillers improves the thermal stability of the polyurethane as well as the thermal conductivity. From the reported literature results it appears evident that process parameters, as well as nanotubes chemical and physical nature are very influencing factors for the final properties of the polyurethane CNT-composite.

A.2 Fabrication and electrical characterization of MWNTs/TPU composites

A thermoplastic polyurethane has been chosen as matrix for the production of MWNTs composites by using the mechanical mixing as dispersion technique without the presence of a dispersing agent.

MWNTs-TPU composites at two different nanotubes content have been prepared by means of extrusion and characterized by DC electrical measurements. Moreover, the alignment of the nanotubes within the polymer has been induced by means of a high electrical field, producing highly conductive material.

Catalytic Carbon Vapor Deposition Multi Walled Carbon Nanotubes (CCVD MWNT 7000) with a purity of 90%, an average diameter of 10 nm and a length ranging from 0.1 to 10 μm have been purchased by Nanocyl. A thermoplastic polyether based polyurethane (Elastollan $\text{\textcircled{R}}$) has been purchased by BASF. Its chemical structure is schematized in figure A.2.

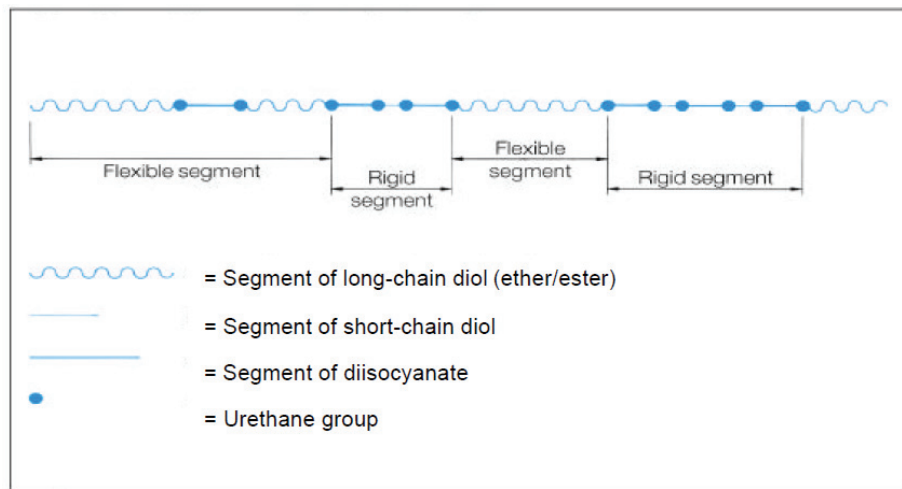


Figure A. 2 - TPU chemistry: hard and soft segments (from BASF)

The soft and hard phases are both semi-crystalline, with different glass transition temperatures.

The nanotubes have been dispersed in TPU by means of hot mixing using a twin-screws miniextruder.

Two concentrations of MWNTs have been used (1 and 3 wt%) while the mixing conditions, such as temperature and screws rounds per minute (RPM) have been varied as illustrated in table A.3. In the following, the samples will be named as “*concentration_sample number*”, for example “1_3” is the composite at 1 MWNT wt% produced at 190 °C, with a mixing speed of 50 RPM for 5 minutes.

Table A. 1 - MWNT/TPU composites mixing conditions

Sample	Temperature [°C]	RPM	Time [min]
1	180	50	10
2	180	100	5
3	190	50	5
4	180	50	5

The pellets obtained from miniextruder have been pressed using a hot press in a circular mold, obtaining disc samples.

A DC electrical characterization has been carried out on the TPU composites by means of a picometer (Keithley Picoammeter and Voltage source 6487) between -50 and 50 Volt.

In figure A.3 a the I-V curves for the samples at 3 wt% are plotted in the range 0 ÷ 50 Volt. For the same applied voltage, an increase of four orders of magnitude can be appreciated, passing from 3_1 to 3_4. The electrical conductivity of all the produced composites is reported in figure A.3 b as a function of the “samples”, such as the mixing conditions. As can be noted, the conductivity of composites at 1 wt% is very low and not influenced by the mixing conditions, while the conductivity of the samples at 3 wt% varies upon process parameters.

The interesting result is that for the same mixing conditions an increase in conductivity can be noted and even a drop of four orders of magnitude can be appreciated passing from sample 1 to sample 4, such as for composites at the same concentration, 3 wt%, prepared at the same temperature and screws speed but mixed for different times. In fact, increasing the mixing time from 5 to 10 minutes, the conductivity strongly increases.

From these results, it seems that a modulation of the electrical properties of the composite at 3 MWNT wt% can be done by varying the processing conditions, while no influence seems to have the variation of the process parameters on the electrical properties of TPU composites at 1 MWNT wt%.

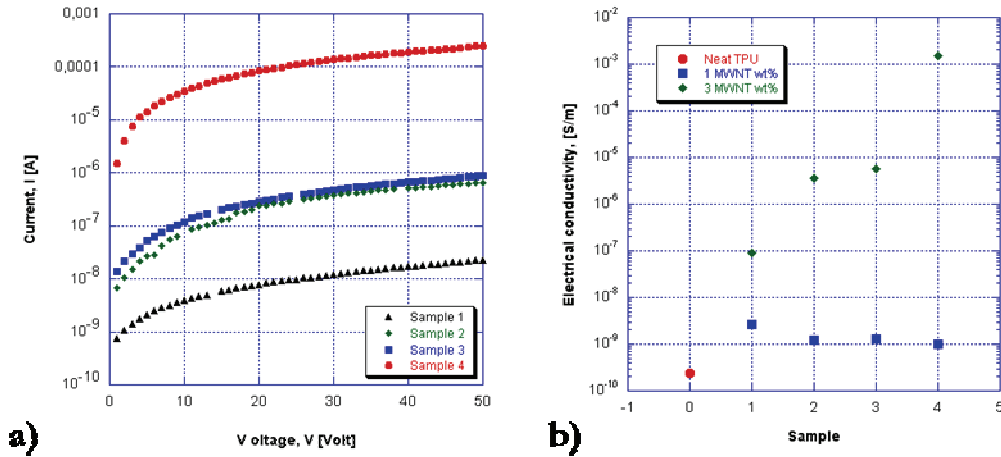


Figure A. 3 - a) Current vs. Voltage curves for TPU/MWNTs composites; b) electrical conductivity of TPU and its composites at 1 and 3 MWNT wt% as a function of mixing conditions

A.3 MWNTs alignment in TPU composites

Here, the alignment process of MWNTs in the TPU composites produced as illustrated in paragraph A.2 and the effects of the nanotubes alignment on their electrical properties will be described.

This study has been patented [1], so a general description of the results is given in the following.

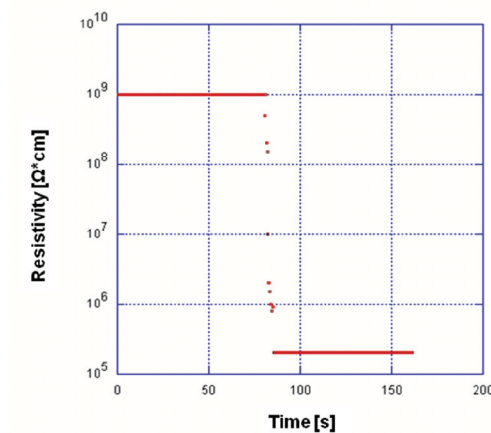


Figure A. 4 - Electrical resistivity of the TPU composite before and after the electrical discharge

The electrical resistivity of the sample has been measured by means of two electrodes embedded within the solid sample. A high voltage has been applied between these two opposite electrodes, that have been subsequently used again as measuring probes. During the voltage application, at a specific voltage value, an electrical discharge occurred inside the dielectric material between the

electrodes. From the electrical measurements after the discharge, the electrical resistivity resulted to be four orders of magnitude lower than before it (fig. A.4).

In order to exclude any type of relaxation phenomena in the composite, electrical measurements have been carried out also after 24 and 48 hours from the discharge and it has been found that the electrical conductivity remained constant.

Microscopic analysis has proved that a substantial modification within the composite occurred during the discharge: the nanotubes aligned between the electrodes along the direction of the voltage application (fig. A.5 a and b).

Before the application of the high voltage the nanotubes appeared coarsely dispersed in the matrix (the black spots in the colored matrix in figure A.5 a), while after the discharge a longitudinal dark pathway can be noted between the electrodes, while any dark spots are present in the surrounding matrix. This observation leads to the conclusion that nanotubes aligned between the electrodes during the discharge, because of the high temperature reached at those voltages, that provided the softening of the matrix allowing the tubes alignment. This highly ordered pathway of nanotubes strongly increased the conductivity of the composite in that region.

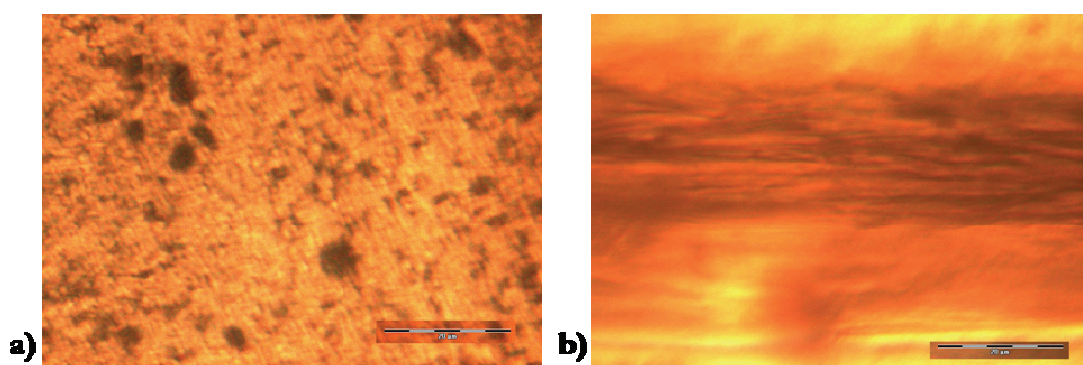


Figure A. 5 - Transmission optical microscopy images of TPU/MWNT composite a) before and b) after the electrical discharge

Possible applications of this technique can be found in the circuits production. One can figure out to build a circuit having a conductive behavior only along determined paths, while in the other parts of it the dielectric behavior can be preserved.

A.4 References

1. Giordano M., Cusano A., Aurilia M., Pilla P.L., Ruggiero V., Faiella G. - Patent N. TO2008A000316 - 23/04/2008

2. Xia H., Song M. - *Soft Matter* 2005; 1:386-394
3. Ni Q-Q., Zhang C-S., Fu Y., Dai G., Kimura T. - *Composite Structures* 2007;81:176-84.
4. Xiong J., Zheng Z., Qin X., Li M., Li H., Wang X. - *Carbon* 2006;44:2701-2707.
5. Xiong J., Zhou D., Zheng Z., Yang X., Wang X. - *Polymer* 2006;47:1763-1766.
6. Frogley M.D., Ravich D., Wagner H.D. - *Composite Science and Technology* 2003;63:1647-1654.
7. Chen W., Tao X., Y. - *Composite Science and Technology* 2006;66:3029-3034.
8. Ryszkowska J. - *Materials Characterization* 2009; 60:1127-1132
9. Abdullah S.A., Iqbal A., Frommann L. - *Journal of Applied Polymer Science* DOI 10.1002/app 28479
196-202

Conclusions and perspectives

This dissertation discusses a number of issues related to carbon nanotubes polymer composites. Starting from the study of CNTs solutions, the experimental work went through the production and characterization of CNTs thermoplastic and thermoset polymer composites using different methods. The use of a wide range of and characterization techniques allowed the investigation of different aspects related to the dispersion of CNTs both in water and in polymer matrices. Moreover, particular attention has been paid to their electrical properties and the dependence between the latter ones and the fabrication methods.

UV-vis and Raman spectroscopies have been used to characterize the degree of exfoliation of SWNTs in surfactant aqueous solutions, finding out a strict correlation between the two spectroscopic techniques and demonstrating that both techniques can be considered effective and reproducible methods to investigate the dispersion state of CNTs in solutions.

Thermoplastic CNTs composites have been produced by means of Latex technology, using a latex of polystyrene as matrix and SWNTs as fillers. The electrical conductivity of such composites has been measured by means of DC and AC electrical measurements, in order to study the percolative behavior of the composites at different CNTs content and their dielectric behavior. A model able to describe the inwardly connected capacitive and conductive natures of the matrix and filler contemporary existent in the composite has been proposed and validated by a good agreement between experimental and fitted data.

Thermoset CNTs composites have been produced using a bi-component epoxy resin as matrix and MWNTs as fillers. Different fabrication parameters have been varied for the production of composites having different morphological and electrical properties. It was found that a strict correlation between the production technique and the final physical properties exists and that the control of the composite process parameters is crucial for the achievement of the desired final performances. Not only conductive epoxy composites have been produced at MWNTs concentrations two orders of magnitude lower than those predicted by statistical percolation theories, but also for the same nanotubes content, those composites show electrical properties finely tunable by a curing temperature variation. A good control on the final electrical properties

of the composites has been acquired during the experimental campaign, even if further analysis, such as SAXS and Raman spectroscopy, could provide helpful information for the comprehension of several aspects related to the CNTs hierarchical morphology existent within the composites, whose structure influences their final electrical behavior.

The process tuning of carbon nanotubes electrical properties is a key factor in fabricating a material where defined values of electrical conductivity are required.

This research opens wide the doors to further studies on CNTs structures forming within polymer composites, enabling to control the final physical properties of the materials with the purpose of engineering their final performances.

Ringraziamenti

Al termine di questi anni di lavoro voglio ringraziare tutte le persone che sono state accanto a me dall'inizio alla fine di quest'avventura e tutte quelle che lungo il percorso in un modo o nell'altro hanno dato il loro contributo per raggiungimento di quest'obiettivo.

Voglio ringraziare il mio tutor Michele Giordano per aver creduto in me e per avermi dato la possibilità di fare ricerca e Enza Antonucci, per il suo supporto tecnico e le chiacchiere tra donne.

Un ringraziamento speciale va a tutti i miei colleghi, amici di laboratorio e di "merenda"...che tutti i giorni hanno trovato il modo di rendere il lavoro piacevole con la loro presenza.

Alla mia famiglia dedico tutto il lavoro di questi tre anni, che non avrei mai potuto portare avanti senza il suo supporto. Grazie a mia madre, per le sue premure e per aver sempre condiviso le gioie e i dolori di una figlia dottoranda; a mia sorella per aver avuto un sorriso dolce per me nonostante il mio frequente caratteraccio...

Il significato che ha per me questo traguardo lo dedico al mio "papà collega", che nonostante avesse per me altri progetti, mi ha guidato nel mio fin qui e con i suoi preziosi consigli mi ha spronata a fare di meglio ogni giorno.

La passione che ho messo in ogni cosa del lavoro che ho fatto in questi anni la dedico al mio fidanzato, Mario, che ringrazio per amare anche questo di me e che mi ha sempre ricordato quanto fosse importante per me questa passione, nei momenti difficili in cui mi sembrava di averla persa.

Gabriella

Curriculum Vitae

Gabriella Faiella was born in Naples, Italy, on the 30th November 1981.

She received the bachelor degree in Materials Science and Engineering in 2003 with 100/100 cum laude and in 2005 the Laurea degree in Materials Engineering with 100/100 cum laude.

During her master studies, she spent six months at Queen Mary and Westfield College University of London, working in Materials Engineering department on polymer nanocomposites, starting there her master thesis project. Since 2003 she has been collaborating with Italian National Research Council, at Institute for Composite and Biomedical Materials (IMCB) working first on shape memory alloys hybrid composites and then, during her Ph.D. program, on carbon nanotubes polymer composites.

Her main research interest field is set in the context of advanced composites materials.

Selected publications

V. Antonucci, G. Faiella, M. Giordano, F. Mennella, L. Nicolais, - “Electrical resistivity study and characterization during NiTi phase transformations” - *Thermochimica Acta*, 462 (1), pp.64-69, (2007)

V. Antonucci, G. Faiella, M. Giordano, L. Nicolais, G. Pepe - “Electrical Properties of Single Walled Carbon Nanotube Reinforced Polystyrene Composites” - *Macromolecular Symposia* 247 (1), pp. 172–181 (2007)

G. Faiella, V. Antonucci, F. Daghia, M. Giordano, F. Daghia, E. Viola - “Effect of the loading history on shape memory alloy transformation temperatures” - *Advances in Science and Technology* 59, pp 57-62 (2008)

Faiella G., Musto P., Di Florio G., Buosciolo A., D'Orazio L., Antonucci V., Giordano M. - *Journal of Nanoscience and Nanotechnology* 9, pp 6026-6033 (2009)

G. Faiella, F. Piscitelli, M. Lavorgna, V. Antonucci, M. Giordano – “Tuning the insulator to conductor transition in a Multi Walled Carbon Nanotubes/Epoxy composite at sub statistical percolation threshold” - *Applied Physics Letters* 95, 153106 (2009)